Distance dependent excited-state relaxation of *MePTCDI* on semiconductor substrates in the isolated molecule limit

Von der Fakultät Mathematik und Physik der Universität Stuttgart
zur Erlangung der Würde eines
Doktors der Naturwissenschaften (Dr.rer.nat.)
genehmigte Abhandlung

vorgelegt von

Eugenio Lunedei

aus Rimini, Italien

Eingereicht am 23.5.2003

Hauptberichter:	Prof. Dr. H.C. Wolf
Mitberichter:	Prof. Dr. G. Mahler
Prüfungsvorsitzender:	Prof. Dr. T. Pfau
Tag der mündlichen Prüfung:	5.8.2003

---

3. Physikalisches Institut der Universität Stuttgart

2003

Contents

Zusammenfassung

Wechselwirkungen zwischen Molekül und Substrat
Die Fluoreszenzeigenschaften eines elektronisch angeregten Moleküls ändern sich nahe der Oberfläche eines Festkörpers dramatisch. Die Änderung hängt von dem Abstand d zum Substrat, sowie von dessen physikalischen Eigenschaften ab.

Hauptaspekt der vorliegenden Arbeit ist die Messung und quantitative Beschreibung der Wechselwirkung zwischen elektronisch angeregten organischen Molekülen und anorganischen Halbleitersubstraten in Abhängigkeit des Molekül-Festkörper-Abstandes.

Die hierzu verwendete experimentelle Technik ist die zeitaufgelöste Fluoreszenzspektroskopie. Die Proben wurden im Ultrahochvakuum (UHV) bei tiefen Temperaturen in-situ präpariert und untersucht.

Konkurrenz zw. Schicht-internem und Schicht-Substrat Anregungstransfer
Abhängig von Molekülsorte, Wachstumsparametern und experimentellen Bedingungen wechselwirken die Moleküle innerhalb der Schicht stärker oder schwächer miteinander. Unabhängig von der Nähe eines Substrats induziert eine solche Wechselwirkung nach optischer Anregung eines Moleküls der Schicht einen Anregungstransfer zwischen den Molekülen, was zur Bindung der Anregungsenergie an Excimerplätzen führt, und damit die Lumineszenzausbeute schwächt. Im Falle einer Molekülschicht auf einem Subtrat kommt nun ein weiterer Mechanismus hinzu: Der Transfer von Anregungsenergie von der Molekülschicht auf den darunterliegenden Festkörper. Die zwei Anregungtransferpfade, schicht-intern und Molekül-Substrat, konkurrieren miteinander, und sind für lateral ausgedehnte Filme ununterscheidbar. Ihre Trennung ist eine Voraussetzung für jede experimentelle Untersuchung.

Die Untersuchung abstandsabhängiger Molekül-Substrat-Wechselwirkungen kann auf zwei Arten erfolgen, abhängig von der Methode, mit der der Abstand d definiert und fixiert wird. Einerseits können verschiedene d durch Einbau einer inerten Abstandshalter-Schicht definierter Dicke zwischen den isolierten Molekülen und dem Substrat realisiert werden. Eine zweite Möglichkeit ist das direkte Aufbringen verschieden dicker Molekülschichten auf das Substrat. In diesem Fall muss man versuchen, die schicht-internen Wechselwirkungen und die, die zwischen den einzelnen Schichten auftreten, numerisch von den Substrat-induzierten Effekten zu trennen. Für diese Arbeit wurde der Weg der inerten Abstandshalter-Schichten gewählt.

Theoret. Modelle zur Beschreibung der Molekül-Substrat-Wechselwirkung
Im ursprünglichen Modell von Kuhn [10] wird das elektronisch angeregte Molekül als gedämpfter klassischer Oszillator betrachtet: die Dämpfung des Dipols rührt von der

Interferenz seines Strahlungsfeldes mit seiner eigenen vom Substrat reflektierten (retardierten) Partialwelle her. Ausgehend von dieser Interpretation wird nur das Fernfeld des Dipols berücksichtigt. Als Ergebnis wird ein oszillierendes Verhalten der vom Dipol emittierten Intensität und Lebensdauer als Funktion des Molekül-Substrat-Abstandes d vorhergesagt.

In den frühen Siebzigern entwickelten Chance, Prock und Silbey ('CPS' [11]) ein neues klassisches Modell (eine Erweiterung des Kuhn-Modells), in dem explizit das Nahfeld des Moleküls berücksichtigt und seine Auswirkungen auf dessen Anregungslebensdauer diskutiert werden. Dieses vollkommen phänomenologische Modell, welches nur von der dielektrischen Konstante des Substrats abhängt, sagt ausser dem von Interferenzeffekten verursachten oszillatorischen Verhalten eine dramatische Reduzierung der beobachteten Lebensdauer als Folge eines strahlungslosen Energietransfers vom Molekül zum Substrat bei Abständen von $d < 500\,\text{Å}$ voraus.

Die Tatsache, dass ein rein klassisches Modell eine Lebendsdauerverkürzung bei Nähe zum Substrat fordert, impliziert, dass der Löschmechanismus vollständig von der dielektrischen Funktion des Festkörpers beschrieben wird. Dennoch war die Natur des Mechanismus, der die Lebendauerverkürzung im Nahfeld verursacht unklar, bis die Analogie zu dem Problem der Radiowellenfortpflanzung in Nähe der Erdoberfläche erkannt wurde [12]: Der Energietransfer von Emitter zu Substrat über kurze Distanzen ist abhängig von der Möglichkeit, über die kurzwelligen Komponenten des molekularen Nahfelds Oberflächen-Ladungsdichtewellen (Oberflächenplasmonen) zu erzeugen.

Speziell für direkte und indirekte Halbleitersubstrate und Abstände ($d < 100\,\text{Å}$) wurde im Rahmen der Störungstheorie von Stavola, Dexter und Knox ('SDK' [13]) ein weiteres semiklassisches Modell entwickelt. Nach diesem Modell wird eine stark abstandsabhängige Lebensdauerverkürzung im Bereich des Nahfeldes erwartet. Dieser Energietransfer auf das Substrat wird durch strahlungslose Dipol-Dipol-Wechselwirkung zwischen dem angeregten Molekül und einem durch seine kurzwelligen Nahfeldkomponenten induzierten Elektron-Loch-Paar im Halbleiter erklärt.

Das SDK-Modell sagt voraus, dass für einen direkten Halbleiter abhängig von seiner elektronischer Bandstruktur und der molekularen Emissionsenergie eine strahlungslose Transfer-Rate proportional zu d^{-3} beobachtet werden sollte, für einen indirekten Halbleiter wird eine Rate proportional zu $\sim d^{-4}$ erwartet. Bei noch kleineren Abständen ($d < 20\,\text{Å}$) reduziert die Energieerhaltung die Effizienz von Elektron-Loch-Paarbildung und damit die des Anregungstransfers von Molekül zu Substrat.

Fluoreszenz nahe an Halbleiteroberflächen

Neben der grossen Zahl von Untersuchungen an Metallsubstraten wurde den photophysikalischen Eigenschaften angeregter Moleküle auf Halbleitersubstraten nur wenig

Aufmerksamkeit zuteil. Während bei Metallen der Anregungstransfer vom Molekül zum Festkörper von Wechselwirkungen mit den ungebundenen Elektronen des Substrats abhängt, wird er bei Isolatoren und Halbleitern hauptsächlich von den gebundenen Elektronen beeinflusst.

Da das klassische theoretische Modell (CPS) keine mikroskopische Beschreibung des Festkörpersubstrats beinhaltet, sollte es auch für Halbleiter erfolgreich angewendet werden können. Obwohl bereits über experimentelle Untersuchungen berichtet wurde, ist noch offen, ob sich die Transferrate proportional zu d^{-3} im Quenchregime verhält. Die vorliegende Arbeit hat eine Antwort auf diese Frage zum Ziel.

Darüberhinaus wurden alle veröffentlichten experimentellen Arbeiten zu den Wechselwirkungsprozessen zwischen organischen/anorganischen Molekülen und organischen/anorganischen Substraten ausschliesslich an direkt oder indirekt auf dem Substrat deponierten Molekülschichten durchgeführt, nie an einem einzelnen isolierten Molekül, wovon die theoretischen Modelle jedoch ausgehen. Als Konsequenz wurden nicht die Auswirkungen der Wechselwirkung eines Moleküls mit dem Substrat, sondern derer zwischen einem Satz gemeinsam wechselwirkender Moleküle (in kristallinen, polykristallinen und amorphen Schichten) und dem Substrat gemessen. Dieser Aspekt wurde bisher fast völlig vernachlässigt, bis frühere Forschungsprojekte unserer Gruppe (M. Daffertshofer [34], U. Gomez [43]) zeigen konnten, dass der schichtinterne Transport von dem Anregungstransfer zum Substrat separiert werden kann.

Das Ziel der vorliegenden Arbeit

Ausgehend von früheren experimentellen Arbeiten ist das Ziel der vorliegenden die Untersuchung der Wechselwirkungsmechanismen zwischen Molekül und Substrat gemäss dem Ansatz des 'isolierten Moleküls' (z. B. durch Aufdampfen ultradünner Schichten), mit einem Schwerpunkt auf Halbleitersubstraten.

Diese Studie wurde mit N,N'-Dimethylperylen-3,4:9,10-bis(dicarboximide) (*MePTCDI*, ein Perylenderivat) als Molekül und MoS_2 (Molybdändisulfid), sowie *Si(111):H* (wasserstoffterminiertes Silizium) als Substrate durchgeführt, Schichtdicken betrugen deutlich weniger als eine Monolage (ML), zur Präparation wurden verbesserte Techniken verwendet.

MePTCDI ist grösser als andere früher verwendete Moleküle, (z. B. Anthracen) und hat eine geringere laterale Mobilität, bei flüssig Helium temperatur erweist es sich als fast unbeweglich. Daher ist es besonders geeignet zur Deposition im UHV und wohldefinierte molekulare Schichten können gewachsen werden.

Als Substratmaterialien wurden *Si(111):H* und MoS_2 wegen ihrer wohlbekannten Eigenschaften, den bewährten Präparationstechniken und den verschiedenen Bandstrukturen gewählt. Beide sind indirekte Halbleiter, aber in einem Fall (MoS_2) ist die Energie des

angeregten *MePTCDI* grösser als die direkte Bandlücke des Materials, in dem anderen Fall (*Si(111):H*) kleiner. Dieser Unterschied sollte einen dramatischen Einfluss auf die Energietransferrate vom Molekül auf das Substrat haben.

Die Substratpräparation wurde ebenfalls weiter verbessert: Insbesondere die Anwendung eines nasschemischen Passivierungsprozesses (ein modifizierter RCA-Prozess) im Falle des Silizium *Si(111)* führte zu einem vollständigen Entfernen der natürlichen Oxidschicht von der Siliziumoberfläche und einer Wasserstofferminierung aller ungesättigten Bindungen; dies erlaubt durch die Herstellung einer chemisch inerten Oberfläche die wohldefinierte Einstellung des Abstandes zwischen dem Molekül und dem Silizium.

Experimentelle Ergebnisse

Bei schrittweisem Ändern des Bedeckungsgrades (von 1 ML bis hinunter zu 0.01 ML) konnte ein kontinuierlicher Rückgang der intermolekularen Wechselwirkung innerhalb der Schicht bis hin zu einer völligen Unterdrückung des schichtinternen Anregungstransports experimentell beobachtet werden. Bei 0,01ML Bedeckung auf einem nicht wechselwirkenden Substrat (z.B. Quarz) hat die Fluoreszenz monomeren Charakter mit einfachem exponentiellem Zerfall und nahezu intrinsischer Fluoreszenzlebensdauer (was auf fehlende Wechselwirkung mit anderen Molekülen oder dem Substrat hinweist). Ganz im Gegensatz dazu ist bei aktiven Substraten neben einem monomeren Fluoreszenzspektrum eine verkürzte Fluoreszenzlebensdauer zu beobachten, da nun Anregungstransfer zum Substrat stattfindet. Die Verkürzung der Lebensdauer kann quantitativ mit der Art des als Substrat verwendeten Festkörpers in Bezug gebracht werden.

Ausserdem ist durch Aufbringen einer solchen ultradünnen Schicht in einer Entfernung d vom Substrat (mit Abstandshalter-Schicht) möglich, die Abstandsabhängigkeit der Molekül-Substrat-Wechselwirkung im Bereich zwischen 0 und 500 Å direkt zu untersuchen, und zwar in Abwesenheit aller anderen normalerweise konkurrierenden Prozesse.

Die Hauptergebnisse lassen sich wie folgt zusammenfassen:
Elektronisch angeregte *MePTCDI* Moleküle im Nanometerabstand zu einer Halbleiteroberfläche (sowohl MoS_2, als auch *Si(111):H*) weisen schnellere Fluorezenzzerfälle auf, als in verdünnter Lösung (die Referenz für intrinsische molekulare Fluoreszenzlebensdauer). Die Abstandsabhängigkeit der *MePTCDI* Fluoreszenzlebensdauer bei Abständen von $0-500$ Å (MoS_2) bzw. $0-130$ Å (*Si(111):H*) zeigt bei den beiden Halbleitern quantitativ unterschiedliche Verkürzungseffekte: Auf MoS_2 verringert sich die Lebensdauer um zwei Grössenordnungen (von 3.95 ns auf 25 ps), auf *Si(111):H* um eine (auf 145 ps).
Das CPS-Modell wurde unter Berücksichtigung der dielektrischen Funktionen der Materialien zur quantitativen Beschreibung der beobachteten Änderungen der Fluoreszenzlebensdauern bei Abstandsvariationen zwischen Molekül und Substrat verwendet. Im Falle des MoS_2 bestätigen die experimentellen Daten das CPS-Modell über den gesamten $d-$Bereich quantitativ.

Bei Verwendung von *Si(111):H* als Substrat kann die experimentelle Abhängigkeit jedoch nicht durch das CPS-Modell erklärt werden: Bei minimalem Abstand besteht eine Diskrepanz von mehr als einer Grössenordnung zwischen Modell und Experiment. Das semi-klassische, speziell für Halbleiter entwickelte Modell (SDK) führt einen neuen Energietransfermechanismus ein, um die beobachtete Verkürzung der molekularen Lebensdauer zu erklären. Es liefert eine qualitative Beschreibung der Abstandsabhängigkeit der Fluoreszenzlebendsdauer unter Berücksichtigung der Halbleiterbandstruktur.

Die Ergebnisse wurden im Rahmen des SDK Modells wie folgt interpretiert:
– MoS_2 ist ein typischer Fall, in dem die molekulare Emissionsenergie grösser ist als die Bandlücke des Halbleiters. Das Nahfeld des Moleküls kann ein Elektron des Valenzbandes strahlungslos in das Leitungsband des Halbleiters heben. Auf diese Weise transferiert das Molekül seine Energie durch einen Dipol-Dipol-Mechanismus (Elektron-Loch-Paar im Halbleiter) zum Festkörper. Dieser Prozess funktioniert effektiv bei Abständen, die kleiner als 300 Å sind. Die Transferrate sollte sich wie im CPS Modell proportional zu d^{-3} verhalten. Zusätzlich sollte bei sehr kleinen Abständen ($d < 50$ Å) eine Abweichung von diesem Verhalten auftreten. Dies konnte wegen der begrenzten Zeitauflösung jedoch nicht beobachtet werden.
– Ein Fall, in dem die Bandlücke die Emissionsenergie des Moleküls übersteigt, ist *Si(111):H*. Hier kann das Nahfeld nicht-vertikale Übergänge durch eine spezielle Verteilung seiner Wellenvektoren anregen, also ohne Beteiligung von Phononen, und auf diese Weise ebenfalls Elektron-Loch-Paare erzeugen. Dieser Mechanismus sollte eine d^{-4}-Abhängigkeit der Transferrate zeigen. Bei extrem kleinen Abständen zum Substrat ($d < 25$ Å), abhängig von der Überschussenergie des Moleküls, sollte eine Abweichung von diesem Verhalten auftreten. Unter Verwendung dieses zweiten Modells können die experimentellen Daten qualitativ erklärt werden.

1 Introduction
State of knowledge and goal of the present research

The overall performance of optical devices (as the OLEDs [a]) based on organic active layers strictly depends on the efficiency of the radiative recombination of the exciton. Upon charges injection and molecular exciton formation, the most significant channels of radiationless exciton decay competing with the light emission include: intersystem crossing to triplet state [5, 6], exciton dissociation induced by the field applied to the device [7, 8] and non radiative transfer of the excitation [9]. In particular, exciton quenching at the surface of the metallic cathode or at the interface with other semiconductors drastically reduces the emission of light.

The study and the comprehension of mechanisms of non radiative interaction between electronically excited organic molecules and metallic or semiconductor substrates has therefore a significant applicative interest besides a considerable scientific importance.

1.1 The molecule-substrate interaction

The fluorescence properties of an electronically excited molecule change drastically when it is brought in proximity of the surface of a solid, as a function of the molecule-substrate distance d and of the specific physical characteristics of the solid.

The main subject of the present research is the measurement and the quantitative description of the interaction between electronically excited organic molecules and inorganic semiconductor substrates, as a function of molecule-solid separation.

The used experimental technique is the time-resolved fluorescence spectroscopy applied to the study of samples prepared and analyzed at low temperature, in–situ, under Ultra High Vacuum (UHV) conditions.

In the following sections, the state of the theoretical and experimental knowledge on the subject, updated to the time of the present research, is briefly summarized (a detailed description of the theoretical models is given in § 6 and § 8.6.3); the importance of an appropriate experimental approach and the earlier results obtained by our group are successively pointed out and the goal of present experimental work connected to those.

1.1.1 Theoretical models to describe the molecule-substrate interaction

A number of theoretical models have been developed to describe the interaction between an electronically excited molecule and a solid and to analyze the dependence of its emission properties as a function of the separation d from the substrate.

[a] Organic Light Emitting Diodes [1–4]

In the original model of Kuhn [10] the electronically excited molecules are considered as damped classic oscillators: the damping of the dipole originates from the interference between its radiating field and the reflected (retarded) field from the surface. On the basis of this interpretation, only the far-field (radiative component) of the dipole is taken into account. As a result of such interference phenomena, an oscillating behaviour of the dipole emission intensity and lifetime as a function of the molecule-substrate separation d is predicted.

In the earlier '70s Chance, Prock and Silbey ('CPS' [11] and references therein) developed a new classical model (extension of the Kuhn's model) in which the *near-field* components of the dipole field are explicitly considered and their effect on the lifetime of the excited molecule studied. The model, *entirely phenomenologic* and based only on the value of the substrate dielectric constant predicts, beside the oscillatory behaviour caused by interference effects, a drastic reduction of the observed lifetime as a result of *non-radiative* energy transfer from the molecule to the substrate in the short molecule-substrate distance range ($d < 500$ Å). For the molecular fluorescence lifetime a distance dependence $\sim d^3$ is predicted.

The fact that a classical model predicts also a drastic lifetime shortening in short distance domain implies that the quenching mechanism is *entirely described* by the dielectric function of the solid. Nevertheless, the *nature of the mechanism* that causes the shortening in molecular lifetime within the near-field range was unclear until the analogy between this experiment and the problem of radio-wave propagation near the surface of the earth became apparent [12].

On metallic substrates, the mechanism of energy transfer from the emitter to the substrate within the short distance regime turns out to be related to the possibility to excite resonantly surface charge density oscillations (Surface Plasmons, SP) by the high-wave-vector components of the molecular near field.

A further semiclassical model has been developed explicitly for direct and indirect *semiconductor* substrates and short distances ($d < 100$ Å) in the frame of the perturbation theory by Stavola, Dexter and Knox ('SDK' [13]). According to this model, a strong distance-dependent molecular lifetime shortening is predicted in the near-field range. Such energy transfer to the substrate is explained in terms of non-radiative dipole-dipole interaction between the excited molecular dipole and an *induced electron-hole pair* in the semiconductor, via the high-wave-vector components of the molecular near field.

The SDK model predicts that, according to the specific electronic band structure of solid and to the molecular emission energy, a non-radiative energy transfer rate proportional to d^{-3} should be observed on *direct* semiconductor, whereas a rate $\sim d^{-4}$ is expected on an *indirect* one. At short molecule-substrate distances ($d < 20$ Å) energy conservation reduces the efficiency of the e-h pair generation and therefore of the excitation

transfer from molecule to the substrate; a *deviation* from both d^{-3} and d^{-4} dependences is consequently expected (*see* § 8.7).

Beside these two models, other theoretical works have been focussed on the subject especially for the short molecule-substrate separation range. In particular, Persson and Lang [14, 15] following a quantum mechanical approach discussed (for metals) the contribution to the excitation transfer rate from electron-hole pairs generation; an energy transfer rate $\sim d^{-4}$ from surface states or $\sim d^{-3}$ from volume contribution is predicted. Rempe [16] proposed a further quantum mechanical model to describe the molecule-substrate interaction for large separation d: the vacuum fluctuation of the electromagnetic radiation field is modified by the presence of the substrate; as a consequence, the Einstein coefficients for the spontaneous emission at the position of the excited molecule (i.e. the fluorescence lifetime) are also modulated as a function of the molecule-substrate separation.

1.1.2 Competition between intra-layer and molecule-substrate excitation transfer

The experimental work concerning the interaction processes between (organic/inorganic) molecules and (organic/inorganic) substrates reported by all the other groups has been carried out exclusively on *films* of molecules deposited (directly or indirectly) on the substrate: *never on 'single isolated molecule'*, as generally assumed in the theoretical models. As a consequence, what has been measured is not the effect of interaction between *one* molecule and the substrate, but between a set of mutually-interacting molecules (in crystal, in polycristalline film or in amorphous film) and the substrate.

Depending on the type of the molecule, on the film growth and on the experimental conditions, the molecules are more or less preferentially *interacting* within the molecular layer. Such interaction induces (independently from the presence of the substrate in the proximity) a transfer of the excitation *inside the film*, generally followed by excitation trapping in traps or excimer sites and subsequent reduction of luminescence efficiency.

In addition, when the film is deposited on (or near) an 'interacting' substrate, a further competing mechanism takes place: the excitation transfer from the molecular film *to the solid* underneath.

The two excitation transfer pathways, intra-layer (i.e. from molecule to molecule) and molecule-substrate, act competingly and their effects are undistinguishable for laterally extended films; their separation is a prerequisite for any experimental study.

1.1.3 The two experimental approaches

The previous experimental works aimed to study the distance dependent molecule-substrate interaction can be divided into two groups according to the method to define

and fix the separation d. Following the first method, different separations d are obtained by inserting an inert 'spacer' layer of defined thickness between the thin molecular film and the substrate; in the second approach, the variation of the distance is obtained by depositing molecular films of various thickness directly on the substrate.

1.) Molecule-substrate distance variation by means of a spacer layer
Already in the pioneering experimental work of Drexhage [17–19] the spacer layer technique was used to vary the distance between a monolayer of molecular Eu^{3+} complexes and metallic substrates (*Ag, Au, Cu*). As spacer, a fatty-acid layers (each layer 26.4 Å thick) of different thicknesses ($d = 60-700$ Å) were deposited on the substrate by LB[b]-technique. Such samples were studied by time-resolved fluorescence spectroscopy: fluorescence intensity and lifetime versus spacer thickness were measured. Both quantities were found to change in an oscillating functional dependence on the distance d. In the large distance range ($d > 1500$ Å), the oscillations could be described with very good approximation by Kuhn's model, whereas the observed deviations from the predicted curves stimulated further researches that led to the development of the CPS model.

Relevant experimental work on energy transfer from organic molecules to inorganic substrates was carried out in the Harris' group since the '80s. As substrates were used both metals (*Au, Ag, Ni*) [20–22] and semiconductors [23,24] (see further § 1.1.4), prepared and measured under *UHV* conditions. As spacer layer *Ar*, NH_3 or *Xe* were condensed at 20 K, with thicknesses in the range of $10-420$ Å. As emitting layer, on metals, a monolayer of pyrazine was used and the intensity and lifetime of its phosphorescence measured, in–situ, at helium temperature; on semiconductors the fluorescence of a sub-monolayer pyrene film was measured for just a number of distances. While on the metals the pyrazine phosphorescence lifetime dependence vs. distance could be adequately described in the frame of the CPS model, on the semiconductors the fluorescence lifetime distance dependence of pyrene could be only qualitatively compared with the classical model expectations owing to a strong non-monoexponentially of fluorescence transients that did not permit a reasonable estimate of lifetime.

Strong deviations from monoexponentiality are very often observed in fluorescence lifetime measured in organic films [24–34]. Differently, phosphorescence exhibits less deviation from monoexponential decay. This aspect is explained in terms of reduced interaction between the molecule within the organic layer: because of the lack of Coulomb interaction, the interactivity among the molecules in triplet states is lower than that among molecules in singlet states. On the base of this difference, the excitation transport inside the singlet manifold is more effective than that in triplet one; the excitation trapping probability (consequence of the intra-layer transfer) is also higher. As a result, an increase of non-

[b] Langmuir-Blodgett

radiative component of deexcitation rate and often a non-monoexponential fluorescence decay are observed.

The presence of this second deexcitation pathway, whose energy transfer rate is difficult to separate, makes the quantitative application of models developed for isolated emitters to thick molecular films complicate.

2.) Molecule-substrate distance variation by change of the film thickness
The second experimental way to study the distance dependence of the optical properties of molecules on a substrate, is depositing a homogeneous molecular film and to increase successively its thickness. Following this approach, the experimental difficulties are greatly reduced (one layer to deposit instead of spacer and molecular film) but the distance between molecule and substrate is no more well define. Actually, it is no longer possible to specify the 'distance', but only an *averaged* distance: in fact, molecules lying within the film in different layer parallel to the substrate experience different distances from the solid surface and consequently a different level of interaction with the substrate. Nevertheless, this approach has been followed, because of its experimental convenience, by a number of researchers.

According to this approach, the precedently described models have to be modified to take into account a distribution of distances from the substrate (integration along a perpendicular direction within the film is necessary); further, the existence of uncontrolled excitation transfer inside the film has to be considered.

Suto et al. [35–38] extended the CPS model and by integration over the total film thickness they calculated the distance dependence of the fluorescence lifetime. The sample was tetraphenylporphyrin (H_2TPP) deposited in high vacuum on gold and on SnO_2. Also in this case, the fluorescence decays were far of to be monoexponential, so that it was not possible to determine exactly the distance dependent fluorescence lifetime of H_2TPP molecules in the film. The reason for this lack of monoexponentiality lies once more in the intra-layer excitation transfer (whose rate is not directly accessible).

1.1.4 Fluorescence near semiconducting surfaces

In contrast to the large number of studies of electronically excited molecules above metals, only little effort has been devoted to the photophysical properties of molecules above semiconductor surfaces.

In case of metallic substrates, the excitation transfer from the molecule to the solid is accounted for by the interaction between the molecule and the *unbound electrons* of the metal, which dominate the dielectric response of the solid. On the contrary, in the case of insulating materials and semiconductors, the dielectric function is mainly contributed by the *bound electrons*.

Since the classical model (CPS) approach is based uniquely on the use of the dielectric function to characterize the material (without any microscopical description of the solid), such a classical model should be successful also when it is applied to semiconductors. Although some experimental work has been undertaken, it is still not clear whether the transfer rate depends as d^{-3} in the quenching regime.

Hayashi et al. [39] studied fluorescence of 50 Å thick films of tetracene at $\lambda = 580\,\text{nm}$, separated from Si and GaAs by LiF spacer layers. The molecule-substrate distance range was spanned with spacer thicknesses of $20\,\text{Å} < d < 400\,\text{Å}$; the transfer rate to the substrate was inferred from fluorescence intensity data. On Si the rate is claimed to show an exponential distance dependence instead of d^{-3} , on GaAs the rate was found to be even constant for $d < 100\,\text{Å}$. In both cases, a very large discrepancy in comparison to the CPS-predictions have been observed. In case of tetracene on Si, a fluorescence intensity reduction more than two orders of magnitude larger than the predicted one has been reported. However, such experimental approach, based only on fluorescence intensity measurements, is inadequate since the radiation pattern changes quite dramatically as the spacer layer thickness is changed [40].

In the group of Harris, Whitmore et al. studied the fluorescence from one monolayer pyrazine ($\lambda = 380\,\text{nm}$) above GaAs(110) using ammonia (NH_3) as spacer layer [23]. The fluorescence lifetime of the molecular film was directly measured and a classical d^{-3} distance dependence was found in the short-distance range, with the tendency of a slightly faster dependence in the range $20\,\text{Å} < d < 100\,\text{Å}$. Furthermore, Alivisatos et al. examined the lifetime of submonolayer pyrene ($\lambda = 390\,\text{nm}$) above Si(111) (Xe as spacer layer) [24]. The distance dependent excitation transfer to Si was somewhat inconclusive, as only few experimental points were reported and since a significant intra pyrene layer energy transfer took place in addition to energy transfer to the Si. Brandstätter et al. [41] reported no energy transfer to the substrate in their study of cyanine ($\lambda = 440\,\text{nm}$) above Si. Also in this case only fluorescence intensity measurements were carried out.

In a more recent study, Sluch et al. [42] investigated fluorescence from palmitic acid ($\lambda = 450\,\text{nm}$) above Si using LB layers of tricosenoic acid as spacers. The data show a d^{-3} dependence of the lifetime for $100\,\text{Å} < d < 300\,\text{Å}$ but for $30\,\text{Å} < d < 80\,\text{Å}$ the distance dependence was weaker, in contrast to the results of Alivisatos et al. [24].

In all the experimental works reported above, the interaction that gives origin to excitation transfer takes place between the excited molecules *within the molecular film* and the substrate, *not between one molecule and substrate*. This aspect has been almost totally disregarded until the earlier research activities undertaken by our group (M. Daffertshofer, 1995 [34]; U. Gómez, 1997 [43]), in which it has been clearly shown that the effect of intra-layer transport can be separated from the effect of excitation transfer to the substrate, as described in the following section.

1.1.5 The research of our group and the goal of this work

In the 3. Physikalisches Institut, the study of molecule-substrate interaction was the main subject of the Ph.D. Theses of M. Daffertshofer [34] and U. Gómez [43]. In both cases, time resolved fluorescence spectroscopy techniques were applied to measure, in–situ, ultrathin films of organic molecules deposited at $T = 10\,\mathrm{K}$. Daffertshofer's work was dedicated to anthracene, Gómez's one to *MePTCDI*[c].

Anthracene

The fluorescence spectra and decays of thin anthracene films, deposited at helium temperature, have been measured upon variation of temperature ($10-300\,\mathrm{K}$). The substrate was systematically changed (*KCl, Si, Ag, Au, Cu* were used), as well as its distance to the anthracene molecules: in one case, by variation of anthracene film thickness between 3.5 Å (~ 1 monolayer) and 1000 Å [32]; in another case, by depositing an inert spacer of solid nitrogen (N_2) with various thicknesses between the substrate and *a single* anthracene monolayer [33].

Similarly to what was observed in Harris' group experiments on other molecules, a strong fluorescence quenching and fluorescence lifetime shortening was measured when anthracene is deposited at short distances from the substrates. Nevertheless, a quantitative description via CPS classical model was difficult for the following reasons: a) the fluorescence from 3.5Å thick anthracene films exhibits two superimposed components (excimeric and monomeric in nature), with different emission energies and lifetimes. The initial assumptions needed to perform the numerical CPS calculations introduce a large uncertainty in the results. b) For film thicknesses in the range of one monolayer, even if no excimer emission is detectable, the dispersive transport inside the anthracene film (hopping among monomer energy levels) introduce a strong non-exponential behaviour in the fluorescence transients that makes decay analysis rather complicate. c.) Even at helium temperature due to the relative small molecular mass, the dimensions of anthracene molecule and the weak binding with the substrates, 'scrambling' phenomena were observed in thin films (with final aggregation of molecules). As a consequence, the films could not be considered as a regular layer of molecules parallely oriented to the substrate surface.

Even with this difficulties, in the work of Daffertshofer the problematic of the two competing processes (excitation transfer intra-layer and across the layer to the substrate) was correctly pointed out, many experiments performed and the experimental results modelled through a modified version of Suto's approach to CPS theory (for thick films).

MePTCDI

Starting from the experimental work of Daffertshofer, Gómez approached the study of the

[c] N,N'-dimethylperylene-3,4:9,10-bis(dicarboximide)

molecule-substrate interaction using *Ag* and *Si(111):H* (hydrogen passivated silicon) as substrates and changing the molecule (*MePTCDI* instead of anthracene), the thickness of the film (well below one monolayer instead of ~ 1 monolayer) and the preparation method of the substrates.

The reasons to do that: *MePTCDI* molecule, in comparison to anthracene, is larger and has a smaller lateral mobility; at helium temperature it turns out to be almost immobile. It is therefore possible to deposite in *UHV* well defined molecular thin films.

The thickness of the film was changed: varying from ~ 1 monolayer to 0.1 or 0.01 of a monolayer the intra-layer transport can be definitely interrupted. Depositing such an 'ultra'-thin film at a distance d from the substrate by spacer layer technique, it is possible to study *directly* the distance dependence of molecule-substrate interaction without other competing processes. Naturally, reducing the organic film thickness in a controlled way by a factor 100 is technically difficult.

The substrate preparation was also improved: in the case of silicon *Si(111)* the use of a wet chemical passivation process (modified RCA-process, *see* § 2.3.2) resulted in a complete removing of the natural oxide layer from the silicon surface and in a hydrogen passivation of any unsaturated dangling bond; this permitted to obtain a chemically inert surface and to define appropriately the distance between the molecule and the *bare* silicon surface. Further, for metallic substrates the introduction of an argon-ion sputtering system resolved the problems connected to the presence of residual contaminants on the sample surface.

The starting point of the research was a conventional approach (progressive variation of film thickness in the range $1-50$ ML[d]), with deposition of the molecules on various kinds of solids: insulator (quartz), metal (*Ag*) and semiconductor (*Si(111):H*) in order to study the different competition between the two components of energy transfer (intra-layer vs. molecule-substrate).

Then, by progressive coverage reduction (from 1 ML down to 0.01 ML) it was possible to *reduce* continuously the intermolecular interaction inside the film down to stop definitely the intra-layer excitation transport (*isolated molecule limit*). As a result, at 0.01 ML coverage on non-interacting substrate (quartz) a monomeric spectrum was detected, with monoexponential decay and nearly intrinsic fluorescence lifetime (typical of non-interacting molecules, without excitation transfer to the substrate). In contrary, on interacting substrates (as *Ag* and *Si(111):H*) beside a monomeric spectrum a *shortened* fluorescence lifetime was detected (typical for non-interacting molecules, but including excitation transfer to the substrate). The amount of the fluorescence lifetime shortening was quantitatively placed in relation with the type of solid used as substrate.

[d] ML= nominal MonoLayer

By using the spacer technique, the distance dependent *MePTCDI* lifetime was measured on *Ag* in a wide range of molecule-substrate distances (0−300 Å). Such a dependence could be quantitatively described by the classical CPS model.

On *Si(111):H* semiconductor, the molecular lifetime in the isolated molecule limit was measured *only at minimum distance* (d=5.7 Å) and a deviation of more than one order of magnitude from the CPS predictions was found. Furthermore, by using a method similar to Suto's approach, it was possible to yield data on the distance dependent fluorescence lifetime as measured on thick films. In this case, a deviation (weaker dependence) from CPS predictions on films with thickness below 5 ML was also observed.

The goal of this research

Starting from the earlier experimental work of our group, the goal of this research is to study, according to the *isolated molecule approach* (i.e. depositing ultra-thin film) the *interaction mechanism* between molecule and substrate, with focal point on *semiconductor* substrates.

Whereas on metals the interaction between molecule and substrate is adequately explained in terms of excitation of surface charge oscillations (surface plasmons) via the near field of the excited molecule, on semiconductors the interaction mechanism is not still obvious.

The research made use of the spacer layer technique to fix the distance between the molecular film and the substrate. All the measurements were carried out in–situ at helium temperature.

As molecule, *MePTCDI* was used, as its physical characteristics and fluorescence properties are well suited for our scope and because of a direct comparison with earlier results.

As substrates, *Si(111):H* and MoS_2[e] were considered, because of their well known properties and preparation techniques and their different band structures. They are both indirect semiconductors, but in one case (MoS_2) the energy of excited *MePTCDI* molecule lies *above* the direct band gap of the material, in the other case (*Si(111):H*) it lies *below* the direct band gap (and above the indirect band gap) of the solid. Such a difference is expected to have a drastic influence on the energy transfer rate from the molecule to the substrate.

As experimental technique, the time-resolved Single Photon Counting (trSPC) was used. During this research an updated experimental setup (based on an integrated acquisition board) was constructed, throughly tested and finally used for the measurements.

[e] Molybdenum Disulphide

2 Setup

In this section the experimental setup and the methods used for the preparation and measurement of ultrathin films ($< 0.1\,\mathrm{ML}$[a]) of *MePTCDI* deposited at $T = 10\,\mathrm{K}$ on semiconductor substrates are briefly described.

The deposition of the film takes place in Ultra High Vacuum (*UHV*) at helium temperature to avoid rearrangement of the molecules on the surface of the substrate. The experimental setup used to deposited the ultrathin organic films and the argon spacer layers are described in § 2.1.1.

The characteristics of the *MePTCDI* molecule, those of its crystal and the purification methods are described in § 2.2. The substrate preparation is described in sections § 2.3.1 (MoS_2) and § 2.3.2 (*Si(111)*).

The optical measurements on the films take place in–situ, at helium temperature, directly after the deposition. The setup for the time-resolved Single Photon Counting Fluorescence Spectroscopy (fluorescence spectra and decays) is described in § 2.4.

2.1 Sample production and analysis

2.1.1 Setup of *UHV* system

The *UHV* system used for the deposition and analysis of the organic films is shown in fig. 1; the system consists of a *preparation* chamber and a *deposition/measurement chamber* (main chamber).

Transfer system and preparation chamber
The preparation zone (fig. 1, on the right) consists of a load lock and a *substrate preparation chamber*, equipped with a turbomolecular pump (Edwards EXT 100) that enables a base pressure of $5 \cdot 10^{-9}\,\mathrm{mbar}$.

The transfer section is connected to the preparation chamber by a gate valve and consists of a separately *UHV*-pumped volume equipped with a flange to introduce the sample (fixed on a sample-holder made of copper or steel) and of a transfer rod. Under atmospheric pressure, the sample-holder is introduced and fixed at the end of the rod; the volume is successively pumped down to $< 10^{-7}\,\mathrm{mbar}$ in within ~ 15 min. The gate valve between transfer and preparation chamber is opened and the sample is moved therein.

In the preparation chamber the substrates are treated to remove residual contaminants from their surface. The sample-holder is screwed on a 360 degrees rotatable vertical rod at the centre of the chamber. The preparation is different depending on the type of

[a] MonoLayer

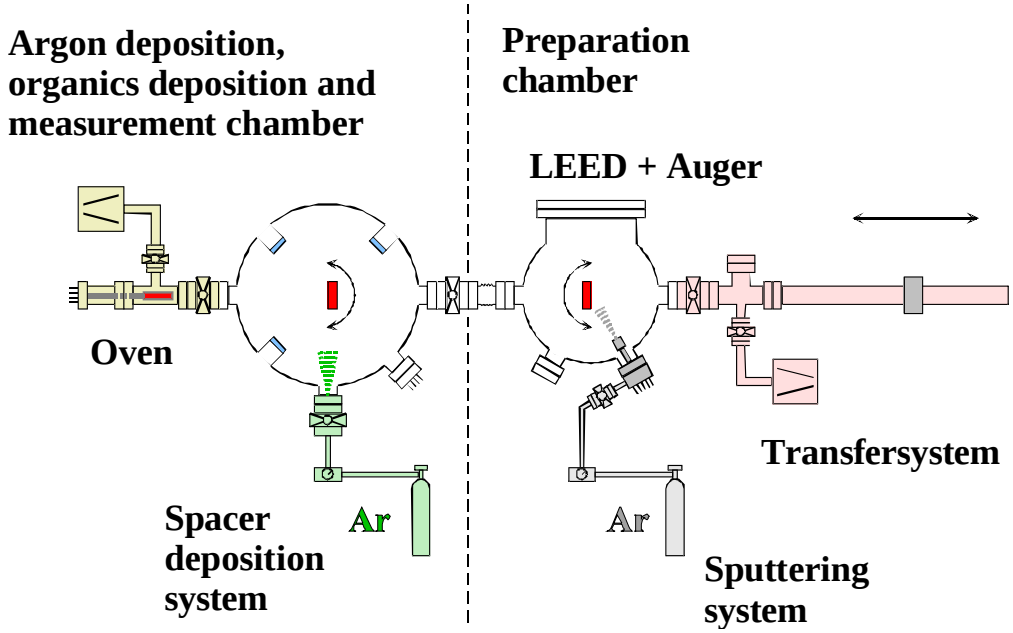

Fig. 1: Schematic drawing of the used *UHV* system; it consists of two parts connected by a transfer line: a "preparation" chamber containing high-temperature flushing, argon Ion–Sputtering, *LEED* analysis and *Auger* spectroscopy and a "main" chamber for the deposition and measurement in–situ. Here a He–flux cryostat mounted inside the chamber allows controlling the sample temperature in the range of 10–400K (*see* text)

the substrate. In case of semiconductors, after the preparation *ex*-situ (*see* below) the treatment in–situ consists essentially in annealing, in the case of metallic surfaces a series of sputter-annealing cycles provides near contaminant-free surfaces.

The annealing process consists of a continuous heating of the sample by a tungsten filament up to 240 °C. For higher temperatures electron-bombardment is applied accelerating thermoelectrons from the filament by a high bias voltage (1000-1500 V). The accelerated electrons impact on the rear of the sample-holder and by this enable a sample temperature up to $\sim$500 °C. The temperature can be regulated by monitoring the flowing current.

The sputter-annealing process is suited to treat metallic surfaces. By means of a sputter source (Specs IQE 11/35), ionized argon atoms are accelerated by a high potential difference (300-5000 V) and shot against the sample surface. The argon ion flux can be controlled by controlling the injection of argon gas in the chamber through a leak-valve.

Deposition/measurement chamber (main chamber)

The part of the device destined to deposition and measurement is shown in fig. 1, on the left. It consists of an evaporator (oven) and of a deposition and measurement chamber,

equipped with a turbomolecular pump (Edward EXT 200) that provides a base pressure of 2-4 $\cdot 10^{-10}$ mbar during the measurement.

The evaporation system is connected to the main chamber by means of a gate valve and it is separately *UHV*-pumped: in this way the crucible of the oven can be effectively refilled without airing the main chamber. The evaporation oven is constructed as a copper block indirectly warmed by a filament. The crucible is a small steel cylinder closed by a cover with a 1.5 mm large aperture, filled with the organic substance and deeply inserted inside the copper block to ensure the higher temperature uniformity on its surface.

The deposition chamber is equipped with sapphire windows to ensure the highest transparency on whole spectral range. A helium-flux cryostat (Cryovac Konti) is mounted by an *UHV*-flange inside the chamber; the temperature of the sample, screwed at the end of cryostat's cold finger can be in this way continuously regulated between 10 K and 450 K by a temperature controller. Even without helium flux, the external tank of the cryostat (filled with liquid nitrogen) ensures 12 hours long cooling time at 77 K. The cold finger is 360 degrees rotatable and the sample position can be vertically varied up to ~ 1 cm.

Furthermore, in this chamber it is possible to deposite (at helium temperature) argon layers with defined thickness by letting the injected argon gas condense directly on the cold sample surface; the argon gas injection is controlled by a leak valve (details on this procedure in § 2.1.3).

2.1.2 Organic film evaporation system

The deposition of *MePTCDI* films follows the OMBD (Organic Molecular Beam Deposition) method. The oven, filled with *MePTCDI* microcrystalline powder, is continuously warmed up to the sublimation temperature of the material. If the temperature ramp has been slow enough, the crucible reaches thermal equilibrium, for which part of the molecules sublimate and part condense back. Some molecule can escape through the small aperture on top and reach the sample ~ 20 cm away from the oven. Extreme low deposition rates can be so obtained and particularly well defined films deposited. As the oven has no mechanical shutter, the cold finger has to be rotated so that the sample is faced towards the molecular beam or away from it.

To obtain a reliable deposition of ultrathin films (< 0.1 ML) a rate of 0.1$-$0.2 Å/min has to be chosen; to measure such a rate a quartz crystal mounted in proximity of the sample has been used and the amount of deposited material has been measured through the change in its oscillation frequency. In the following section it is explained how this measurement is carried out.

Interference calibration measurements and ultrathin film deposition protocol
The proper resonance frequency of an oscillating quartz crystal is in good approximation

proportional to the mass of the oscillator. If this mass is supposed to change in time, because of evaporating molecules that stick on the quartz surface, its proper oscillation frequency is supposed to change (in particular, it is expected to become slower).

During the organic film deposition, the quartz oscillation frequency is continuously monitored by a frequency meter (Conrad FZ310, internally modified to be interfaced to an acquisition computer). From the change in frequency, making use of calibration measurements that put in relation the number of deposited monolayers to the observed change in frequency, the amount of deposited material can be calculated. At constant evaporation rate, it is therefore possible to estimate the thickness of the deposited film by measuring the deposition time.

The calibration has been carried out by interference measurement [44] on a *MePTCDI* film deposited on *Si(111)* at room temperature; as a source, a Helium-Neon laser was used ($\lambda = 632.8\,\mathrm{nm}$, since at such wavelength *MePTCDI* does not absorb).

During the deposition of the film, the intensity (normalized respect to the laser intensity) of the reflected signal from the sample surface has been recorded together with the frequency of the quartz balance as a function of the deposition time. The observed oscillations in the reflected signal originate from the interference effect between the beams reflected from the substrate and that reflected from the surface of the film deposited on it. Since the refraction index of *MePTCDI* at laser wavelength is known [45] as well as the optical arrangement, the thickness of the film (in Å) can be immediately related to the time interval between two interference fringes. From the *MePTCDI* crystal structure (in particular the distance between two molecular planes, that amounts to 3.40Å [46]), the thickness in nominal monolayer (ML) is obtained. The simultaneous measurement of the quartz frequency vs. the deposition time permits to determine the dependence of the thickness (in ML) vs. change of quartz frequency. From a series of measurements an average value of 1.78 ML/Hz is obtained. Making use of this value, it is possible to estimate the thickness of any successively deposited film by measuring the change of the quartz frequency during the evaporation.

The calibration measurements have been carried out at room temperature; at this temperature the *MePTCDI* film grows in *polycrystalline* form. Nevertheless, when deposited at helium temperature ($T = 10\,\mathrm{K}$), the film grows in *amorphous* form (*see* § 3.3). The film density decreases (30% reduction of packing density) and the resulting thickness per monolayer changes consequently; a film deposited at low temperature at parity of deposited mass turns out to be up to 40% thicker [43]. The quartz thickness calibration in any case is still valid, since the value of thickness expressed *in nominal monolayer* depends only on the deposited mass: for a crystalline film 1 ML corresponds to 3.40 Å [46], for an amorphous film 1 ML corresponds to 3.40+40%(3.40)=4.76 Å, but the change in frequency (ΔHz) to get 1 ML is always the same.

2.1.3 Argon-spacer evaporation system

The production of reasonably flat argon spacer layers with well-defined thickness has been one of the more difficult aspect of the whole experimental activity (*see* also § 5.2).

The deposition of argon layers is carried out via condensation of argon gas on the sample surface kept at helium temperature. Owing of the fact that argon doesn't condensate on sufficiently warm surfaces (with $T > 60-80\,K$) it is not possible to use the quartz balance (which is thermally isolated from the sample holder) to estimate the thickness of the deposited layer. As alternative method, the deposition is indirectly controlled by monitoring the *partial pressure of the chamber* when argon is injected.

The pressure of the chamber ($\sim 4 \cdot 10^{-10}$ mbar at $T = 10\,K$) is assumed negligible with respect to the argon partial pressure during the injection of the gas. The measured partial pressure during the gas injection thus corresponds to the argon partial pressure. All Ar atoms are supposed to possess similar velocity (depending on the temperature), i.e. the pressure turns out to be proportional to the number of particles. But also the condensation rate is proportional to this quantity, therefore it is proportional to the argon partial pressure; i.e. the argon condensation *rate* is proportional to the measured chamber partial pressure, too.

Through a series of calibration measurements, the *rate of growth* at various partial chamber pressures has been estimated via interference methods. The effect on the growth rate of changing the angle between sample surface and argon jet has been also investigated. As a result, during the argon gas injection at a partial chamber pressure of $8.0 \cdot 10^{-7}$ mbar, condensation rates of $0.82\,Å/s$, $0.70\,Å/s$ and $0.65\,Å/s$ are obtained when the sample surface is perpendicular to the jet, parallel to the jet and on the opposite side with respect to the jet, respectively.

The critical aspect in the condensation of the spacer concerns the substrate temperature during the spacer deposition. As extensively discussed in § 5.2, if the condensation occurs at $T = 10\,K$ and the layer *is not further processed*, the spacer appears to be *rigid* and stable over several hours [43, 47], *but not flat*.

On semiconductors, to avoid undulations and to get a homogeneous coverage it was found to be more effective condensating the argon at the minimum temperature ($T_S = 10\,K$), then progressively warm the sample up to $T = 25\,K$ (in 10-15 minutes) to let the atoms in the argon layer settle in, lowering back the temperature to $T = 10\,K$ and continue with the successive deposition of the organic molecules on the top of the spacer.

All the experimental results reported in chapter 4 have been obtained following this argon deposition procedure that ensures planarity of the spacer layer; nevertheless, the effects of untreated spacer undulation have been thoroughly studied: the results of this research are exemplified in § 5.2.

2.1.4 Ultrathin films: evaporation techniques

When the target film thickness goes down below one monolayer, the deposition of organics at $T = T_S = 10\,\mathrm{K}$ becomes critical. To get reliability and a good reproducibility the deposition must be error free and with a correct timing.

For thin coverages, extreme low evaporation rate has to be used ($0.1-0.2\,\text{Å/min}$), with a deposition time of the order of just few seconds. In the case of extreme low coverage ($0.01\,\mathrm{ML}$), usually no more than 5 sec are needed.

The preexistent setup has been improved to get a better control on the various evaporation parameters. In particular, the integration between oscillating quartz frequency counter, oven temperature controller and computer permitted to follow the thermalization dynamics of the quartz balance during the cryostat cooling down and to monitor the evaporation rate with an accuracy of ~ 4 over 10^7. Since the quartz balance is placed in proximity of the sample holder, which is fixed on the coldfinger block, its elastic constant (and therefore its resonance frequency) is indirectly influenced by any change in coldfinger temperature. For this reason, during the cooling down, a drift in the resonance frequency of the quartz balance is observed.

Fig. 2 (*above*) shows the drift in quartz resonance frequency, when the sample holder temperature goes down from $T = 300\,\mathrm{K}$ to $T = 10\,\mathrm{K}$, on a temporal interval of many hours. The nominal oven temperature is shown on the right vertical axis, whereas the dashed horizontal lines indicate the target oven temperatures. This temperature is only indicative, strongly depending on the position of the sensor on the copper block inside the oven. The evaporation starting time is pointed out by a vertical arrow.

Fig. 2 (*below*) shows (the plot is rescaled) the observed quartz frequency when a complete thermalization occurred (Ⓐ) and its change of slope when evaporation of the molecules starts (Ⓑ). After the thermalization (usually $6-7$ hours are needed to get a frequency stability of $\pm 0.2\,\mathrm{Hz}$ over $\approx 6\,\mathrm{MHz}$) by slowly increasing the oven temperature the molecules begin to evaporate and to reach the quartz balance. The observed quartz frequency starts again to change (to slow down, Ⓑ) because of its own mass increase. From the curve slope change (Hz versus minutes), the evaporation rate can be estimated (according to the calibration § 2.1.2) and the deposition of the molecules on the sample can take place (by rotating the sample holder to put the sample faced the molecular beam).

Nevertheless, at the required rate, the change in frequency is significant only on a temporal scale of hours after the beginning of the evaporation; for this reason, a good estimation of the deposition time (needed to get the target thickness) can be made only at least one hour after the start of the evaporation. In the case shown, the final deposition time has been 5 seconds long.

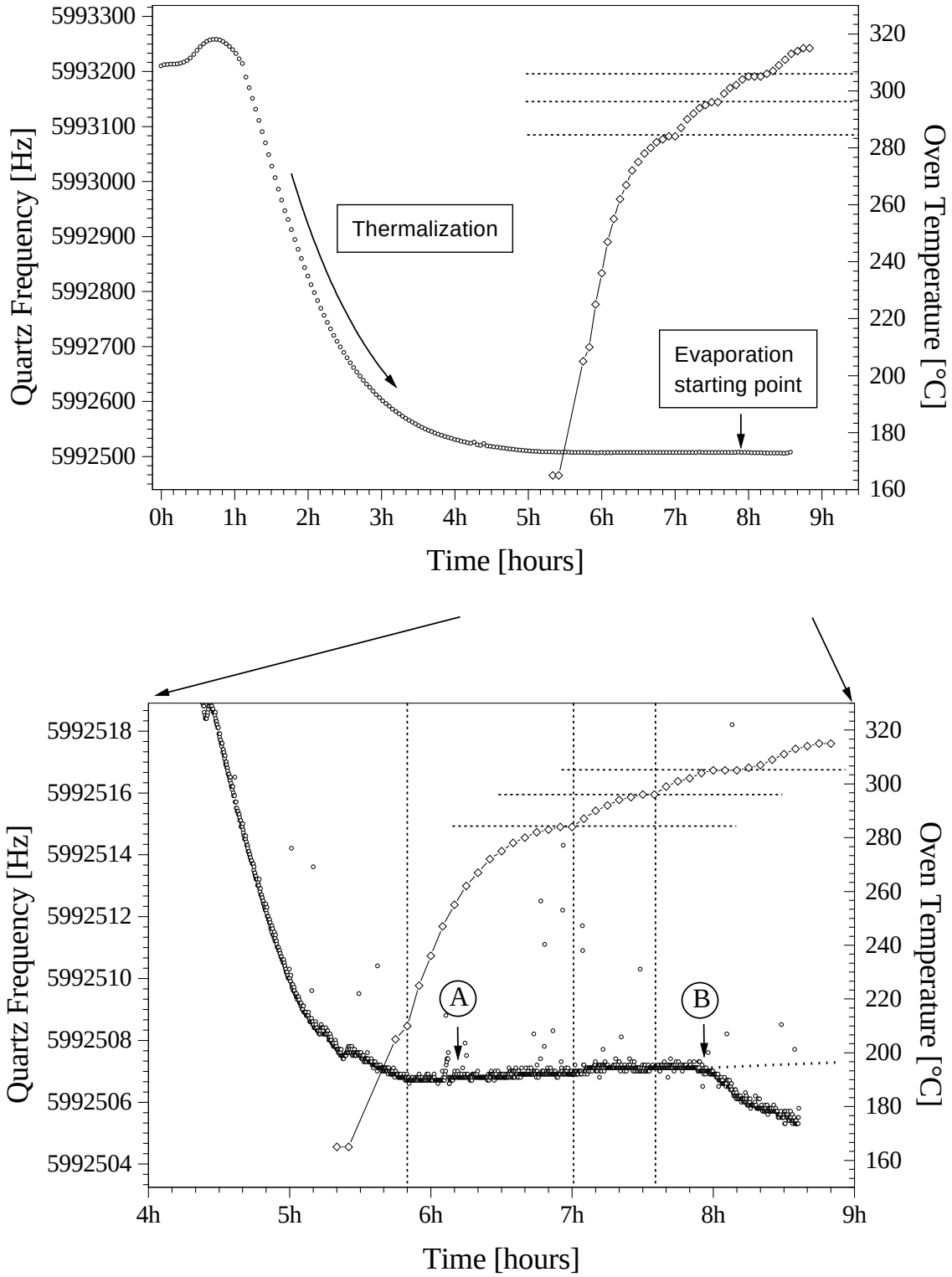

Fig. 2: Typical ultrathin (0.01 ML) *MePTCDI* film deposition at $T = T_S = 10\,\mathrm{K}$.
Above: Quartz frequency thermalization curve during the sample cooling down from $T = 300\,\mathrm{K}$ to $T = 10\,\mathrm{K}$ (*left*) and oven warming up ramp (*right*)
Below: Expansion of scale of the plot above. Ⓐ indicates the definitive thermalization time, Ⓑ the evaporation starting point; the molecule deposition begins one hour later and it is 5 seconds long (*see* text).

After the deposition, the oven must be left cool down to at least 100 °C below the substance evaporation temperature to avoid uncontrolled further deposition. The time resolved fluorescence spectra and fluorescence decays can be then measured.

Due to the extreme low fluorescence intensity (from *few photons* per second, down to less than *one* photon per second) very long spectrum scan times and transient acquisition times are necessary. A duration of the single measurement up to two hours is common (*see* also § 2.4), whereas a measurement session is in average 14−18 hours long.

The optic alignment to couple the collected signal to the monochromator was carefully optimized to reduce any fluorescence intensity loss. A Peltier-cooled photomultiplier with a very low dark current ($< 1\varphi$/sec, *see* § 2.4 for details) has been used, in single-photon mode, to collect the fluorescence.

Following this procedure, it was possible to prepare and observe ultrathin films in the coverage limit of the not interacting molecules, as described in the chapter 4.

2.2 The *MePTCDI* molecule

In this section, the properties of the *MePTCDI* molecule and of its crystal are presented.

N,N'-dimethylperylene-3,4:9,10-bis(dicarboximide) (*MePTCDI*)
MePTCDI belongs to the family of the perylene-derivative molecules; it is a plain, photochemically stable, difficult to dissolve, dye molecule with intense orange colour. The molecule structure is sketched in fig. 3, a collection of physical data is reported in tab. 1.

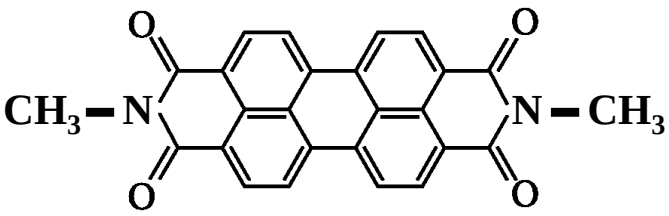

Fig. 3: Sketch of the molecular structure of *MePTCDI*.

Because of its low vapour pressure at room temperature and of its thermal stability, *MePTCDI* is particularly suited for the production of sublimated films under ultra high vacuum conditions.

***MePTCDI* crystal structure**
The *MePTCDI* crystal structure is monoclinic, presents two molecules in the single cell and belongs to the spatial group $P2_1/c$ (or C_{2n}^5 following the Schönflies notation); the structural data are listed in tab. 1.

	MePTCDI
Molecule	
Formula	$C_{26}H_{14}N_2O_4$
Mass [amu]	418
Symmetry	D_{2h}
Crystal	
Spatial group	$P2_1/c$
Mol. per cell	2
a [Å]	3.874
b [Å]	15.580
c [Å]	14.597
β [°]	97.65
V [Å^3]	873.2
ρ [g/cm^3]	1.59

Tab. 1: Collection of physical and cristallographic data for *MePTCDI* [48].

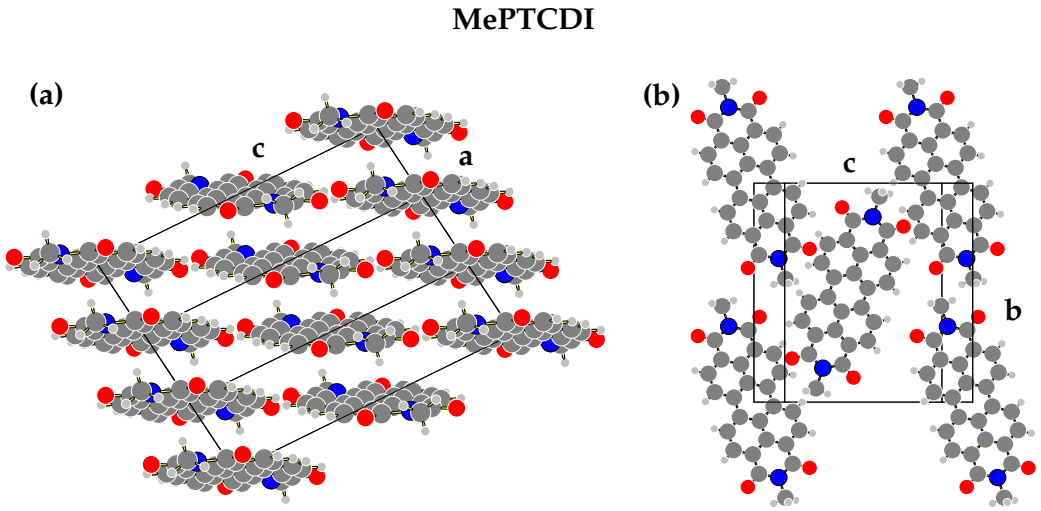

Fig. 4: Sketch of *MePTCDI* crystal structure (after [46,48]): (a) projection on the (010)-plane, (b) on the (102)-plane. The molecule are organized in a stack structure, parallel to (102)-plane; The molecular planes are inclined by 9 degrees with to respect to the stacking plane. The long molecular axes of the non-translational invariant *MePTCDI* molecules form an angle of $\sim$36.7 degrees.

Fig. 4.a shows the *MePTCDI* crystal structure as projected on the (010)-plane, whereas Fig. 4.b shows the projection of the crystal on the (102)-plane. The molecules form a *stack structure*, with stacking planes parallel to (102)-crystal plane; it forms an angle of 33.7 degrees with the a-axis of the crystal. The distance between two successive molecular layers amounts to $d_{102} = 3.40$ Å. Within the single stack plane the molecules do not lie flat, but form an angle of ~ 9 degrees: for this reason, the stacking is not ideal. Within the stacking plane the *MePTCDI* molecules form a herring-bone structure, with an angle of ~ 36.7 degrees between the long axis of the non-translational equivalent molecules.

Purification of *MePTCDI*

The used substance was bought by Hoechst as powder with a minimum purity of $> 98\%$. As the internal molecular bounds tends to break before reaching the melting point, it is not possible to use a zone-purification method on *MePTCDI*; owing to the very poor solubility of the substance also the purification via recristallization is not applicable.

For this reason the substance purification has been carried out via *double vacuum gradient sublimation* in the Kristallabor of the University of Stuttgart. After the first sublimation, it turned out the presence of only one homogeneous fraction of material: this implies that the starting substance was actually pure and that it has not been modified in its internal bounds during the sublimation process.

The purity level of the sublimated material has been proofed by mass spectrometry and X-ray spectroscopy on the microcrystalline material [43] and already after the first sublimation step, no presence of impurities was revealed.

2.3 Substrates and their preparation

In the present research a number of different substrates has been used. The choice of the substrates was mainly driven by considerations about their dielectric functions (which completely determine their optical properties as explained in § 6), their preparation easiness and their *UHV* compatibility.

The following substrates have been taken into account:

- Molybdenum Disulphide (MoS_2): indirect semiconductor, with direct gap energy $E_{gap}^{MoS_2} = 1.95\,\text{eV} < E_{Me} = 2.32\,\text{eV}$ (*MePTCDI* emission energy)
- Silicon (*Si(111)*): indirect semiconductor, with direct gap $E_{gap}^{Si(111)} = 3.4\,\text{eV} > E_{Me}$
- Quartz: insulator, as reference material.

Further measurements, not reported in this thesis, were performed on gold (*Au(111)*) and gallium phosphide (*GaP*).

Most of all, the two semiconductors (MoS_2 and *Si(111)*) have been particularly studied; the reason of this choice, their characteristics and the experimental details on their prepa-

ration techniques are given in the following sections, whereas their dielectric properties are reported in Appendix (A.1).

2.3.1 MoS_2

Molybdenum disulphide (together with the graphite) is a typical representative of the layered crystals, characterized by strong covalent bounds among atoms *inside* a layer and weak van der Waals bounds between the layers (fig. 5, left).

Such a crystal structure derives from the nature of the single layer formed by a sandwich S–Mo–S (fig. 5, right), where each Mo (filled circle) is in 6-fold coordination with the chalcogen (sulphur, hollow circle).

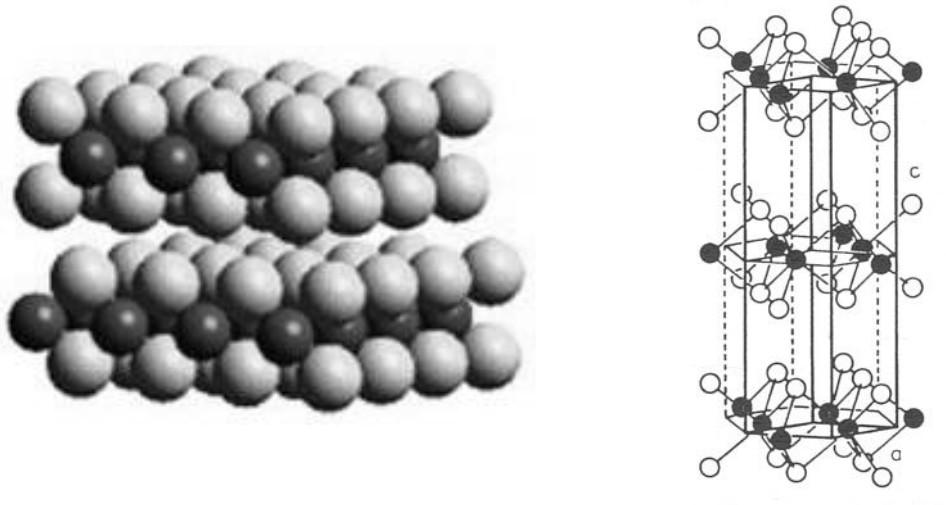

Fig. 5: MoS_2: sketch of the layered structure and of the crystal. The weakness of van der Waals bounds between the layers makes the cleavage easiest along the plane (0001).

The weakness of binding between the layers explains the exceptional cleavability along the plane (0001). The exposed surface exhibits, after the cleavage, sulfur atoms arranged in hexagonal symmetry, described by the two dimensional spatial group *p6mm*.

Since, after cleaving, there are no unsaturated valence electrons on the surface (because the cleaving breaks only van der Waals bounds), MoS_2 turns out to be chemically *inert*.

The first layer of molybdenum atoms is arranged 1.49 Å below the external layer of sulfur atoms. Further 1.49 Å deeper follows the second layer of S atoms. The underlying sandwich S–Mo–S layer is laterally displaced of a half lattice constant with the respect to the first one, so that the lattice constant c amounts to the double of the value of interlayer distance.

The direct band gap energy of 1.95 eV makes the MoS_2 substrate an ideal candidate

(used together with *MePTCDI* molecule) to study the molecule-semiconductor interaction when the emitter energy is *greater* than the absorption edge of the solid (*see* § 8.6).

A collection of physical and crystallographic data for MoS_2 is given in the second column of tab. 2. The band gap energies for the first indirect and direct transition are also tabulated.

	MoS_2	*Si*
Spatial Group	$P6_3/mmc$	Fd3m
a [Å]	3.1604	5.4301
c [Å]	12.295	5.4301
(0001)-plane	p6mm	–
ρ [g/cm^3]	4.92	2.42
T_{subl} [°C]	450	
T_{melt} [°C]	1185	1412
ind. trans. [eV]	1.1	1.16
dir. trans. [eV]	1.95	3.4

Tab. 2: Collection of physical data and structural parameters of MoS_2 [49–51] and silicon crystals [52].

Preparation of the MoS_2 substrate

The molybdenum disulphite substrates have been cut (in square shape, 5 mm × 5 mm) from a piece of natural mineral provided by Prof. Dr. N. Karl (3.Phys.Inst. - University of Stuttgart). Because of its layered structure, MoS_2 is extremely easy to prepare by peeling by means of adhesive-band. After peeling the substrate is immediately brought in *UHV* and annealed at 240 °C to desorb water and any residual organic contaminant. The exposed sulfur basal plane turns out to be nearly defect-free on large scale. Extremely sharp LEED[b] patterns ensure high surfacial order. Moreover, Auger spectroscopy applied on the bare MoS_2 confirms the cleanness of the surface, on which only a residual percentage ($< 5\%$) of contaminant carbon atoms can be detected.

2.3.2 *Si(111)*

Silicon has been chosen because of its attractivity in photonics, its optical characteristics and the possibility to obtain a well defined chemically inert surface by wet-chemical etching and H-passivation.

[b] LEED: Low Energy Electron Diffraction

Moreover, its direct band gap energy of $E = 3.40\,\text{eV}$ makes silicon indicated to study the molecule-semiconductor interaction when the emitter energy is *lower* than the direct absorption edge of the solid (*see* § 8.6).

A collection of physical, optical and cristallographic data for silicon is given in the third column of tab. 2.

Preparation of the *Si(111)* substrate

The silicon substrates (square shaped, $5\,\text{mm} \times 5\,\text{mm}$) have been cut from *Si(111)*-wafers (Wacker-Chemitronic) with various doping levels ($\rho = 0.5 - 1000\,\Omega\cdot\text{cm}$) and doping types (p and n).

As a result of the exposition to air, the silicon surface (fig. 6, above) is covered by a natural layer of oxide, whose thickness amounts to 5−20Å [53]. The importance to take into account the existence of the oxide layer on silicon surface is pointed out in § 2.3.3.

By means of a wet chemical etching process, it is possible to remove completely this oxide layer from the surface and moreover passivate all the reactive, 'dangling' (unsaturated) bonds with hydrogen atoms. The result is a near perfectly hydrogen-passivated surface [54]. The preparation method is in detail described in the following. During this work, all the silicon substrates have been prepared in collaboration with G. Untereiner (1. Physikalisches Institut - University of Stuttgart).

Apart from oxide layer, an untreated silicon crystal can exhibit also contamination by OH-bonds and by heavy metals. The used cleaning process, based on the RCA[c]-method [55, 56], eliminates organic and inorganic contaminants from the surface.

The steps of the process are the following:

- Pre-cleaning of the surface through bath in aceton and methanol.
- 4 min in $H_2O - H_2SO_4 - H_2O_2$ solution $\rightarrow$ controlled oxidation of the surface.
- 4 min in $H_2O - NH_4OH - H_2O_2$ solution $\rightarrow$ dissolving of organic bounds and formation of ammonia-complexes of some metals (*Ag, Cu, Ni, ...*).
- 4 min in $H_2O - HCl - H_2O_2$ solution $\rightarrow$ Alkali- and heavy metals are captured from the surface and hold in solution.

After each step, the substrate is dipped into high purity water ($\varrho \geqslant 10^{18}\,\Omega\cdot\text{cm}$). At the end of the process the so treated sample is etched for 4 min in a solution of $H_2O - NH_4F$ to saturate the free bounds of the surface by hydrogen atoms.

The so prepared surface turns out to be hydrophobic, whereas the H-passivation prevents for long time (also in air) the growth of a new oxide layer [57]. After the preparation, since the sample is still sensible to contamination by hydrocarbons, it is immediately transferred in nitrogen atmosphere and within 10-15 minutes brought into *UHV*. To avoid

[c] RCA Laboratories, Princeton, N.J.

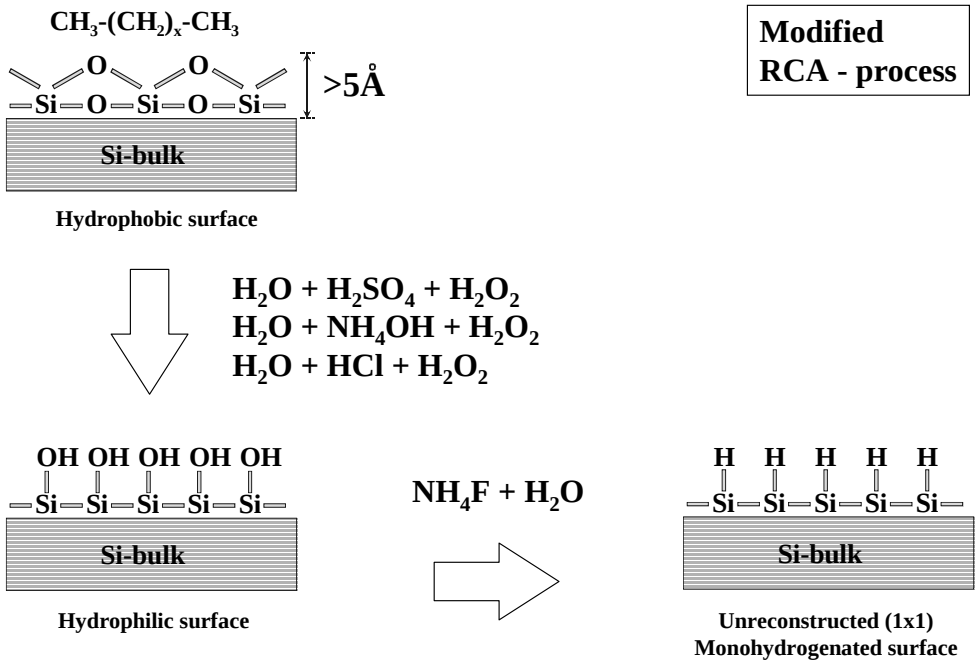

Fig. 6: Scheme of the Hydrogen passivation process of *Si(111)* substrates by means of modified RCA-method [55, 56].

any risk of after-contamination the sample is not further treated in preparation chamber, but directly moved into the measurement chamber.

Other researches [58] evidenced how *Si(111)* samples prepared in a similar way exhibit a *non* reconstructed, monohydride-terminated surface, where residual contamination by carbon atoms can be still present.

2.3.3 Problems related to the sample preparation

The preparation of the sample is a step of crucial importance to get reliability in the results. The substrate preparation methods described in the precedents sections ensure good final results and high reproducibility; in this section further aspects related to the sample preparation are pointed out, in particular:

- Presence of natural oxide layer on the surface of the substrate and its treatment
- Chemical reactivity of substrate and effects due to the presence of contaminants bound on it
- Argon spacer layer: difficulties related to the undulation and the inhomogeneity of the spacer

1) Native oxide layer as a natural spacer

Dealing with distance-dependent measurements, the role of the thin *oxide layer* naturally

grown on the substrate surface has to be carefully taken into account. In particular, it has to be considered that the oxide layer acts as a *natural spacer* between the substrate and the molecules deposited on top. Since the deposited organic thin layer is far from the bare surface of the substrate by an amount equal to the oxide layer thickness (up to tens of Angstroms) and being the emitter-substrate distance just the key parameter in the molecule-substrate interaction, the observed fluorescence decay and the measured fluorescence lifetimes are evidently affected[d].

The common methods are usually inadequate to prepare surfaces (both of semiconductors or metals) covered with an oxide layer. The chemical treatment based on spectroscopic grade solvents and on successive annealing at few hundreds of grads for hours in *UHV*, is not effective in the present case, since the thick oxide layer that covers the substrate is not actually removed, but only 'cleaned'.

In order to definitively remove the oxide layer and deal with the real surface of the substrate, the metallic substrates have always been treated by a number of sputtering-annealing cycles (*see* § 2.1.1), whereas the wet chemical treatment (described in § 2.3.2) has been used in the case of *Si(111)* crystals.

2) Silicon unsaturated dangling bonds and surface reactivity

The presence of contaminants on the surface of the substrate affects drastically the de-excitation pathways of excited molecules successively deposited on it at a distance d and their fluorescence dynamics. This perturbation is particularly strong on silicon and it has been thoroughly studied, in its distance dependence, by means of time resolved fluorescence spectroscopy techniques (*see* § 5.1.2). Origin of such contamination is the presence of unsaturated dangling bonds (free bonds of surfacial silicon atoms) on the surface, result of annealing treatment of the sample or of incomplete H-passivation. Such free bonds act as chemically highly reactive centers and external 'contaminant' molecules are captured and tightly bound to the surface.

The ways an organic molecule can be trapped on the top of an only partially saturated silicon surface have been object of a series of studies performed by a number of different techniques. In particular, it has been found that unsaturated silicon dangling bonds are capable, also at low temperature, of dissociating π bonds in hydrocarbon species [59–61] [62, and ref. therein]. Recently, it has been demonstrated that on a hydrogen passivated silicon surface a 'chemical contrast' can be generated desorbing *single* hydrogen atom by an UHV-STM (*UHV*-Scanning Tunnelling Microscope) tip [63–66]; upon successive deposition of organic molecules, they are seen to bind to the surface *exclusively* at prepatterned dangling bond sites. An example of this site selective reaction

[d] A variation of 100% in *MePTCDI* fluorescence decay time with and without natural oxide layer was precedently observed on *Si(111)* [43].

is the [2+2] cycloaddition reaction between C=C double bond in norbornadiene (NBE, bicyclo[2.1.1] hepta-2,5-diene) and a reactive free silicon dimer bond on the surface [67]. These observations show that: 1.) *even a single* unsaturated dangling bond act as a trapping center for organic molecules and 2.) trapped organic molecules can be locally deformed or altered in their chemical structure.

Adsorption of *MePTCDI* on *Si(111)* surface

When organic molecules (and in particular the extended perylene derivatives) are deposited on *Si(111)* surface, the strong local chemical interaction can actually cause (re)hybridization and formation of local bonds between the substrate and the reactive groups of the organic molecule [68]. Moreover, the presence of adsorbates on the surface perturbs locally the electronic properties of the interface.

Different possible orientations (depending on simultaneous occurrence of different adsorption sites) and the partial dissociation of the adsorbated molecules are reported in literature [68–70] to be the cause for the observed disorder and random orientation of big perylene derivatives on *Si(111)*.

As an example, neutron spectroscopy, photoemission experiments and NEXAFS[e] [69, 70] and [68, and ref.18,19 therein] carried out on *PTCDA* on *Si(111)* indicate a strong chemical interaction of the anhydride group with the substrate as derived from significant changes in the corresponding features of carbon and oxygen, whereas the perylene core (i.e. the aromatic ring) system remained essentially unperturbed.

On the base of these observations and due to similarity between *MePTCDI* and other perylene derivatives as *PTCDA* (methyl instead of anhydride as radical group), it is reasonable to assume that adsorbed *MePTCDI* molecules on reactive silicon tend to maintain the perylene core structure unaffected. This aspect will be experimentally considered on § 5.1.1.

Similarly to the case of metals, a good method to prepare a contaminant-free silicon surface (and regenerate the substrate after a measurement), would be a 'gentle' argon ion-sputtering ($E \leqslant 500\,eV$, with current density of $3-5\,\mu A/cm^2$ for $30-40\,min$) followed by a strong annealing of the sample up to 1000-1200 °C. This process ensures the removing of any organic residuum. After the treatment the silicon surface presents a reconstructed (7×7) surface [54, 71, 72]; recursive sputtering-annealing cycles create however a large amount of *structural defects* and induce roughness of the surface. Due to limitations of the used experimental setup (highest annealing temperature, $T_{max} = 500\,°C$), it was not possible to apply this method to treat the silicon substrates; for this reason every time a new, freshly prepared (via the wet chemical method described in § 2.3.2) *Si(111)* substrate was used.

[e] Near Edge X-ray Absorption Fine Structure

3) Argon spacer layer inhomogeneity
Finally, the argon spacer can be not completely flat immediately after the deposition. The experimental effects related to the inhomogeneity of the argon spacer will be extensively considered and discussed in § 5.2.

2.4 Time resolved Single Photon Counting fluorescence spectroscopy

The fluorescence measurements have been carried out with high detection sensitivity and a ps-time resolution; the setup used for the time resolved Single Phonon Counting fluorescence spectroscopy is sketched in fig. 7.

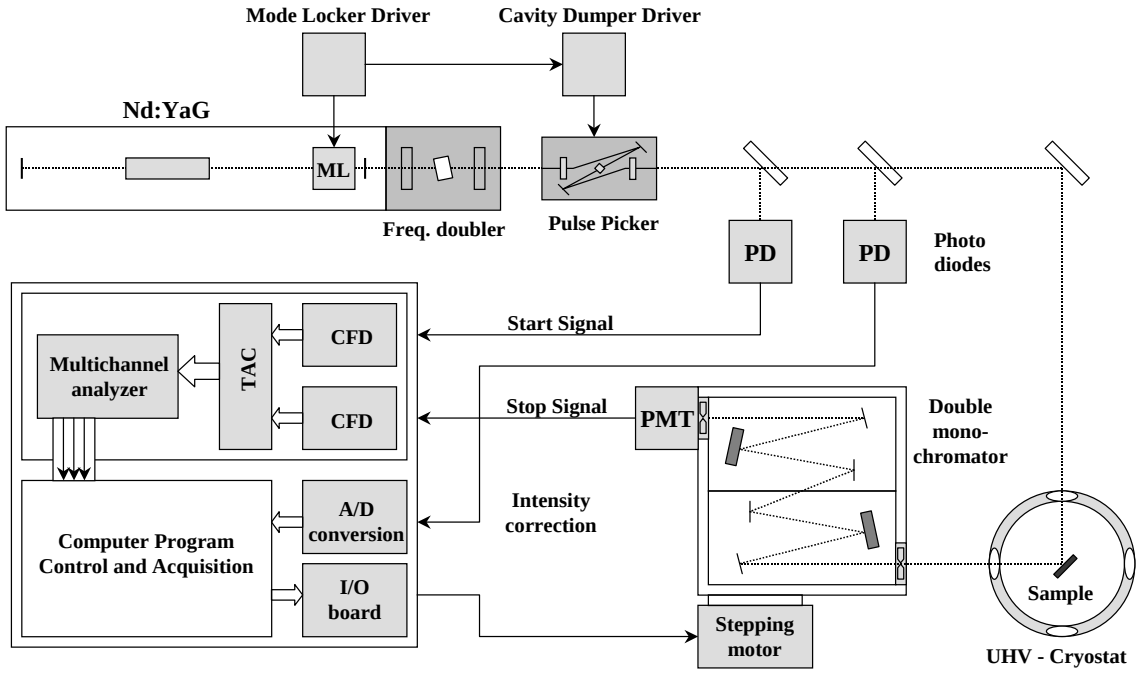

Fig. 7: Sketch of the device for the low temperature time-resolved Single Photon Counting fluorescence spectroscopy.

The basic principle
In ps-time resolved Single Photon Counting (trSPC) the time difference between a laser pulse that excites the sample and the emitted photon is measured for each emitted photon. The time difference values are accumulated for a statistically large ($\sim 10^4 - 10^6$) number of emitted photons and plotted as number of photons vs. delay time; such a curve is called fluorescence decay curve (fluorescence transient) and its shape reflects the fluorescence properties of the sample.

The collected photons are detected at a defined spectral position. If the detection frequency is changed, it is possible to measure a 'time resolved fluorescence *spectrum*' by measuring at each frequency a fluorescence decay curve and than dividing the histogram in a number of 'time windows' (i.e. time ranges after the excitation pulse). By summing, at each frequency, all the photons inside the various time intervals it is possible to obtain fluorescence spectra at different delay. This allows to study phenomena characterized by spectrally superimposed emission, but distinct in time.

The Single Photon Counting (SPC) technique is particularly indicated for studying weakly fluorescent samples (with very low photon count rate) as those considered in this work.

The excitation source

Short excitation pulses are effectively produced by high repetition active mode-locked Nd:YaG[f] Laser (Quantronix 416) working at a repetition rate of 76 MHz with a pulsewidth of ~ 100 ps. The cw-output power amounts to 11 W at $\lambda = 1064$ nm. The laser emission line frequency is doubled through a KTP[g]-crystal with Type-II phase matching. The cw-power after frequency doubling ($\lambda = 532$ nm, $\bar{\nu} = 18796\,\mathrm{cm}^{-1}$) amounts to ~ 1.5 W.

The doubled laser line is passed through a Pulse Picker (Coherent 7220), that enables to reduce the repetition rate down to 3.8 MHz. The minimum time separation between two successive pulses amounts to 260 ns. In operative configuration the average power after rate reduction amounts to 8-10 mW, corresponding to an average energy per pulse of 2.6 nJ. The limit FWHM of the pulse is $\sim$ 65-70 ps.

The detection system

The spectral selection of the fluorescence is performed by a double monochromator ($f = 0.5$ m) with subtractive dispersion (Dilor). The covered spectral range spans from $11335\,\mathrm{cm}^{-1}$ to $41580\,\mathrm{cm}^{-1}$.

The spectral resolution, using typical slit width (600 μm), on the base of a total dispersion of 0.9 nm/mm, amounts to $< 15\,\mathrm{cm}^{-1}$ on the whole spectral range.

After the spectral selection, the signal is finally detected by a fast microchannel plate photomultiplier (Hamamatsu R-3809U-01 with multi alkali cathod). The photomultiplier is cooled to -30 °C to minimize the dark counts (< 1 photon/sec). The PMT (Photo Multiplier Tube) provides a current pulse with average rise-time of ~ 170 ps and Transit-Time-Spread (TTS) of < 25 ps. The absolute quantum efficiency of the detector is between 1% and 10% on the whole spectral range.

[f] Neodymium:Yttrium-Aluminum-Granat
[g] Potassium-Titanyl-Phosphate

The new integrated system for *trSPC*

During the present experimental work, the preexistent acquisition device based on a HP-2100 computer has been replaced by an updated system based on an integrated Single Photon Counting board (Becker & Hickl) and two other accessories modules (A/D conversion and I/O controller). The software for the calibration, system control, data acquisition and analysis has been newly programmed and tested.

The logical building blocks of the acquisition system are: Constant Fraction Discrimination (CFD), Time to Amplitude Conversion (TAC) and Multi Channel Analysis (MCA). The CFD prevents time shift of the start/stop pulse due to amplitude jittering of signal, the TAC converts linearly the time delay of the emitted photons with respect the excitation pulse in a voltage, which is successively converted in digital form, the MCA accumulates events and generates finally the histogram of the number of photons vs. delay (with a discretization on 4096 channels).

Maximal time resolution

The maximal time resolution of the system is determined on one hand by the electronic components of the detection system, on the other hand by the width of the excitation laser pulse. This value can be estimated from the FWHM of the System Response Function (SRF) obtained by measuring the fluorescence decay of scattered excitation light.

The observed fluorescence transient is described by the *convolution* of the instrumental function and the real decay behaviour [73]. By knowing the response of the system, it is however possible to deconvolute numerically the fluorescence decay time from the experimental transient. Slow fluorescence decays are negligibly affected by such convolution, whereas the fast transients exhibit strong modulation induced by the folding with the instrumental effects (*see*, for example, the fluorescence decay on MoS_2 in fig. 19). It is possible to deconvolute decay times as fast as some fraction (down to 50%) of the width of the SRF [74].

The maximal time resolution of the whole system amounts to $\sim 25\,\mathrm{ps}$. Since the SRF dependents on many experimental parameters, for the highest reliability of the results it is important to measure frequently the SRF during the mesurement session.

Experimental results: organization of the chapters

In the following three chapters, the results concerning the research about the interaction between the *MePTCDI* molecule and semiconductor substrates will be considered under different points of view.

- In **Chapter 3** - *reference measurements*, here are presented and briefly discussed the results concerning *MePTCDI* molecules in dilute solution, in crystalline films and in amorphous films.
  - In § 3.1, the time resolved fluorescence measurements carried out on a dilute solution of *MePTCDI* molecule give the possibility to derive the intrinsic properties of the *isolated MePTCDI* molecule (spectrum and fluorescence decay). A numerical value of the molecular fluorescence lifetime can be accordingly drawn out from the fluorescence decay curves.
  - Section § 3.2 is dedicated to the temperature dependent measurements of absorption and fluorescence spectra of *MePTCDI* in crystalline form. The optical properties related to the existence of an organized structure of molecules in the space are put in evidence and briefly discussed.
  - In § 3.3, amorphous *MePTCDI* films are considered: the temperature dependent fluorescence spectra and fluorescence decays are described and discussed and the observed fluorescence properties are put in relation to the lack of spatial order inside the molecular film.
  - Finally, in § 3.4, upon progressive molecular film thickness reduction, it is shown how is experimentally possible to stop the intermolecular interaction and consequently the excitation transfer inside the film, coming to a real 'isolated' molecule condition in solid state.

- **Chapter 4** - *Experimental results I* is dedicated to ultrathin molecular films (isolated molecule limit): in this chapter, only ultrathin (0.01 ML) *MePTCDI* film either *directly* deposited on semiconductor surfaces or deposited on a *spacer* precedently condensed on the substrate are explicitly considered.
  - In § 4.1, the time resolved fluorescence spectra and decays of *MePTCDI directly* deposited on quartz, MoS_2 and *Si(111):H* are shown and the excitation transfer rate from the excited *MePTCDI* molecule to the substrate are calculated for these three cases.
  - In § 4.2, the *distance dependence* (spacer measurements) of fluorescence spectra and fluorescence transients for *MePTCDI* deposited on MoS_2, as a function of the spacer thickness is reported.
  - In § 4.3, the distance dependence of the fluorescence spectra and transients for *MePTCDI* deposited on *Si(111):H*, as a function of the spacer thickness is reported.

– In **Chapter 5** - *Experimental results II*, the effects of particular treatments applied to the sample are described and discussed.
  · In § 5.1, a silicon surface characterized by *an enhanced chemical reactivity* is used as substrate and its effects on the distance dependent fluorescence of the *MePTCDI* molecules are described and discussed.
  · In § 5.2 an *undulate* spacer layer is explicitly considered; the effects of the undulation on the fluorescence properties of the *MePTCDI* molecules deposited on it and the modifications induced by a controlled annealing of the sample are investigated.

---

3 Measurements on *MePTCDI* in different environments

MePTCDI can be studied (1) as *non–interacting* molecules in dilute solution (*see* § 3.1), (2) as *crystalline* films deposited at room temperature in High-Vacuum (*HV*, $\sim 10^{-6}$ mbar) (*see* § 3.2), (3) as amorphous films deposited at helium temperature ($T = 10$ K) in Ultra-High-Vacuum (*UHV*, $\sim 5 \cdot 10^{-10}$ mbar) (*see* § 3.3).

A large number of reference measurements have been carried out varying the thickness of the deposited molecular films, the sample temperature and the preparation conditions; by changing the experimental conditions, it is actually possible to modify the environment of the *MePTCDI* molecules and consequently their fluorescence properties.

Being the goal of this research the study of the interaction between *isolated MePTCDI* molecules and semiconductor substrates, the results concerning 'thick' molecular films (whose thickness is greater than one monolayer), although representing a large amount of experimental work, are only briefly reported and exclusively within this chapter.

3.1 The intrinsic properties of the molecule: *MePTCDI* in solution

The *intrinsic* optical properties of the *MePTCDI* molecules can be actually studied only when they *do not interact* each other. This condition, extremely difficult to obtain in solid state, is quite easy to reach in dilute solution. A dilute solution of *MePTCDI* molecules offers therefore a reliable way to measure the pure *molecular* properties. In this section the

absorption and fluorescence spectra of *MePTCDI* dissolved in chloroform are considered and their characteristics discussed.

Fig. 8 shows (see Ref. [43] for complete details) the quantitative absorption spectrum and the steady-state fluorescence of two–times gradient–purified *MePTCDI* in dilute solution of chloroform ($CHCl_3$). To calculate a quantitative value of the extinction coefficient ε, a number of absorption measurements have been carried out with increasing concentration (between $5 \cdot 10^{-8}$ mol/l and $2 \cdot 10^{-7}$ mol/l). The resulting numerical value is shown on the right vertical axis, the error is $\pm$ 5%.

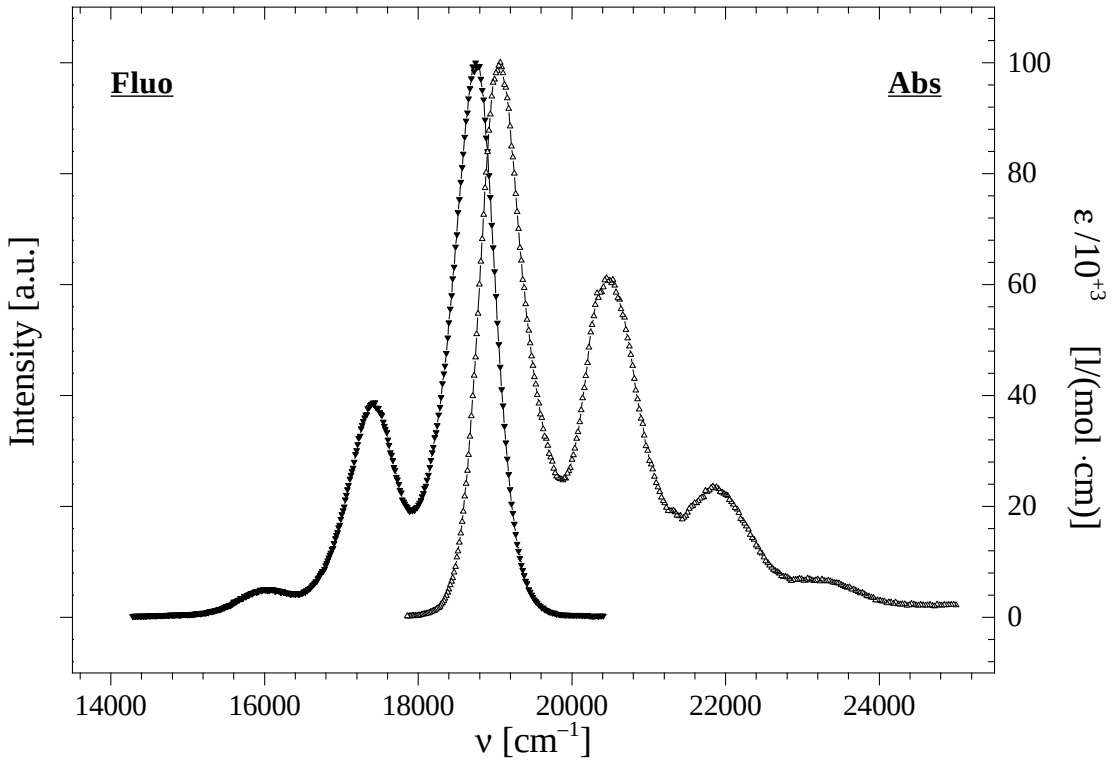

Fig. 8: Room temperature absorption and fluorescence spectra of *MePTCDI* in dilute solution of chloroform ($CHCl_3$), after Gomez [75]. These spectra will be considered in the following the prototypes of absorption and emission spectra of the isolated *MePTCDI* molecules.

MePTCDI has a chemical structure derived from the perylene and as in all the other perylene derivatives its lowest electronically excited states are mainly governed by the extension of $\pi-$electron conjugation and by its vibronic coupling to carbon backbone, whereas the small outer substituents hardly affect the lowest state. As a result, the solution absorption spectra of all the perylene derivatives are quite similar [76].

The four-bands absorption spectrum shown in fig. 8 spans the energy range of the lowest molecular π-π^* electronic transition ($S_0 \rightarrow S_1$). This transition is polarized along

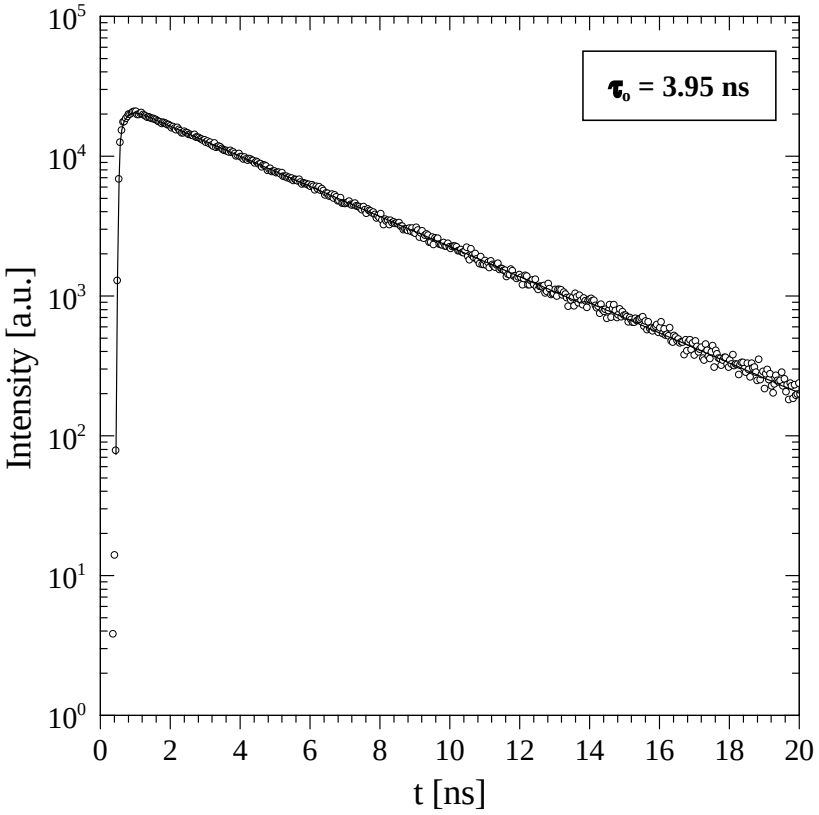

Fig. 9: Fluorescence transient of *MePTCDI* in $CHCl_3$ solution a room temperature. Excitation at $\bar{\nu} = 18796\,\mathrm{cm}^{-1}$, detection at $\bar{\nu} = 17300\,\mathrm{cm}^{-1}$ [75]. The continuous line represents a monoexponential fit curve assuming a decay time estimated in $\tau_0 = 3.95\,\mathrm{ns}$; this value is the intrinsic fluorescence lifetime of the isolated *MePTCDI* molecule.

the long molecular axis [43, 77] and from the absolute absorption cross-section the total electronic transition dipole is estimated to amount to 9.05 Debye [43]. The next dipole-allowed singlet state S_2 has a much smaller transition dipole (directed along the short axis in the molecular plane) and a frequency of $\bar{\nu} = 27400\ \mathrm{cm}^{-1}$.

The $0-0$ transition ($\bar{\nu}_{00} \approx 19050\,\mathrm{cm}^{-1}$) couples mainly to C−C and C−O vibrational modes of the perylene carbon backbone leading to the well-developed vibronic progression visible in the figure. Following a theoretical analysis [78] only seven (on a total of $3N$-6 [a]) vibrational modes have a significant intensity in absorption spectrum of *MePTCDI*; they are however not resolved in the spectrum in solution and they can be treated as one effective mode ($\Delta\bar{\nu} \approx 1400\,\mathrm{cm}^{-1}$) with an effective coupling constant [79].

A typical emission spectrum of *MePTCDI* in $CHCl_3$ at room temperature is shown on the left side of fig. 8. The emission is a mirror image of the absorption with a Stokes–shift

[a] N is the number of atoms in the molecule

of $\Delta\bar{\nu} \sim 310\,\mathrm{cm}^{-1}$. The excitation energy is $\bar{\nu} = 20830\,\mathrm{cm}^{-1}$.

Fig. 9 shows (in half-logarithmic scale) the fluorescence decay of *MePTCDI* in $CHCl_3$ solution (with concentratio $c \sim 10^{-7}$ mol/l) at room temperature in a $[0-20\,\mathrm{ns}]$ time range [43]. The excitation energy is $\bar{\nu} = 18796\,\mathrm{cm}^{-1}$, whereas the detection energy is $\bar{\nu} = 17300\,\mathrm{cm}^{-1}$. The fluorescence transients are independent on the spectral position and show a *monoexponential* decay with time $\tau_0 = \mathbf{3.95\,ns}$. **This value will be in the following considered as the intrinsic fluorescence lifetime of the *isolated molecule*.**

Moreover, in order to estimate the *absolute fluorescence quantum yield* Φ_{Me} of *MePTCDI* in $CHCl_3$, the method of Parker and Rees [80] was applied; as reference, a degassed solution of anthracene in n-hexane was used. An average (on 10 measurements) value of $\mathbf{\Phi_{Me} = 0.93}$ with an error of $\pm 5\%$ was found [43].

3.2 Thin microcrystalline films

In this section are reported and briefly discussed the temperature dependent absorption and time resolved fluorescence measurements carried out on a prototypical *crystalline* 500 Å (~ 150 ML) thick *MePTCDI* film. The film has been deposited on quartz, at room temperature, under High Vacuum (HV) conditions with a base pressure of $\sim 5 \cdot 10^{-6}$ mbar and a deposition rate of 0.75 ML/min.

The crystalline *MePTCDI* films are characterized by a complex energy level structure related to the formation of *delocalized crystal states* or to the presence of *different crystalline phases*. That emerges in non-monomeric absorption and fluorescence spectra, as shown in the next paragraph.

3.2.1 Temperature–dependent absorption and time resolved fluorescence

Fig. 10 (right) shows the absorption spectrum of a 150 ML thick crystalline film, when the temperature spans the range $[10-295\,\mathrm{K}]$. Fig. 10 (left) shows the relative quasi-*cw* (quasi steady-state) fluorescence spectrum of the same film. The spectra are normalized to their maxima; in fluorescence spectra the excitation takes place at $\bar{\nu} = 18796\,\mathrm{cm}^{-1}$.

The **absorption spectrum** turns out to be *drastically different* from that in solution (irrespectively of the temperature at which it is measured). It exhibits a first series (the only visible in fig. 10 and in the following considered) of four features between $\bar{\nu} = 16000\,\mathrm{cm}^{-1}$ and $\bar{\nu} = 25000\,\mathrm{cm}^{-1}$ (i.e. between ~ 2.0 eV and ~ 3.0 eV). A progressive broadening of the features upon increasing of the temperature is observed, accompanied by an apparent shift of the first peak from $\bar{\nu} = 17170\,\mathrm{cm}^{-1}$ (at $T = 10$ K) to $\bar{\nu} = 17420\,\mathrm{cm}^{-1}$ (at room temperature). The absorption spectrum turns out to be however only *slightly affected* by the temperature change.

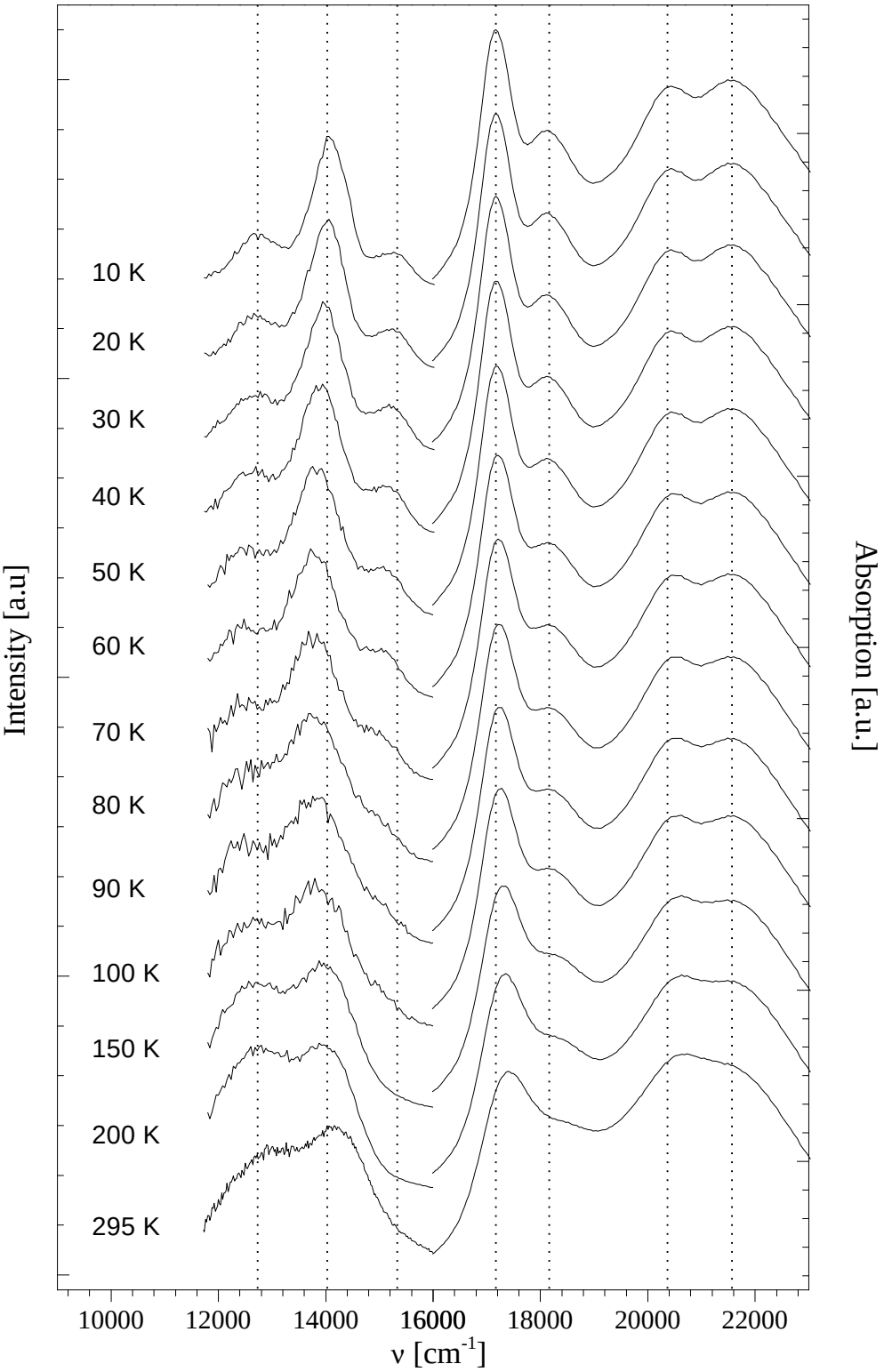

Fig. 10: *Right*: Temperature dependent unpolarized absorption spectra of a 500 Å ($\sim$150 ML) thick crystalline *MePTCDI* film deposited at room temperature on quartz. *Left*: temperature dependent quasi-*cw* fluorescence spectra. The spectra are normalized to their maxima, excitation at $\bar{\nu} = 18796\,\mathrm{cm}^{-1}$. Time interval $[\,0-50\,\mathrm{ns}\,]$. *See* text for details.

The **fluorescence spectrum** is also dissimilar from what observed in solution, moreover drastic spectral variations are evidenced upon raising the temperature: the three-features structure visible at $T = 10\,\mathrm{K}$, progressively changes in a less structured form centered at lower energies. The dominant feature at $\sim 14000\,\mathrm{cm}^{-1}$ apparently shifts to red and then back to blue with the temperature. Under constant excitation and detection geometry the measured fluorescence intensity drastically decreases passing from helium to room temperature.

Making use of time resolved techniques, it is possible to evidence the temperature dependence of different fluorescence components in the spectrum [b]: the fluorescence collected within the first 200 ps after the excitation pulse does not change appreciably (apart the temperature broadening of the peaks) and it reminds the form of quasi-*cw* fluorescence shown in fig. 10. A drastic variation is instead observed in the delayed fluorescence as a consequence of thermally activated excitation transfer phenomena among the various crystalline states.

Such a temperature dependence, together with the low temperature three-bands structure are commonly observed in fluorescence spectra of $\alpha-$perylene crystals [81–85], $\alpha-$perylene crystalline films [86] and *PTCDA* films [75]. This kind of emission is indicated in literature as 'Y'-fluorescence. Its origin, nowadays not completely clear, is associated to a stable low-temperature arrangement of the molecules in the crystal.

Molecular stacking and fluorescence properties

During the past years a big experimental effort was devoted to study the nature of the *lowest energy state* in crystals of *MePTCDI* and *PTCDA*. Experimental investigations were carried out with a number of different techniques [c] and the theoretical activity on the subject has been very intense ([77] and ref. therein).

In the crystalline phase the excited states of the monomer are influenced by intermolecular interactions, which lead to strong changes in the absorption spectra with respect to that of the molecules in dilute solution. As an effect the solution absorption spectra of the various perylene derivatives are usually very similar, whereas the crystal spectra differ each other considerably ('crystallochromy' [46, 48]), depending on the relative arrangements among the molecules in the crystal. In the perylene derivatives the steric effect of the radical substituent groups is mainly responsible of the different molecular packing geometry and therefore of the different crystalline states.

The crystal structure of *MePTCDI* is characteristic, in the sense that it presents a large anisotropy along particular spatial directions: the molecular planes are arranged

[b] The study of time evolution of the various fluorescence components in the spectrum of fig. 10 lies out of the scope of this research and it is therefore here not treated.

[c] UV-VIS absorption [46, 87], photo-luminescence [88–92], IR and Raman spectroscopy [93, 94], electro-absorption [95], photo-conductivity [96] and photo-emission [97].

(fig. 4) in stacks where the molecules lie in a face-to-face configuration in closely packed one-dimensional structures; the distance between planes of near-neighbours in stack is 3.40 Å [46], in comparison the length of a molecule amounts to $\sim$11 Å. This causes a strong interaction between the $\pi-$electrons along the stack and weak interaction in the other directions.

According to a recently developed model [98] that takes into account the effect induced by the interaction among the molecules along a molecular stack, the absorption spectrum structures and their polarization behaviour are interpreted as the result of a strong *mixing* between lowest crystal states (Frenkel excitons, superposition of neutral excited states of molecules, considered isolated, that build up the crystal) and the charge-transfer (CT) excitons (ionized states of the nearest-neighbour molecules). For large intermolecular distances or negligible π-orbitals overlap (as, e.g., in anthracene where two molecules are laterally shifted by 5.4 Å and they do not lie at all above each other) the CT levels lie energetically well above the lowest Frenkel exciton and the effects of interaction between the two are not important (for this reason the lowest crystal state in anthracene is adequately described by Frenkel excitons); on the contrary, for smaller intermolecular distances or larger π-orbitals overlap (as in the case of *MePTCDI*) the CT exciton energy decreases towards the lowest Frenkel exciton levels and the interaction integral between the two (and therefore their mixing) increases. As a consequence, the lowest exciton state becomes strongly mixed Frenkel-charge-transfer exciton in character.

On the contrary, according to a second interpretation [99], making use of time-dependent density functional techniques the CT energies were found *below* the Frenkel exciton. For this reason the mixing of both type of excitons by electron and hole transfer is not expected to influence strongly the absorption lineshape; as a consequence, the absorption and photoluminescence data are interpreted uniquely in terms of Frenkel exciton [100, 101]. The low energy band in fig. 10 can be accordingly interpreted as having only Frenkel exciton character.

The goal of this research is the study of the properties of *non-interacting* molecules, therefore samples in crystalline form are not suited for the scope. Their spectra have been shown here as a reference to exemplify the optical properties of *ordered* molecular structures, but they are not further considered.

3.3 Thin amorphous films

In this section, the optical properties of a prototypical amorphous *MePTCDI* film are experimentally studied, together with their variation with the temperature.

The growth of organic films under particular experimental conditions (base pressure

$\sim 5{\cdot}10^{-10}$ mbar, $T = T_S = 10\,\mathrm{K}$ [d]) occurs *amorphous*, independently from the substrate [34, 43]; instead of a regular crystalline molecular environment a non-ordered structure results, i.e. without spatial periodicity and with very few small crystallization nuclea enclosed.

The formation of large crystalline phases inside such molecular films is prevented by energetic reasons: at $T_S = 10\,\mathrm{K}$ the *MePTCDI* molecules have not enough lateral mobility [43,102] to reach, after the deposition, positions and mutual orientations that minimize the configurational energy and to form crystalline structures. Such low lateral mobility is, however, a characteristic rare among the organics, since only bigger and heavier molecules are observed to rest fix on the substrate after the deposition [e].

3.3.1 Temperature dependent time resolved fluorescence

In order to study the fluorescence properties of amorphous samples and to proof their degree of structural stability with the temperature, *temperature dependent* time resolved fluorescence spectra and transients of a film deposited on quartz have been measured for temperature from $T = 10\,\mathrm{K}$ to 370 K. The results have to be compared with those obtained for a *crystalline* film in the same temperature range (fig. 10).

Fluorescence spectra and transients

Fig. 11 shows the quasi-*cw* (quasi steady-state) fluorescence spectra of a 70 ML thick *MePTCDI* film evaporated and measured in–situ in *UHV* at $T_S = 10\,\mathrm{K}$ on quartz (base pressure $\sim 4 \cdot 10^{-10}$ mbar, deposition rate $\sim 0.5\,\mathrm{ML/min}$). The temperature has been successively raised to 370 K. Fig. 12 shows the temperature dependent fluorescence transients of the considered film, as detected at $12200\,\mathrm{cm}^{-1}$. In both cases the excitation is at $\bar{\nu} = 18796\,\mathrm{cm}^{-1}$. After reaching the target temperature, the complete thermalization of the system coldfinger + sample holder + sample was waited (at least 30 minutes pause before a new measurement). In the course of the measurements the experimental geometry was not changed. The acquisition time has been kept constant for all the fluorescence transients up to 250 K, then it has been prolonged four times for the last two measurements. The temperature has been set by a temperature controller and by timely balancing the flux of liquid helium. Fig. 11 and fig. 12 evidence that there is *no significant change* in both quasi-*cw* fluorescence spectra and fluorescence transients over a large temperature range. In particular, between $T = 50\,\mathrm{K}$ and $T = 150\,\mathrm{K}$, the quasi-*cw* fluorescence spectra remain practically unaffected, whereas a corresponding *crystalline* thin film exhibits radical changes (fig. 10). The unstructured fluorescence and the negligible change

[d] T without subscript indicates the temperature at which the measurement is carried out, T_s indicates the temperature at which was hold the substrate during the deposition of the molecular film.

[e] Anthracene, for example, due to its small dimensions and weight, has been demonstrated [34] to have a marked tendency to move and to form aggregates also at very low temperature and to crystallize irreversibly for temperature above $T = 270\,\mathrm{K}$.

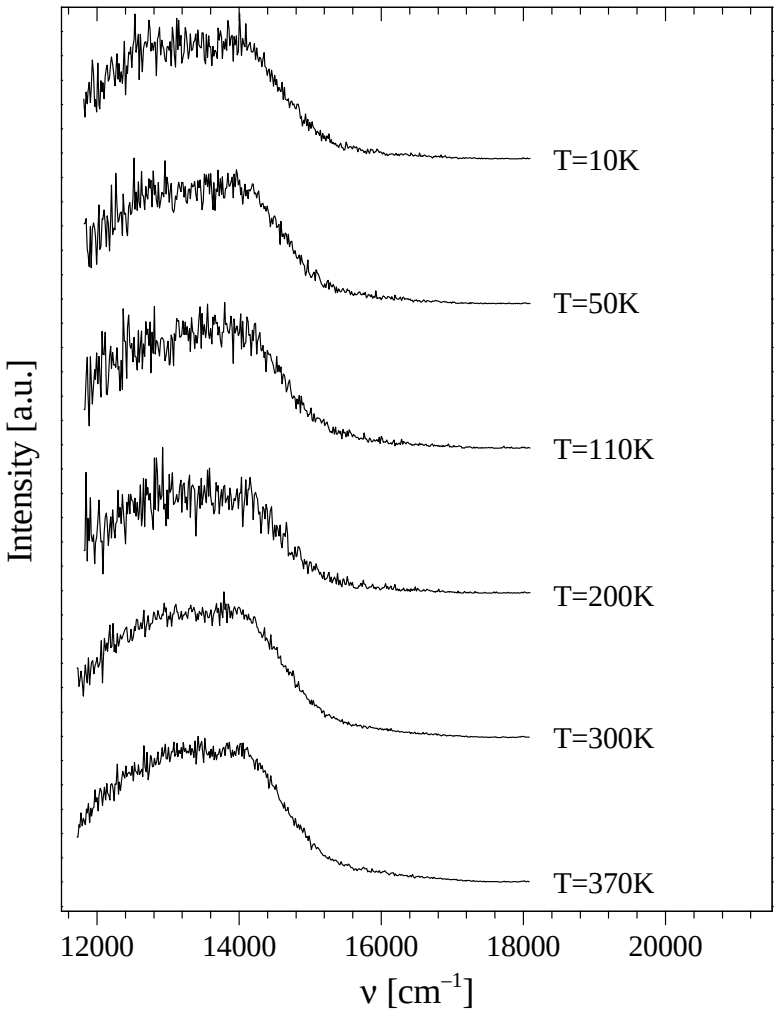

Fig. 11: Temperature dependent quasi-*cw* fluorescence spectra of a 70 ML thick *MePTCDI* film deposited at $T = T_S = 10\,\mathrm{K}$ on quartz. Excitation at $\bar{\nu} = 18796\,\mathrm{cm}^{-1}$. The unstructured fluorescence and the negligible change in the spectra upon temperature variation are the main evidences of the amorphous nature of the film.

in spectra upon temperature variation are the main evidences of the amorphous nature of the film. Also the fluorescence decay time measured at $\bar{\nu} = 12200\,\mathrm{cm}^{-1}$ does not change appreciably over the considered range of temperatures. At room temperature in–situ, the molecular film turns out to be still non-ordered even if crystalline nucleation sites inside the film are evidently already present [f]. No appreciable variation upon temperature change is visible also at different detection frequencies ($\bar{\nu} = 16000\,\mathrm{cm}^{-1}$ and $\bar{\nu} = 18370\,\mathrm{cm}^{-1}$, not shown). In amorphous *MePTCDI* films, contrary to crystalline ones, the presence of thermal activated processes can be therefore excluded on an extended temperature range.

[f] Actually it has been experimentally observed that 24 hours annealing at 150 °C are sufficient to come to a complete crystallization of the film

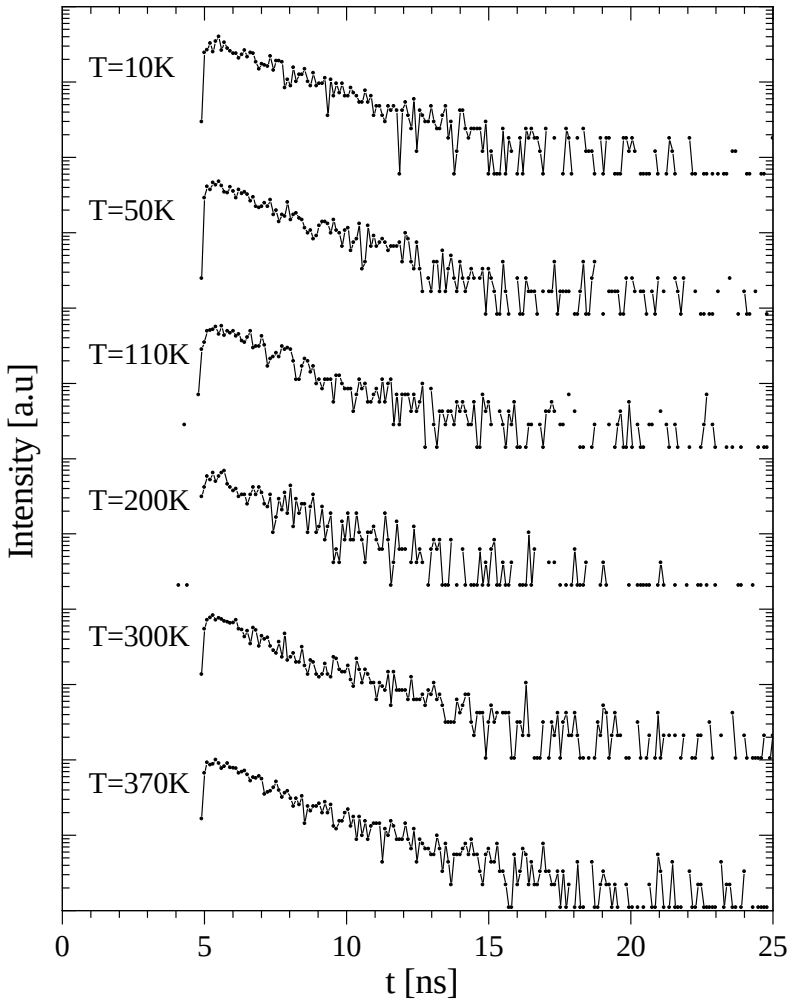

Fig. 12: Temperature dependent fluorescence transients of the amorphous film of fig. 11. Excitation at $\bar{\nu} = 18796\,\mathrm{cm}^{-1}$. Detection at $12200\,\mathrm{cm}^{-1}$.

3.3.2 Amorphous films and excimers

Concerning the optical properties, two are the main characteristics of amorphous films:

a) They exhibit a **monomeric absorption** spectrum, with a general shape *independent of film thickness* [89,102]. This aspect reflects the disordered internal film structure characterized by *iso*tropic interaction among the molecules (unlike the *an-iso*tropic interaction typical of a crystalline environment): the excited state of the film is actually a distribution of excited states of *monomer* and for this reason the absorption remains monomeric.

b) The amorphous films exhibit nearly **structureless fluorescence** spectrum in a large temperature range (fig. 11). This is quite different from the complex temperature dependent emission of crystalline films (fig. 10) and from the monomer fluorescence in solution (fig. 8). Furthermore, amorphous films usually exhibit a big Stokes-shift (thou-

sands of cm^{-1}, that increases with the film thickness) and non-exponential fluorescence decays.

The lack of features in quasi-*cw* low temperature fluorescence spectra of fig. 11 and the strong Stokes–shift (estimated [g] to $\sim 4100\,cm^{-1}$) can be interpreted as the experimental evidence of an **excimer type fluorescence**. The nature of excimers and their fluorescence properties are described in the following.

Excimers and excimer fluorescence

Two identical molecules, the mutual interaction of which causes in the *ground* state a bond to be built up, form a dimer [103,104]. In contrast, if a bond between two equal molecules can be built up only when one of two is in its *excited* state, the state associated to such a pair is called **excimer** (*exci*-ted di-*mer*). Upon deactivation, the coupling between the two molecules is lost and the excimer dissociates: its ground state is actually repulsive. The excimer formation is a dynamic process that takes place between two appropriately oriented molecules; the state associated to this pair is energetically favoured and lies lower with respect to the energy level of the excited molecule. The excimer formation causes delocalization of excitation on both molecules. Since the interaction between excited aromatic molecules is generally attractive, the excimer formation is already observed in concentrate solution of a number of organic compounds [104, 105].

On the base of its characteristics an excimer exhibits the following optical properties: 1.) The excimer state is built starting from excited states of molecular monomers, therefore *its optical absorption is identical to absorption of molecular monomers*. 2.) The excimer energy level is lower than monomer one, consequently the excimer fluorescence spectrum is *red shifted* with respect to that of monomer. 3) Since the excimer is not bound in its ground state, its fluorescence is essentially *unstructured*. 4) The optical transition from excited to ground state is not allowed for parity in excimer states [104], therefore the fluorescence lifetime of excimers is generally *longer* than monomer one.

The excimer formation is extremely sensitive on the relative orientation of the two molecules of the pair. In the case of organic molecules with extended π-electron systems their overlap is a prerequisite for a strong interaction [104, 106].

If the molecular environment is highly ordered (as in molecular crystals) the excimer formation is possible only if the molecular arrangement permits such overlap; this is the case of coronene [86], α-perylene [82] or pyrene [104] crystals, where a pairwise packing structure does exist; but it is *not* the case of anthracene [107], naphthalene [108], tetracene [109] or β-perylene [82], where no excimer fluorescence is visible.

[g] The Stokes–shift is estimated as difference between the position of the fluorescence maximum in spectra of fig. 11 and the maximum in fluorescence excitation spectra [43] measured under similar experimental conditions.

If the molecular environment is *not* ordered (as in amorphous molecular films), there is a statistic distribution of relative orientations of the molecules. There is therefore a distribution of molecular pairs that, in the excited state, can give rise to excimer formation; for this reason a typical excimer emission can be observed also in amorphous films of those molecules that do not exhibit excimer fluorescence in single crystals.

Differently from the case of excimers in molecular crystals, in amorphous films not one, but a *distribution* of different excimer configurations exists. Consequently, there is a distribution of excimer energy levels and different fluorescence spectra and fluorescence lifetimes [34, 110]. This causes a more complex dynamics in the excited states.

Intermolecular excitation transfer and trapping

The fluorescence spectra of amorphous films (fig. 11) can be described making use of the excimer concept, as follows.

Upon electronic excitation of a *MePTCDI* molecule, the interaction between nearby molecules inside the film does favour an incoherent excitation transport (i.e. by *hopping*) within the manifold of *monomer* levels [34, 43]. At a stage of this transfer, the excitation can reach a molecule with a properly oriented neighbour, so that an excimer pair can be formed acting as an effective *trapping site*: since at $T = 10\,\mathrm{K}$ the excitation cannot be thermally detrapped, it cannot be transferred anymore and the deexcitation takes place from this site.

Furthermore, the fluorescence spectrum of an amorphous *MePTCDI* film generally exhibits a strong *spectral inhomogeneity*, i.e. the shape of the spectrum changes from early to late times after the excitation pulse, shifting the position of the emission peak and that of the fluorescence onset to lower energies within successively measured time intervals [104]. Such effect is shown in fig. 13 (below); there, the room temperature fluorescence of a 70 ML amorphous film is plotted as collected in the first 1.2 ns after the excitation pulse and in a delayed time interval ($[\,8.4-40\,\mathrm{ns}\,]$), respectively. Fig. 13 (above) shows the quasi-*cw* fluorescence of the same film as collected in the full time interval $[\,0-40\,\mathrm{ns}\,]$.

The observed spectral behaviour can be interpreted as fluorescence originating from a distribution of excimers with different spatial orientations and consequently different ordering of energy levels (i.e. different fluorescence spectra and lifetimes). In such a distribution the high energetic components (corresponding to less stabilized configurations) exhibit a shorter fluorescence lifetime than the lower energy ones. When the fluorescence is collected by time resolved spectroscopy techniques, it is possible to separate temporally the various fluorescence components, whereas the quasi-*cw* fluorescence spectrum results from the superposition of the various fluorescence components contributing in different amount.

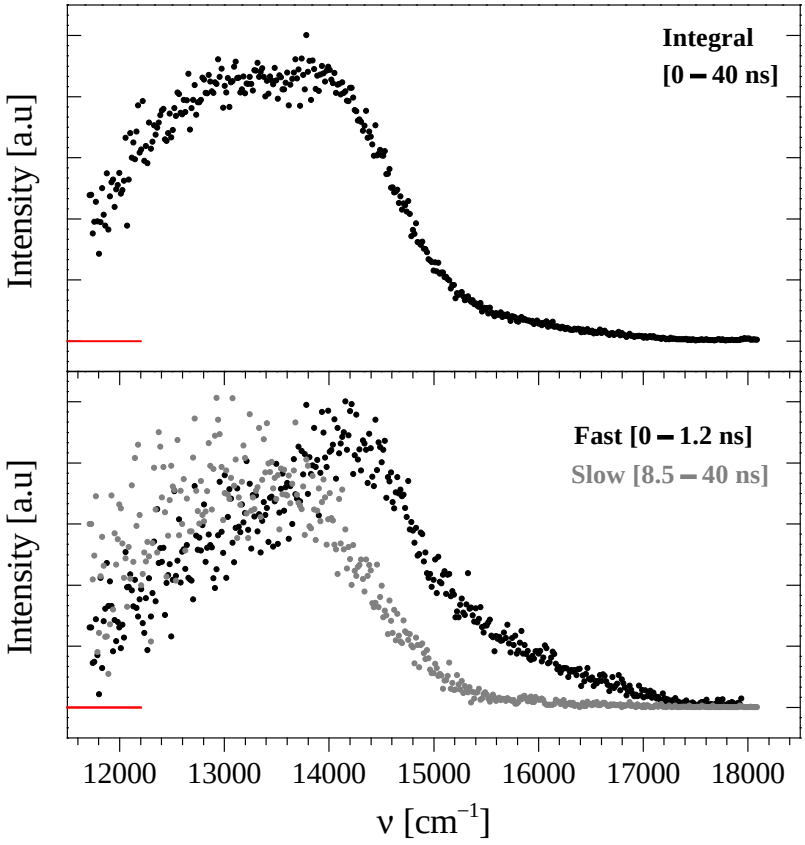

Fig. 13: Room temperature time resolved fluorescence spectra of amorphous *MePTCDI* film (70 ML) on quartz (below) and relative quasi-*cw* fluorescence spectrum (above). Time range [0 – 40 ns], excitation at $\bar{\nu} = 18796\,\mathrm{cm}^{-1}$. All spectra are normalized to their maximum.

Since the quasi-*cw* fluorescence spectrum of the *MePTCDI* film (fig. 11) seems nearly unaffected upon temperature change (as well as the observed spectral inhomogeneity), the molecular reorganization during the film crystallization process is supposed to take place slowly in the temperature range below room temperature.

Summarizing, the fluorescence in amorphous molecular films can be described as the result of molecular monomer excitation, excitation hopping among the monomer levels, excitation trapping in excimer trap and de-excitation. In the following, an unstructured excimer-like emission is considered the fingerprint of an amorphous structure in the organic film.

From now on, only molecular films deposited and measured in–situ at $T = T_S = 10\,\mathrm{K}$ are considered, without further variation of the temperature.

3.4 Submonolayer films

In the precedent activity of our group [34, 43, 111] it has been shown how, depending on the nature of the substrate and on the thickness of the deposited organic film, *two* competing excitation transfer processes a) the *intra*-layer transfer and b) the molecule-substrate transfer affect the sample fluorescence with different balancing.

When the organic film is deposited on a *non-interacting* substrate, the observed change in fluorescence dynamics upon film thickness variation is dominated by the excitation transfer phenomena *inside* the film [43].

On quartz, prototype of non-interacting material, the measured fluorescence decay time *increases* upon progressive decreasing the film thickness (particularly for thickness below few ML) [43]. This is explained in terms of reduced excitation transfer rate from molecule to molecule: since, below the single monolayer coverage, the molecular density decreases with the film thickness, the excitation hopping rate decreases, too and the possibility to reach sites where the deexcitation occurs non-radiatively is reduced. The observed radiative decay time therefore increases.

Nevertheless, a similar experiment performed on metallic or semiconductor substrates gives opposite results [43,111]: by reducing the organic film thickness down to the single monolayer range, the observed fluorescence decay time is strongly *reduced*. The existence of a *competing* deexcitation process (via non-radiative interaction between molecule and substrate) qualitatively explains the effect. The experimental findings have been successively also quantitatively described [h] in the case of anthracene [34] and of *MePTCDI* on *Ag* and *Si* [43].

Upon *further* reduction of coverage well below the single monolayer (*ultrathin* film: 0.5 ML−0.01 ML), the interaction between the molecules diminishes until is completely blocked (*isolated* molecule limit), the inter-molecular excitation transfer rate becomes progressively slower, whereas its inverse becomes comparable or even longer than the molecular lifetime. As a result, due to such very low hopping rate the deexcitation takes prevalently place from the originally excited site.

Since the observed fluorescence dynamics is no more affected by *intra*-layer transport phenomena, the measured fluorescence properties are determinated only by the interaction between the molecules (now isolated from each other) and the substrate.
Only in the isolated molecule limit the molecule-substrate interaction phenomena can be *directly* measured.

[h] A modified version [37] of the model described in § 6.1 was applied.

3.4.1 Submonolayer film thickness dependent fluorescence on MoS_2

In this section, it is shown how is experimentally possible to change, upon film thickness reduction in sub-monolayer range, the balancing between the competing *intra*-layer excitation transport and the molecule-substrate interaction phenomena in favour of this latter and at limit to stop completely the former.

A series of time resolved fluorescence measurements has been carried out on a particular kind of sample (fig. 14), using MoS_2 as substrate and depositing on it a decreasing amount of molecules between 0.5 ML and 0.01 ML. MoS_2 is known to have a large effect on the optical properties of organic molecules deposited on it and a strong reduction both in fluorescence intensity and fluorescence decay time has been observed [111].

The molecular film has been deposited not in direct contact with the substrate surface, but *separated 170 Å* apart from the surface by means of a solid argon layer. The argon condensed at helium temperature on the MoS_2 surface (details on the condensation techniques in § 2.1.3) acts like a well defined *spacer*, optically and chemically inert, on which the *MePTCDI* molecules are successively deposited following the procedure described in § 2.1.4.

Because of the separation, a direct chemical-physical interaction between the molecules and the surface can be excluded; as a result, any variation observed in fluorescence properties upon thickness reduction is a consequence of the different trade-off between intra-layer excitation transport and molecule-substrate interaction.

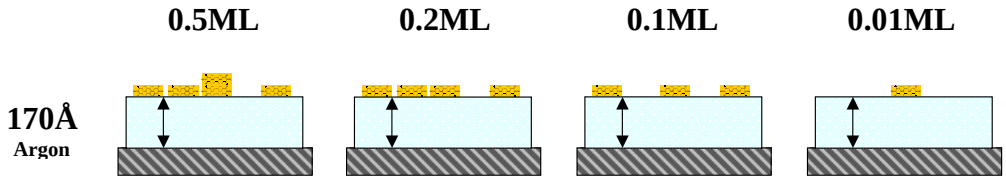

Fig. 14: *Inter*-layer transfer *vs* molecule-substrate interaction and their effects of the fluorescence properties of *MePTCDI* films. Sketch of the studied samples structure: a *MePTCDI* thin film is deposited at a fixed distance (170 Å) from a freshly cleaved MoS_2 substrate by means of an argon spacer. The balancing between the two effects can be modified by a progressive reduction of molecular coverage (0.5−0.01 ML).

Steady-state fluorescence spectra

Fig. 15 shows the in–situ quasi-*cw* fluorescence spectra ($T = T_S = 10$ K) of ultrathin *MePTCDI* films with different thicknesses (0.5 ML−0.01 ML) separated by a 170 Å thick argon layer from a freshly cleaved MoS_2 surface (time range [0 − 10 ns]).

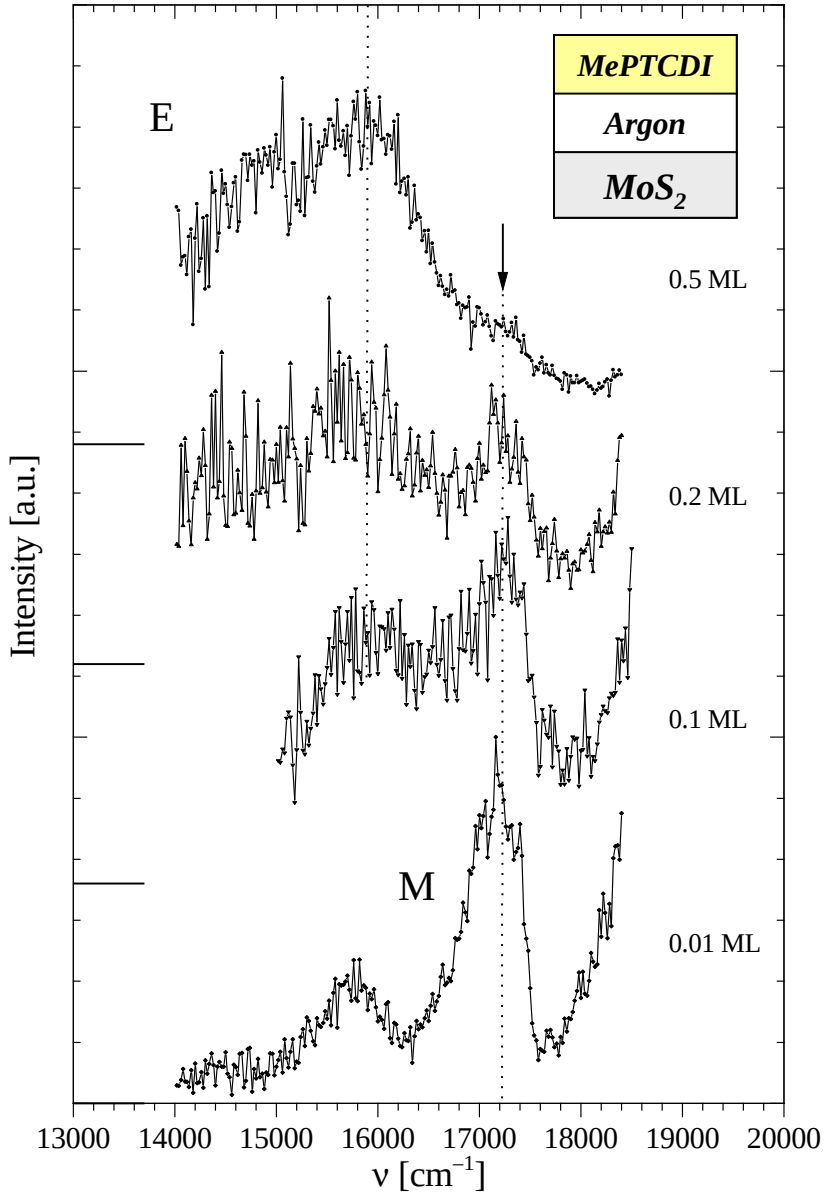

Fig. 15: In–situ quasi-*cw* fluorescence spectra of ($MePTCDI$ / 170 Å Ar / MoS_2) samples for four different molecular coverages (0.5, 0.2, 0.1 and 0.01 ML) separated by a 170 Å thick argon layer from a freshly cleaved MoS_2 substrate. $T = T_S = 10\,\mathrm{K}$. Time range $[\,0-10\,\mathrm{ns}\,]$. The spectra are normalized to their maxima, excitation at $\bar{\nu} = 18796\,\mathrm{cm}^{-1}$.

The 0.5 ML film exhibits a broad and unstructured fluorescence spectrum with maximum at $\sim 15900\,\mathrm{cm}^{-1}$ similar to that of the thick amorphous film (fig. 11) and for this reason assigned to excimer type emission ('E'). With respect to such emission a strong blue-shift of the fluorescence ($\sim 1800\,\mathrm{cm}^{-1}$) is observed [i]; it is related to the decreasing of the dimensionality of inter-molecular interaction: below the monolayer coverage each *MePTCDI* molecule has statistically less neighbours and they are spatially more confined on the plane; the resulting possible excimer states are less relaxed and their fluorescence is higher in energy.

Upon progressive reduction of the coverage, at fix spacer thickness (170 Å), a high-energy structure (indicated by 'M') gains intensity on 'E'; it becomes dominant for the (0.2 ML−0.1 ML) films. In the limit of 0.01 ML thick film only a 'M'-type fluorescence characterized by a strong apparent $\Delta\bar{\nu} = 1400\,\mathrm{cm}^{-1}$ vibronic progression is visible. The peak positions (tab. 3) and the intensity ratio are in good agreement with those observed in fluorescence of *MePTCDI* dilute solution (apart from an additional small $\Delta\bar{\nu} \simeq 100\,\mathrm{cm}^{-1}$ solvent shift, fig. 8).

Order n $S_{10} \rightarrow S_{0n}$	$\nu_S\,[\mathrm{cm}^{-1}]$ $[\pm\ 30\,\mathrm{cm}^{-1}]$
0	18650 *
1	17200
2	15800
3	14420

Tab. 3: Spectral position of monomer ('M') fluorescence peaks (*see* fig. 15). The * indicates an extrapolated value taking into account an apparent vibronic progression with $\Delta\bar{\nu} = 1400\,\mathrm{cm}^{-1}$.

Such spectrum has been identified in § 3.1 with the prototypic fluorescence of *isolated MePTCDI* molecules; consequently the 'M'-type fluorescence is here attributed to the *MePTCDI* **monomer**.

At 0.01 ML coverage level, the fluorescence originates from *isolated*, *non-interacting MePTCDI* molecular monomers.

Summarizing, when the thickness of the *MePTCDI* film deposited on the argon spacer is progressively reduced within a thickness range well below the single monolayer, the change in fluorescence spectrum appears to be *monotonic* and a homogeneous transition from an excimer 'E' emission to a monomer emission 'M' is observed. Below 0.03 ML the fluorescence has a pure monomer character.

[i] A blue-shift upon film thickness reduction was observed also on quartz, *Si(111)* and *Ag*.

Time resolved fluorescence spectra

Time resolved spectroscopy technique permits to separate the temporal evolution of the two distinct emission components ('E' and 'M') upon variation of the coverage. Fig. 16 shows, from left to right, three different films characterized by a continuous molecular coverage reduction (from 0.5 to 0.01 ML), whereas from top to bottom it is shown the fluorescence spectrum as collected from the same sample, in different time intervals after the excitation pulse (Fast $[0-200\,\mathrm{ps}]$, Medium $[200-700\,\mathrm{ps}]$, Slow $[700-8400\,\mathrm{ps}]$ and quasi-*cw* $[0-8.4\,\mathrm{ns}]$). The last row shows three of the four quasi-*cw* fluorescence spectra of fig. 15.

With reference to fig. 16, it can be observed that: at 0.5 ML coverage, the emission 'E' turns out to be dominant in all the time intervals, whereas the 'M' component appears only in the early times after the excitation pulse and then *tends to disappear*. At 0.2 ML coverage, the component 'E' gains intensity in the delayed times, whereas 'M' emission persists up to delayed times. At 0.01 ML coverage, 'E' emission does not appear at all, whereas 'M' gains intensity, from early to delayed times. In this limit the film fluorescence has pure monomer character in all the considered time intervals.

These experimental results confirm that the excitation transfer inside the system of monomer levels is effective already at film thickness above 0.1 ML . As a consequence excimer formation and excitation trapping can occur and therefore 'E' emission is observed. Below 0.1 ML the excitation trapping becomes less probable: 'M' and 'E' emission coexist and areas with non-interacting monomers can already exist. At 0.01 ML the excitation transfer and the consequent excitation trapping inside the film is completely blocked and only a pure 'M' emission can be observed.

Fluorescence transients

The monomer fluorescence in the system (*MePTCDI* / 170Å Ar / MoS_2) can be analysed as a function of the molecular film thickness. Fig. 17 shows the fluorescence decays as detected at $\bar{\nu} = 17250\,\mathrm{cm}^{-1}$ (arrow in fig. 15).

Down to film thicknesses of 0.2 ML, the fluorescence has predominant excimer character and its decay is strongly non-exponential; upon a further coverage reduction (0.1 ML) the fluorescence decays become progressively slower. In the limit of ultrathin film (0.05−0.01 ML) the excitation cannot be transferred and the deexcitation takes place from monomer sites. The fluorescence spectrum exhibits monomer character, whereas the relative fluorescence transients become in the limit nearly monoexponential, with a decay time that depends uniquely on the properties of the substrate on which the molecule is deposited.

At a distance of 170 Å from a MoS_2 substrate, the isolated *MePTCDI* molecule fluorescence lifetime amounts to $\tau_{\mathrm{obs}} = 1.8$ ns.

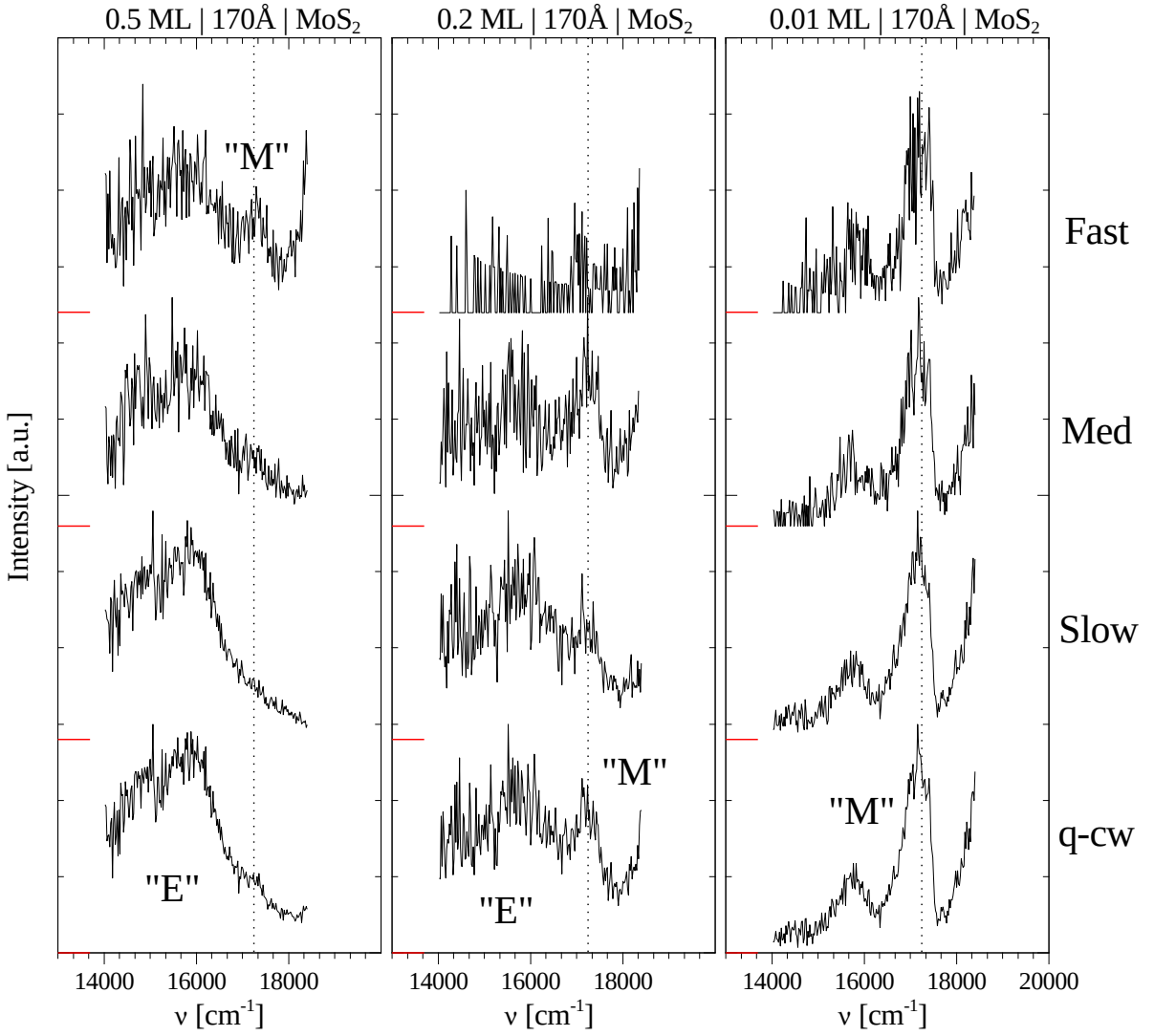

Fig. 16: In–situ time resolved fluorescence spectra of systems (*MePTCDI* / 170 Å Ar / MoS_2) for three different nominal thicknesses (0.5, 0.2 and 0.01 ML) at $T = T_S = 10\,\mathrm{K}$. The spectra are normalized to their maxima, excitation at $\bar{\nu} = 18796\,\mathrm{cm}^{-1}$ Time intervals after the excitation pulse: Fast [0 – 200 ps], Med [200 – 700 ps], Slow [700 – 8400 ps] and quasi-*cw* [0 – 8400 ps].

Nevertheless, this value turns out to be only 45% of the *MePTCDI* fluorescence lifetime as measured in solution ($\tau_0 = 3.95\,\mathrm{ns}$) in spite of a comparable (monomeric) fluorescence spectrum and an exponential fluorescence decay.

The only difference between the two experimental configurations is that the isolated *MePTCDI* molecule is now placed in **proximity of a substrate**: when the molecule is brought at a short distance from the MoS_2 surface, **its fluorescence lifetime is drastically affected**. It is possible to account for the observed fluorescence lifetime shortening

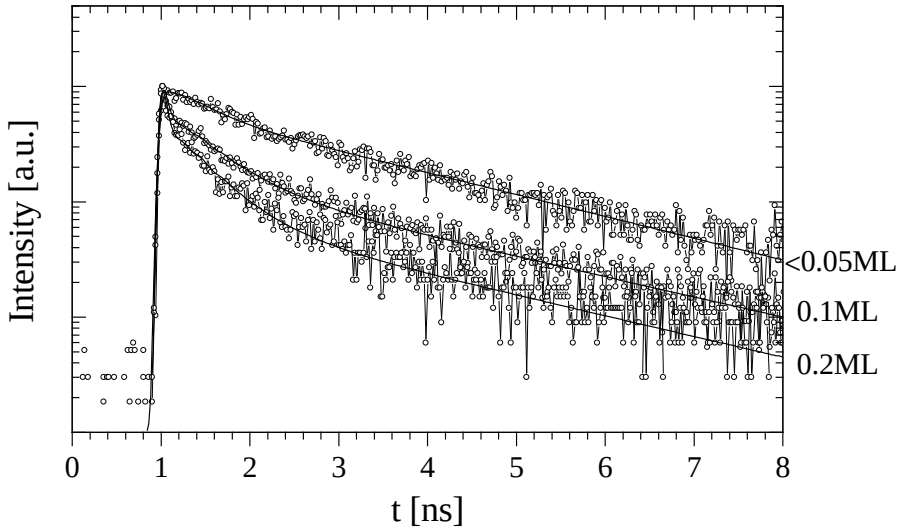

Fig. 17: Coverage dependent fluorescence decays of systems (*MePTCDI* / 170Å Ar / MoS_2) at $T = T_S = 10\,\mathrm{K}$. At ultrathin coverage ($< 0.05\,\mathrm{ML}$), the fluorescence lifetime amounts to 1.8 ns. Detection at 'M' peak ($\bar{\nu} = 17250\,\mathrm{cm}^{-1}$) in fig. 15. Excitation at $\bar{\nu} = 18796\,\mathrm{cm}^{-1}$.

by introducing in the system a non-radiative deactivation channel with a deactivation rate *function of the separation* between molecule and substrate.

Making use of the isolated molecule approach and of the spacer technique to define the distance between the molecule and the substrate, it is possible to study the *dependence on the distance* of the non-radiative interaction between the molecule and the substrate in the nanometric and subnanometric distance regime. This aspect will be considered in the next chapter.

Summary of § 3.4.1

In this section it has been shown how it is possible, by the progressive reduction of deposited *MePTCDI* film thickness, to change the balancing between the intra layer transport (that causes excitation trapping and excimer fluorescence) and the non-radiative molecule-substrate interaction. On MoS_2 the two effects always *coexist*. Nevertheless, in the limit of non-interacting molecules, the intralayer excitation trapping can be *however* effectively reduced and at limit can be completely blocked.

The observation of a pure *monomeric* fluorescence and *monoexponential* decay will be considered in the following as the experimental fingerprint of the isolated molecule regime.

4 Experimental results I
Measurements in the isolated molecule limit

In the precedent sections it has been shown how through a progressive film thickness reduction the intra-layer transport phenomena via molecule-molecule interaction is strongly suppressed. At this stage, the intrinsic molecular properties appear and the effect of the interaction between molecule and the substrate on the dynamics of the electronically excited states can be directly measured.

The subject of this chapter is the study of the distance-dependent molecule-substrate interaction between isolated *MePTCDI* molecules and two prototypical semiconductor substrates (MoS_2 and *Si(111):H*) by means of low temperature time resolved fluorescence spectroscopy, making use of the spacer technique to vary the distance.

In section § 4.1, the particular case of deposition of the molecules *directly* on the substrate is considered; fluorescence spectra of ultrathin (0.01 ML) *MePTCDI* films deposited *without spacer* on MoS_2 and *Si(111):H* are compared with those measured when the molecules are deposited on the surface of a prototypical insulator (quartz).

In sections § 4.2-4.3, *spacer measurements* on MoS_2 and *Si(111):H* are reported (distance dependent measurements); the time resolved fluorescence technique is applied to the study of the fluorescence properties of ultrathin *MePTCDI* films separated from the substrate by a spacer of solid argon. In particular, the progressive shortening of the molecular lifetime upon reduction of the separation between molecules and the semiconductor is put in evidence.

4.1 Isolated molecules *directly deposited* on semiconductors: effect of molecule-substrate interaction

In this section, fluorescence measurements carried out on ultrathin (0.01 ML) *MePTCDI* films *directly* deposited on MoS_2, *Si(111):H* and quartz are reported. The experimental methods used for the preparation of the substrates are described in § 2.3.1 and § 2.3.2 for MoS_2 and *Si(111):H*, respectively; quartz has been cleaned by spectroscopic grade solvents and by successive annealing in–situ at $\sim 500\,^{\circ}\mathrm{C}$.

Fluorescence spectra

Fig. 18 shows the quasi-*cw* fluorescence spectra measured on the three substrates in a time range of $[\,0-10\,\mathrm{ns}\,]$ at $T = T_S = 10\,\mathrm{K}$. As already seen in fig. 15, at 0.01 ML coverage the fluorescence spectra have monomeric character; changing the substrate they remain similar in shape and no appreciable band shift is visible.

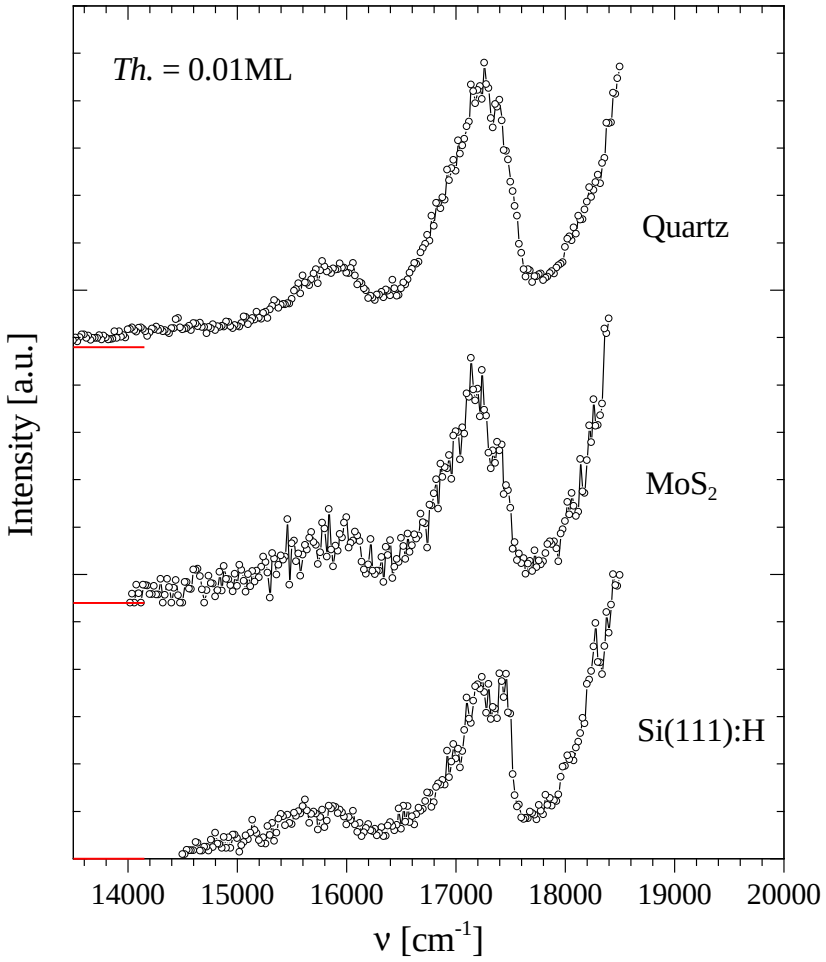

Fig. 18: In–situ, quasi-*cw* fluorescence spectra $[0-10\,\mathrm{ns}]$ of ultrathin (0.01 ML, isolated molecule limit) *MePTCDI* films *directly deposited* on quartz, *Si(111):H* and MoS_2 at $T = T_S = 10\,\mathrm{K}$. The spectra are normalized to their maxima, excitation at $\bar{\nu} = 18796\,\mathrm{cm}^{-1}$. Due to the proximity of the excitation line, the 0-0 transition peak on the high-energy side of spectra is only partially detectable.

Only the substructure (with peaks at $\bar{\nu} = 17400\,\mathrm{cm}^{-1}$ and $\bar{\nu} = 17200\,\mathrm{cm}^{-1}$), related to the main vibrational modes of the perylene core (*see* § 5.1.1), is more pronounced in the spectrum on *Si(111):H* rather than in the other two cases.

For molecules directly deposited on the three considered surfaces, the fluorescence shape turns out to be *substrate-independent*. It reveals that in these three cases the electronic levels of *MePTCDI* are *unaffected or only weakly affected* by the contact with the substrate surface.

Fluorescence transients

Beside no change in fluorescence spectra, the monomer fluorescence lifetime is *extremely* affected by the change of the substrate: fig. 19 shows the normalized fluorescence decays

of the ultrathin *MePTCDI* films of fig. 18, as detected at $\bar{\nu} = 17250\,\mathrm{cm}^{-1}$, maximum of the second emission band. The fitting curves (result of the convolution between exponential decay curves and system response function) are mono- or biexponential (with very similar decay times). While the isolated molecule fluorescence on quartz exhibits a decay time ($\tau_Q = 3.91\,\mathrm{ns}$) similar to that of the *MePTCDI* molecule in solution ($\tau_0 = 3.95\,\mathrm{ns}$), on *Si(111):H* and MoS_2 the lifetime is ***shortened*** respectively to a $\sim 1/40$ ($\tau_{Si} = 145\,\mathrm{ps}$) and to a $\sim 1/160$ ($\tau_{MoS_2} \leq 25\,\mathrm{ps}$) of this value.

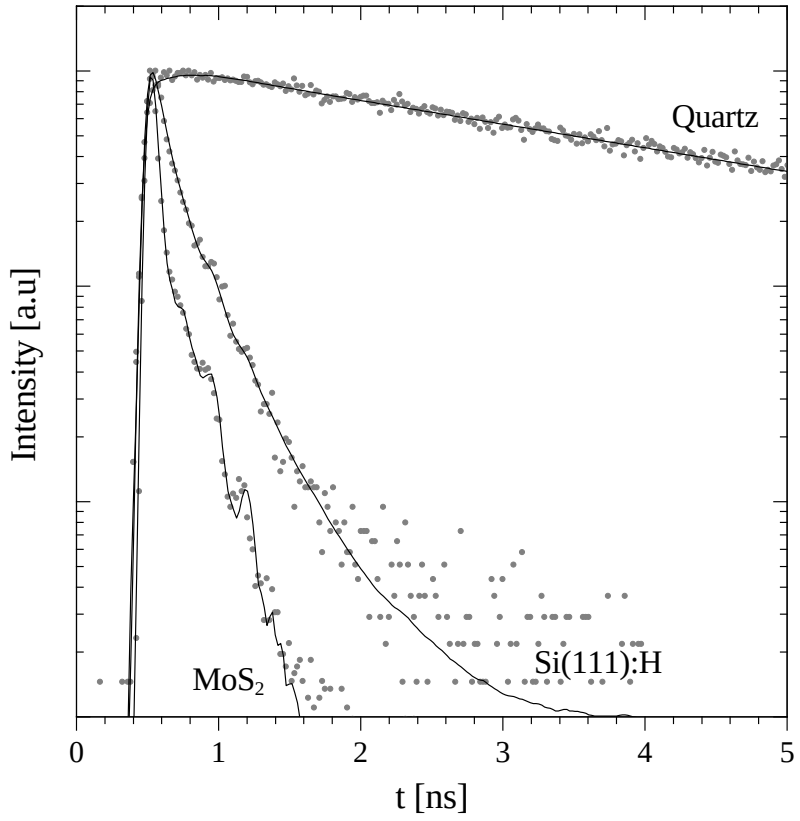

Fig. 19: In–situ normalized fluorescence decays of ultrathin *MePTCDI* films on quartz, *Si(111):H* and MoS_2 at $T = T_S = 10\,\mathrm{K}$. Detection at $\bar{\nu} = 17250\,\mathrm{cm}^{-1}$. Excitation at $\bar{\nu} = 18796\,\mathrm{cm}^{-1}$. Fitting: convolution between the system response function and mono- or bi-exponential decay curves.

Two aspects have to be pointed out:

a) compared to an insulator (quartz) *both* semiconductors present monomer fluorescence lifetime shortening

b) the shortening is quantitatively very different (about a factor 7).

The observed fluorescence lifetime shortening can be phenomenologically taken into account by adding to the system a *non-radiative deexcitation channel* for the excited state of *MePTCDI* molecule, with an effective rate k_s^{nr} independent from the radiative

one. The *nature* of this deactivation channel will be extensively discussed in the next chapter.

If k_0 is the intrinsic *MePTCDI* fluorescence decay rate in dilute solution, the *observed* decay rate k_s in presence of the substrate (with $s = Si, MoS_2$, etc.) can be expressed as the sum of two decay rates:

$$k_s = k_0 + k_s^{nr} \tag{1}$$

or, correspondingly, for the decay time:

$$\frac{1}{\tau_s} = \frac{1}{\tau_0} + \frac{1}{\tau_s^{nr}}$$

therefore

$$\tau_s^{nr} = \frac{\tau_s \tau_0}{\tau_0 - \tau_s} \tag{2}$$

that gives the non-radiative deexcitation time τ_s^{nr} (its inverse k_s^{nr} is the molecule-substrate excitation transfer rate) in terms of the experimentally observed lifetime τ_s and the intrinsic molecular lifetime τ_0.

In case of quartz, the rate turns out to be only $k_Q^{nr} = 2.59 \cdot 10^6\, s^{-1}$. The excitation transfer time from the molecule to the substrate ($\tau_Q^{nr} = 386$ ns) is almost *hundred times* greater than the intrinsic molecular lifetime.

Since the molecule-substrate excitation transfer rate is appreciably shorter than the intrinsic molecular fluorescence rate k_0, the excited molecules decay almost only in a radiative way; the presence of the quartz substrate does not affect substantially the deactivation pathway of the excited molecules and therefore it is considered as a *non-interacting* material.

In case of *Si(111):H* and MoS_2, the calculated non-radiative transfer rate amounts to $k_{Si}^{nr} = 6.7 \cdot 10^9\, s^{-1}$ and to $k_{MoS_2}^{nr} = 39.7 \cdot 10^9\, s^{-1}$, respectively about 40 and 160 times that of the molecule deposited on quartz.

Substrate	τ_s [ps]	$b_s^{-1} = \tau_s/\tau_0$ [$\cdot 10^{-3}$]	k_s^{nr}[$\cdot 10^9 s^{-1}$]	τ_s^{nr} [ps]
quartz	3910	989	$2.59 \cdot 10^{-3}$	$386 \cdot 10^3$
Si(111):H	145	37.9	6.7	150
MoS_2	≤ 25	≤ 6.3	≥ 39.7	≤ 25.1
Ag(111)	< 10	< 2.5	> 99.8	< 10

Tab. 4: Measured fluorescence lifetime τ_s, fluorescence damping rate b_s^{-1} and calculated molecule-substrate excitation transfer rate k_s^{nr} for *MePTCDI* on quartz, *Si(111):H* and MoS_2. The values for *Ag(111)* [43] are given in comparison.

The experimental value of τ_s and some related quantities are listed in tab.4, where the (extrapolated) value of monomer lifetime on *Ag(111)* substrate [43] is reported in comparison, too.

The presence of the substrate, beside a decrease of molecular fluorescence lifetime induces a decrease of fluorescence quantum yield, too. The quantum yield of fluorescence (the ratio between emitted and absorbed photons) in presence of a substrate Φ_s can be referred to that of the *free MePTCDI* molecule in dilute solution ($\Phi_{sol} = 0.93$, *see* § 3.1) by:

$$\Phi_s = \Phi_{sol} \frac{k_0}{k_0 + k_s^{nr}} \quad \rightarrow \quad \frac{\Phi_s}{\Phi_{sol}} = \frac{\tau_s}{\tau_0} \equiv b_s^{-1} \tag{3}$$

where b_s^{-1} is the damping rate of fluorescence in presence of the substrate.

In the next sections, it is shown how the *MePTCDI* monomer fluorescence properties change upon variation of the *distance* between isolated molecules and the semiconductor substrate.

Distance dependent molecule-substrate interaction on semiconductors: spacer measurements

In the following sections, the *distance dependent* time resolved fluorescence measurements of ultrathin *MePTCDI* molecular films (0.01 ML) deposited on the two semiconductor substrates are considered (*spacer measurements*).

The spacer layer technique has been already used in § 3.4.1 to separate thin *MePTCDI* films from MoS_2 substrate. There, the spacer thickness was kept constant (170 Å), whereas the thickness of the film deposited on it was progressively reduced; on the contrary, in the following sections the *spacer* thickness is varied, whereas on the top of it an ultrathin *MePTCDI* film of constant thickness (0.01 ML) is deposited.

All the following spacer-measurements were carried out in a similar way, differing only the pre-treatments of substrate; for MoS_2: cleaving and in–situ annealing, § 2.3.1; for *Si(111):H*: wet chemical treatment (modified *RCA*-process, § 2.3.2).

4.2 *Spacer* measurements on MoS_2

In this section the spacer measurements on MoS_2 are presented. All the samples have been created exclusively using freshly prepared MoS_2 substrates; the experimental method to obtain a defect free MoS_2 surface are described in § 2.3.1. The spacer of solid argon is condensed following the process reported in § 2.1.3. The argon spacer has been *preventively annealed* to minimize possible residual undulations of the spacer surface (§ 5.2). The ultrathin (0.01 ML) *MePTCDI* film was finally deposited following the method described in § 2.1.4.

Fluorescence spectra

Fig. 20 shows the *distance dependent* quasi-*cw* fluorescence spectra of 0.01 ML *MePTCDI* films separated from a MoS_2 substrate by an argon spacer of variable thickness d_{sp} in the range [0-500 Å]; time interval $[\,0-10\,\mathrm{ns}\,]$, $T = T_S = 10\,\mathrm{K}$.

The spectra exhibit a typical monomer fluorescence that *does not depend* on the distance from the substrate and *no monotonic shift* in peak positions and shape can be observed. Both at $d_{sp} = 500\,\text{Å}$ as well as at direct contact with the substrate ($d_{sp} = 0\,\text{Å}$), only the fluorescence from isolated molecules can be detected. No red excimer-like emission appears.

Similarly to fig. 18, it is not possible to resolve completely the high energy emission band because of the proximity of the laser excitation line (at $\bar{\nu} = 18796\,\mathrm{cm}^{-1}$).

Fluorescence transients

In contrast to negligible changes in fluorescence spectra, the fluorescence decays exhibit

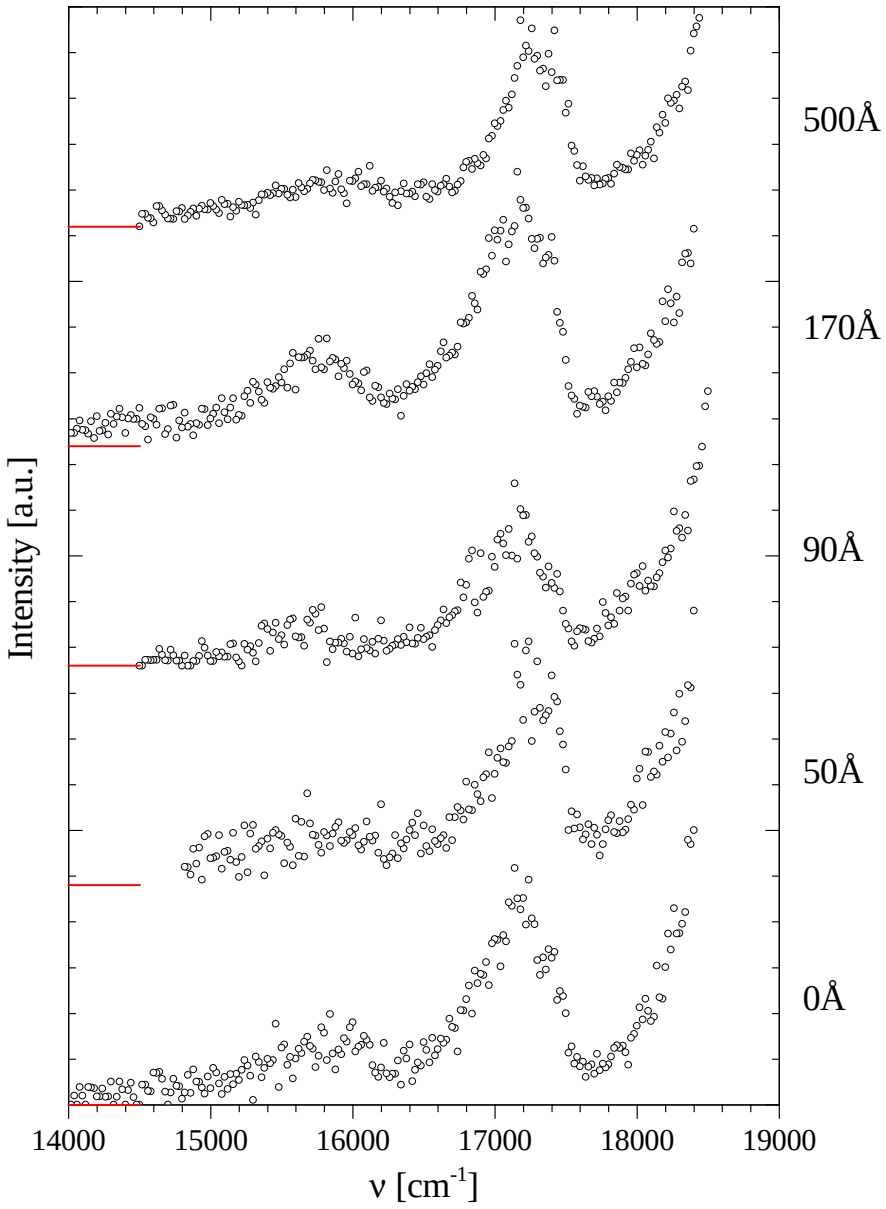

Fig. 20: In–situ distance dependent quasi-*cw* fluorescence spectra of ultrathin (0.01 ML) *MePTCDI* films on MoS_2, at $T = T_S = 10\,\mathrm{K}$. The distance is defined by a spacer of solid argon of thickness d_{sp} [0-500 Å] indicated on the right side. The spectra are normalized to their maxima, excitation at $\bar{\nu} = 18796\,\mathrm{cm}^{-1}$. Time range $[\,0-10\,\mathrm{ns}\,]$.

a *strong* change upon spacer thickness reduction. Fig. 21 shows the distance dependent [0-500 Å] fluorescence decays, as measured at $\bar{\nu} = 17300\,\mathrm{cm}^{-1}$ in the time range $[\,0-10\,\mathrm{ns}\,]$.

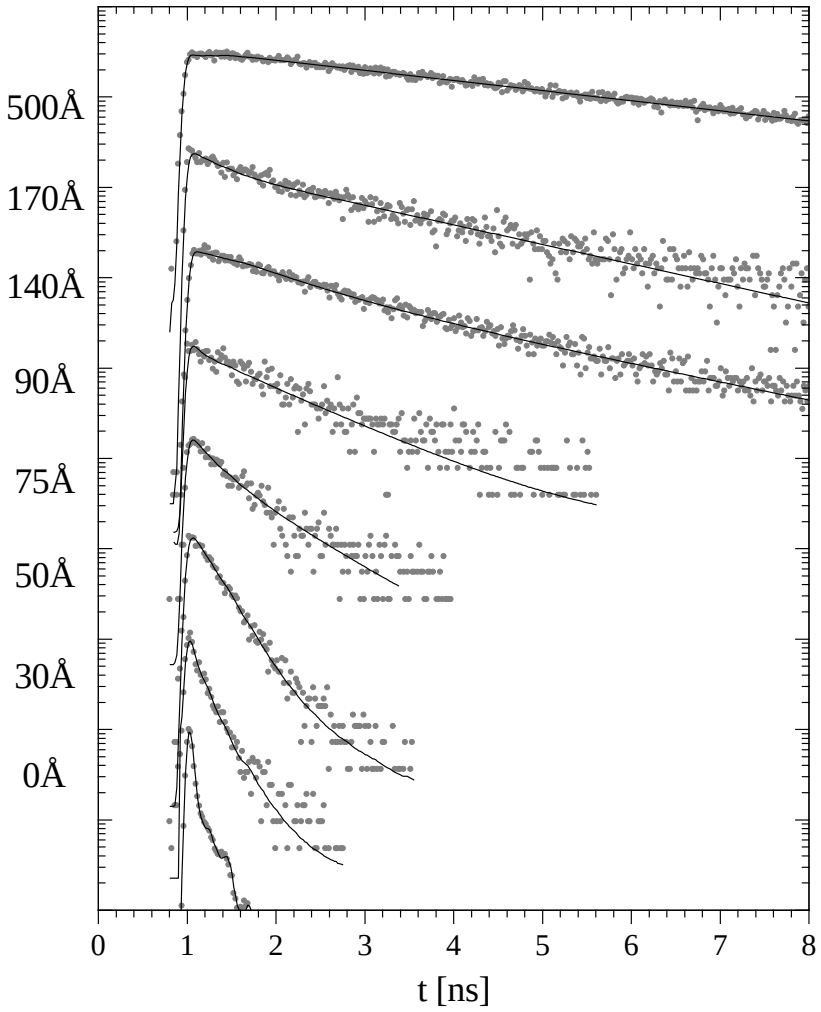

Fig. 21: In–situ distance dependent [0-500 Å] fluorescence decays of ultrathin (0.01 ML) *MePTCDI* films on MoS_2, at $T = T_S = 10\,\mathrm{K}$. The distance is defined by a spacer of solid argon whose thickness d_{sp} is indicated on the left side. Excitation at $\bar{\nu} = 18796\,\mathrm{cm}^{-1}$, detection at $\bar{\nu} = 17300\,\mathrm{cm}^{-1}$, time range $[\,0-10\,\mathrm{ns}\,]$. Fitting mono- and bi-exponential (*see* p. 58).

In tab. 5 the observed monomer lifetime (τ_{obs}) and the normalized lifetime ($\mathrm{a} = b^{-1} = \tau_{obs}/\tau_0$, with $\tau_0 = 3950\,\mathrm{ps}$, lifetime in solution) are tabulated as a function of the argon spacer thickness d_{sp}.

Upon decreasing the molecule-substrate distance from 500 Å down to the direct contact, the observed *MePTCDI* fluorescence lifetime (as drawn out by a mono- and bi-exponential fitting of the experimental decay curves, see below) exhibits a more than two orders of magnitude shortening.

d_{sp} [Å]	τ_{obs} [ps]	a [%]
0	$\leq$25	0.6
35	75	1.9
50	220	5.6
75	510	12.9
90	880	22.3
140	1730	43.8
170	1790	45.3
500	3860	97.7

Tab. 5: *MePTCDI* monomer fluorescence lifetime (τ_{obs}) and normalized lifetime ($a = \tau_{obs}/\tau_0$) as measured on freshly cleaved MoS_2 substrate for different argon spacer thicknesses (d_{sp}). Average values drawn out from mono- and bi-exponential fitting of fluorescence transients (*see* p. 58).

In particular, whereas the molecular fluorescence lifetime on the top of a 500 Å thick spacer ($\tau_{500\,A} = 3860$ ps) is of the same order of magnitude of that of molecule in solution, the fluorescence at $d_{sp} = 0$ Å (direct contact) exhibits (as already shown in § 4.1, fig. 19) a decay hardly distinguishable from the system response function ($\tau_{0A} < 25$ ps).

As at 0.01 ML intra-layer transport and trapping phenomena are excluded, the fluorescence lifetime shortening has to be completely ascribed to an effective *excitation transfer* to the substrate.

If the observed molecular fluorescence lifetime (τ_{obs}) is plotted versus the argon thickness d_{sp}, the shortening effect as a function of the emitter-substrate distance is evidenced (fig. 22). The strong dependence of τ_{obs} on the molecule-substrate distance is non-linear. According to eq. 3 also the excitation transfer rate k_s^{nr} varies non-linearly with the emitter-substrate distance.

A quantitative description of these phenomena obtained by applying the theoretical model described in chapter 6, will be given in the section dedicated to the discussion of results on MoS_2 (§ 8.3).

Origin of the residual non-exponentiality in fluorescence transients

The observed deviation of fluorescence transients from a mono-exponential behaviour (and therefore the necessity, sometimes, to use a sum-of-exponentials (typically 2) function to fit the decays) is essentially due to:

a) residual spacer undulation or roughness

b) orientation of *MePTCDI* molecules with respect to the substrate

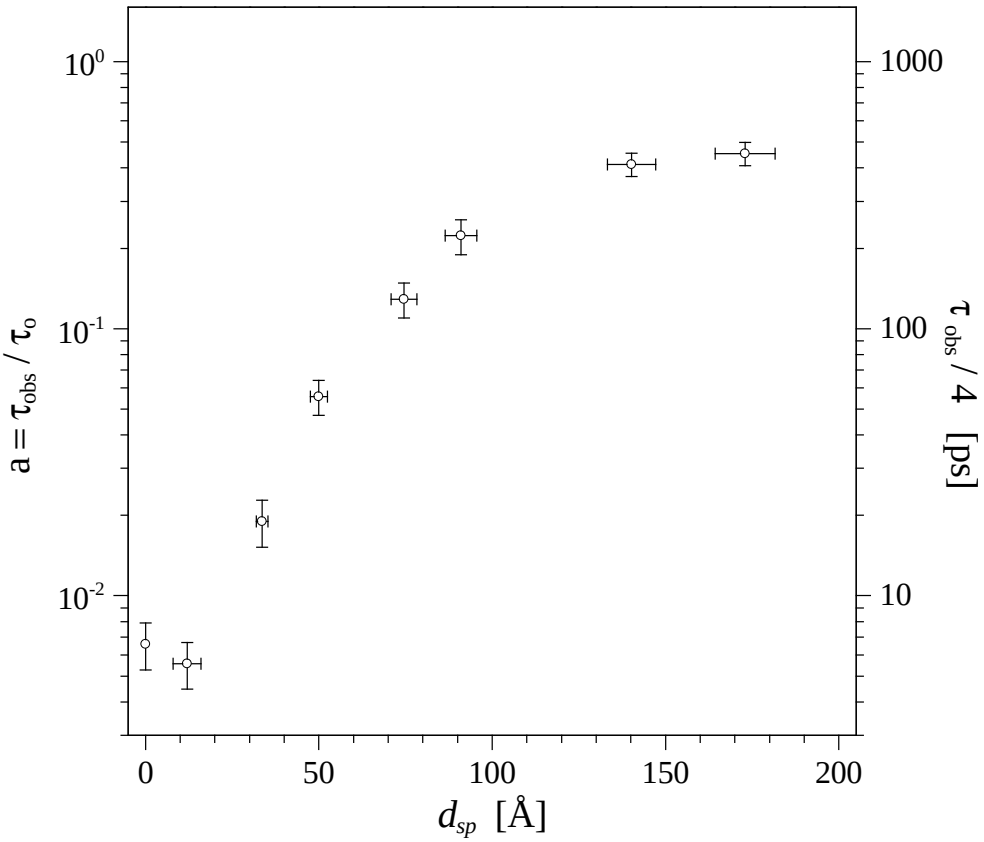

Fig. 22: *MePTCDI* monomer lifetime (τ_{obs}) and normalized lifetime ($a = \tau_{obs}/\tau_0$, with $\tau_0 = 3950$ ps, lifetime in solution) on MoS_2 as a function of argon spacer thickness d_{sp}, at $T = T_S = 10$ K.

c) residual transfer inside the ultrathin molecular film (limited 'isolated molecule' condition)

- The argon layer is actually planar, but only because a preparation process (*see* § 2.1.3) to reduce the initial inhomogeneity has been carried out. In spite of this, a residual undulation can still exist after the applied treatment. As explained in § 5.2, the residual non planarity results in a deviation from mono-exponentiality of the fluorescence decay.
- Apart from the distance from the substrate, the fluorescence lifetime shortening effect depends also on the relative orientation (*see* § 6.1) between molecule and substrate (i.e. the effect is slightly different for parallel or perpendicular molecules). As the deposited *MePTCDI* molecule can assume every orientation with respect to the substrate (even if the flat lying and 'on edge' positions turn out to be the more probable, *see* § 8.3 and § 8.4), the observed fluorescence transient is a superposition of decays with slightly different times, therefore non-monoexponential in nature.
- Finally, if the molecular coverage is only some percent higher than 0.01-0.02 ML, the residual excitation transfer between the molecules inside the film causes a change in the

statistic of the radiative decay of molecular excited state and once more a deviation from an exact mono-exponential fluorescence decay behaviour [34, 43].

4.3 *Spacer* measurements on *Si(111):H*

In this section the spacer measurements on *Si(111):H* are presented. The experimental method to obtain an inert, oxide-free, hydrogen-terminated silicon (111) surface is reported in § 2.3.2. All the samples were prepared from *freshly* passivated silicon substrates, chemically treated *ex*-situ (modified RCA-process) and immediately transferred in *UHV*. The argon layer is prepared following the process described in § 2.1.3. The argon spacer was *annealed* to minimize possible residual spacer surface undulations (*see* § 5.2). The ultrathin (0.01 ML) *MePTCDI* film was deposited as described in § 2.1.4.

Details on the samples

As a substrate, 5×5 mm samples cut from a *Si(111)* wafer (Wacker-Chemitronic) were used, with the following properties : n-type doping (phosphor), room temperature resistivity $\rho = (1.05-1.95)\,\Omega\cdot$cm, dopant concentration $N_{D,A} = (2-4)\cdot 10^{15}\,\mathrm{cm}^{-3}$, crystal thickness $\theta = 505\,\mu$m. These values, in particular that of resistivity, were chosen to permit a direct comparison with the precedent experimental research in our group. The substrate resistivity however is not a key-parameter in the molecule-substrate interaction.

In fact, as assessed in a precedent study on *Si(111):H* [43] the electric conduction properties of the silicon substrate have *no effect* on the molecule-substrate interaction phenomena and therefore on the fluorescence lifetime of an electronically excited *MePTCDI* molecule. In particular, temperature dependent molecular fluorescence lifetime measurements of films directly deposited on *Si(111):H* show no change in fluorescence decays upon a temperature change from $T = 10$ K to $T = 200$ K, corresponding to a change of silicon conductivity of a number of orders of magnitude. The molecular fluorescence lifetime shortening effect does not appear therefore to be related to the carrier density inside the semiconductor.

Fluorescence spectra

Fig. 23 shows the distance-dependent quasi-*cw* fluorescence spectra of ultrathin films separated from a *Si(111):H* substrate by a variable thickness argon spacer in the range [0-130 Å]; time interval $[0-10\,\mathrm{ns}]$, $T = T_S = 10$ K. The high-energy fluorescence band is only partially detectable because too close to the excitation line. As already observed on MoS_2, also in films deposited on silicon the spectra exhibit a pure monomer fluorescence whose position and shape *does not depend* on the distance from the substrate. Both at $d_{sp} = 130$ Å as well as at direct contact with the substrate ($d_{sp} = 0$ Å), only the fluorescence from isolated molecules can be detected without excimer-like emission. Moreover, the

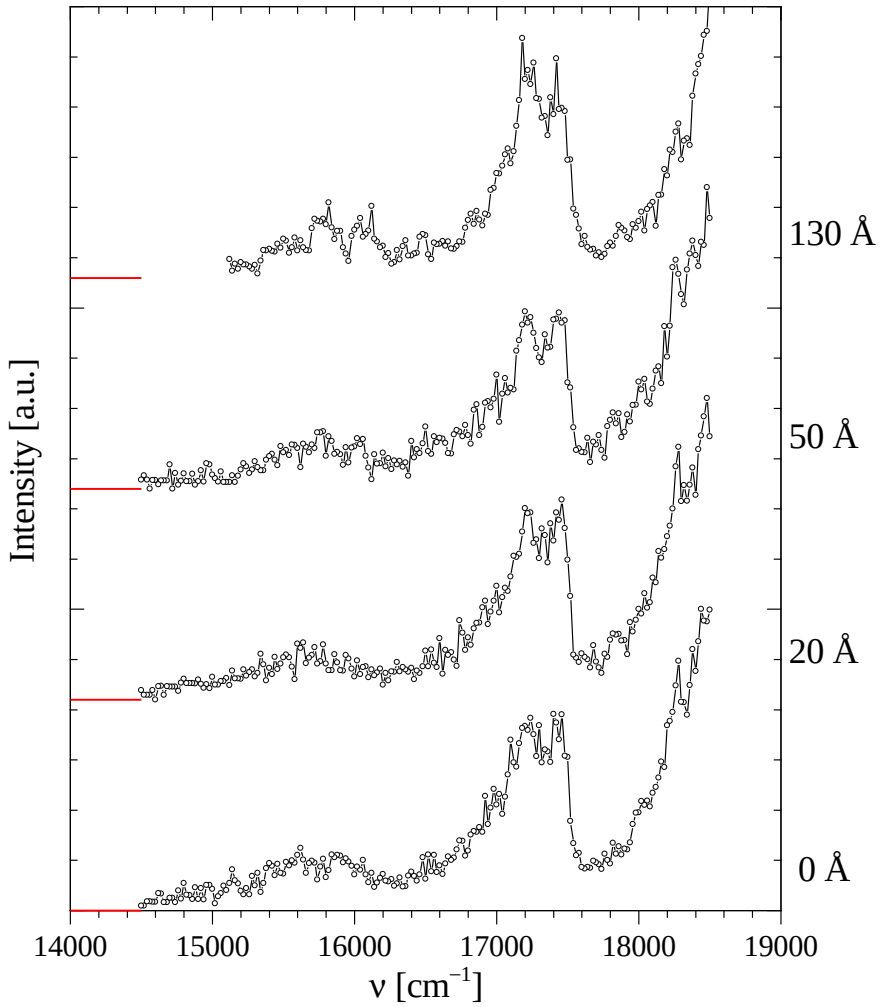

Fig. 23: In–situ distance dependent quasi-*cw* fluorescence spectra of ultrathin (0.01 ML) *MePTCDI* films on freshly prepared *Si(111):H*, at $T = T_S = 10\,\mathrm{K}$. The distance is defined by a spacer of solid argon, whose thickness d_{sp} [0-130 Å] is indicated on the right. The spectra are normalized to their maxima, excitation at $\bar{\nu} = 18796\,\mathrm{cm}^{-1}$. Time range $[\,0-10\,\mathrm{ns}\,]$.
Peak positions of the vibrational structure visible in the fluorescence spectra: $\bar{\nu} = 18230\,\mathrm{cm}^{-1}$, $17440\,\mathrm{cm}^{-1}$, $17215\,\mathrm{cm}^{-1}$, $16040\,\mathrm{cm}^{-1}$ and $15800\,\mathrm{cm}^{-1}$.

spectra exhibit a strong vibrational substructure, whose peak positions are given in the caption of fig. 23.

Fluorescence transients

Fig. 24 and Fig. 25 show (with and without offsetting of the curves) the distance dependent [0-130 Å] fluorescence decays as measured at $\bar{\nu} = 18400\,\mathrm{cm}^{-1}$ in the time range $[\,0-10\,\mathrm{ns}\,]$.

Similarly to the case of MoS_2 also on *Si(111):H*, beside a negligible change in fluorescence spectra, the fluorescence decays exhibit a pronounced shortening upon spacer

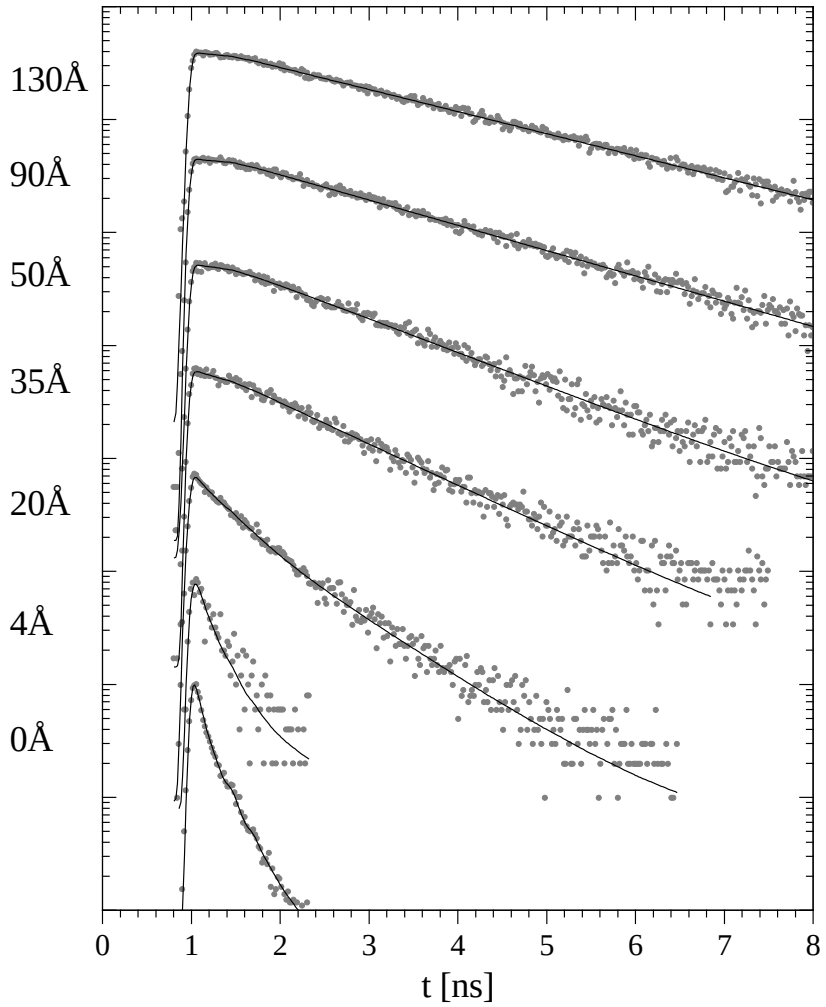

Fig. 24: In–situ distance dependent fluorescence decays of ultrathin (0.01 ML) *MePTCDI* films on *Si(111):H*, at $T = T_S = 10\,\mathrm{K}$, for d_{sp} in the range [0-130 Å]. Excitation at $\bar{\nu} = 18796\,\mathrm{cm}^{-1}$, detection at $\bar{\nu} = 18400\,\mathrm{cm}^{-1}$, time range $[0 - 10\,\mathrm{ns}]$. The decays are normalized to their maxima.

thickness reduction.

The *MePTCDI* fluorescence lifetime shortening effect measured on *Si(111):H* is however not as strong as that observed on MoS_2 (sligthly more than one order of magnitude on with respect to more than two orders of magnitude on MoS_2). Furthermore, in contrast to the MoS_2 case, even on thin argon spacer ($d_{sp} \leqslant 15$Å) the observed fluorescence decay is still well above the system detection limit.

Upon decreasing the spacer thickness from 130 Å to 0 Å, a shortening of ~ 30 times in *MePTCDI* monomer lifetime can be drawn out by the fitting of fluorescence decays.

In tab. 6 the monomer lifetime (τ_{obs}) and normalized lifetime ($\mathrm{a} = \tau_{obs}/\tau_0$, with $\tau_0 = 3950\,\mathrm{ps}$, lifetime in solution) of the films deposited on *Si(111):H* are tabulated as

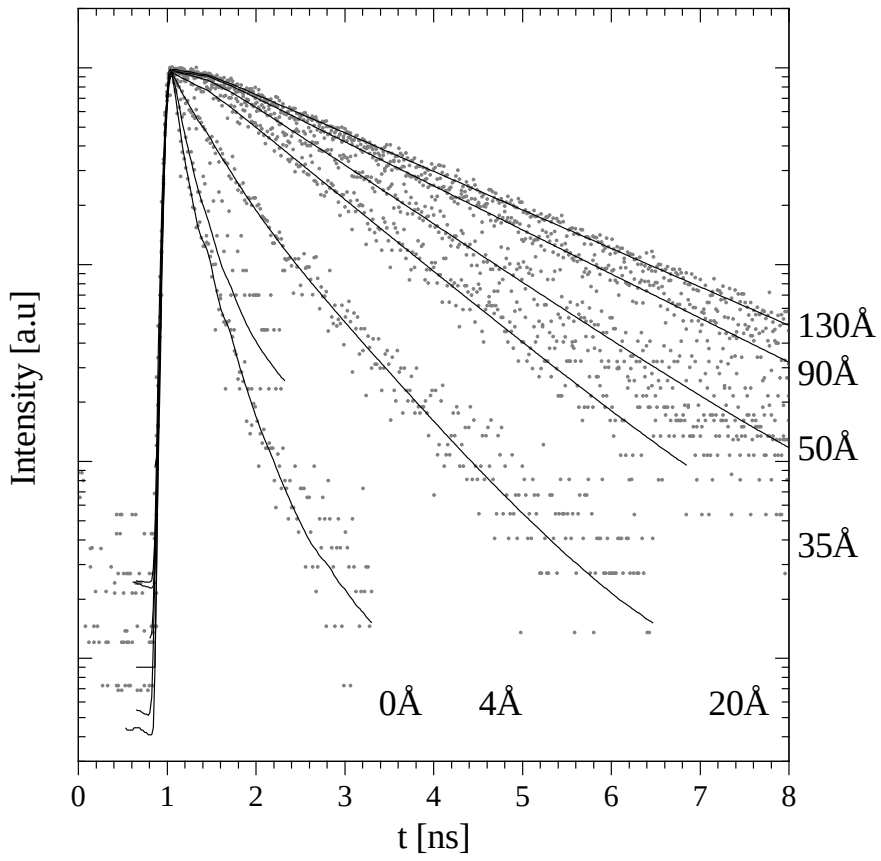

Fig. 25: Same fluorescence decays of fig. 24 plotted without vertical offset to evidence the progressive fastening in fluorescence decay upon reduction of the spacer thickness.

d_{sp} [Å]	τ_{obs} [ps]	a [%]
0	145	3.6
4	257	7.0
20	840	21.3
35	1175	29.7
50	1460	37.0
90	1935	49.0
130	2205	55.8

Tab. 6: *MePTCDI* monomer lifetime (τ_{obs}) and normalized lifetime ($a = \tau_{obs}/\tau_0$) as measured on *Si(111):H* for different argon spacer thickness (d_{sp}). Average values drawn out from mono- and bi-exponential fitting of fluorescence transients (*see* p. 58).

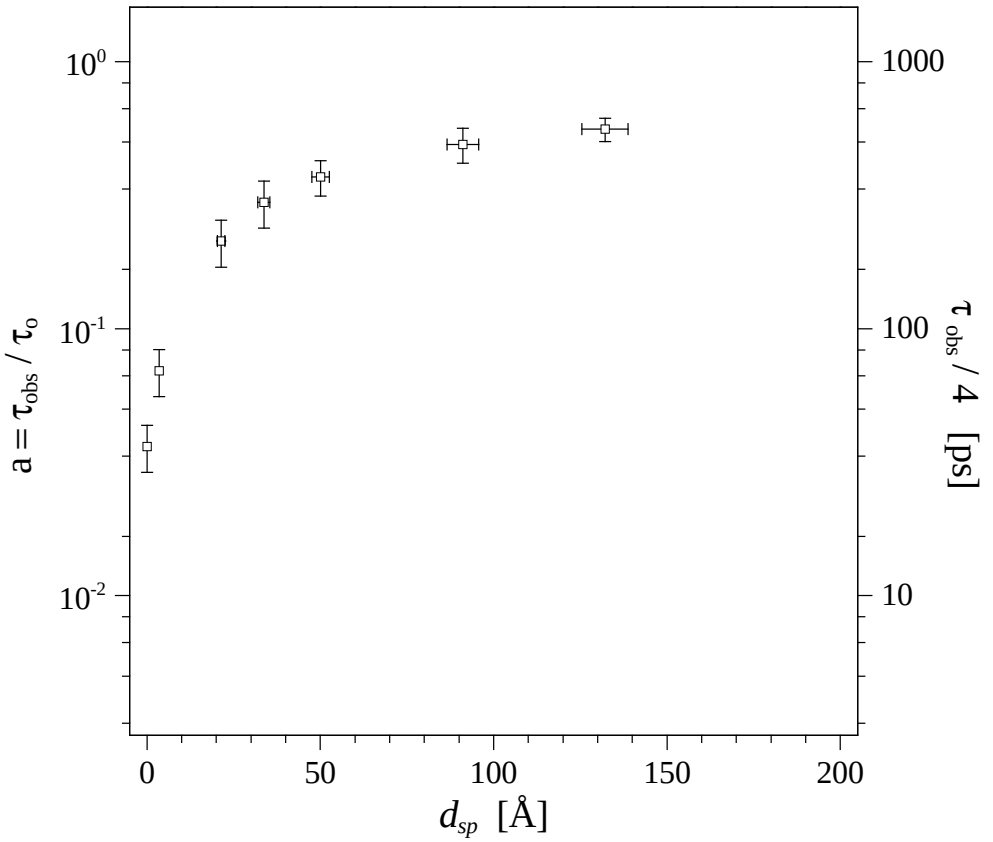

Fig. 26: *MePTCDI* monomer lifetime (τ_{obs}) and normalized lifetime ($a = \tau_{obs}/\tau_0$) on *Si(111):H* as a function of the argon spacer thickness d_{sp}, at $T = T_S = 10\,\mathrm{K}$. Same x and y scales as in fig. 22.

a function of argon spacer thickness d_{sp}.

In Fig. 26 the distance dependent *MePTCDI* fluorescence lifetime is plotted versus d_{sp} in semilogarithmic scale to evidence the shortening at distances d_{sp} below 50 Å. The x and y scales are the same as in fig. 22 and permit a direct comparison between the effect on *Si(111):H* and on MoS_2.

In the case of *Si(111):H* the fluorescence lifetime shortening exhibits a dependence on the spacer thickness different from that observed on MoS_2. In particular, whereas on silicon this effect is remarkable only below 50 Å spacer thickness, on MoS_2 already below 120-130 Å spacer thickness the lifetime shortening is more than 50%.

A quantitative description of these experimental results obtained by applying the theoretical model described in chapter 6 will be given in the section dedicated to the discussion of results on *Si(111):H* (§ 8.4).

5 Experimental results II
Sample treatments and their effect on film fluorescence properties

The measurements on MoS_2 and on *Si(111):H* described in the last chapter were based on use of always new, *freshly prepared* substrates and on optimized experimental procedures. A great number of other measurements has been however carried out to study what kind of effect have the treatments applied to the substrate surface and to the argon layer on the fluorescence properties of the ultrathin *MePTCDI* films deposited on top.

While the use of the MoS_2 substrate does not give particular problems, various aspects have to be taken into account by using *Si(111)*. As pointed out in § 2.3.3, the necessary condition for a correct estimation of the actual distance between the *MePTCDI* molecules and the *bare Si(111)* substrate is the *removal of the oxide layer* naturally grown on the surface.

The wet chemical process (RCA-modified method, *see* § 2.3.2) used to prepare the *Si(111)* substrate does result in a complete oxide layer removal from the surface. However, the price to pay for this is an enhanced reactivity of the surface due to the unsaturated free (dangling) silicon bonds that are created [54]. For this reason the last step of the preparation is the passivation of the free bonds by means of hydrogen atoms (H-passivation).

Nevertheless, differently from the naturally grown oxide layer the H-passivation layer is unstable (especially upon annealing at $T > 200\,^{\circ}\mathrm{C}$ of the sample) and the possibility of loosing part of hydrogen atoms does exist also under normal experimental conditions.

The lost of hydrogen atoms causes the enhancing of silicon surfacial reactivity that usually results in its 'contamination' through the binding on the surface of molecules and residual gas atoms.

In § 5.1, the effects of the annealing applied to passivated silicon substrates ($T \sim 200-450\,^{\circ}\mathrm{C}$) are analysed. In particular in § 5.1.1, the effect of the presence of adsorbed molecules on the *Si(111)* surface (result of a contamination, consequence of the annealing treatment) is studied by time resolved fluorescence techniques. Successively, in § 5.1.2 silicon surfaces with adsorbed molecules on it *are used as substrate* for a series of distance-dependent measurements; the effect of the presence of bound-to-the-surface *MePTCDI* molecules on the fluorescence properties of a molecular film deposited at a distance d_{sp} is exemplified and discussed.

The section § 5.2 is dedicated to a different (but related to the precedent) aspect: the analysis of the effects of a treatment consisting in a slight warming up of the system (substrate/spacer/molecules) up to $\sim 70\,\mathrm{K}$. The *MePTCDI* molecular fluorescence is used

in this case as a *sensor* to monitor the change of thickness of the argon spacer on which the molecules are deposited.

5.1 *Si(111)*, surfacial reactivity and adsorption of *MePTCDI* molecules

During the experiments on *Si(111)*, it has been an open question if it was somehow possible to 'regenerate' the substrate after each measurement session by flushing away any deposited organic molecule from the surface. The advantage would be that the substrate remains permanently under well controlled *UHV* conditions and the average level of contaminants could be kept very low [j].

Differently from the case of metals, using silicon as substrate the chemical passivation treatment needs to be carried out (ex-situ) to obtain a suitable surface for the present scopes (*see* § 2.3.2). After the first low-temperature experimental run (argon spacer condensation and organic film deposition), the surface cannot be however easily 'flushed' just by annealing the sample above the *MePTCDI* desorption temperature, because the H-termination becomes unstable and many silicon atoms loose their hydrogen atom. It has been observed as the loosing of H atoms starts already at $T = 280\,^{\circ}\mathrm{C}$ and it is practically completed at $T = 450\,^{\circ}\mathrm{C}$ [54, 113, 114]. As a consequence, the surface acquires again all its strong reactivity because of the presence of newly free dangling bonds.

In the following section, it is experimentally shown and discussed how, upon annealing of the silicon substrate, organic molecules can be captured and strictly bound in chemically active trapping centers localized in the unsaturated bonds of the surface.

5.1.1 *MePTCDI* adsorption on *Si(111)* surface

In the course of the present work, it has been found that if instead of a fresh one, the *same Si(111)* substrate is used for further depositions after an annealing treatment ($6-12$ hours at $T_{ann} = 450\,^{\circ}\mathrm{C}$, in–situ) and a new experimental run is carried out, both fluorescence spectra and transients exhibit *evident modifications* with respect to what observed on freshly passivated substrates.

Molecular films successively deposited on such substrates exhibit (1) a very weak monomeric fluorescence spectrum, slightly deformed and with *sharp peaks* superimposed to the three typical broad emission bands, (2) the fluorescence transients are very fast and strongly non-exponential.

[j] Any metallic single crystal can be re-used upon a treatment consisting in an annealing at $T = 450\,^{\circ}\mathrm{C}$ to desorb the majority of deposited organic molecules, followed by diverse sputtering-annealing cycles within preparation chamber; after this treatment, the metallic substrate presents a reconstructed surface, regular and nearly contaminant free [58, 112].

These two experimental findings are interpreted as the result of a contamination of the silicon surface, consequent the annealing treatment. The hypothesis is that upon annealing the surface partially looses its passivation and its reactivity is enhanced.

In the next paragraphs, it is studied how the observed change of fluorescence properties can be ascribed to the *chemical binding* of *MePTCDI* molecules on the reactive centers of *Si(111)* surface.

a) Preparation of a reactive test-*Si(111)*-surface
To study the effect of the existence of a chemical bond between the molecules and the reactive silicon surface on the fluorescence properties of *MePTCDI*, time resolved fluorescence measurements have been carried out on molecular films directly deposited on *Si(111)* substrates characterized by *incomplete* passivation. In these substrates a number of unsaturated dangling bonds make the surface reactive.

A partially reactive *Si(111)* surface ('test-substrate') was obtained by annealing (12 hours long) in–situ at $T = 400\,^{\circ}\mathrm{C}$ a freshly-passivated silicon sample. At this temperature nearly all the passivating H atoms are desorbed [54, 113] and the surface acquires great chemical reactivity. Successively, the *MePTCDI* molecules are deposited (at $T_S = 10\,\mathrm{K}$) on it, following the procedure described in § 2.1.4.

b) Fluorescence spectra of *MePTCDI* molecules adsorbed on reactive *Si(111)*
Fig. 27 shows (A) the fluorescence spectrum of a 0.01 ML *MePTCDI* film *directly* deposited on the reactive *Si(111)* test-substrate as collected in the time interval $[\,0-200\,\mathrm{ps}\,]$ after the excitation pulse rise, in comparison to (B) a low temperature, substrate-independent ordinary fluorescence spectrum of a 0.01 ML *MePTCDI* film measured in the same time interval.

When the *MePTCDI* molecules are deposited directly on the reactive silicon test surface, the observed fluorescence spectrum strictly reminds what is normally observed using a re-used *Si(111)* substrate. This confirms that upon sample annealing, the consequent 'contamination' of its surface happens mainly through the capture of *MePTCDI* molecules [k] by its surfacial free bonds. Further, the integrity of the *MePTCDI* molecule on the surface cannot at this stage be proofed.

Nevertheless, on the base of previous researches concerning the binding properties of large perylene derivatives on *Si(111)* (*see* p. 25 and references therein), it is possible to represent the 'contaminated' silicon surface as covered by a random distribution of immobilized *MePTCDI* molecules, distorted in their external chemical bonds, with a percentage of coverage estimated from deposition parameters to be below 0.05 ML.

[k] but contributions from any other molecule in the *UHV* chamber are not excluded

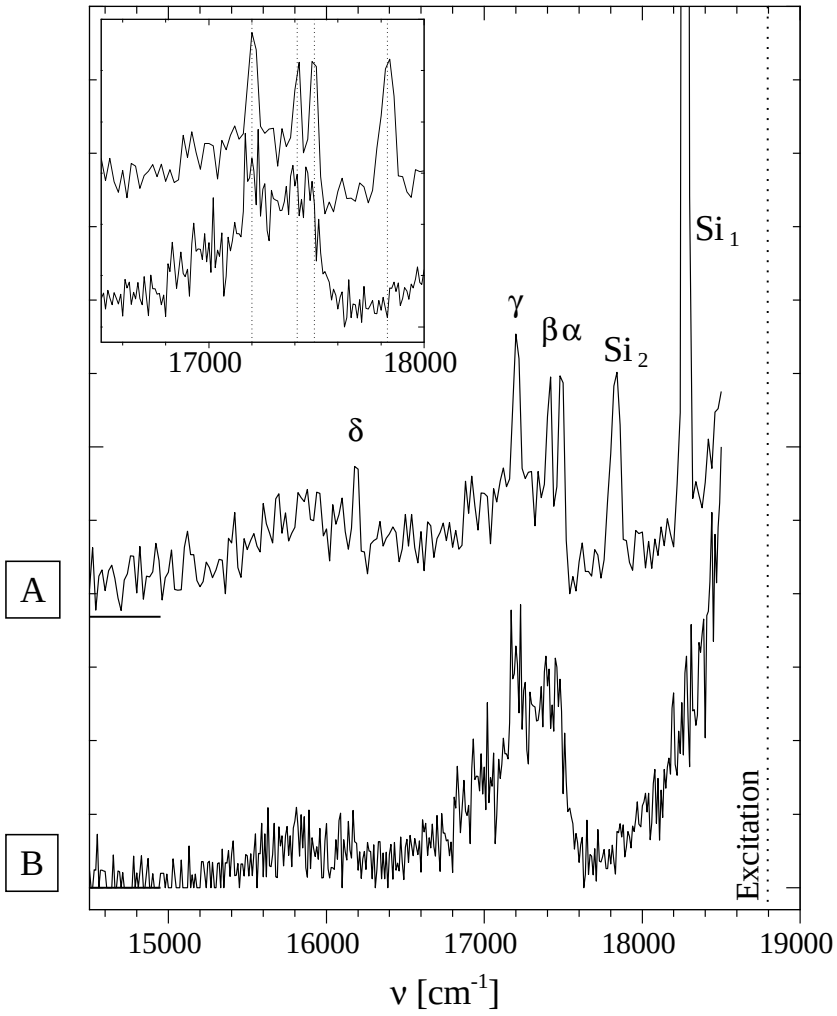

Fig. 27: A) In–situ fluorescence spectrum of ultrathin (0.01 ML) *MePTCDI* film directly deposited on reactive *Si(111)* in the time interval $[0-200\,\mathrm{ps}]$ after the excitation pulse rise. The spectra generally exhibit narrow lines overlapping to a broad band structure. In comparison B), prototype of substrate-independent fluorescence spectrum of 0.01 ML *MePTCDI* film, measured in the same time interval. The inset shows the region around $\bar{\nu} = 17400\,\mathrm{cm}^{-1}$: the lines in A) are $\sim 20\,\mathrm{cm}^{-1}$ blue-shifted with respect to the substructure in B). *See* text for details. $T = T_S = 10\,\mathrm{K}$. Excitation at $\bar{\nu} = 18796\,\mathrm{cm}^{-1}$.

The two spectra of fig. 27 can be so commented:

A) when a 0.01 ML *MePTCDI* film is deposited on a reactive *Si(111)* substrate, its fluorescence spectrum consists of two components: a broad one and series of lines. The broad features, owing to the similarity with the spectrum in B, are interpreted as monomer fluorescence, whereas the series of narrow lines has the following characteristics:

- The sharp lines Si_1 and Si_2 are related to bulk silicon substrate: they are visible in the emission spectra of the *bare* silicon substrate (passivated or not) without *MePTCDI* molecules deposited on, under strong excitation condition.
- The remaining peaks ($\alpha-\delta$) are visible exclusively in fluorescence spectra of *MePTCDI* film deposited on a reactive silicon surface.

The fluorescence transients, as measured both at the position of the broad features and at that of the sharp peaks, are indistinguishable from the system response function: in both cases, the fluorescence lifetime is *below* the system time resolution.

B) when a 0.01 ML *MePTCDI* film is deposited on a well prepared substrate (indipendently from the type of substrate), again two overlapping fluorescence components are observed (broad and narrow bands), but with different characteristics with respect to case A. In fact:

- The relative intensity of the narrow peaks with respect to the broad monomer emission as well as their spectral position are substrate independent [a].
- The fluorescence decay related to the broad and the narrow bands does not present difference and the correspondent fluorescence lifetime value depends on the substrate type (as in fig. 19).

Further, from the comparison of the two spectra, as shown in the inset of fig. 27, the $\alpha-\delta$ peaks in A) appear slightly blue-shifted ($\sim 20\,\mathrm{cm}^{-1}$) with respect to that of B).

Although it was not possible to change the energy of the excitation line ($\bar{\nu}_{exc} = 18796\,\mathrm{cm}^{-1}$), the ratio between the intensity of the line (Si_1) at $\bar{\nu} = 18275\,\mathrm{cm}^{-1}$ as measured in two successive time intervals ([0 − 240 ps] and [240 − 980 ps]) is in agreement with the ratio between the integrated number of incoming photons in these two time intervals. This suggests the origin of all the lines is related to scattering phenomena. As the excitation energy ($\bar{\nu} = 18796\,\mathrm{cm}^{-1}$) is located just $\sim 100\,\mathrm{cm}^{-1}$ below the maximum of low-temperature absorption of *MePTCDI* ultrathin film (estimated at $\bar{\nu} = 18890\,\mathrm{cm}^{-1}$ [43]) *resonant Raman* scattering can take place in the molecule and Raman lines are expected to appear overlapped to the fluorescence spectrum; under these conditions the Raman scattering cross section is predicted to be increased by a factor up to 10^3 [115]. The experimental findings can be therefore interpreted as follows.

[a] Measurements with the same results were carried out on *Ag(111)*, *Si(111)*, MoS_2 and quartz.

−*MePTCDI* backbone vibrations and assignment of the features in fig. 27.A
The fluorescence spectra can be described by the superposition of a broad monomeric fluorescence originating from isolated *MePTCDI* molecules and Raman scattering lines both from the substrate and from the organic molecules deposited on it.

The two lines Si_1 and Si_2, present also on the bare *Si(111)* substrate, are assigned to phonon modes of silicon crystal. In particular, the dominating feature at about $\bar{\nu} = 18275\,\mathrm{cm}^{-1}$ corresponds to the Transverse Optical (TO) phonon mode ($\Delta\bar{\nu} \simeq 520\,\mathrm{cm}^{-1}$) of the bulk silicon [116] [117].

The intensity of this line depends on the detection geometry and it is negligible in presence of strong monomer fluorescence. The second sharp line (Si_2, at $\bar{\nu} = 17830\,\mathrm{cm}^{-1}$) is related to overtones and combinations of various low energies optical phonons [118].

Beside these two strong lines, a number of other Raman peaks are visible in the region $\Delta\bar{\nu} = 1300-1600\,\mathrm{cm}^{-1}$, between $\bar{\nu} = 17500\,\mathrm{cm}^{-1}$ and $\bar{\nu} = 17000\,\mathrm{cm}^{-1}$. This range of energies is known to be the Raman scattering 'fingerprint' of the perylene derivatives, according to measurements carried out on thin films [119–122] and on single crystals [123].

In several perylene derivatives (i.e. *PTCDA*, *MePTCDI*, *PTCDI*, *PTCDS*), the influence of the heteroatoms on the optical properties and on the vibrational modes is generally found to be small [78]. In particular, the main vibrations (basically in-plane stretching and bending modes) are those of the *perylene core*; for this reason it is reasonable to describe the observed lines in term of experimental Raman modes of the *MePTCDI* molecule [94] and of theoretical analysis generally valid for all the perylene derivatives.

Due to symmetry restrictions (*MePTCDI* belongs to D_{2h} symmetry point group), as already observed on *PTCDA* [123,124], only fully symmetric A_g vibrations of the molecule are supposed to be active in the resonant Raman process involving transitions between the highest occupied and the lowest unoccupied molecular orbital [120].

Making use of the results of density-functional tight-binding calculations of molecular dynamics originally applied to *PTCDA* [120], it possible to assign the two intense Raman lines $\Delta\bar{\nu} = 1306\,\mathrm{cm}^{-1}$ (α) and $\Delta\bar{\nu} = 1386\,\mathrm{cm}^{-1}$ (β) to molecular vibrational modes containing a large contribution of C−H in-plane bending elongations. The strong peak at $\Delta\bar{\nu} = 1596\,\mathrm{cm}^{-1}$ (γ) is assigned to modes with dominant contribution of C−C vibrations located at the perylene core. Further, the weak feature at $\Delta\bar{\nu} \simeq 1790\,\mathrm{cm}^{-1}$ is assigned to C=O vibrations (breathing mode). The spectral positions of the lines, the distance in wavenumbers from the excitation and the proposed assignment are summarized in Tab. 7.

Moreover, the high Raman intensity can be on one hand tentatively explained as a substrate-induced 'chemically enhanced' scattering phenomenon (enhancing of scattering cross section by a factor of 10 to 100 are possible in presence of new electronic states due to adsorbate-substrate bonding interactions [115, 125]), on the other hand just as

	$\bar{\nu}$ $[\mathrm{cm}^{-1}]$	$\Delta\bar{\nu} = \bar{\nu}_{exc} - \bar{\nu}$ $[\mathrm{cm}^{-1}]$	Exp. Raman modes and proposed assignment
Si_1	18275	521	Si: 519, TO phonon mode (bulk)
Si_2	17830	966	Si: 930-985, overtones of opt. modes
α	17490	1306	1301, C−H (in plane bending)
β	17410	1386	1380, C−H (in plane bending)
γ	17200	1596	1570, 1587 C−C (stretching)
δ	16190	2606	$2 \times A_g$ (1303)

Tab. 7: Spectral position of Raman lines in fig. 27, distance from the excitation (at $\bar{\nu} = 18796\,\mathrm{cm}^{-1}$), experimental Raman modes of *MePTCDI* [94] and proposed assignment following [94, 120].

the result of a favourable scattering configuration, under strong sample illumination, in resonance conditions and in presence of a very weak monomer fluorescence.

−Ordinary vibronic structure of *MePTCDI* fluorescence spectra (fig. 27.B)
The substructure in fluorescence spectrum B) is ordinarily observed in all *MePTCDI* fluorescence spectra and is *substrate independent*. It exhibits a time dependence typical of the S_1 emitting state of the *MePTCDI* molecule and it has to be interpreted as a vibronic progression built on the molecular ground state S_0. Also in emission, the coupled vibrational modes are the A_g total-symmetric in-plane stretching and bending modes of the molecule. The small energy red-shift ($\Delta\bar{\nu} \simeq 20\,\mathrm{cm}^{-1}$) of vibronic substructure with respect to the Raman lines is accounted by the relative position of the emitting S_1 state with respect to the excitation energy, to which the Raman lines are referred.

The bottom of the emitting band is therefore estimated to $\bar{\nu} = 18796\text{-}20 \sim 18775\,\mathrm{cm}^{-1}$; the main active modes are $\Delta\bar{\nu} = 1306\,\mathrm{cm}^{-1}$, $\Delta\bar{\nu} = 1386\,\mathrm{cm}^{-1}$, $\Delta\bar{\nu} = 1596\,\mathrm{cm}^{-1}$, whereas the modes $\Delta\bar{\nu} = 569\,\mathrm{cm}^{-1}$, $\Delta\bar{\nu} = 542\,\mathrm{cm}^{-1}$ and $\Delta\bar{\nu} = 221\,\mathrm{cm}^{-1}$ [126, 127] are also often observed.

c) Fluorescence transients of *MePTCDI* molecules adsorbed on reactive *Si(111)*

The deposited molecules have a *fast* fluorescence dynamics: after 245 ps from the rise of the excitation pulse the monomer fluorescence is already disappeared and the fluorescence lifetime lies consequently below the system time resolution (below 25 ps). This value has to be compared with a value of $\tau = 145\,\mathrm{ps}$ as measured in case of a film deposited on freshly passivated silicon surfaces (§ 4.3).

The molecules directly deposited on a reactive silicon surface exhibit thus a *further*

shortening of the observed lifetime with respect to the case of molecules deposited on freshly passivated silicon surfaces.

The further reduction of the electronically excited states lifetime is deeply connected with the formation of new bonds between *MePTCDI* molecules and silicon that influence drastically the deactivation pathways of the organic molecule and the fate of the optically created excitations.

5.1.2 Spacer measurements on *Si(111)* in presence of adsorbed molecules

To answer the question whether adsorbed *MePTCDI* molecules bound on the silicon substrate can perturb the fluorescence dynamics of other electronically excited *MePTCDI* molecules lying at a distance d_{sp} from this surface, a series of argon-spacer measurements has been carried out depositing (at $T = T_S = 10\,\mathrm{K}$) ultrathin *MePTCDI* films at various distances from reacted *Si(111)* surfaces. The studied system is shown in fig. 28.

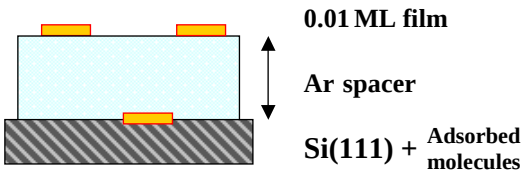

Fig. 28: Experimental configuration used in the described spacer measurements; instead of a freshly passivated silicon surface, a *Si(111)* substrate on which lie adsorbed *MePTCDI* molecules is used.

Both the argon condensation and the deposition of *MePTCDI* molecules follow the sample preparation method already described earlier, being the only difference the use of a silicon surface with *MePTCDI* molecules adsorbed on it.

Distance dependent fluorescence transients

Fig. 29 shows the distance dependent [0-130 Å] fluorescence transients of ultrathin *MePTCDI* films deposited on *Si(111)* substrates on which *MePTCDI* molecules are adsorbed, as detected at $\bar{\nu} = 17300\,\mathrm{cm}^{-1}$, time range $[\,0-10\,\mathrm{ns}\,]$.

The fluorescence decay curves are strongly non exponential. Two decay components with different time constant are observed: a dominant *fast* one, spacer thickness *independent*, with a time constant at system detection limit and a *delayed* one, *strongly spacer dependent*, that varies more than 2 orders of magnitude when the spacer thickness decreases from 130 Å to 0 Å. This latter component can be fitted by a mono- or a biexponential decay curve.

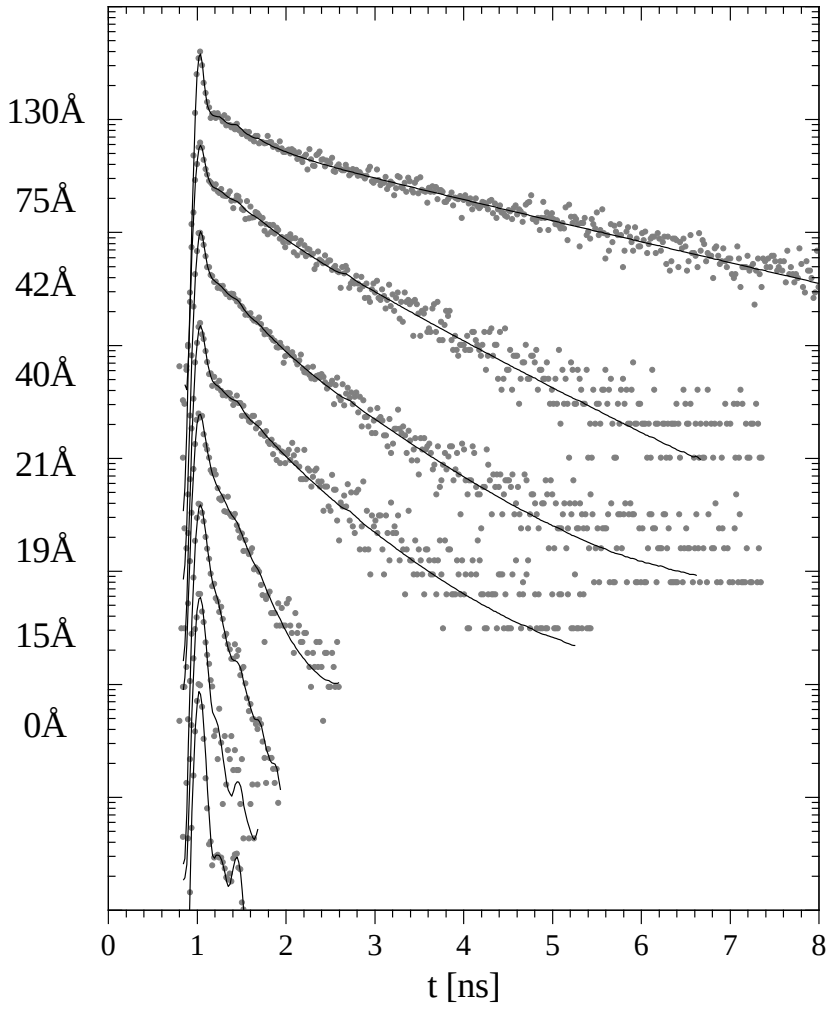

Fig. 29: In–situ distance dependent fluorescence decays of ultrathin *MePTCDI* films on *Si(111)* surface with adsorbed *MePTCDI* molecules, at $T = T_S = 10\,\mathrm{K}$. The distance is fixed by means of solid argon spacer, whose thickness d_{sp} [0-130 Å] is indicated on the left. Excitation at $\bar{\nu} = 18796\,\mathrm{cm}^{-1}$, detection at $\bar{\nu} = 17300\,\mathrm{cm}^{-1}$, time range $[\,0-10\,\mathrm{ns}\,]$. The decays are normalized to their maxima. Fitting: multiexponential with a fixed time component ($\tau \sim 35\,\mathrm{ps}$); *see* text for details.

The relative fluorescence spectra, as measured inside an early time interval ($[\,0-800\,\mathrm{ps}\,]$ after the excitation pulse) or in a delayed one ($\mathrm{t} > 1.5\,\mathrm{ns}$), do not present substantial differences and exhibit monomeric character (apart from the presence of strong Raman lines in the early time interval). This ensures that also the short fluorescence component is a real monomer fluorescence signal, without, for example, any stray light contribution. The fluorescence decay curves have been fitted by a multiexponential fitting keeping *fix* the fast time component (35 ps). If only the remaining decay component (that varies with the spacer) is plotted versus the argon thickness d_{sp}, the dependence is that shown in fig. 30; the x and y scale is the same as in fig. 22 and fig. 26 to permit a direct comparison.

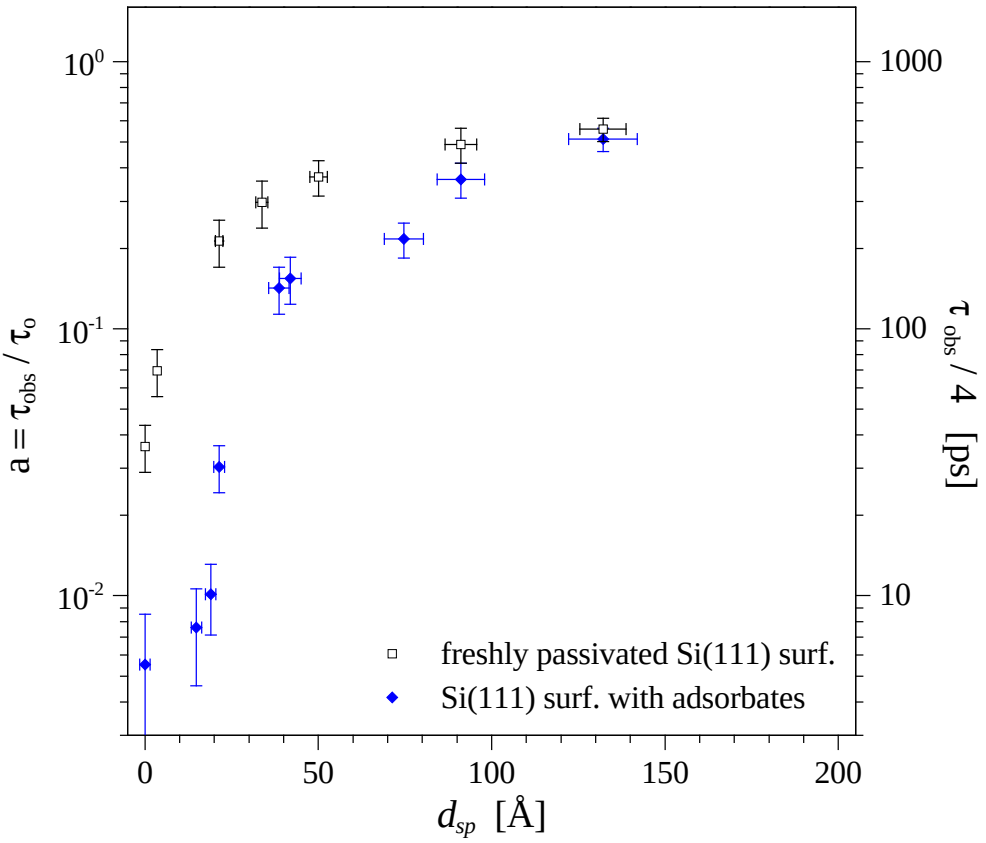

Fig. 30: (Filled diamonds) – *MePTCDI* monomer lifetime (τ_{obs}) and normalized lifetime ($a = \tau_{obs}/\tau_0$) in (0.01 ML) films spacer-separated from *Si(111)* surfaces with adsorbates as a function of the argon spacer thickness d_{sp}, at $T = T_S = 10$ K. After multiexponential fitting of the decays in fig. 29 only the longer living (distance-dependent) component is here plotted as a function of d_{sp}.
(Hollow squares) – *MePTCDI* monomer lifetime as measured on freshly passivated *Si(111):H* (data as in fig. 26), plotted in comparison.

Discussion of the spacer measurements on *Si(111)* surface with adsorbates
In presence of adsorbed *MePTCDI* molecules on the silicon surface, the optical properties of *the whole* system [*MePTCDI* film + spacer + *Si(111)*] are affected. The experimental results can be interpreted as follows.

The time resolved fluorescence spectra are the result of the superposition of two fluorescence components: 1) the fluorescence from adsorbed molecules (see fig. 28), characterized by a fast dynamics due to *the direct contact* with the substrate and 2) the fluorescence originating from the non-interacting molecules deposited on the argon spacer surface, at a distance d_{sp} from the silicon surface.

The fluorescence transients exhibit (consequently) two different decay regimes: a fast one, associated to the fluorescence dynamics of the adsorbate *MePTCDI* molecules (and

for this reason spacer thickness *independent*) and a slow one, distance dependent, related to the excitation dynamic of *MePTCDI* molecules at distance d_{sp} from silicon surface.

Noticeably, this latter does not follow the distance dependence of films deposited on fresh-passivated *Si(111)* substrate (fig. 30), being the monomer fluorescence shortening more pronounced on contaminated silicon surfaces. This enhanced monomer fluorescence lifetime shortening effect at the various spacer thicknesses can be nevertheless phenomenologically accounted for by considering a *further* distance-dependent deactivation channel beside the ordinary molecule-substrate pathway described in § 4.3.

The origin of this further lifetime shortening is to search in the existence of a *non-radiative* excitation transfer channel between the *MePTCDI* molecules deposited on top of argon-spacer and the *adsorbated molecules* on the silicon surface.

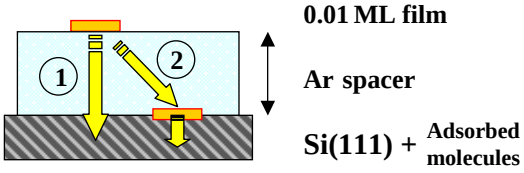

Fig. 31: Proposed deactivation pathways for electronically excited *MePTCDI* molecules deposited at a distance d_{sp} from a *Si(111)* substrate contaminated by adsorbed molecules: beside the non-radiative molecule-substrate excitation transfer channel (1), a further pathway (2) (form *MePTCDI* molecules to adsorbates and from here to the substrate) opens in presence of contaminants. As a result, a further shortening in molecular fluorescence lifetime is observed at every distance d_{sp}.

The favoured face-to-face orientation [1] of the molecules and the average distance between the molecules across the spacer layer (of the same order of magnitude of the Förster radius, estimated to be $R_0 \sim 50$ Å at 0.01 ML coverage [43]) make possible, in competition to the non-radiative energy transfer from the molecules on top of the argon layer directly to the substrate (fig. 31, (1)), an efficient excitation migration from these to the adsorbates and from here to the substrate (fig. 31, (2)).

If k_{MS} is the rate of the direct excitation transfer from the molecule (on the spacer) to the substrate (1) and k_0 is the radiative rate in absence of the substrate, the excitation transfer rate k_{MA} through the molecule $\rightarrow$ adsorbate $\rightarrow$ substrate deactivation channel (2) can be estimated by the observed fluorescence lifetime as measured on substrates *without*

[1] The hypothesis on this mutual orientation of the molecules is based on the comparison between experimental data and expectation values according to the theoretical model, as explained in § 8.4.

adsorbates ($\tau_{obs} = {k_{obs}}^{-1}$) and *with* adsorbates ($\tau'_{obs} = {k'_{obs}}^{-1}$). It follows that:

$$k_{obs} = k_0 + k_{MS}$$
$$k'_{obs} = k_0 + k_{MS} + k_{MA}$$

and therefore

$$k_{MA} = k'_{obs} - k_{obs} = \frac{1}{\tau'_{obs}} - \frac{1}{\tau_{obs}} \tag{4}$$

The numerical value of the transfer rate k_{MA} is estimated to be $k_{MA} = 0.04 \cdot 10^9\,\mathrm{s}^{-1}$ at $d_{sp} = 130\,\text{Å}$ and $k_{MA} = 31.6 \cdot 10^9\,\mathrm{s}^{-1}$ at $d_{sp} = 15\,\text{Å}$; it corresponds to $\tau_{MA} = k_{MA}^{-1} = 24.8\,\mathrm{ns}$ and 31.6 ps, respectively. This second deactivation channel turns out to be extremely efficient at short molecule-substrate separation, becoming the dominating excitation transfer pathway below 70 Å.

5.2 *MePTCDI* fluorescence as a sensor to monitor the argon layer planarity

In chapter 4, the distance-dependent time resolved fluorescence measurements have been presented under the basic assumption that the spacer layer was: 1) *rigid*, 2) *perfectly planar* and 3) *stable* in time and that the molecules were fixed on its top.

Actually, the argon layer preparation method used during the measurements (i.e. progressive annealing of the spacer as described in § 2.1.3) ensures that these three requisites were fulfilled and no remarkable change in fluorescence spectrum or transient was noticed up to a number of hours after the deposition on the film.

It is however known in literature (e.g. from *XPS* measurements carried out on *PTCDA* on xenon spacer [128]) and by precedent researches of our group (anthracene on solid nitrogen [34] and *MePTCDI* on argon [43]) how both a) *molecule rearrangement* on the top of the spacer layer and b) *sinking* of the molecules inside the spacer can take place, depending essentially on the chosen experimental conditions. In the present case, if a clustering of *MePTCDI* molecules on the argon surface at $T = 10\,\mathrm{K}$ can be excluded (differently from what observed for anthracene), their *sinking* by diffusion inside the layer cannot be excluded a priori.

Moreover, during this research it was found that also the argon layer can be critically affected by the preparation conditions: in particular the spacer can be *non completely flat*. Since the fluorescence lifetime of the molecules deposited on the spacer depends dramatically on the distance from the substrate, also little non-planarity of the argon surface has appreciable effects on their fluorescence transients, because different isolated molecules are located at *different distances* from the substrate as sketched in fig. 32.

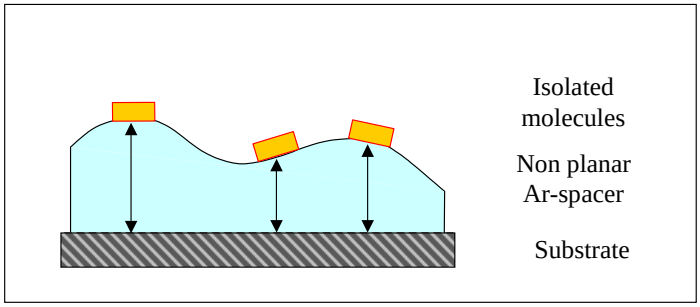

Fig. 32: Effect of the undulation of argon spacer: the *MePTCDI* molecules are mutually not interacting, but their distance from the substrate is distributed. Each molecule experiences a *different substrate-induced lifetime shortening*.

Scope of this section is the analysis of the argon spacer structure. The characteristics of the spacer are studied by using the fluorescence of the *MePTCDI* film deposited on top as a sensing tool:

In (1), an 'untreated' sample (*MePTCDI*/argon spacer/Substrate) is considered, i.e. a system based on a freshly prepared substrate, a not further treated argon spacer and a film of *MePTCDI* molecules deposited on top.

In (2), the annealing of the system is considered: after condensation of the argon spacer and the deposition of the molecular film, the sample temperature is raised up to 70 K to monitor, through the change of the fluorescence properties of the film deposited on top, the evolution of the argon spacer.

(1) – Non-processed (*MePTCDI*/argon spacer/Substrate) system

The effects related to the original inhomogeneity of the argon layer are studied in the following way: the argon layer has been deposited at $T = 10$ K on a freshly prepared MoS_2 substrate and *not further annealed*; an ultrathin *MePTCDI* film has been successively deposited and studied by time resolved fluorescence spectroscopy.

Fluorescence spectra and transients

Fig. 33.A shows the quasi-*cw* fluorescence spectrum of a (0.01 ML) *MePTCDI* film separated by a 300 Å thick argon layer from a freshly cleaved MoS_2 substrate at $T = T_S = 10$ K.

Fig. 33.B shows the corresponding fluorescence decay as detected at $\bar{\nu} = 17380\,\mathrm{cm}^{-1}$, upon excitation at $\bar{\nu} = 18796\,\mathrm{cm}^{-1}$. The fluorescence decay is strongly non-monoexponential and faster than the fluorescence decay of an equivalent film deposited on a *flat* argon spacer of comparable thickness (fig. 21).

Fig. 33.C shows the fluorescence spectra as collected in three different time intervals after the excitation pulse: *fast:* [-20:120 ps], *medium:* [120:610 ps], *slow:* [1880:7980 ps].

The quasi-*cw* fluorescence has monomeric character without any excimer-like low energy emission component; this ensures that on the top of the argon layer the molecules are non-interacting. The corresponding fluorescence decay (fig. 33.B) exhibits however a strong non-monoexponentiality; nevertheless, time resolved spectrum reveals *no apparent change* in shape also at different delay times after the excitation pulse (fig. 33.C).

Discussion of the results obtained on a non-processed system

This experimental findings can be easily explained as follows: if no annealing process is applied to the argon layer, it is rigid, but not flat; *MePTCDI* molecules are successively deposited on it: they are mutually non-interacting and each of them, when electronically excited, decays exponentially with a monomeric fluorescence spectrum. Nevertheless, because of the lack of argon flatness, it does not exist one well defined molecule-substrate distance, but a *distribution of distances*. According to its distance from the substrate each

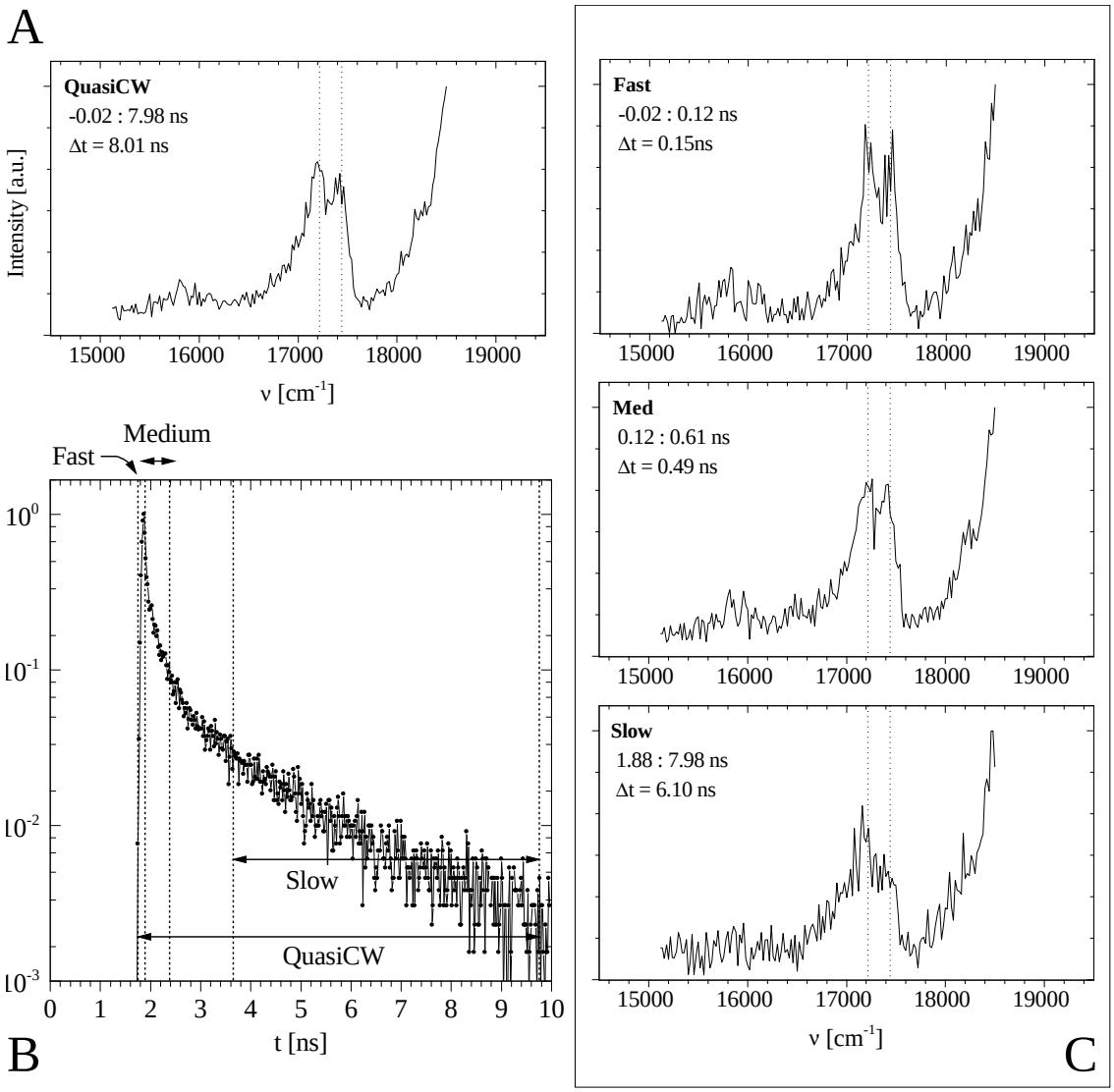

Fig. 33: The effect of argon spacer inhomogeneity on time resolved fluorescence of ultrathin (0.01 ML) *MePTCDI* film separated by means of a 300 Å thick, *not further annealed* argon layer from a freshly cleaved MoS_2 substrate at $T = T_S = 10\,\mathrm{K}$. A): quasi-*cw* fluorescence spectrum; B): fluorescence decay as detected at $\bar{\nu} = 17380\,\mathrm{cm}^{-1}$; C): fluorescence spectrum in three different time intervals after the excitation pulse (at $\bar{\nu} = 18796\,\mathrm{cm}^{-1}$). In this particular configuration, because of argon inhomogeneity, it is possible to have a strong non-monoexponential fluorescence decay even with a pure monomeric fluorescence in all the considered time intervals. *See* text for details.

molecule experiences a different lifetime shortening effect. As a consequence, the observed fluorescence transient is a *superposition* of contributions characterized by different decay times and it appears non-monoexponential. On the contrary, the fluorescence spectrum does not change appreciably, since the emitting states belong to isolated molecules.

Furthermore, the presence of a substrate-independent *vibronic substructure* with peaks at $\bar{\nu} = 17215\,\mathrm{cm}^{-1}$ and $\bar{\nu} = 17440\,\mathrm{cm}^{-1}$ (dotted lines in fig. 33.A−C) ensures that the molecules *did not sink* into the argon layer. If this would be the case, a loss of the substructure in the fluorescence spectrum should be observed. This aspect is pointed out in detail in the next subsection where, as a further step, the effects on the system (*MePTCDI*/argon spacer/Substrate) induced by a slight annealing are studied through the analysis of the variation of fluorescence properties of the molecular film deposited on top of the spacer.

(2) – Effect of the annealing of (*MePTCDI*/argon spacer/Substrate) system

Time resolved fluorescence spectroscopy can be used to study the settling process of the spacer upon slight annealing of the whole sample.

Starting from a distribution of *MePTCDI* molecules deposited at $T = T_S = 10\,\mathrm{K}$ above a spacer condensed on a generic interacting substrate and increasing progressively the temperature of the sample from $T = 10\,\mathrm{K}$ to $T = 40\,\mathrm{K}$, radical changes in fluorescence spectra and decays can be observed.

Actually, although the argon layer is rigid and stable at $T = 10\,\mathrm{K}$, a raising of the temperature will induce mainly 'softening' and settling of the layer. According to the different *initial* configurations of the (*MePTCDI*/argon spacer/Substrate) system, different responses have been found.

a.) Annealing of systems with *flat* spacer

As precedently experimented in our group, if the argon layer is initially *homogeneous* and *flat*, upon warming up of the sample the spacer becomes soft and the molecules on the top of the argon layer tend to sink inside the condensed spacer [43]. Their initially well defined distance from the substrate becomes, due to a diffusion process, a distribution of distances. As a consequence, the observed fluorescence dynamics changes from a monoexponential decay to an overlap of exponential decays with slightly different times, depending on the relative distance from the substrate of each molecule, thus to a multi-exponential curve (fig. 34 and fig. 46 in [43]).

b.) Annealing of systems with *undulated* spacer

If the argon layer is *not* initially flat, it is not straightforward to predict what kind of change can occur (upon warming of the sample) to the fluorescence properties of the organic molecules deposited on it.

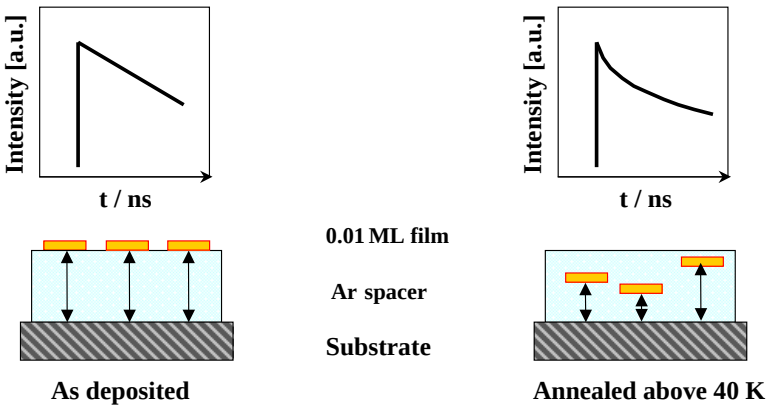

Fig. 34: Effect of a slight annealing applied to a system (*MePTCDI*/argon spacer/Substrate) initially *homogeneous* and *flat*. Upon rising up of the temperature above the 40 K, the argon layer becomes soft and the molecules sink inside; their distance from the substrate is not well defined. Each molecule experiences a different substrate-induced lifetime shortening and the fluorescence transient becomes a multi-exponential curve.

To study the effect of annealing in this particular case, a 35 Å thick argon layer has been evaporated at $T = 10\,\mathrm{K}$ on a freshly prepared *Si(111):H* substrate and *not further annealed*; successively, a 0.01 ML *MePTCDI* film has been deposited on it.

The sample has been successively warmed up and maintained for typically 5 minutes at a target temperature. Afterwards it was cooled again down to $T = 10\,\mathrm{K}$ in order to avoid further uncontrolled layer modifications. The fluorescence decays and spectra have been then measured. Measurements were carried out immediately after the film deposition (without treatment) and after an annealing at 30 K, 40 K and 70 K.

Fig. 35 shows the fluorescence spectra of the system (0.01 ML / 35Å Ar / *Si(111):H*) as measured in the interval $[\,0-240\,\mathrm{ps}\,]$ immediately after the deposition and upon annealing to the indicated target temperatures. Fig. 36 shows the fluorescence transients of the same sample, as measured at $\bar{\nu} = 18500\,\mathrm{cm}^{-1}$.

It can be observed that:

- An annealing of the sample up to $25\,\mathrm{K}-30\,\mathrm{K}$ does not result in any variation both in fluorescence spectra and transients: up to this temperature the argon layer is thus supposed to be stable.
- Upon 5 minutes annealing at higher temperature (40 K) a number of changes can be observed:

  in fluorescence spectra (fig. 35):
  - Increase (up to 2 times) of fluorescence intensity.
  - Fluorescence intensity redistribution on different vibrational components (compare white and grey curves between 16500 cm^{-1} and 17500 cm^{-1})

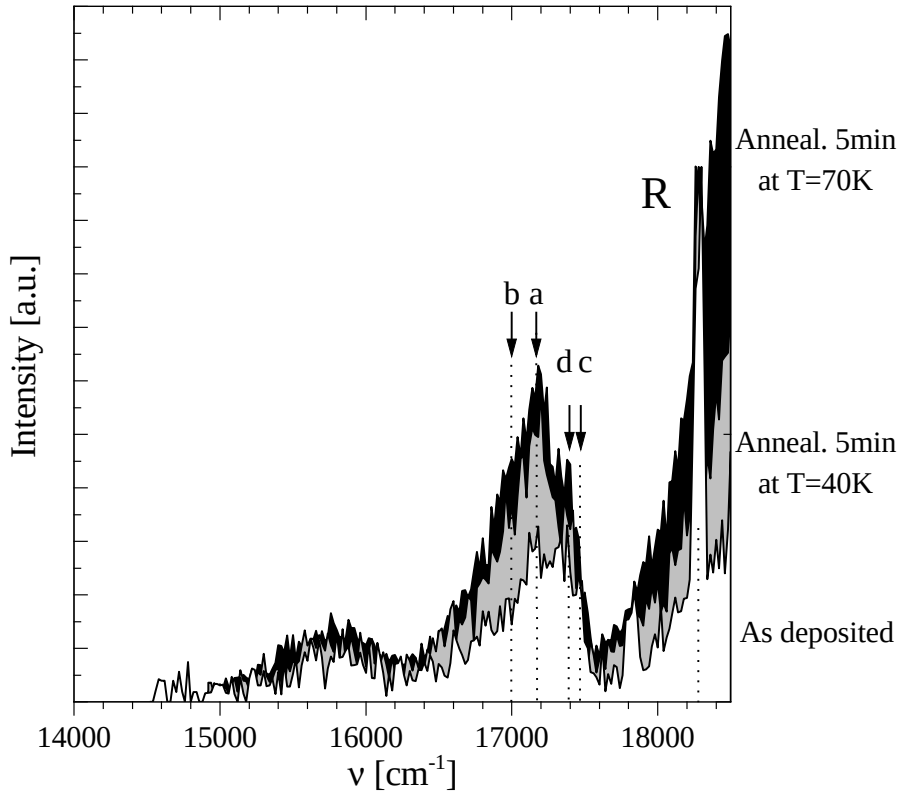

Fig. 35: (0.01 ML / 35Å Ar / *Si(111):H*): fluorescence spectra as measured in the range [0−240 ps] directly after deposition and after annealing at different target temperatures. Excitation at $\bar{\nu} = 18796\,\mathrm{cm}^{-1}$. The spectra are normalized to the maximum of silicon Raman line 'R' at $\bar{\nu} = 18275\,\mathrm{cm}^{-1}$ (mode TO, $\Delta\bar{\nu} = 521\,\mathrm{cm}^{-1}$, *see* tab. 7) to evidence the progressive increasing of fluorescence intensity upon annealing, under constant illumination geometry and excitation conditions. The main vibronic modes are indicated by letters and arrows. *See* text for details.

in fluorescence transients (fig. 36):

- · A sensible 'straightening' in decay form (i.e. the decay curves tend to become more and more monoexponential)
- · An appreciable fastening of fluorescence decay

– Upon further 5 minutes annealing at higher temperature (70 K), a still higher fluorescence intensity is observed (up to 4 times), whereas only further minimal changes are measured both in fluorescence spectrum (fig. 35, black curve) and fluorescence decays; in particular, no drastic further lifetime shortening is observed.

– Upon still longer annealing at higher temperature induces negligible variations in fluorescence spectra, but a 'bending' in fluorescence transients is observed. They tend to become again non monoexponential.

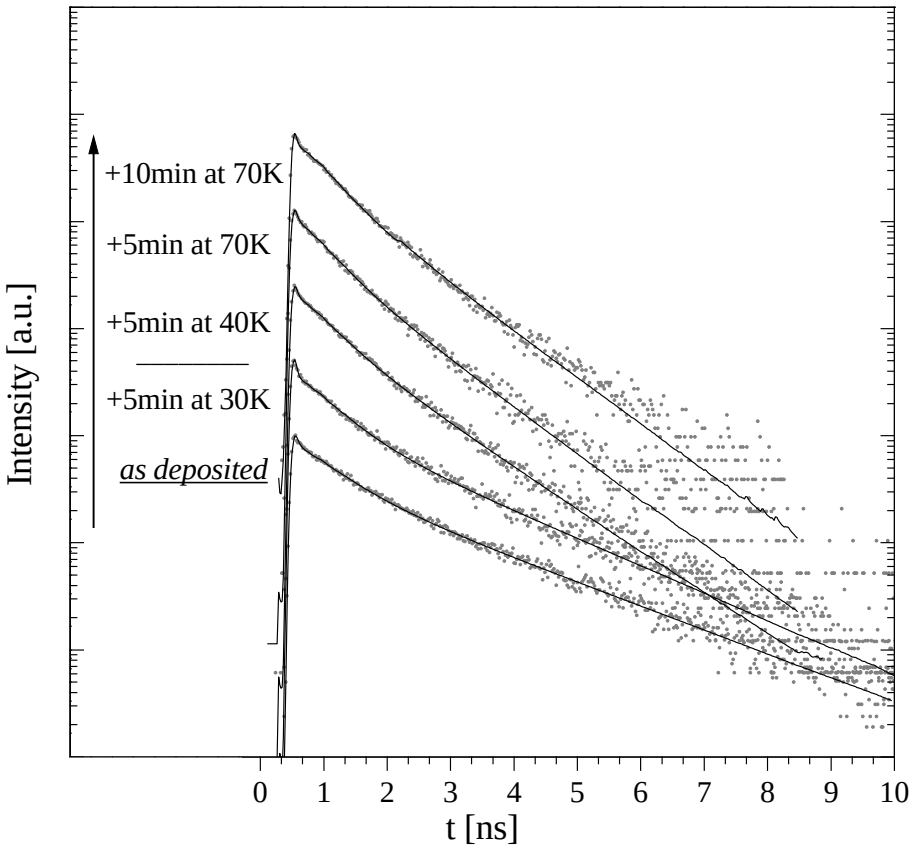

Fig. 36: Changes in *MePTCDI* fluorescence decays as measured at $\bar{\nu} = 18500\,\mathrm{cm}^{-1}$ directly after deposition and after annealing at different target temperatures. The decays are normalized to their maxima and vertically shifted for clarity, excitation at $\bar{\nu} = 18796\,\mathrm{cm}^{-1}$. Fitting multiexponential. The 'straightening' effect and fastening in time behaviour are the results of annealing at a temperature higher than 40 K.

Argon spacer annealing: discussion of results

The experimental findings can be explained making use of the precedent observations and by the knowledge on the argon layer properties.

Immediately after the deposition, as not further thermally treated, the argon spacer at $T = 10\,\mathrm{K}$ is rigid, but not flat. The *MePTCDI* molecules are successively deposited on the top of the spacer; the distance of this 0.01 ML organic film from the substrate is not well defined and shows a *distribution of distances*. For this reason the fluorescence spectrum has monomeric character (the emitters are mutually non-interacting), but the fluorescence decay curves are strongly non-monoexponential (fig. 36, 'as deposited'): the measured fluorescence transients are actually the superposition of fluorescence dynamics with different decay times, since *MePTCDI* molecules lying at various distances from the

substrate experience different fluorescence lifetime shortening effect.

By warming up the system (0.01 ML / 35Å Ar / *Si(111):H*) at temperatures lower than ~ 30 K, only negligible changes happen in the argon spacer and almost no changes in the measured fluorescence properties of the organic film deposited on top (fig. 36, second decay from below).

But at a higher annealing temperature (35 K−40 K) the condensed argon atom layer starts to *settle* and to *flatten*. As a result, the amplitude of argon surface undulation *decreases*, whereas the overlying *MePTCDI* molecules (big with respect to the Ar atoms) initially do not sink completely (see below) but are supposed to follow the variations of the argon surface (fig. 37).

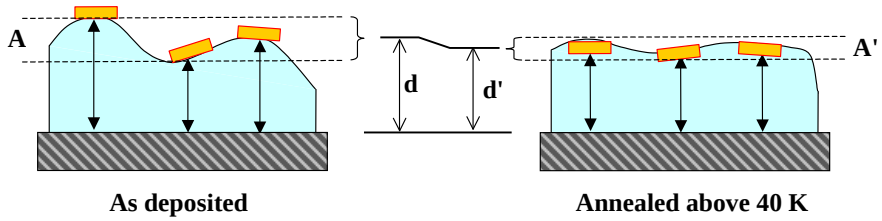

Fig. 37: Effect of a slight annealing applied to a system (*MePTCDI*/argon spacer/Substrate) initially *inhomogeneous*. Rising up the temperature above the 40 K, the argon layer starts to settle: the amplitude A of its inhomogeneity decreases (down to A'). Upon longer annealing the average distance d of the molecules from the substrate starts to decrease, too (down to d') as a result of argon wetting; consequently, the fluorescence decay becomes more monoexponential and the measured fluorescence lifetime shorter. *See* text for details.

- The fluorescence transients

On one hand, this would explain the straightening in fluorescence decay curves: upon argon layer settling the amplitude A of the distribution of distances decreases, the *MePTCDI* molecules arrange to a similar distance from the substrate: they experience a similar substrate-induced lifetime shortening effect and the fluorescence decay becomes statistically more monoexponential.

On the other hand, this explains the *shortening* in measured molecular fluorescence lifetime upon annealing, too: because of the layer settling and argon atoms wetting the *average distance* d between the *MePTCDI* molecules and the substrate slightly *decreases*; the interaction with the substrate becomes stronger and therefore the observed molecular fluorescence lifetime becomes *shorter*.

Comparing the fluorescence decay times drawn out from the transients in fig. 26 with

those measured on a planar argon spacer of equal thickness (fig. 26), it is possible to estimate the order of magnitude of the spacer inhomogeneity before and after the annealing. The spacer has been condensed with a nominal thickness of 35 Å. When not further treated, the thickness is found to vary between 45 Å and 30 Å, corresponding to a variation of ±25-30%. After 5 minutes annealing at 40 K, such amplitude variation reduced to ±5-10%, whereas the average distance from the substrate decreases to ~ 30 Å.

According to the crystallographic parameters of argon (cubic close-packed (fcc) crystal structure, near-neighbour distance 3.76 Å, lattice parameter of the cubic cell 5.31 Å) [129], the effect previously described involves a small number of argon monolayers: only 2 or 3 on ~ 10 in the case of $d_{sp} = 35$ Å; this means that, within this distance range, already a thickness variation of few single argon layers induces an appreciable effect on the fluorescence dynamics of the *MePTCDI* molecules deposited on top, which can be optically detected.

- The fluorescence spectra

Changes in fluorescence spectra (fig. 35) upon annealing were precedently observed [43] and explained as follows: the annealing of the sample induces sinking of the *MePTCDI* molecules into the argon layer and consequently a polarization effect generated by the argon atoms around the *MePTCDI* molecules; this effect was claimed to result in a lowering of the molecular electronically excited state and therefore in *red-shift* (in the order of $\sim 200\,\mathrm{cm}^{-1}$) of the whole emission spectrum.

On the base of the present experimental data and following the proposed assignment of *MePTCDI* vibrational modes active in molecular fluorescence (tab. 7), we tend to interpret the change in fluorescence spectra as the result of a *different balancing* of intensity among the vibrational substructures in emission. In particular, it has been observed that the rising edge of the second emission band at $\bar{\nu} = 17570\,\mathrm{cm}^{-1}$ (fig. 35) is annealing *independent* (no red-shift is observed) and this is in contrast to the hypothesis *of a general shift of fluorescence spectrum*.

On the contrary, it seems more plausible to describe the change in fluorescence spectra as the result of a loss of intensity by the components (c) $\bar{\nu} = 17470\,\mathrm{cm}^{-1}$ and (d) $\bar{\nu} = 17390\,\mathrm{cm}^{-1}$, with respect to those (a) $\bar{\nu} = 17180\,\mathrm{cm}^{-1}$ and (b) $\bar{\nu} = 17000\,\mathrm{cm}^{-1}$ in fig. 35.

Following the proposed assignment, these fluorescence components are associated to transitions to total symmetric vibrational levels of the molecular ground state (S_0): (a) C−C (stretching mode), (b) C=O (breathing mode), (c) and (d) C−H (in plane bending mode).

Upon annealing, only the vibronic coupling with C−H molecular bending modes looses intensity. By excluding symmetry reasons for that, it means that these particular ground

state vibrational modes are perturbed by the physical changes which affect the *MePTCDI* molecules and their environment when the sample temperature is rised above the 40 K; being the *sinking* of molecules the more evident effect of the rise of the temperature, it is highly probable that the diffusion process (that starts at 40 K) of *MePTCDI* through the spacer atoms disturbs mainly the free vibration modes localized at the *perimeter* of molecule (like C−H modes) with respect to those localize *inside* the perylene core (especially C−C) [120]. A general loss of fluorescence substructure has to be thus considered as an indirect evidence of molecular sinking phenomena.

Finally, the fluorescence intensity increase normally observed as a result of the annealing of the sample has to be related to the molecular reorganization on top of the argon layer: starting from a random 3D angular distribution, the *MePTCDI* molecules tend to acquire a flat lying position on the spacer. This favours on one side a better excitation condition (the absorption transition moment lies along the long molecular axis [43, 98]) and on the other side the fluorescence intensity increases since, as it will be seen in chapter 6, the non-radiative interaction with the substrate is less effective for molecules that lye parallel to the substrate.

Argon spacer annealing: summary of the results

In conclusion:

- Under standard experimental conditions, the argon layer turns out to be solid and no sinking of molecules can be noticed.
- Immediately after the deposition, without other further treatments the argon layer appears inhomogeneous (especially for thin layer). The homogeneity can be however effectively increased in a controlled way by annealing the layer (at 25 K−30 K), *before* the deposition of the organic film.
- Upon sample (molecule+spacer+substrate) annealing a number of effects have been observed using the time resolved fluorescence of the deposited molecular film as a sensing tool:

a) if the spacer is originally *homogeneous and flat*, the annealing induces sinking of the molecules, broadening of fluorescence spectra and non-monoexponential fluorescence decays.

b) if the spacer *isn't originally flat*, the annealing results in a settling of the spacer and it is observed: 1.) straightening of fluorescence decay curves (related to the decreases of argon undulation amplitude), 2.) fluorescence lifetime shortening (related to the approaching of molecules to the substrate), 3.) fluorescence intensity increasing. Upon stronger annealing the molecules sink further into the argon layer.

6 Classical model of molecular emission in proximity of interfaces

In this and in the next chapter, the theoretical background necessary to the analysis of the experimental results is elaborated starting from the original macroscopic approach to describe the molecule-substrate interaction worked out, in the frame of classical electrodynamic, by Chance, Prock and Silbey in early '70s ('CPS model').

In § 6.1 the CPS model is briefly introduced and the general expression for the damping constant $\hat{b}$, the rate of the excitation transfer from an electronically excited molecule to a substrate at a distance d, is obtained starting from macroscopic quantities of the system (the dielectric function $\varepsilon(\omega)$ of the materials).

In § 6.2, on the basis of this formulation, the predicted molecular fluorescence lifetime shortening ($\tau = \tau_0/\hat{b}$) is numerically calculated in its distance dependence for various orientations of the molecule with respect to the substrate, choosing a metallic substrate Ag and an argon spacer as reference case.

The CPS model offers however only a macroscopic treatment of the problem: if for large molecule-substrate separations the observed fluorescence lifetime modulation is adequately explained in terms of interference phenomena (fig. 39), in the short distance domain the model offers no microscopical explanation about the *interaction mechanism* that gives origin to the strong excitation transfer between molecule and substrate (fig. 39, inset).

In the next chapter (§ 7) the interaction mechanism dominant in the *near-field* range is analyzed: both metallic and semiconductor substrates are explicitly taken into account and the differences addressed to the different nature of the solids.

6.1 The CPS model: general aspects

The lifetime τ of an electronically excited molecule at a distance d from a flat surface of a solid is drastically affected by the presence of the substrate.

The CPS model (extensively reviewed in [11]) describes the system as follows. The molecule (fig. 38) is treated as a harmonic point-dipole with dipole moment μ embedded in a non absorbing medium 1 at a distance d from a substrate (medium 2), uniquely characterized by its complex dielectric function $\varepsilon_2(\omega)$:

$$\varepsilon_1 = \varepsilon_1^r \qquad \text{and} \qquad \varepsilon_2 = \varepsilon_2^r + i \cdot \varepsilon_2^i \quad . \tag{5}$$

The CPS model extends the Kuhn's approach [10] to the problem, requiring the cal-

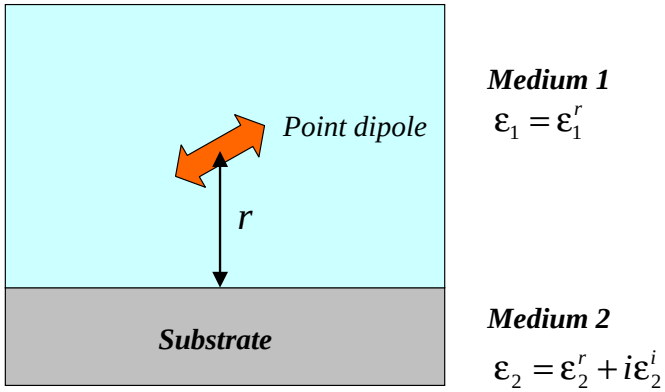

Fig. 38: Sketch of the system considered in the CPS model: the harmonic point oscillator represents the electronically excited molecule that radiates in a lossless medium 1 (ε_1) at a distance d from a infinite half-space (the substrate, medium 2) characterized by a complex dielectric function $\varepsilon_2(\omega)$.

culation of the molecular field reflected from the substrate at the dipole position [a].

The equation of motion of the molecular dipole (considered as a harmonic forced and damped oscillating charge) can be written as:

$$\ddot{\mu} + b_0\,\dot{\mu} + \omega_0^2\,\mu = \frac{e^2}{m}\,E_R \tag{6}$$

where E_R is the reflected field at the position of the dipole, ω_0 is the natural oscillation frequency of the undamped dipole, m is the effective mass of the dipole and b_0 is the dipole decay rate (*inverse lifetime*) in absence of the interface (proper damping constant).

The dipole moment μ oscillates at the same complex frequency of reflected field E_r, so:

$$\begin{aligned} \mu &= \mu_0\, e^{-i\,(\omega_0+\Delta\omega)\,t}\, e^{-b\,t/2} \\ E_R &= E_0\, e^{-i\,(\omega_0+\Delta\omega)\,t}\, e^{-b\,t/2} \end{aligned} \quad . \tag{7}$$

Here, $\Delta\omega$ indicates the shift from resonance frequency and b (without index '0') the damping constant *in presence* of the substrate.

The problem is reduced to that of the driven harmonic oscillator, where the external driving force originates from the reflected radiation field of the emitting dipole. Substi-

[a] A second equivalent approach (based on the energy-flux method [12]) permits further to separate the radiative and non radiative lifetime components.

tuting into eq. 6 and noting that $b^2 \ll \omega_0^2$ and $(e^2/\mu_0\, m)E_0 \ll \omega_0^2$, we have:

$$\begin{aligned} \Delta\omega &= \frac{b_0^2}{8\omega_0} + \frac{e^2}{2\,\mu_0\, m\, \omega_0}\,\mathrm{Re}(E_0) \\ b &= b_0 + \frac{e^2}{2\,\mu_0\, m\, \omega_0}\,\mathrm{Im}(E_0) \quad . \end{aligned} \tag{8}$$

Therefore it is sufficient to evaluate the reflected field at dipole position to solve the problem. From the two expressions (8), it also turns out that the damping rate and the frequency shift in presence of a substrate are related to the out-of-phase and in-phase components respectively of the reflected field. The frequency shift $\Delta\omega$ is found to be always negligible [130] and it will not be considered in the following.

The damping rate without substrate b_0 is composed of a radiative contribution b_r and a nonradiative one b_{nr} (thermal deactivation). Introducing the classical expression for b_r [10]:

$$\begin{aligned} b_0 &= b_r + b_{nr} \\ b_r &\equiv \frac{2\, e^2\, k_1^3}{3\, m\, \omega_0\, n_1^2} \end{aligned} \tag{9}$$

where $n_1 = \sqrt{\varepsilon_1}$ is the refractive index of the medium containing the dipole and k_1 is the propagation constant ($k_1 = \omega n_1/c$) and defining further the quantum yield of the emitting state without substrate $\Phi_0 \equiv b_r/b_0$, it is possible to write the normalized damping rate $\hat{b}$ in a form convenient for numerical calculations:

$$\hat{b} \equiv \frac{b}{b_0} = 1 + \frac{3\,\Phi_0\, n_1^2}{2\,\mu_0\, k_1^3}\,\mathrm{Im}(E_0) \quad . \tag{10}$$

This quantity is directly related to the measured fluorescence lifetime τ:

$$\boxed{\tau = \frac{\tau_0}{\hat{b}} \qquad \longrightarrow \qquad a \equiv \frac{\tau}{\tau_0} = \hat{b}^{-1}} \tag{11}$$

where τ_0 is the intrinsic lifetime of the molecule (without interaction with the substrate) and a indicates the normalized lifetime.

The problem is now reduced to estimate the reflected electric field at the position of the dipole. Following Sommerfeld [131], the Hertz's vectors notation is used in cylindrical coordinates [11]; treating explicitly the case of dipole perpendicular ($\perp$) and parallel ($\parallel$) to the surface, it is possible to calculate the complex quantities $E_r(\perp)$ and $E_r(\parallel)$ and readily the relative damping constants $\hat{b}_\perp$ and $\hat{b}_\parallel$.

$$\hat{b}_{\perp} = 1 - \frac{3}{2}\,\Phi_0\ \mathrm{Im}\left(\int_0^{\infty} du\ R^{\parallel}\, e^{-2l_1\hat{d}}\,\frac{u^3}{l_1}\right)$$

$$\hat{b}_{\parallel} = 1 + \frac{3}{4}\,\Phi_0\ \mathrm{Im}\left(\int_0^{\infty} du\ \left((1-u^2)\,R^{\parallel} + R^{\perp}\right)\, e^{-2l_1\hat{d}}\,\frac{u}{l_1}\right) \qquad (12)$$

The integration variable u is the component of the dipole field wave vector *in the plane of the interface* (k_x) scaled by the far-field wave vector k_1 of dipole radiation field in medium 1:

$$u \;=\; k_x/k_1$$

The $R^{\parallel,\perp}$ are respectively the Fresnel reflection coefficients for incident rays polarized parallel ($R^{\parallel}$, p-polarized) and perpendicular ($R^{\perp}$, s-polarized) to the plane of incidence:

$$R^{\perp} \;=\; \frac{l_1 - l_2}{l_1 + l_2} \quad , \quad R^{\parallel} \;=\; \frac{\varepsilon_1 l_2 - \varepsilon_2 l_1}{\varepsilon_1 l_2 + \varepsilon_2 l_1} \quad , \qquad (13)$$

Finally l_j and $\hat{d}$ are respectively a parameter (related to the wave vector component perpendicular to the substrate) and the dipole-substrate distance, normalized to the dipole wavelength inside medium 1.

$$l_j \equiv -i\sqrt{\frac{\varepsilon_j}{\varepsilon_1} - u^2} \quad , \quad \hat{d} \equiv k_1 d \;=\; \frac{\omega\sqrt{\varepsilon_1}}{c}\,d \;=\; \frac{2\pi\sqrt{\varepsilon_1}}{\lambda}\,d \qquad (14)$$

It should be noticed that the reflection coefficients are calculated for both real and complex angles of incidence: this means that the waves are either propagating or evanescent in nature.

An equivalent approach: the flux method

In the following section the general expression for the damping constant $\hat{b}$ is approximated in short distances domain by an expression (eq. 15) where *only* the non-radiative interaction between molecule and substrate is taken into account. Nevertheless, in the classic approach up to here followed, no way is given to distinguish among the various routes (i.e. radiative, non-radiative) the molecules can deexcite through. Making use of an equivalent approach (flux method) [12] to obtain the decay rate expression, it is possible to break the integral of eq. 12 in two parts and identify the individual contributions corresponding to different energy transfer mechanisms (this aspect will be extensively discussed on page 105).

The value of the ratio $u = k_x/k_1$ discriminates between these coupling mechanisms. The integral over $0 \leqslant u \leqslant 1$ ($k_x \leqslant k_1$) is related to the modification of the dipole decay rate caused by coupling between emitter and *radiative* field, while the integral for $1 < u < \infty$ ($k_x > k_1$) represents the energy transfer through wave vectors in the plane of the interface *greater* than the photon wave vector: these components are contained not in the radiative field, but in the near field of the emitter and cause a transfer not mediated by photons (*non-radiative* transfer). In this last case the excited dipole can actually couple to modes having in plane of interface momentum greater than k_1 (as the Surface Plasmon Polariton SPP, *see* pg. 100), modes that are not directly accessible to the incident plane waves.

In the next section, only the non-radiative contribution (integral for $1 < u < \infty$) will be considered in the approximated expression for the energy transfer rate $\hat{b}$ in short distances domain.

6.2 Calculation of *MePTCDI* fluorescence lifetime on *Ag*

Eq. 12 are not analytical and they have to be numerically solved. The integration in the complex plane has to be carefully performed in order to avoid singularities on or near real axis. A number of computer programs (based on Runge-Kutta [132–134] and Simpson-rule [134] methods) have been written to carry out the numerical computations and calculate the curves shown in the following.

To exemplify, the explicit case of *MePTCDI* separated from a *Ag* substrate by means of an argon spacer is considered. Fig. 39 shows the normalized lifetime *a* (according to eq. 11 and eq. 12) numerically calculated for *MePTCDI* molecule oriented either parallel (——) or perpendicular (– – –) to the *Ag* surface, versus distance *d*. The following parameters have been used: *MePTCDI* emission frequency $\bar{\nu} = 18775\,\mathrm{cm}^{-1}$, argon dielectric constant ε_1 (1.68; 0.0), *Ag* dielectric constant ε_2 (-10.6; 0.9) [135] and fluorescence quantum yield $\Phi_0 = 0.93$.

For a more detailed understanding of the result in fig. 39, it has to be considered that the field around the oscillator (the molecule), embedded in a medium with constant ε_1, consists of *two components*:
1.) the *radiation field*, that extends infinitely in the space around the emitter and obeys the dispersion relation of the light ($\omega = ck/\sqrt{\varepsilon_1}$)
2.) the *near field*, that contains a distribution of wave vectors k; of those, the components with $k > k_1$ (k_1 is the wave vector of far-field radiation) do not propagate into the far field, are evanescent in nature, decays exponentially away from the emitter and does not follow this relation.

For this reason, according to the distance d between emitter and solid surface, different interaction mechanisms can take place (via radiation field or near field) leading to a

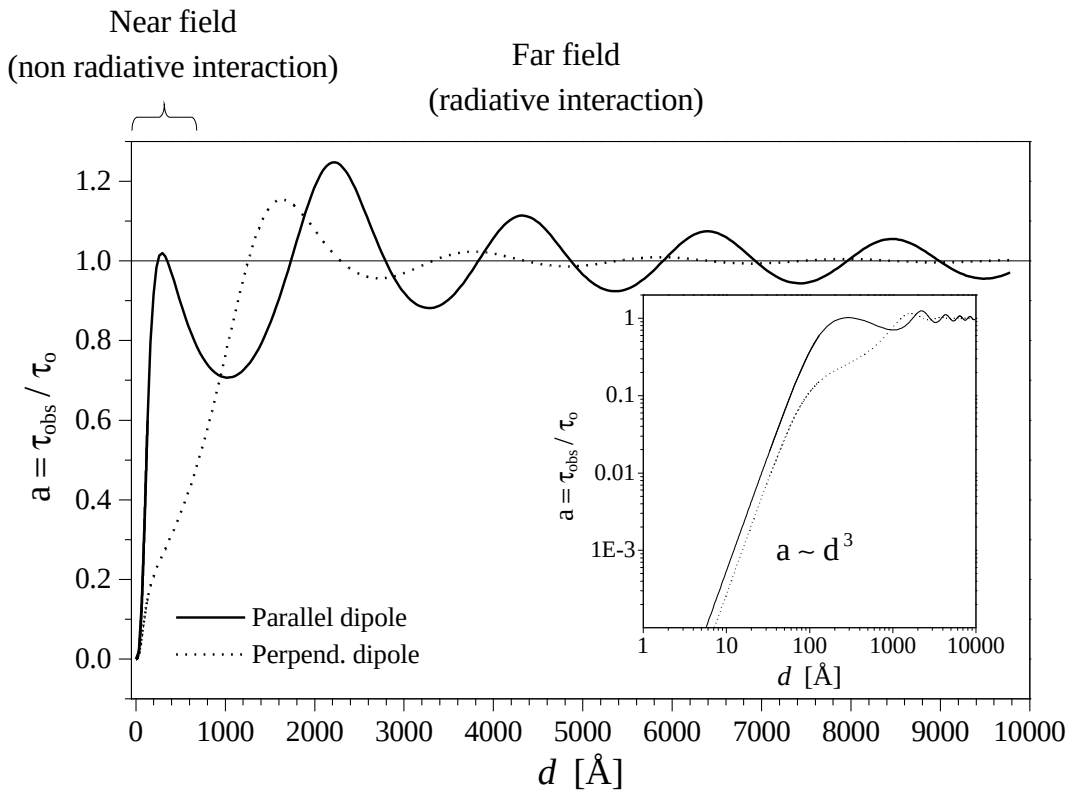

Fig. 39: Normalized lifetime a (according to eq. 11 and eq. 12) numerically calculated for excited dipole oriented either parallel (——) or perpendicular (– – –) to the substrate surface, versus distance d [Å]. The used parameters are those of *MePTCDI* molecule on argon spacer on *Ag(111)* substrate. *Inset:* Same curves plotted in log-log scale to emphasize the short distance domain; for distances $d < 300$ Å the normalized lifetime starts to fall because of an effective energy transfer to the substrate. Within this distance domain, the model predicts an approximated $\sim d^3$ functional dependence for *a(d)* (eq. 15 and eq. 11) that results in a straight line with slope three in the log-log plot.

complicate distance dependence in the observed lifetime τ_{obs}, because of modulations of the emission properties of the electronically excited molecule.

As a consequence, if λ is the wavelength of the dipole radiation, the CPS model predicts the existence of two ranges of distance d in which the behaviour of the emitter lifetime is drastically different:

Far field ($d \sim \lambda$) - (*radiative* interaction)
In this range the rate of radiative emission of the emitter is effectively modulated by its own field, reflected by the solid surface. When the reflected field is in phase with the source field, the emission is enhanced, thus reducing the emitter lifetime; when it is out of phase the emission is suppressed, thus increasing the emitter lifetime. As a result the

measured excited-state lifetime *oscillates* as a function of the distance from the surface. This oscillation will be from now on referred to as 'interference effect'.

Near field ($d \ll \lambda$) - (*non-radiative* interaction)
At distance below about 300 Å the excited-state lifetime begins to fall rapidly, since the emitter near field effectively induces a non-radiative energy transfer to the surface via its high wave vector components.

Near field approximation of damping constant $\hat{b}$
In this distances range, it is possible to approximate analytically the only non-radiative component ($1 < u < \infty$) in eq. 12 in the limit of small $\hat{d}$ ($k_1 d = \hat{d} \ll 1$) [12]; this leads to:

$$\boxed{\hat{b}_{ET} \equiv \lim_{\hat{d}\to 0} \hat{b}\,|_1^\infty = \frac{\Phi_0 \cdot \Theta}{4\,\hat{d}^3}\,\mathrm{Im}\left(\frac{\varepsilon_2 - \varepsilon_1}{\varepsilon_2 + \varepsilon_1}\right) \sim d^{-3}} \tag{15}$$

where Θ is a geometrical coefficient: $\Theta = 3/4$ for parallel, $\Theta = 3/2$ for perpendicular and $\Theta = 1$ for isotropic dipole, respectively.

The near-field damping function $\hat{b}_{ET}$ is found to vary as d^{-3} in this region. In the vicinity of a substrate, the excited-state lifetime is expected to exhibit a linear dependence with slope three on the distance when plotted in log-log scale (fig. 39, inset) [b].

[b] From general dimensional reasons, such a dependence can be explained in terms of Förster type dipole-dipole energy transfer [136]: this transfer is predicted to be proportional to the inverse of the sixth power of the distance between two point dipoles. If a point dipole is above a solid, it will transfer energy to a *volume* of point dipoles. The rate has to be integrated over a volume and the distance dependence of transfer rate is reduced to cubic ($\sim d^{-3}$). By the same reasoning one expects quartic ($\sim d^{-4}$) distance dependence for transfer to a surface or to a thin film.

7 Nature of the interaction mechanism in the near-field range

In this chapter, the nature of the interaction mechanism for molecules placed in proximity of a metal or a semiconductor is studied from a theoretical point of view and numerical calculations are performed taking into account the specific physical parameters of solids.

A.) In § 7.1 *metallic substrates* are explicitly considered. The shortening of the molecular fluorescence lifetime on a metal is quantitatively described in terms of coupling between the molecular near field and the charge density waves on the metal surface. The concept of *surface plasmon polariton* and its dispersion relation are introduced and applied to the study of the system. Further, in § 7.2.1 the *energy transfer rate parameter* $\beta(\omega)$ as a function of the molecule emission energy is explicitly calculated for the case of *Ag*. Successively, the importance to take into account (also on metals), beside the contributions of free charges to the dielectric function, also those originating from the *interband transitions* is pointed out. Their effect on the energy transfer rate predicted by the CPS model are numerically exemplified in case of *Ag*.

In § 7.2.2 the *power dissipated* by the *MePTCDI* molecule as a function of the distance d from the substrate is discussed and numerically calculated for *Ag*; various decay mechanisms (radiative, via coupling to surface plasmons and via interband transitions) and their relative importance as a function of the distance between molecule and substrate are discussed.

B.) In § 7.3 *semiconductor substrates* are explicitly considered. The possibility to apply directly the theoretical approach developed for metals also to semiconductors will be justified and the use of the classical model critically introduced. Since in semiconductors the dielectric response is mainly contributed by transitions across the band gap, the energy transfer rate will be quantified in terms of molecular near field induced electron-hole pair generation in the solid. The results of application of the CPS model to MoS_2 and *Si(111):H* semiconductors will be the focal point of the chapter 8.

Energy transfer rate parameter β

In the near-field range, the expression eq. 15 can be written as:

$$\hat{b}_{ET} = \beta\, d^{-3} \quad \rightarrow \quad \boxed{\beta = \frac{\Phi_0 \cdot \Theta}{4\, k_1^3}\, \mathrm{Im}\left(\frac{\varepsilon_2 - \varepsilon_1}{\varepsilon_2 + \varepsilon_1}\right)} \tag{16}$$

with $k_1 = \frac{2\pi\sqrt{\varepsilon_1}}{\lambda}$, the propagation constant. The functional dependence d^{-3} of $\hat{b}_{ET}$ on the distance is *independent* from the nature both of emitter and of substrate; in the

short distance domain, keeping valid the initial assumptions of the model, the *physical* properties of the system are accounted for in β [cm^3], the energy transfer rate parameter, by the values of the dielectric function of medium 1 and medium 2.

7.1 Energy transfer to metals

Metallic substrates are now explicitly considered. To estimate the energy transfer rate parameter $\beta(\omega)$ the value of the dielectric function $\varepsilon_2(\omega)$ on the whole frequency range has to be provided.

Independently from the nature of medium 2, it is worthwhile to try to approximate its dielectric function by means of an analytical *model* function.

Drude's dielectric function

In metals the dielectric behaviour results largely from collective excitations of the free carriers. To derive the dielectric properties of metals, the plasma concept can be referred to: the free electrons of a metal are treated as an electron liquid of high density ($\sim 10^{22}\,\mathrm{cm}^{-3}$), while the interaction between electrons and the ion-lattice background is taken into account by introducing an inverse collision (relaxation) time.

Starting from the equation of motion for the displacement of the electron gas relative to the ion cores, it is possible to model a complex dielectric function ($\varepsilon_D(\omega)$, Drude's dielectric function) in the form [129, 137]:

$$\varepsilon_D(\omega) = 1 - \frac{\omega_p^2}{\omega(\omega + i\delta)} \tag{17}$$

or, separating real and imaginary part:

$$\varepsilon_D(\omega) = \varepsilon_D^r + i \cdot \varepsilon_D^i = \left(1 - \frac{\omega_p^2}{\omega^2 + \delta^2}\right) + i\frac{\omega_p^2 \delta}{\omega(\omega^2 + \delta^2)} \tag{18}$$

with δ the inverse collision time and ω_p, the plasma frequency (a quantity depending only on free carrier density n), defined as:

$$\omega_p^2 \equiv \frac{ne^2}{\varepsilon_0 m} \tag{19}$$

where e is the electron charge, ε_0 the dielectric constant of vacuum and m the mass of charge carriers (here electron mass, m_e). In eq. 17 $\varepsilon(\infty)$, the value of ε in the limit of high frequency, has been replaced for simplicity with 1 (approximation largely valid in metals).

For weak damping ($\delta \sim 0$, large collision time $\tau_c = \delta^{-1}$), ω_p is the frequency at which $\varepsilon(\omega) = 0$. At this frequency a collective *longitudinal* oscillation of free electron gas can be

sustained by the material. Such oscillations of near free electron gas are known as *plasma oscillations*. As in the case of a simple harmonic oscillator, the energy of plasma oscillations can be quantized. The quantized entity is called *plasmon*. Since electromagnetic waves are transverse in nature they can couple only to transverse excitations, but not to longitudinal ones. Plasmons cannot therefore be directly excited by an electromagnetic wave because of their longitudinal character (i.e. the displacement of electrons is parallel to the direction of propagation).

Energy transfer rate in Drude's approximation
It is now possible to calculate the dependence of energy transfer rate parameter β on the *frequency* of the emitter, by inserting the model dielectric function (eq. 17) in the expression for β (eq. 16). Formally, this is equivalent to examine the effect on β of change of emitting molecule keeping fix the substrate, in the short distance domain. In the limit for small δ ($\tau \to \infty$), with some algebra, it is possible to write:

$$\beta(\omega) \propto \frac{\omega_p^2\, \omega\, \varepsilon_1\, \delta}{(1+\varepsilon_1)^2 \left[\left(\omega^2 - \frac{\omega_p^2}{1+\varepsilon_1} \right)^2 + \frac{\omega_p^4 \delta^2}{\omega^2} \right]} \cdot k_1^{-3} \tag{20}$$

According to this formula, β exhibits a strong resonance at $\omega = \omega_p / \sqrt{(1+\varepsilon_1)}$; this increase of transfer rate will be demonstrated in the following to correspond to the excitation of a longitudinal *surface* wave of charge density that propagates along the *interface* between medium 1 and medium 2 (the substrate). This surface wave is called surface plasmon (SP) and its properties are derived as follows.

7.1.1 Derivation of Surface Plasmon resonance frequency

1.) From the differential wave equation, the dispersion law of a transverse electromagnetic wave propagating inside a non-magnetic ($\mu = 1$) medium with dielectric function $\varepsilon(\omega)$ can be expressed as [138]:

$$k^2 c^2 = \omega^2 \varepsilon(\omega) \tag{21}$$

2.) Eq. 21 has to be modified when an abrupt change in space of the dielectric function occurs, therefore in the presence of an interface (between medium 1 and medium 2). Starting from Maxwell's equations, with some mathematics (*see*, for example, Appendix I in ref. [139]), it is possible to conclude that the presence of an interface *implies* the existence of surface charge density waves described by the following dispersion relation:

$$k_x^2 c^2 = \omega^2 \frac{\varepsilon_1(\omega)\, \varepsilon_2(\omega)}{\varepsilon_1(\omega) + \varepsilon_2(\omega)} \tag{22}$$

Where k_x is the wave vector that characterizes the charge compression and rarefaction along the surface.

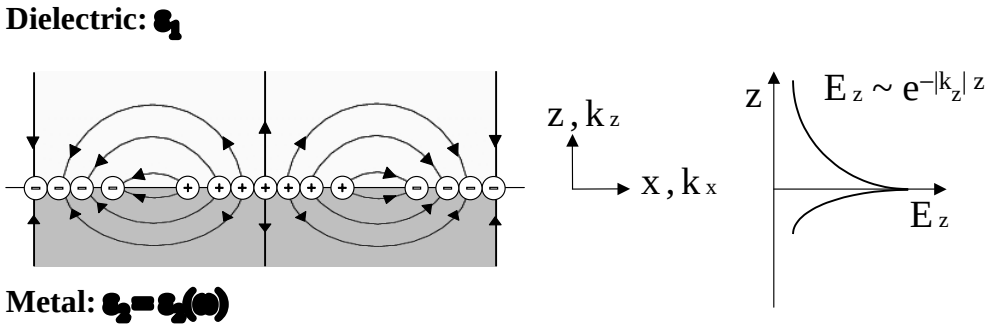

Fig. 40: Charges and field distribution of a surface plasmon travelling (parallel to the x-axis) along the interface between a dielectric ε_1 and a metal modelled as a semi-infinite half-space $z < 0$ described by the dielectric function $\varepsilon_2(\omega)$. The field intensity (sketched on the right side) decays exponentially in the direction z, inside and outside the surface (*evanescent field*).

The electric field lines associated to this longitudinal surface charge oscillation are sketched in fig. 40. The frequency of these oscillations is tied to its wave vector k_x by the dispersion relation $\omega(k_x)$. These charge fluctuations can be localized within a length of about 1 Å from the interface [139]. The associated electric field has the maximum intensity on the plane $z = 0$, and is described by:

$$E = E_0^{\pm} \exp[+i(k_x\, x \pm k_z\, z - \omega t) = E_0^{\pm} \exp[+i(k_x\, x - \omega t)]\, \exp(-|k_z|\,|z|) \qquad (23)$$

with + for $z \geqslant 0$, − for $z \leqslant 0$ and imaginary k_z: this causes an exponential decay of field amplitude (*evanescent field*) along z direction, inside and outside the surface.

Comparing eq. 21 (valid for bulk excitations) with eq. 22 (valid for surface excitations), it is formally correct to define a 'surface dielectric function' $\varepsilon_s(\omega)$:

$$\varepsilon_s(\omega) = \frac{\varepsilon_1(\omega)\,\varepsilon_2(\omega)}{\varepsilon_1(\omega) + \varepsilon_2(\omega)} \quad \rightarrow \quad \frac{1}{\varepsilon_s(\omega)} = \frac{1}{\varepsilon_1(\omega)} + \frac{1}{\varepsilon_2(\omega)} \qquad (24)$$

From bulk dispersion relation eq. 21, the frequency of the bulk plasmon is obtained in the limit $k \to \infty$ and it results defined by the pole in $\varepsilon(\omega)$. Similarly, the frequency ω_s of the interface wave (for $k_x \to \infty$) is the pole in $\varepsilon_s(\omega)$: from eq. 24 the condition is:

$$\boxed{\varepsilon_2(\omega_s) = -\varepsilon_1(\omega_s)} \qquad (25)$$

Since eq. 22 is directly derived from Maxwell's equations, it is valid to describe the dispersion of *any* surface mode, depending the description of solid only on the choice of dielectric function $\varepsilon_2(\omega)$.

In case of metals, Drude's dielectric function eq. 17 can be once more used to approximate $\varepsilon_2(\omega)$. The frequency of surface mode is finally obtained in terms of ε_1 (property of medium 1) and ω_p (property of medium 2). From eq. 17 and eq. 25, it turns out that, in the limit of small δ:

$$\varepsilon_2(\omega_s) = 1 - \frac{\omega_p^2}{\omega_s^2} = -\varepsilon_1 \tag{26}$$

and hence, the frequency ω_{sp} of the surface mode (surface plasmon, SP) becomes

$$\omega_{sp} = \omega_s = \frac{\omega_p}{\sqrt{1+\varepsilon_1}} \tag{27}$$

But this is exactly the frequency at which the energy transfer rate parameter β (eq. 20) has a resonance. The result is this: the energy transfer rate parameter β, derived by the CPS model, is found to be maximal at the emitter frequency with the highest matching with the resonance frequency ω_{sp} of the surface plasmon.

The mechanism of energy transfer from emitter to metallic substrate in the short distance regime is therefore related to the possibility to excite surface charge density oscillations by means of the emitter field.

However a coupling between emitter field and surface plasmon is possible only if energy *and* momentum are simultaneously matched. Beside energy matching also wave vector k matching has to be fulfilled. The excitation of surface modes by means of emitter field is therefore strictly constrained by the dispersion relation, as shown in the following.

7.1.2 Coupling of molecular EM field with Surface Plasmons

When an electromagnetic field couples to a surface plasmon mode of the metal, the resulting *coupled* mode is called *surface plasmon polariton* (SPP); its dispersion relation is obtained as follows.

The dispersion relation of SPP

By inserting eq. 17 (Drude's dielectric function) in eq. 22, the dispersion relation of surface plasmon polaritons is obtained in terms of ω_p and ε_1:

$$k_x^2 = \left(\frac{\varepsilon_1\omega^2}{c^2}\right) \cdot \frac{\omega^2 - \omega_p^2}{\omega^2(1+\varepsilon_1) - \omega_p^2} \tag{28}$$

The dispersion curve is drawn as a solid curve in fig. 41. Since eq. 28 is a quadratic equation in ω^2, for every value of k_x there are two solutions in ω^2 and the dispersion

curve exhibits two branches. It is easy to show that for $k_x \to 0$ the lower branch (a) approaches $\omega = ck_x/\sqrt{\varepsilon_1}$, whilst the upper branch (b) the constant value ω_p; on the other side, for $k_x \to \infty$, the upper branch approximates $\omega = ck_x/\sqrt{\varepsilon_1}$, while the lower branch the constant value $\omega_{sp} = \omega_p/\sqrt{1+\varepsilon_1}$.

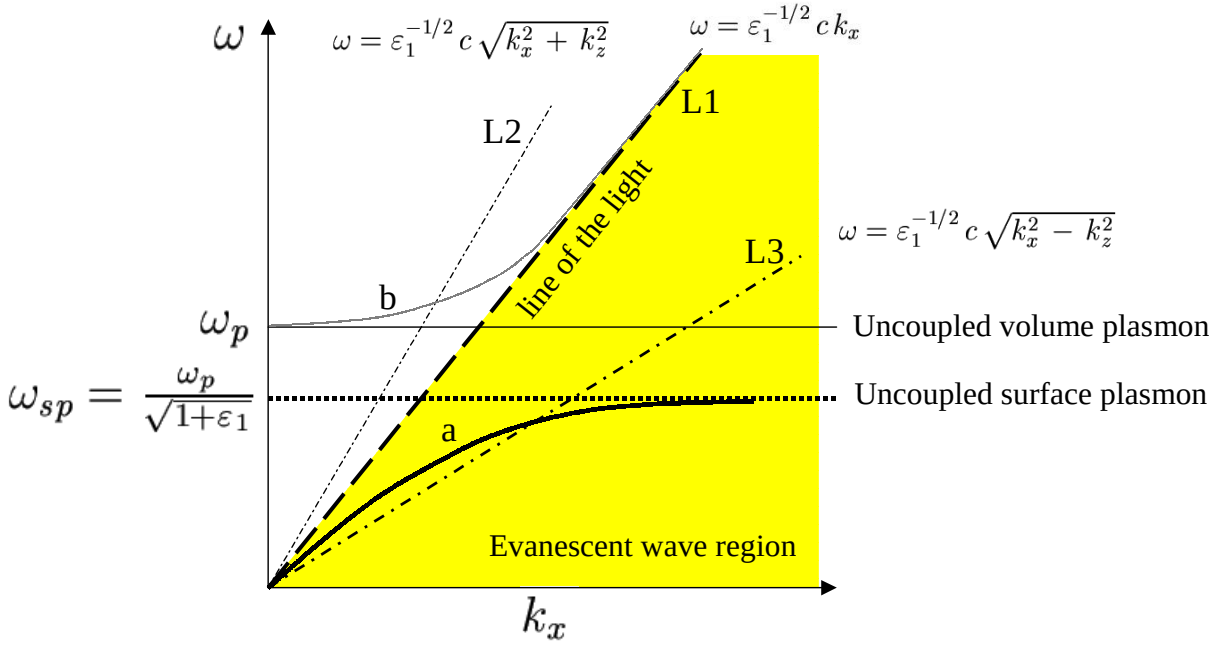

Fig. 41: a,b: branches of the dispersion relation of plasmon polariton modes in a metal. The surface plasmon dispersion curve (a) lies *right* of the 'line of the light' L1 (dispersion relation for the light in the medium 1 at grazing incidence): the mode has therefore a *longer* wave vector than the light of the same energy $\hbar\omega$ propagating along its surface and cannot be excited by these photons. Only evanescent waves (dot-line curve, L3), with imaginary (perpendicular to surface)-wave vector k_z, can effectively couple with the surface mode on the metal, because their dispersion curve cross that of SPP at finite k_x. But this is just the case of the field around an excited molecule (near field): it is evanescent in nature and it can therefore excite SPP in a metal when the emitter is brought to the vicinity of the substrate surface fig. 42. *See* text for further details.

The two branches exhibit an 'avoided crossing' behaviour and approach only asymptotically the light dispersion relation curve inside the medium 1 ('light line', L1) drawn as a dashed line for the case $k_z = 0$, i.e. at grazing incidence.

Since the surface plasmon polariton dispersion curve (a) *nowhere* intersects the light line L1 (even for grazing incidence), no external electromagnetic wave can excite this polariton: energy and momentum cannot be simultaneously conserved.

Differently speaking, the SPP modes on a metallic surface cannot be directly excited

by the light incident on the surface, because the component of the wave vector of the light parallel to the surface is smaller than that of the surface plasmon polariton and the requirement of momentum conservation is not satisfied.

Furthermore, if the incident beam is tilted toward the perpendicular (L2, $k_z \neq 0$), it intersects both the continuum of transverse bulk waves (the region with $\omega^2 > \omega_p^2 + c^2 k_x^2$) giving rise to normal refraction and the upper branch (b) of SPP dispersion curve. However in this case the energy leaks immediately in the degenerate bulk modes and no excitation of the surface mode is possible. Remarkably, in the range of frequencies between ω_p and ω_{sp} no direct coupling with the external field is possible.

In conclusion, there is *no* angle of incidence for which a true (lower branch) surface plasmon polariton can be excited by an external EM wave. The SPP dispersion curve lies *right* of the light line: this surface mode is therefore a *non-radiative* mode and for this reason is not involved in the theory of optical refraction.

The excited molecule as SPP exciter

The only way to permit a coupling between an EM wave and the surface polaritons is to use waves with *imaginary* wave vector component in z-direction k_z (so that $(k_z)^2 = -k_z^2$ in the argument of square root), therefore an *evanescent* field perpendicularly to the metal surface. The dispersion relation of such a wave is visualized in fig. 41 by the line L3: this line crosses the SPP dispersion curve and a coupling between evanescent field and surface mode becomes possible.

An evanescent wave, nothing else than a particular solution of Maxwell's equations, can be experimentally obtained when the condition for light propagation is not satisfied, as in devices (like prisms) used in total internal reflection technique (*see*, for example [140, and reference therein]).

On microscopic scale, *the field around an excited molecule is nevertheless evanescent* in nature. This field (*near field*), has an imaginary wave vector z-component, it decays exponentially away from the emitter and therefore it can fulfil the wave vector matching requirements for the excitation of surface modes on the metals.

Within the near-field distance range (i.e. $d < 300\,\text{Å}$ for *MePTCDI*), an excited molecule can therefore non-radiatively excite a surface charge oscillation mode on the metal by means of its evanescent field and in this way transfer effectively energy to the substrate. This effect is sketched in fig. 42

The excitation of SPP in metals by the near field of the excited molecules in thin film deposited in the vicinity of a metal surface has been experimentally confirmed by means of momentum-matching techniques (like ATR, Attenuated Total Reflection), in a series of experiments of *Weber and Eagen* [141] and *Pockrand and Brillante* [142].

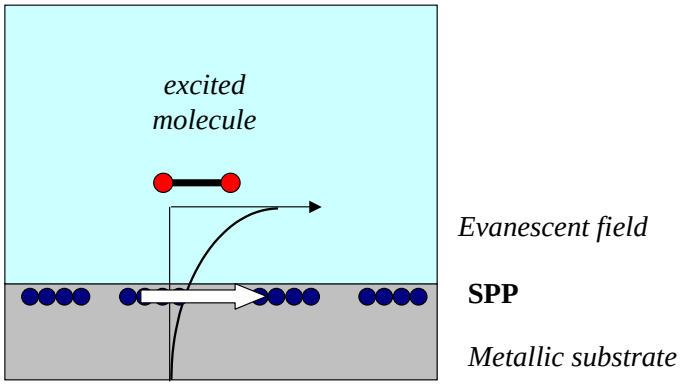

Fig. 42: At small distance from a metallic substrate, the near field of an excited molecule can non-radiatively excite a SPP in the metal by means of its evanescent field and in this way transfer effectively energy to the solid.

7.2 Calculations for *MePTCDI* on *Ag* in the near-field range

It is now possible to exemplify the theoretical approach up to now developed and to calculate both the *parameter of energy transfer rate* β as a function of emitter frequency in the near-field distance domain and the *dissipated power* from the emitter as a function of k_x, the wave vector of emitted field projected on the surface. The two curves are shown in Fig. 43 and Fig. 45, respectively.

A specific system is chosen for the calculations: the interface between a non-absorbing medium (argon), on which an emitting dipole (the *MePTCDI* molecule) is deposited and a metal (*Ag(111)*) used as a substrate. The emitter is placed at a near field distance from the surface of the metal, so that the assumptions of eq. 16 are valid.

7.2.1 Calculation of the energy transfer rate parameter β

Following eq. 16 and eq. 20 the energy transfer rate parameter $\beta(\omega)$ has been calculated for energies of the dipole ranging from 2 to 10 eV, being the emitter separated by an argon spacer with $d < 100$ Å from the *Ag(111)* surface, whose properties are described either by a model dielectric function or by an experimentally determined one.

In the first case, to calculate $\beta(\omega)$ the dielectric function of the metal has been analytically expressed by the Drude's model (eq. 17) using the values $\omega_p = 13.9 \cdot 10^{15}$ rad/s [140] ($\hbar\omega_p = 9.14$ eV) and relaxation (collisional) time $\tau_c = 31 \cdot 10^{-15}$ s [135], whereas the dielectric constant of argon is valued $\varepsilon_1 = 1.68$. Real and imaginary part of Drude's $\varepsilon(\omega)$ for *Ag* are plotted as dashed lines in fig. A.1.

The so calculated $\beta(\omega)$ curve is plotted (in semi-log scale) as a black line in fig. 43. The curve exhibits a strong resonance at $\hbar\omega = 5.58$ eV. At this energy, the condition (eq. 27) for

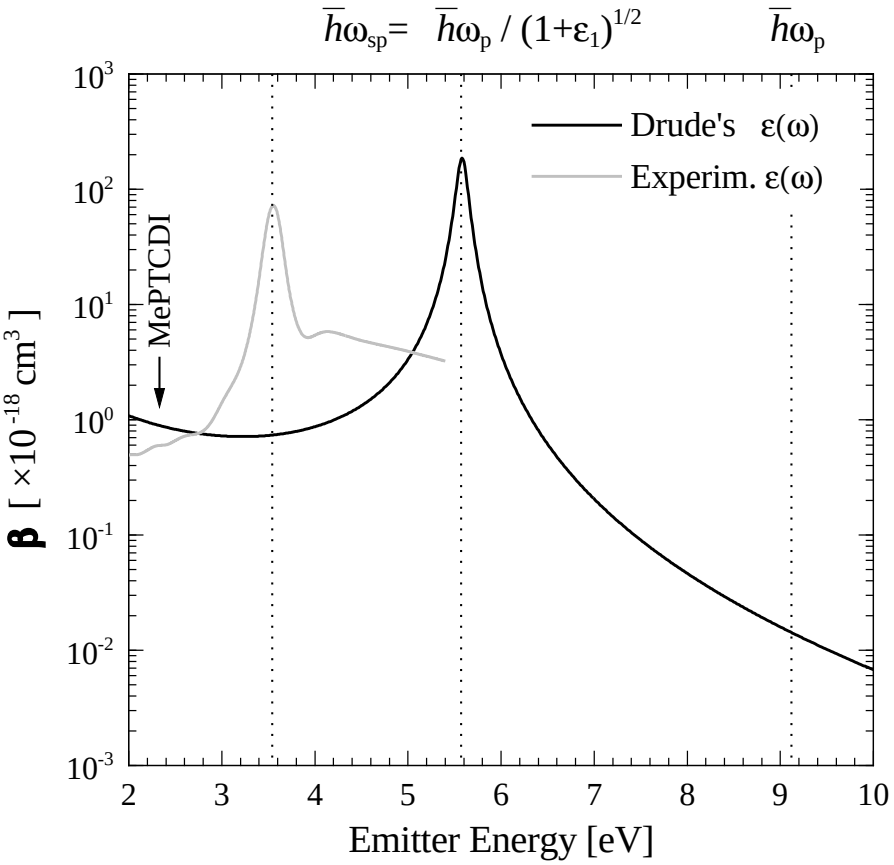

Fig. 43: (Black line) - Calculated energy transfer rate parameter (β, eq. 20) as a function of the emitter energy when it is deposited on a non-absorbing medium (argon, $\varepsilon_1 = 1.68$) at a distance $d < 100$ Å from a metallic substrate (here, *Ag(111)*). The dielectric function of the metal has been analytically expressed by a Drude's dielectric function (with $\hbar\omega_p = 9.14\,\text{eV}$, $\delta = 3.2 \cdot 10^{13}\,\text{s}^{-1}$ [135]). The curve exhibits a strong resonance at $\hbar\omega = \hbar\omega_{sp} = 5.58\,\text{eV}$, corresponding to the excitation of the surface charge density oscillation mode (SPP) at the metal-dielectric interface. The plasma resonance energy $\hbar\omega_p$ is also indicated.
(Grey line) - β-curve calculated keeping into account the actual *experimental* values [135] of $\varepsilon(\omega)$ for silver. The position of the surface resonance peak ($\hbar\omega = 3.56\,\text{eV}$) turns out to be strongly red-shifted because of the large contribution to the dielectric function from the interband transitions in the metal. The emission energy of *MePTCDI* molecule is indicated by an arrow.

the resonant excitation of surface charge density oscillations (SPP) at the metal-dielectric interface is fulfilled ($\omega = \omega_{sp} = \omega_p / \sqrt{(1+\varepsilon_1)}$) and a strong energy transfer from emitter to substrate is predicted to take place. Furthermore, the peak width is related to δ (the inverse electron collision time), becoming the FWHM smaller when $\tau_c \to \infty$ ($\delta \to 0$, limit for undamped electron gas).

Since a *model* dielectric function has been used (based exclusively on free electrons contributions) a number of effects as, for example, contributions to $\varepsilon(\omega)$ coming from interband transitions in the metal [135,143,144] are not taken into account. In Appendix A, the Drude's model dielectric function of silver is compared with the experimental dielectric function to evidence how large can be the discrepancy between the two quantities at energies *above* the interband transition in the metal.

Such a discrepancy in $\varepsilon(\omega)$ is reflected in a complex way (through eq. 16) also in the form that $\beta(\omega)$ assumes when the emitter energy is thought to scan the visible range across the interband transition energy. In fact, if instead of a model function the actual experimental values of the dielectric function are used, the features of $\beta(\omega)$ change drastically.

The grey line in fig. 43 shows the energy transfer rate parameter calculated using the experimental values of $\varepsilon(\omega)$ [135]. The curve exhibits a resonance, that can be still partially described in terms of coupling to surface charge oscillations, but the position of the peak ($\hbar\omega = 3.56\,\mathrm{eV}$) turns out to be strongly red-shifted and the general shape of the curve to be different. Responsible for that are the interband transitions in the metal which induce a large modulation in the dielectric function, superimposed to the Drude's term (*see* Appendix A for a detailed discussion of this point).

From now on, where not differently indicated, only experimental dielectric functions will be considered, in order to correctly estimate the expected value of energy transfer rate.

This approach is useful since it permits to visualize and estimate how strong is the energy transfer rate (once chosen spacer and substrate) at the emitting frequency of a given excited molecule.

1) Energy transfer rate $\hat{b}_{ET}$ value for *MePTCDI* at d=10 Å from *Ag*

Fig. 43 plots the expected values of $\beta(\omega)$ for different emitter frequencies by supposing to keep fix the substrate, the spacer and the distance between emitter and substrate ($d < 100\,\mathrm{Å}$). Since every molecule does emit at its own energy, the plot can be imagined as representative of the effect of a particular configuration spacer/substrate when various molecules are alternatively deposited on it.

The same figure shows clearly that in the case of the system *MePTCDI*/argon/*Ag(111)*, the molecular emission (indicated by an arrow) takes place at a nearly off-resonance energy

with respect to the peak at 3.56 eV: the energy transfer (and therefore the observed molecular lifetime shortening) is nevertheless rather *strong* in absolute value.

In fact, the rate parameter amounts to $\beta_{Me} \sim 0.6 \cdot 10^{-18}\,\mathrm{cm}^3$. From β's defining equation (eq. 16), it holds: $\hat{b}_{ET} = \beta\, d^{-3}$; if $d = 10$ Å ($d = 10^{-7}$ cm, $d^{-3} = 10^{21}\,\mathrm{cm}^{-3}$), then $\hat{b}_{ET} \sim 0.6 \cdot 10^{-18} \cdot 10^{21} \sim 600$; since $\tau = \tau_0 / \hat{b}_{ET}$, the measured fluorescence lifetime is expected to be shortened more than two orders of magnitude, when the molecule is brought in proximity of the substrate.

2) Effect of changing the spacer type
Kept fixed the substrate and the emitting molecule, it is evident that the resonance frequency ω_{sp} is defined (eq. 27) by the value of ε_1, therefore by the choice of the medium 1, in the present case the spacer. Different values of β at the molecule emission frequency are therefore observed just by changing the type of spacer layer (for example using LiF, ammonia, xenon or krypton instead of argon) on the same substrate, because of the change of the position of the resonance peak.

3) Effect of changing the molecule
Changing the emitting molecule, its own emission energy $\hbar\omega$ is different and therefore the value of β, too. In this way, different molecules experience different lifetime shortening effects on the *same* spacer and substrate.

As an example, it is worthwhile to calculate the expected lifetime shortening when various molecules are placed (by argon spacer) at a fixed distance ($d = 10$ Å) from a silver substrate. The molecule is supposed to be aligned *parallel* to the surface and possesses a fluorescence quantum yield q. The value found for $\hat{b}_{ET}$ has to be scaled with respect to the quantum yield of *MePTCDI* molecule ($q = 0.93$ [43]).

When *MePTCDI* is deposited on silver, the total damping $\hat{b}_{ET}$ amounts to more than two orders of magnitude. If, for example, instead of *MePTCDI* $^3n\pi^*$ pyrazine is considered ($\hbar\omega \sim 3.3$ eV, $\beta(\omega) \sim 5.25\,[10^{-18}\,cm^3]$) at $d = 10$ Å the damping is expected to be about five thousand. On the contrary, by depositing $^3n\pi^*$ biacetyle on silver ($\hbar\omega \sim 2.29$ eV, $\beta(\omega) \sim 0.58\,[10^{-18}\,cm^3]$)) a very similar effect to that on *MePTCDI* should be observed.

As a consequence (from eq. 16 and fig. 39, inset) upon change of the molecule, the normalized lifetime model curve ($a \sim d^3$) is expected to shift down (more energy transfer) or up (less energy transfer) depending on the β value.

7.2.2 Calculation of power dissipated by *MePTCDI* on *Ag*

The only energy matching is not a sufficient condition to have coupling between excited molecules and the surface mode of the substrate: momentum matching is necessary, too.

The excited dipole looses energy radiatively and non-radiatively and its emitted power is distributed over a complete spectrum of wave vectors.

The essential value of the theoretical framework of the CPS model lies in the possibility to examine *where* the power of the excited dipole is dissipated as a function of $u = k_x/k_1$ (with k_x the dipole field wave vector in the plane of the substrate and k_1 the radiative dipole far field wave vector in medium 1).

As originally discussed by CPS [11] and later by others [14, 22, 145] (and already briefly pointed out at p. 90) the integral in eq. 12 can be broken down into various components: the integral over $0 \leqslant u \leqslant 1$ represents the modification of the dipole decay rate due to coupling to the *radiation* field (the value of u dictates the direction of emission), whereas the integration over the range $1 < u < \infty$ represents the total energy transfer rate through *non-radiative* loss mechanisms all having a wave vector greater than the photon wave vector.

Fig. 44 helps to understand qualitatively the point. In far field the excited dipole does radiate, within the medium 1, propagating plane waves with wavelength λ and propagation vector ($k_1 = 2\pi\sqrt{\varepsilon_1}/\lambda$) with real z-component. Depending on the incidence angle, the projection of this wave vector on the plane of the interface (k_x) varies, but it cannot be in any case bigger than k_1. For the normalized wave vector u, it holds: $u = (k_x/k_1) \leqslant 1$, with sign equal only at grazing incidence.

The normalized wave vector values u associated to the radiative field of the dipole are therefore in any case $0 \leqslant u \leqslant 1$. The values $u > 1$ are associated exclusively to components of the emitter field with wavelength shorter then that of radiation, i.e. to the near, evanescent field components of dipole field.

Furthermore, in the near-field domain the emitter field contains not only one, but a complete spectrum of wave vectors k; their projection k_x on the interface forms also a distribution of values. If the wave vector of SPP mode is matched by one of these, the excitation of longitudinal charge oscillation on the surface takes efficiently place. Since the SPP modes dissipate their energy within the solid (or also re-radiate), the net result of this process is an effective energy transfer from the emitter to the substrate.

Fig. 45 shows the imaginary part of the integrand in eq. 12 in log-log scale. The plotted quantity is directly related to the *power dissipated* by the emitter as a function of the normalized wave vector $u = k_x/k_1$ and it has been calculated for the case of a perpendicular *MePTCDI* molecule, placed at various distances ($d = 0-600$ Å) above a silver surface by means of argon spacers.

The plot exhibits three key features, corresponding to three different ranges for u:

I The region $0 \leqslant u \leqslant 1$ represents the modification of the radiative decay rate of the dipole due to the presence of the surface.

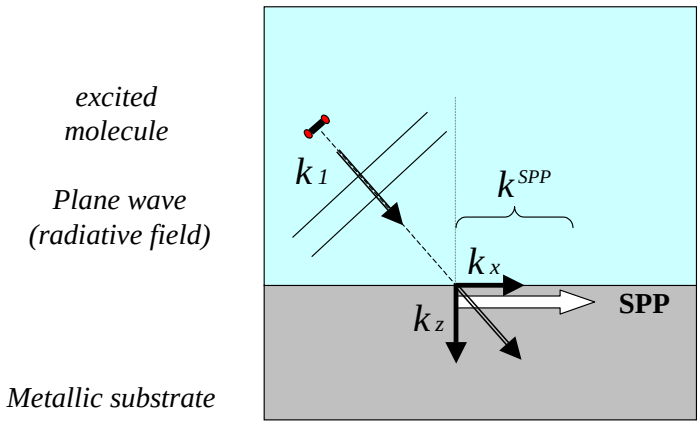

Fig. 44: Far away from the substrate the excited dipole does radiate, within the medium 1, plane waves with wavelength λ and propagation vector $k_1 = 2\pi\sqrt{\varepsilon_1}/\lambda$. Depending on the incidence angle, the projection of this wave vector on the plane of the interface (k_x) can assume all the values with $k_x \leqslant k_1$, with '=' valid at grazing incidence. If $u = (k_x/k_1)$, the $0 \leqslant u \leqslant 1$ are associated with the radiative component of the emitter field. The surface plasmon polariton (SPP) has a wave vector larger then every k_x of photons: for this reason the SPP can *not* be excited by the radiative field of the dipole.

II The sharp spike at $u \sim 1.09$ is related to the strong increase in emitted power when *resonant* coupling to the SPP *eigen*mode of the interface argon-silver occurs. Since for this mode $u > 1$, the coupling to it can only occur via non-radiative components of the emitter field.

III The region with $u \gg 1$, where a broad feature develops and increases rapidly in strength as d falls. This additional non-radiative decay route represents the coupling between the near field of the emitter to the interband transitions in the solid with simultaneous scattering of the excited electron with phonons and impurities of lattice [146]. These modes, called also 'lossy modes' (LM) [145], totally dissipate their energy in scattering within the substrate.

So defined, the emitted power (unphysically) diverges at $d = 0$ when $u \to \infty$, whereas at $u = 1$ the integrand function exhibits a singularity.

To put in evidence the correspondence between peak at $u \sim 1.09$ (as numerically derived from the CPS model) and the excitation of SPP on the interface argon-silver, it is worthwhile to calculate the normalized wave vector u_{spp} at which the surface mode is expected to resonate, keeping into account the actual interface parameter.

Making use of the dispersion relation of the electromagnetic wave in medium 1 (eq. 21) and that of the mode on the interface (eq. 22) it is possible to express analytically u_{spp}

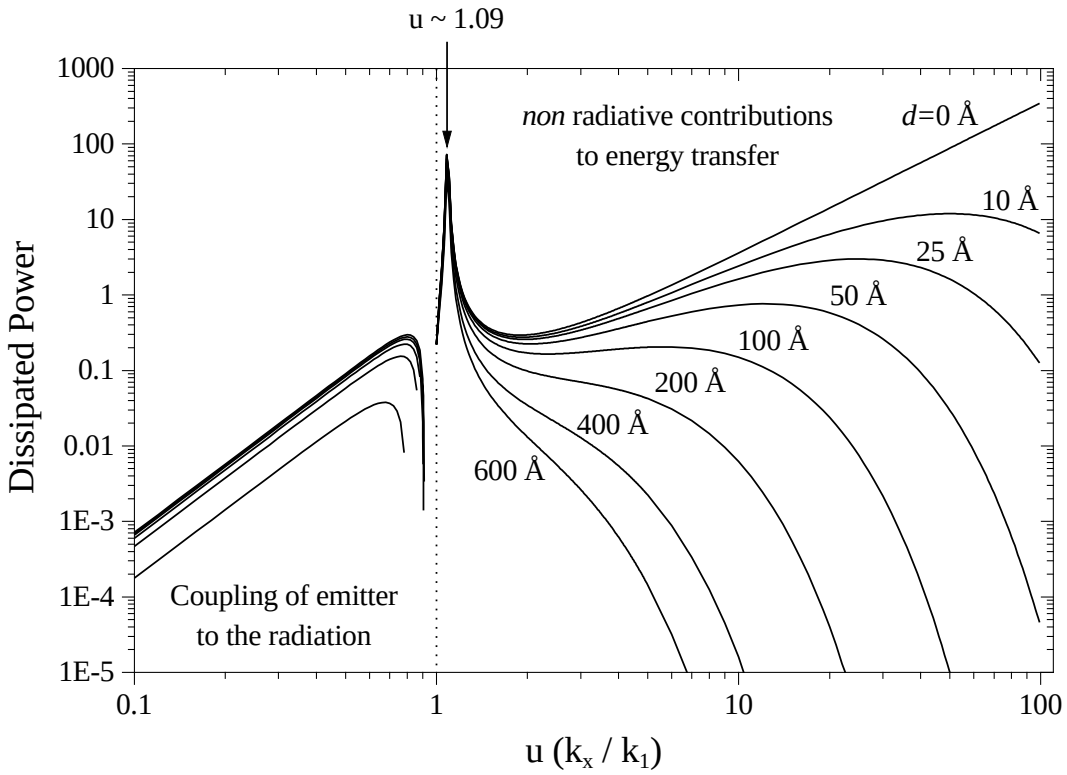

Fig. 45: Imaginary part of the integrand in eq. 12 (related to the power dissipated by the emitting dipole) calculated as function of the normalized wave vector $u = k_x/k_1$, for a perpendicular *MePTCDI* molecule located at various distances ($d = 0-600$ Å, argon spacer) above a silver surface. The area under these curves is proportional to the energy transfer rate from the excited molecule to the substrate. The range $0 \leqslant u \leqslant 1$ represents the *radiative* contribution to decay rate, the range $1 < u < \infty$ the *non-radiative* contribution; the spike at $u \sim 1.09$ is caused by strong energy transfer via resonant coupling to the SPP mode at the argon-silver interface. Furthermore, as the distance is shorter, proportionally more important becomes the energy transfer through high wave vector ($u \gg 1$) components. At $d = 0$, so defined, the power diverges. Log-log plot.

as:

$$u_{spp} = \frac{k_{spp}}{k_1} = \frac{1}{\sqrt{\varepsilon_1}} \cdot \sqrt{\frac{\varepsilon_1 \varepsilon_2}{\varepsilon_1 + \varepsilon_2}} = \sqrt{\frac{\varepsilon_2}{\varepsilon_1 + \varepsilon_2}} \tag{29}$$

Using the values $\varepsilon_1 = 1.68$ (argon) and $\varepsilon_2 = -10.6 + i\,0.9$ (silver) at *MePTCDI* molecule emission energy, it turns out: u_{spp}=1.087, in agreement with the position of the peak as numerically derived from the CPS model.

7.2.3 Calculation of decay probability through the 3 competing mechanisms: Rad, SPP and LM

It is possible to calculate which is the fraction of power dissipated by the dipole via emission of photons (RAD), via SPP coupling and via lossy modes (LM) respectively, as a function of the distance from the substrate.

The decay probabilities have been calculated for *MePTCDI* on *Ag* by scaling, with respect to the total decay rate (eq. 12), the dissipated power (fig. 45) integrated on the range $0 \leqslant u \leqslant 1$ (for RAD), on the range $1 < u \leqslant (2u_{spp} - 1)$ (for SPP, with Lorentzian approximation of the peak) and on the range $(2u_{spp} - 1) < u < \infty$ (for LM).

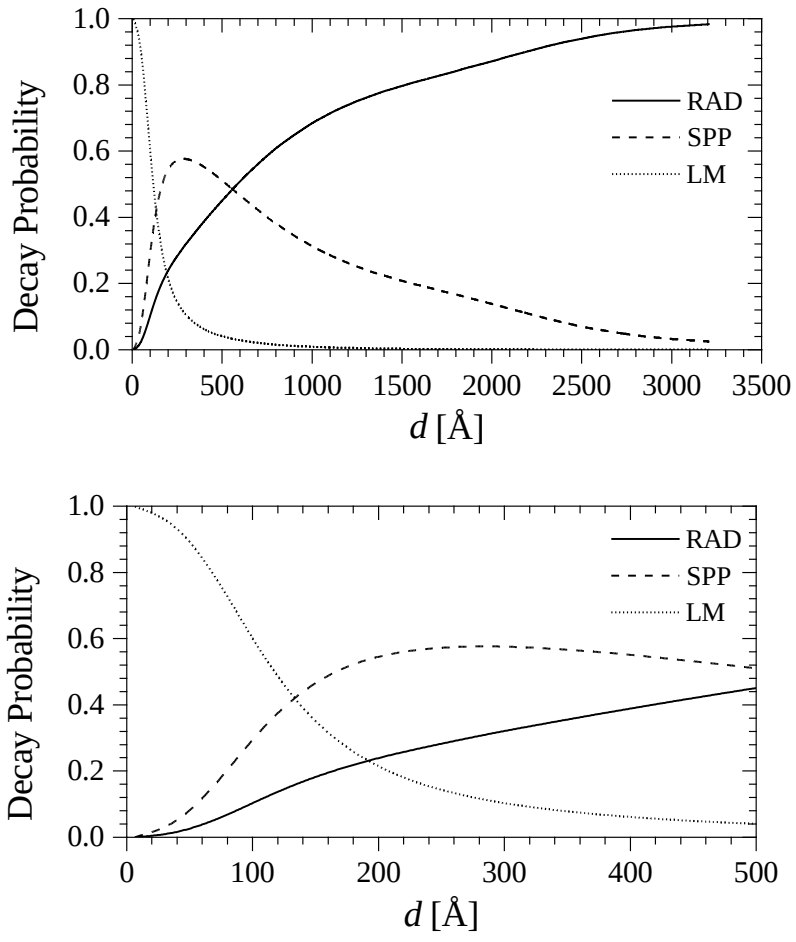

Fig. 46: Calculated relative (sum=1) decay probability (fraction of power dissipated) for isotropically oriented *MePTCDI* molecules separated from a metal (*Ag(111)*) by an argon spacer, as a function of the distance d from the substrate. Three main mechanisms contribute to the decay: via emission of photons (RAD), via resonant excitation of SPP or via interband transitions (LM) in the substrate. Two different x-scale ranges of the same plot are shown. *See* text for details.

Fig. 46 shows (in two different distance ranges) the three relative contributes. The change in importance of each of these decay route is plotted as a function of distance d of the emitter from the surface. The plot can be analysed as follows.

At distances d comparable with the emission wavelength ($d \gtrsim 1500\,\text{Å}$), the emission is primarily into photons and the decay probability via radiative emission (RAD, continuous line) is found to dominate on the other processes.

At distances of the order $d = 150-500$, i.e., much larger than atomic dimensions but less than the emission wavelength, energy transfer via surface plasmon polariton (SPP, dashed line) becomes the predominant decay route.

At smaller values of d ($d < 100\,\text{Å}$), the dissipation arises from non-resonant coupling between the evanescent field associated with the near field of dipole and the solid. The coupling between emitter and lossy modes (LM, dotted line) represents the most effective intrinsic loss mechanism in the metal and it is found definitely to dominate the decay rate at short distances.

Isotropically oriented dipoles exhibit a probability to decay in SPP equal to $\sim 55\%$ at $d \sim 250\,\text{Å}$; nevertheless the SPP coupling probability can be very higher in some configuration ($> 90\%$ for a perpendicular dipole). It is somewhat surprising that SPP coupling is maximal *away* from the metal surface: the SPP coupling rate decreases exponentially with increasing d and it should actually be maximum at zero distance. What observed is a consequence of the competition between the SPP decay channel and the interband-transition in the solid (LM). As the separation is reduced, this latter decay route proportionally increases more rapidly and it becomes the dominant fraction of the whole decay. The distance dependence of coupling between emitter and the SPPs was experimentally confirmed [142] and a maximum coupling distance of approximately 200 Å was found.

7.2.4 Removing the divergence of power dissipated at $d = 0$ Å

The classical model is actually based on assumptions which lead to *un*physical behaviour at very small molecule-surface separations. Namely, as shown in fig. 45, both the energy transfer rate and the dissipated power diverge for large u values (large k-vectors) as the distance d approaches zero.

To describe the coupling between emitter to photons, which dominate at large distance from the surface, the full retarded solution of Maxwell's equations have to be used, but the substrate can be treated in a simple *local* approximation ($\varepsilon(\omega)$ does not dependent on k-vector) with a sufficient accuracy.

On the contrary, to describe the decay processes occurring at small distances from the solid, a simplified quasi-static approximation for the electromagnetic fields can be used, but a *non-local* solid response is required.

By including (although *a posteriori*, taking the electron-electron interaction partially into account) a k-vector dependence in dielectric constant $\varepsilon(\omega)$, this unphysical behaviour can in any case be corrected [145, in particular § 3.2 therein]. In the 'corrected' model, the metal is thought to absorb energy from the emitting dipole only when electrons below Fermi level are excited to states above it. The excitation of an electron is possible only when the momentum conservation condition is satisfied; once fixed the excitation energy, the 'excitable' electrons are inside a thin shell in k-space, depending on k_F (the Fermi wave vector of the solid) and on the frequency of the emitter field.

If the emitter k-vector lies outside this range in k-space, the emitter incident field cannot obey the momentum conservation condition for the electron-hole pair excitation in the solid and hence *no energy* is transferred to the substrate. Taking into account the k-vector dependence it is found that the dissipated power does not diverge anymore (as it happens in fig. 45), but it exhibits a maximum at large u and then it goes to zero, because with still higher k-vectors do not fulfil anymore the momentum matching condition.

By including the wave vector dependence of dielectric constant, the unphysical behaviour of classical theory can be therefore corrected.

In the following section, the possibility to extend the application of the classical model to semiconductor solids will be discussed and in § 8.3 and § 8.4 the theory will be quantitatively applied to analyse the observed distance dependent lifetime-shortening of *MePTCDI* molecules deposited on MoS_2 and *Si(111):H*.

7.3 Energy transfer to semiconductors

The theoretical approach followed up to here has been developed and exemplified by considering exclusively *metallic* substrates. From eq. 6 to eq. 12, the effect of the presence of the substrate on the emission properties of an electronically excited molecule is schematically accounted for as follows:

- The molecular emitting dipole field incident on the solid is partially reflected and partially absorbed according to the value of the complex dielectric function $\varepsilon(\omega)$.
- The reflected fields are appropriately summed to give the electric field at the position of the emitting dipole.
- The modified lifetime of the emitting state in presence of the substrate is directly related to the imaginary part of the electric field at the emitting dipole (eq. 10).

Within this classical model the energy transfer to the substrate is taken into account phenomenologically, by describing the solid by its dielectric function $\varepsilon(\omega)$, without any microscopic description of the material.

In the short distance approximation, the decay rate $\hat{b}_{ET}$ exhibits a d^{-3} dependence (eq. 15). This functional dependence is independent of the *nature* of the solid, depending

the lifetime shortening effect only on $\varepsilon(\omega)$.

The fact that the classical model predicts, beside oscillations in observed emitter lifetime, also a drastic lifetime-shortening in the small distance domain **implies that the quenching mechanism is entirely described by the dielectric function of the solid**.

It is thus formally correct to apply the CPS model also to the study of the interaction between excited molecules and a *semiconductor*, making use of the appropriate dielectric function to describe the solid [c].

7.3.1 Limits of application of the classical model to semiconductors

By extending the classic model to semiconductors, it is still possible to maintain a large correspondence with the approach earlier developed. Starting from the expression for the energy transfer rate $\hat{b}_{ET}$ valid in short-distance domain (eq. 15), the energy dissipation can be still described in terms of resonant excitation of surface modes.

As dispersion relation of these surface modes (now on the semiconductor surface) eq. 22 can be immediately adopted, since this formula was directly derived from Maxwell's equations in presence of a interface (without reference to solid structure).

Further, in order to describe the dielectric properties of the semiconductor (as the n-type doped silicon presently used), it is still consequent to introduce the Drude model and the Drude dielectric function (eq. 17) [d], since free carriers usually introduced into semiconductors by doping behave in may ways like those in simple metals [138].

As shown for the metals, the energy transfer rate can be successively expressed in terms of excitation of surface charge density oscillations (SPP) (eq. 20, eq. 27 and fig. 43), whose frequency ω_{sp} is related with the physics of the solid through the plasma frequency value ω_p (eq. 27). The plasma frequency is defined as in eq. 19 and it depends only on the *free carrier density* n.

But, whereas in a metal the carrier concentration is on the order of $n \sim 10^{22}\text{cm}^{-3}$ and the corresponding plasmon energies are on the order of $8-10\,\text{eV}$, in a semiconductor the density of free electrons in the *conduction band* amounts to $n \sim 10^{17}\text{cm}^{-3}$ and the corresponding plasmon energies (and consequently surface plasmon energies ω_{sp}) are in the range of $10-30\,\text{meV}$, therefore in the Infra-Red (IR) region of the spectrum.

[c] A complete *non-local* treatment is required to describe correctly the energy transfer to semiconductor substrates [13], but at least formally the application of the classical model to non-metallic solid is however possible.

[d] In reality the best approximation for the dielectric function of a doped semiconductor is given in terms of a component Drude-like that takes quantitatively into account the *free carrier* density and of a component of *harmonic oscillator* where the resonance frequency is the frequency ω_{TO} of the transverse optical bulk phonon [71]; this simplification does not influence however the result.

For molecules that emit in the visible range (as *MePTCDI*) there is no possibility to couple to modes so far in energy and consequently the energy transfer is expected to be very low.

7.3.2 Interband transition contributions in semiconductors: use of realistic dielectric function

As seen in the case of *Ag* (Appendix A.1), the free electron dielectric function is useful in describing the properties of the solid only when the emitter photon energy lies *below* the threshold for the onset of any interband transition. Above this threshold the form of $\varepsilon(\omega)$ (and most of all the form of $\mathrm{Im}(\varepsilon(\omega))$) depends almost exclusively on the specific *band structure* of the material.

The observation (fig. 43) that even on metallic substrates as *Ag* the description of the solid uniquely by the Drude's model fails and that the interband transitions must be taken into account in $\varepsilon(\omega)$ to permit reliable quantitative analysis of the energy transfer rate does justify the possibility to extend to semiconductors the methods and the ideas developed for metals.

In fact, in semiconductors (particularly in *UV-Vis* spectral range) the dielectric response is almost exclusively contributed by *bound electrons* and by the *band structure* of the electronic states in the crystal lattice. **Thus, the direct application of the classical model to semiconductors is still justified on condition that the *actual* dielectric function of the solid is used in the calculations.**

7.3.3 Numerical calculations for *MePTCDI* on semiconductors

The expected energy transfer rate parameter $\beta(\omega)$ and the dissipated power have been numerically calculated in the case of *MePTCDI* deposited both on MoS_2 and *Si(111):H* substrates, keeping into account the experimental value of dielectric function of these materials. The spacer dependent measurements have been successively analysed by the light of these calculations. The results will be shown and discussed in § 8.3 and § 8.4.

8 Discussion

Organization of the chapter

In this section, the low-temperature in–situ time resolved fluorescence measurements carried out on ultrathin (0.01 ML) *MePTCDI* film deposited on semiconductor substrates are *quantitatively* analysed.

In particular, the results of the measurements on structures formed by *isolated* organic molecules, deposited on argon *spacer* of well defined thickness, condensed on inorganic *semiconductor* substrates are discussed.

The non-radiative interaction mechanism between electronically excited *MePTCDI* molecules and MoS_2 or *Si(111):H* substrates and its dependence on the molecule-substrate distance is analysed by applying the CPS theoretical model.

The chapter is organized as follows:

- § 8.1 is a summary of the essential aspects of the experimental approach followed during the research and of the main results.
- In § 8.2 the criteria for application of the CPS model to semiconductors are revisited, the physical quantities used in the calculations are introduced and the method commented.
- In § 8.3– 8.4 the experimental results are *quantitatively* discussed in the framework of the CPS model:
  - *CPS and MePTCDI on* MoS_2 (§ 8.3)
  - *CPS and MePTCDI on Si(111):H* (§ 8.4)
    1) The calculated fluorescence lifetime shortening curves are compared with the experimental data.
    2) The plot of the frequency dependent energy transfer rate parameter $\beta(\omega)$ is calculated starting from the experimental values of the dielectric function of MoS_2 and *Si(111):H* respectively.
    3) The plot of the power dissipated by the electronically excited molecule in proximity of the semiconductor surface is calculated for a number of different emitter-substrate distances.
- In § 8.6 the importance of considering the band structure of the semiconductor substrates in the study of their interaction properties is pointed out. A model (SDK) explicitly dealing with the band structure is introduced, briefly described and finally applied to the cases of *MePTCDI* on MoS_2 and on *Si(111):H*.

8.1 Essentials of the experimental results

Isolated molecule approach

In § 3.4 it has been experimentally shown how, by continuously reducing the molecular film thickness well below the single monolayer coverage, the intermolecular interaction among the *MePTCDI* molecules within the amorphous organic film are reduced and by this the excitation transfer inside the film.

In the limit of 0.01 ML coverage these *intra*-layer excitation transport phenomena are interrupted and the fluorescence exhibits pure monomeric character without any residual excimeric component (fig. 18) and monoexponential decay (fig. 19).

Using the isolated molecule approach it has been possible to analyse the *direct interaction* between the isolated *MePTCDI* molecules and different kinds of substrate. These measurements have been described in section 4.1.

Argon spacer measurements

Furthermore, by condensing (at helium temperature) an argon layer (*spacer*) on the substrate before deposition of the *MePTCDI* molecules, it was possible to study the *distance dependence* of the excitation transfer rate from the molecules toward the substrate (fig. 47). The spacer measurements have been described in section § 4.2 and § 4.3 for MoS_2 and *Si(111):H*, respectively.

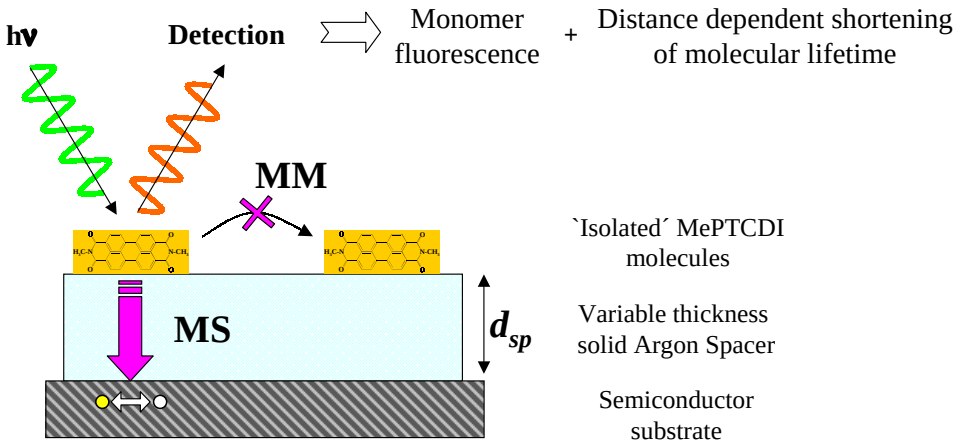

Fig. 47: Inside ultrathin molecular films the Molecule-Molecule interaction (MM) is negligible (isolated molecule limit). It is thus possible to quantify directly the effect of Molecule-Substrate interaction (MS) (i.e. the non-radiative energy transfer from electronically excited molecule to the solid) by measuring the distance dependent variation of the fluorescence properties of the molecule. The molecule-substrate relative distance is set by a spacer of solid argon.

The more evident effect (fig. 21 and fig. 24) of this interaction is the fastening of

molecular fluorescence transients by orders of magnitude upon distance reduction from hundreds of Angstrom down to direct contact with the substrate.

The isolated molecule approach permitted an easier and more reliable data analysis: no other competing process has to be taken into account and all the changes observed in molecular fluorescence transients upon spacer thickness variation have to be ascribed to the interaction with the substrate. In this particular case the fluorescence decays are easier to analyse, since the fitting (continuous lines in fig. 21 and fig. 24) of the fluorescence transients is usually monoexponential.

The interaction mechanism on semiconductor substrates
The fluorescence lifetimes drawn out from these fit curves are the main result of this experimental work; they are shown in Fig. 22 (for MoS_2) and fig. 26 (for *Si(111):H*) as a function of the spacer thickness d_{sp} in the range $[0-200\,\text{Å}]$. A fluorescence lifetime shortening by more than two orders of magnitude is observed on MoS_2, by more than one order of magnitude on *Si(111):H*.

The physical meaning of this drastic molecular lifetime shortening upon approaching the substrate and why the same molecule seems to experience a different shortening effect when deposited on different semiconductor substrates will be studied in the following subsections.

8.2 Numerical application of the CPS model to semiconductors

In the following sections the CPS model is applied to quantify the molecular lifetime shortening effect, when electronically excited isolated *MePTCDI* molecules are brought in proximity of a semiconductor substrate.

As extensively discussed in § 7.3, within the CPS model there is no hint at the *nature* of the substrate: the solid is described only by its dielectric function (through the Fresnel reflection coefficients): lacking any kind of microscopic treatment, it turns out thus formally correct to apply the model to description of any non-metallic solid, too.

Naturally, the physical contributions to $\varepsilon(\omega)$ are different in nature for different solids: in the case of metals, the complex dielectric function is mainly contributed by the properties of *free carriers*, for semiconductors the dielectric response is governed by the behaviour of *bound electrons* [129, 147].

Disregarding the different origin of contributions to the dielectric function, the application of the CPS model to the study of energy transfer from excited molecules to semiconductors like MoS_2 and *Si(111)* is accomplished by inserting the appropriate local, complex dielectric function value of the solid in the calculations of properties of the emitter in presence of the substrate (eq. 11, eq. 12 and eq. 15).

Scheme of numerical calculations

A number of programs have been written to compute the curves and the numerical values shown and used in the following. In some detail:

- the distance dependent fluorescence damping constant ($\hat{b} = \hat{b}(d)$) has been computed by numerically integrating the eq. 12 in the k-space (by the Runge-Kutta's method [132–134]) for distances in the range $[\,0-10000\,\text{Å}\,]$, both for parallel and perpendicular to surface emitting dipole.
- inside the short distance domain ($d < 100$ Å) the damping constant can be developed in a simplified form ($\hat{b}_{ET}$, eq. 15); making use of the experimental dielectric function of the substrate it is possible to express the energy transfer parameter rate $\beta(\omega)$ (eq. 16) in terms of the energy of the emitting dipole.
- furthermore, the power dissipated by the excited dipole as a function of the parameter u has been calculated starting from the integrand of eq. 12.

Parameters used in calculations

The expressions for the damping constants $\hat{b}$ and $\hat{b}_{ET}$, for the energy transfer rate parameter $\beta(\omega)$ and for the dissipated power *do not contain any free parameter*, being every quantity either tabulated (as the frequency dependent dielectric function of the substrates) or just directly measured (as the molecular lifetime in solution, τ_0) or calculated (as the molecular fluorescence quantum yield, Φ_0 [43]).

The following values have been used in the calculations:

- Molecule emission energy (E_{mol}): $\bar{\nu} = 18775\,\text{cm}^{-1}$, (p. 71)
- Argon dielectric constant at molecular emission energy:
  $\varepsilon_1 = (1.68 + \text{i } 0.0)$ [148, 149]
- Substrate dielectric constants at molecular emission energy:
  MoS_2: $\varepsilon_2 = (20.0 + \text{i } 5.0)$ [51]
  Silicon: $\varepsilon_2 = (17.2 + \text{i } 0.43)$ [150, 151]
- Molecular fluorescence Quantum Yield: $\Phi_{Me} = 0.93$ [43]
- Intrinsic molecular fluorescence lifetime in solution: $\tau_0 = 3.95\,\text{ns}$ (*see* § 3.1)

In the next two sections the experimental results obtained on MoS_2 and on *Si(111)* are compared with the predicted curves calculated according to the CPS model.

8.3 CPS model and *MePTCDI* on MoS_2

In this section, the CPS model is used to describe *quantitatively* the distance dependent interaction between excited *MePTCDI* molecule and the MoS_2 substrate.

MoS_2 is an indirect semiconductor, which at $\bar{\nu} = 18775\,\text{cm}^{-1}$ efficiently absorbs ($\alpha = 5 \cdot 10^4\,\text{cm}^{-1}$, [152]) above its direct band gap, located at $\bar{\nu} = 15730\,\text{cm}^{-1}$ (fig. A.2). In

the present case, the energy of the molecular dipole *exceeds* the direct band gap of the substrate solid.

Fig. 48 reports, in semi-log scale, the *MePTCDI* fluorescence lifetime as a function of the *effective* distance (d_{eff}[a]) from a freshly cleaved MoS_2 substrate. Together with the experimental values (§ 4.2, fig. 22) are plotted the theoretical curves calculated according to the CPS model.

Two CPS model curves have been numerically computed for *parallel* (——) respectively *perpendicular* to the surface (– – –) emitting dipole.

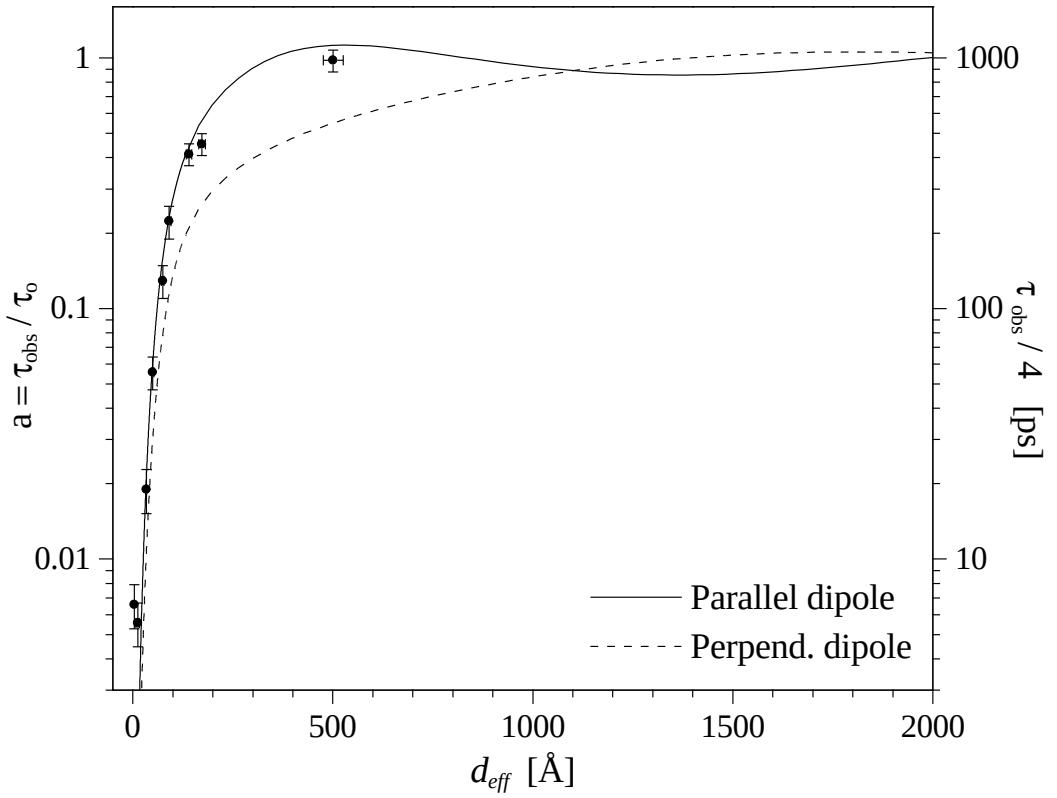

Fig. 48: Normalized *MePTCDI* monomer fluorescence lifetime as a function of the effective distance d_{eff} from a MoS_2 substrate (data points as in fig. 22) plotted together with the CPS curves calculated for parallel (continuous line) and perpendicular (dashed line) oriented emitting dipole. The physical properties of the semiconductor are phenomenologically accomplished by using its dielectric function within the calculations. The value $d_{eff} = d_{sp}$+3.5 Å (with d_{sp} argon spacer thickness) accounts for the effective distance of the molecule from the MoS_2 surface (*see* fig. 50). Semilogarithmic plot.

[a] The reason to use an effective distance d_{eff} instead of the simple argon thickness to quantify the separation between dipole and surface is connected with the finite dimensions of the *MePTCDI* molecule and will be explained in § 8.3

The CPS model predicts for perpendicular to the surface dipoles a more effective coupling with the substrate and therefore an enhancing of the fluorescence lifetime shortening effect with respect to the case of parallel lying dipoles. For this reason, in fig. 48, the dashed curve runs, in the short-distance domain, *below* the continuous one.

Furthermore, the plot evidences that the sequence of experimental measurements has been preferentially focussed on the small-distance range ($d_{eff} \leqslant 200$ Å), where a strong lifetime shortening effect is observed and where eventual deviations from the classical model are expected to be larger.

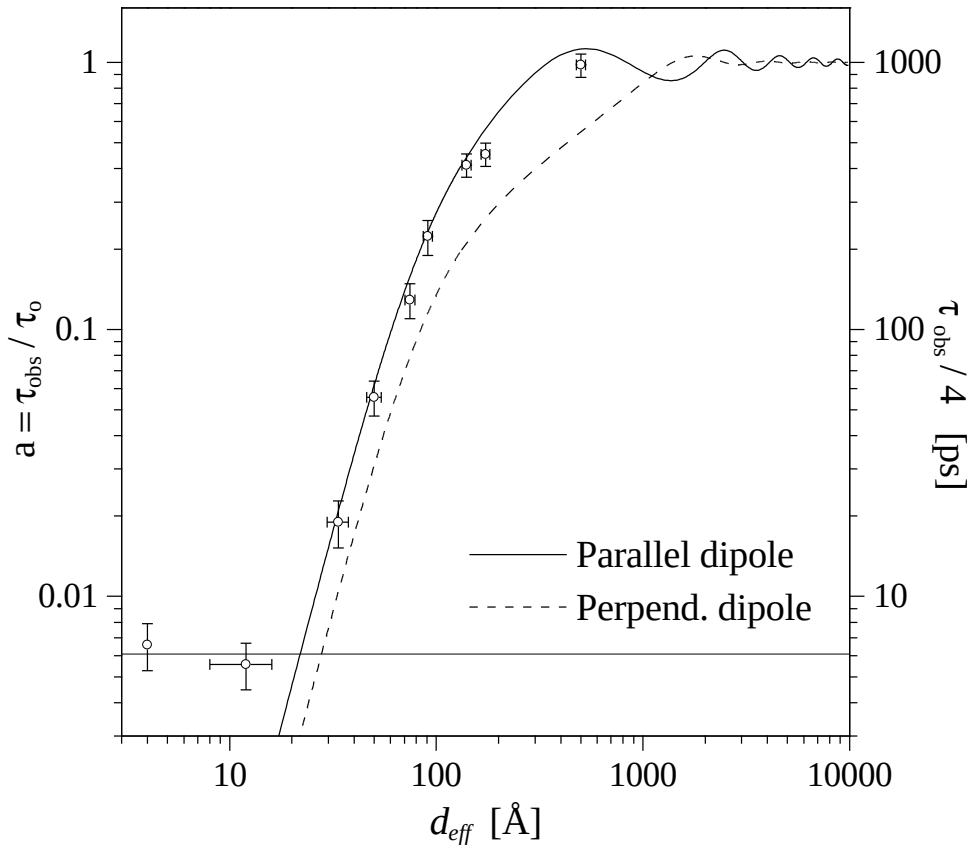

Fig. 49: Same experimental points and calculated CPS curves as in fig. 48, but in log-log scale to emphasize the near-field range (d_{eff}<100 Å). The thin horizontal line at 25 ps indicates the time detection limit of the system. The d^3 dependence in normalized fluorescence lifetime appears as a straight line with slope 3.

The curve calculated for dipoles *parallel* to the surface describes excellently the experimental data, both at large distances, where the interference effects are expected to prevail (with oscillations in fluorescence lifetime) and in the near-field range ($d_{eff} < 100$ Å), where strong energy transfer phenomena are predicted to take place (resulting in a drastic lifetime reduction). Fig. 49 shows the same curves of fig. 48, but in double logarithmic plot to stretch the scale and to emphasize the short-distance domain. The agreement with the

measured molecular lifetimes is found very good for distances down to $\sim 20-30$ Å. Below this limit the lifetime decreases more slowly and it deviates from the predicted curve.

The model would not seem to describe appropriately the observed experimental distance dependence. Nevertheless, inside this distance domain the shortening effect turns out to be so strong that the measured molecular lifetime falls under the time-detection limit of our system ($\tau \sim 25$ ps, thin horizontal line in fig. 49). Any lifetime measurement carried out on very small d_{eff} would result in a value around the system-limited minimum value. As an example, the molecules *directly* deposited on the semiconductor are predicted to experience a lifetime shortening of ~ 40000 times ($a = 2.53 \cdot 10^{-5}$ at $d_{eff} = 3.5$ Å). A lifetime of $\tau \sim 0.1$ ps is expected by extrapolation, a value of ~ 25 ps is instead measured.

The limited time resolution of the system does not permit to consider the values measured at short d_{eff} as deviating from CPS expectations.

As discussed in § 6.1, within the near-field domain the molecular lifetime is predicted to exhibit a d^3 distance dependence (i.e. a straigth line with slope 3 in log-log plot). The *numerical value* of the lifetime shortening is quantified by the energy transfer rate parameter $\beta(\omega)$ (eq. 16), which defines the *vertical offset* of the d^3 curve on the graph. In § 8.3.1, the value of $\beta(\omega)$ is calculated in a large frequency range and the specific value for *MePTCDI* on MoS_2 is given.

The effective distance from the substrate

Because of the better agreement found between the experimental data and the model curve calculated for a *parallel* dipole with respect to a perpendicular one, it is assumed that the transition dipole of the molecules is predominantly oriented along a direction parallel to the solid.

Since the transition dipole is directed (within the *MePTCDI* molecule) along the *long* molecular axis (§ 2.2), it implies that also the *molecules* are preferentially lying with this axis parallel to the substrate.

In order to calculate the actual distance between the molecular dipole and the substrate, the finite dimensions of the molecule have to be taken into account, too.

A molecule can lie parallel to the substrate either 'flat' or 'on edge' (fig. 50): according to the lateral dimension of the molecule and to the Van der Waals radii of component atoms, in the first case the transition dipole results to lie at 2.3 Å, in the second at 4.7 Å away from the substrate. Considering an uniform distribution of molecules "flat" and "on edge", the average offset value of 3.5 Å has to be added to get the effective dipole-substrate distance d_{eff}.

If an argon spacer of thickness d_{sp} is placed between molecule and substrate, the effective dipole-substrate distance d_{eff} amounts to $d_{eff} = d_{sp} + 3.5$ Å. For molecules directly

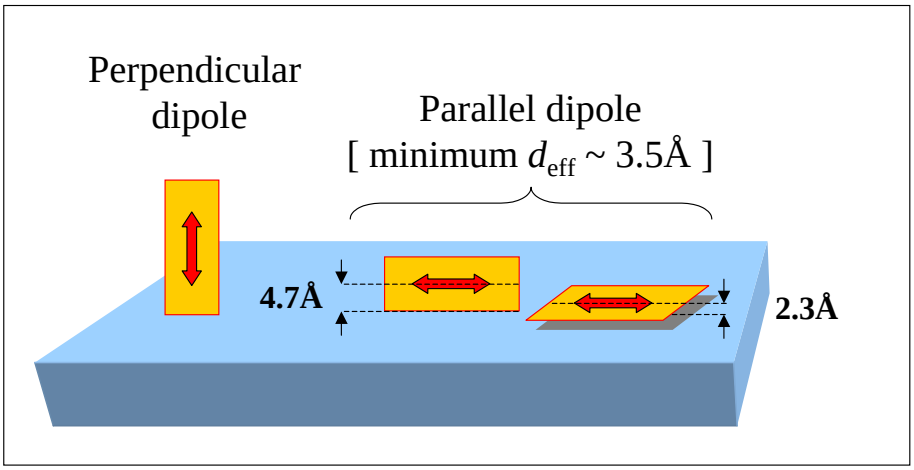

Fig. 50: Sketch of the three possible extreme orientations of the *MePTCDI* molecule. The transition dipole moment (indicated by a double arrow) lies along the long axis of the molecule [43, 98]. If the molecule is parallel to the substrate, the distance of its dipole from the surface has to be calculated as the average of half lateral dimensions for 'flat' lying and 'on edge' molecule. For *MePTCDI*, the average minimal distance amounts thus to 3.5 Å.

deposited on the MoS_2 (no argon spacer, $d_{sp} = 0$) the *minimum* dipole-substrate average distance amounts to $d_{eff} = 3.5$ Å. The correction becomes appreciable only at very small argon thicknesses ($d_{sp} < 30-40$ Å).

8.3.1 Calculation of the energy transfer rate parameter $\beta(\omega)$ for MoS_2

According to the theoretical approach developed in § 7.1 for metallic substrates and making use of the assumptions on the applicability of the model to semiconductors (§ 7.3), it is possible to estimate by eq. 16 the rate of energy transfer $\hat{b}_{ET}$ from an excited dipole to a MoS_2 substrate *as a function of the frequency of the emitter*, when the distance d is small: $\hat{b}_{ET} = \beta(\omega)d^{-3}$.

$\beta(\omega)$ does express, in its functional dependence on the frequency, the predicted change of the energy transfer rate when the emitting molecule is supposed to be substituted with another kind of molecule, with different emission frequency. The numerical value for the specific case of the *MePTCDI* molecule on MoS_2 is calculated in the following.

The emitter is considered at a distance $d_{eff} < 100$ Å from a MoS_2 surface, separated from it by the argon spacer. Within this distance range the approximation that leads to the near-field expression (eq. 15) of energy transfer rate actually holds.

Instead of any model function only the *experimental* dielectric function of MoS_2 [51] and of argon has been used in the calculations.

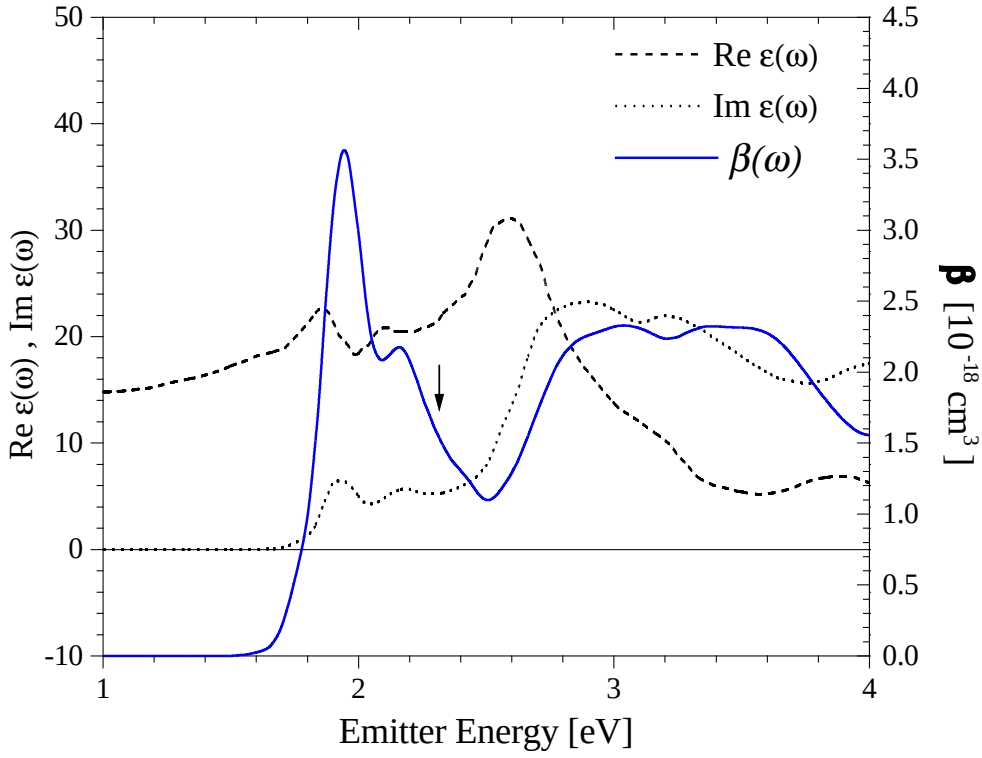

Fig. 51: MoS_2 dielectric function's real and imaginary part [51] and calculated energy transfer rate parameter β as a function of emitter energy $\hbar\omega$, for a parallel dipole at a distance $d_{eff} < 100$ Å from MoS_2 substrate. The spacer is argon. The abrupt increase in transfer rate at 1.80 eV is related to the onset of direct absorption across the band gap. The arrow indicates the emission energy of the *MePTCDI* molecule; a number of emitters, with emission energy ranging hypothetically from $\hbar\omega = 2$ eV to 2.5 eV are predicted to experience a lifetime shortening effect whose value changes almost four times. A so strong modulation is to ascribe to the band structure of the semiconductor.

Fig. 51 shows, together with the real (dashed) and imaginary (dotted) part of MoS_2 experimental dielectric function, the energy transfer rate parameter $\beta(\omega)$ (thick line) numerically derived as a function of emitter frequency. $\beta(\omega)$ has been calculated for a *parallel* emitting dipole (with fluorescence quantum yield equal to *MePTCDI*'s one, q=0.93). The small arrow indicates the actual energy of $S_0 \rightarrow S_1$ electronic transition in the *MePTCDI* molecule.

The strong increase predicted in $\beta(\omega)$ for energies above 1.80 eV is related to the onset of the transition across the band gap in MoS_2, evidenced by a change in absorption coefficient (in the figure, proportional to $\mathrm{Im}(\varepsilon(\omega))$). The *MePTCDI* emission energy ($E_{\mathrm{mol}} = 2.32$ eV) turns out to lie well above the band gap, although far from the resonance

at 1.95 eV.

Numerical value of β for *MePTCDI* on MoS_2

In the particular case of *MePTCDI* on MoS_2, the energy transfer rate parameter is calculated to be $\beta_{MoS_2} \sim 1.7 \cdot 10^{18}$ [cm^3] at the molecular emission frequency.

As discussed for silver, from β's defining equation (eq. 16) the energy transfer rate $\hat{b}_{ET}$ at a distance d can be readily calculated: if $d = 10$ Å ($d = 10^{-7}$ cm, $d^{-3} = 10^{21}$ cm^{-3}), then $\hat{b}^{ET}_{MoS_2} \sim 1.7 \cdot 10^{-18} \cdot 10^{21} \sim 1700$; since $\tau = \tau_0/\hat{b}_{ET}$, the measured *MePTCDI* fluorescence lifetime is expected to be shortened on MoS_2 more than three order of magnitude. It is interesting to compare this large quenching effect on MoS_2 with that estimated when the *MePTCDI* molecule is supposed to be deposited on a metallic substrate (for example on *Ag*, $\hat{b}_{ET} \sim 600$, p. 104).

In this particular case, the *MePTCDI* fluorescence lifetime can be shortened *more on a semiconductor than on a metal*.

This result demonstrates that the interactivity of a material cannot be guessed *a priori* and that, depending on the frequency of the emitter and on the band structure of semiconductor, also non-metallic materials can affect drastically the fluorescence properties of the molecules deposited.

8.3.2 Calculation of the power dissipated by *MePTCDI* on MoS_2

It is now possible to calculate the distributions of wave vectors on which the emitting dipole dissipates its power, when it is brought in the proximity of the MoS_2 surface. Following the approach developed at p. 105, the imaginary part of the integrand in eq. 12 can be plotted as a function of $u = k_x/k_1$ for various emitter-surface separations (k_x is the projection of dipole field wave vector on the plane of the interface and k_1 the dipole far field wave vector in medium 1).

As already discussed for *Ag*, the value of the ratio k_x/k_1 discriminates between various energy transfer mechanisms: the integral over $0 \leqslant u \leqslant 1$ ($k_x \leqslant k_1$) is related to the coupling to radiation, while the integral for $1 < u < \infty$ ($k_x > k_1$) represents the non-radiative contributions to energy transfer.

Fig. 52 shows (in log-log plot) the power dissipated by the emitting dipole, calculated as a function of the normalized wave vector u, for a parallel *MePTCDI* molecule placed at various distances ($d_{eff} = 0{-}600$ Å, by argon spacer) above a MoS_2 surface. The area under each of these curves is proportional to the energy transfer rate $\hat{b}$ from excited molecule to substrate, i.e. it corresponds to a point of the curve $a = \hat{b}^{-1}$ in fig. 49 at a defined distance d_{eff}.

From the comparison between fig. 45 (power dissipated by the *MePTCDI* molecule on *Ag*) and fig. 52 (*MePTCDI* on MoS_2), a number of considerations can be made.

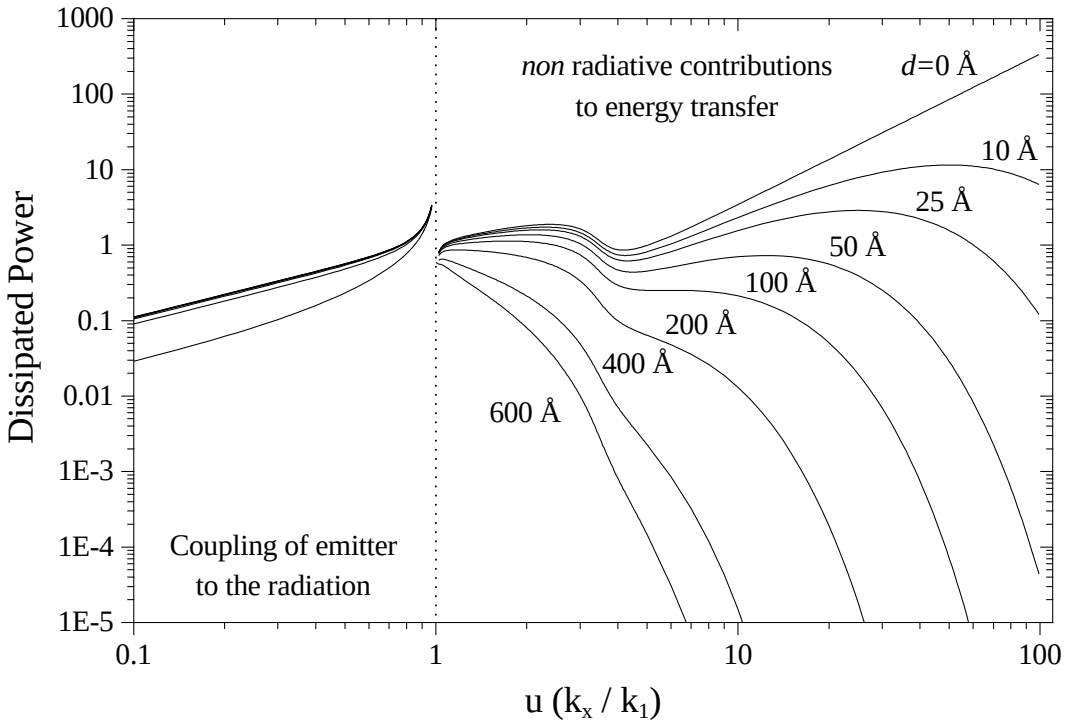

Fig. 52: Imaginary part of the integrand in eq. 12 (related to the power dissipated by the emitting dipole) calculated as a function of the normalized wave vector $u = k_x/k_1$, for a parallel *MePTCDI* molecule located at various distances (d_{eff}=0−600 Å, by argon spacer) above a MoS_2 surface. The area under these curves is proportional to the energy transfer rate from excited molecule to substrate. Log-log plot.

- The range $0 \leqslant u \leqslant 1$ exhibits few differences: the contribution of radiatively dissipated power does not change appreciably in absolute value between the two cases.
- There is no strong resonance for u slightly above 1; the curve shows only the usual divergence at $u = 1$ (corresponding to l_1=0 in eq. 12) and only a further slight modulation about $u = 4$ (corresponding to the zero of l_2). *The peak associated to the resonant excitation of surface charge oscillations (SPP) is not present.*
- The region with $u \gg 1$ shows the importance, also in the case of MoS_2, of the additional non-radiative decay route represented by coupling between the near field of the emitter and an induced electron-hole generation in the solid ('lossy modes', LM). As already observed in *Ag* the dissipated power via this mechanisms increases progressively with decreasing distance and represents the *main decay route* at short separations.

The results of application of the CPS model to the study of the interaction between *MePTCDI* and MoS_2 are summarized in § 8.5.

The real nature of the interaction mechanism between *MePTCDI* and MoS_2 and why

the CPS model is able to adequately describe the experimental data on a large distance ranges will be discussed in § 8.6.

8.4 CPS model and *MePTCDI* on *Si(111):H*

In this section the CPS model is applied to describe *quantitatively* the distance dependent interaction between the *MePTCDI* molecule and a *Si(111):H* substrate.

Silicon at $\bar{\nu} = 18775\,\mathrm{cm}^{-1}$ still does not absorb across the direct energy gap (since direct $E_{gap} = 3.4\,\mathrm{eV}$, $27420\,\mathrm{cm}^{-1}$, fig.A.3). In case of *Si(111):H* the energy of molecular dipole <u>does not exceed</u> the direct band gap of the semiconductor, but only its indirect band gap.

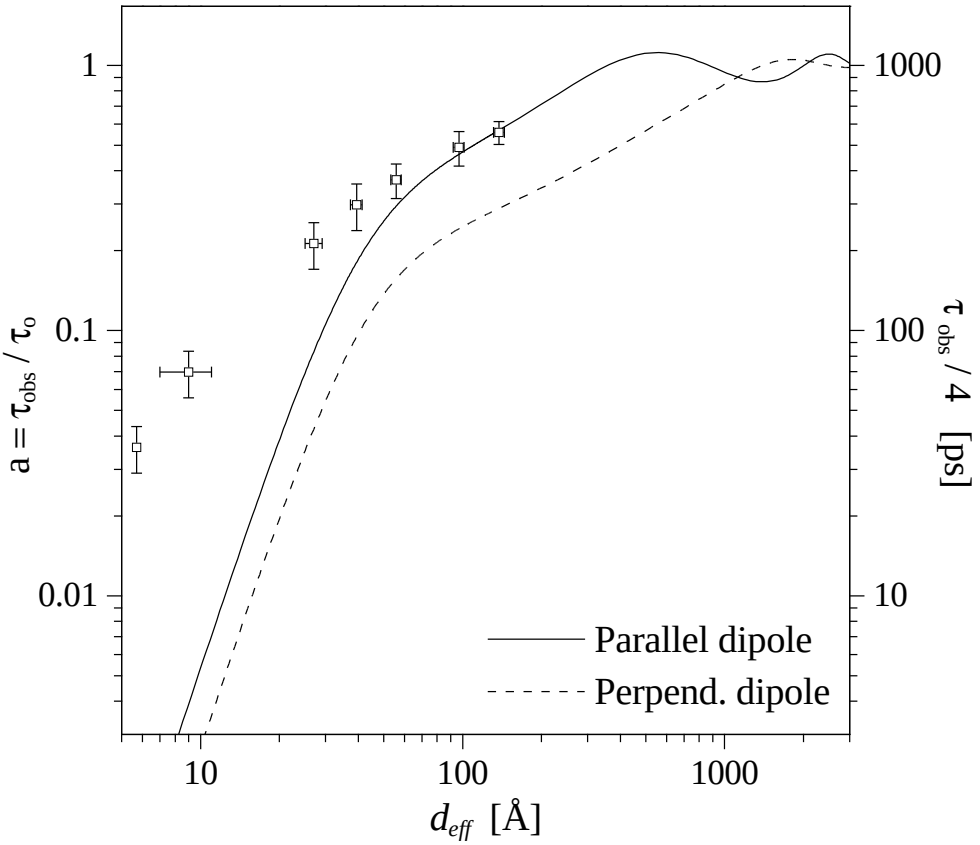

Fig. 53: Normalized *MePTCDI* monomer fluorescence lifetime as a function of the distance from a *Si(111):H* substrate (data point as in fig. 26). CPS model curve calculated for parallel (continuous line) and perpendicular (dashed line) oriented emitting dipole with respect to the semiconductor surface. The value $d_{eff} = d_{sp}$+5.7 Å accounts for the effective distance of the emitting dipole from the bare silicon surface (fig. 54).

Fig. 53 shows, in log-log scale, both the experimental data (from fig. 26) and the curves calculated according to CPS-model using for *MePTCDI* and *Si(111):H* the parameters

reported in § 8.2.

Much as made for MoS_2, also for *Si(111):H* an effective average distance has to be chosen (fig. 54) to account for the finite dimensions both of the molecule and of the additional passivation layer, whose thickness is estimated to 2.2 Å. Consequently, the minimum distance between the dipole and the *bare* silicon substrate amounts to 5.7 Å (for parallel *MePTCDI* molecules).

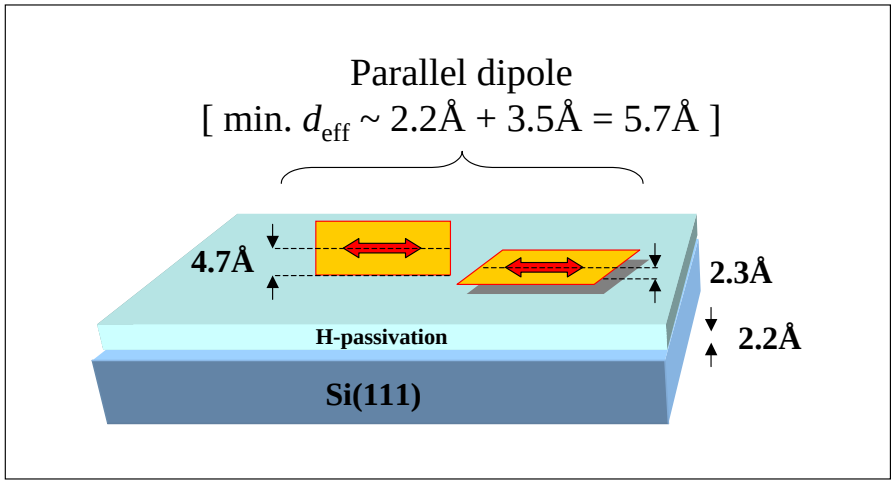

Fig. 54: *MePTCDI* on hydrogen passivated *Si(111)*. When the molecule lies parallel to the surface, to get the actual separation between transition dipole and the bulk, the average value (3.5 Å) has to be further increased by the hydrogen layer thickness (2.2 Å). The minimum dipole-substrate distance for parallel *MePTCDI* molecules on *Si(111):H* amounts to 5.7 Å.

Two CPS curves have been calculated for parallel (continuous line) respectively perpendicular (dashed line) emitting dipole; the physical properties of *Si(111):H* are also here phenomenologically accomplished by inserting in the calculation the values of the semiconductor optical dielectric function at emitting dipole frequency ($\varepsilon = (17.2 + \mathrm{i}\ 0.43)$ [150]).

Differently from the case of MoS_2, the observed distance-dependent *MePTCDI* fluorescence lifetime *is not* adequately described by the CPS model. Both curves calculated for parallel and perpendicular emitting dipole locally strongly *overestimate* the energy transfer to the substrate and consequently underestimate the observed lifetime, especially in the small-distances domain ($d_{eff} < 50$ Å). At the shortest distance ($d_{eff} = 5.7$ Å) the model predicts a value of $\tau \sim 4$ ps, a value of $\tau = 145$ ps is instead observed; the discrepancy amounts here to a factor of ~ 35.

8.4.1 Calculation of the energy transfer rate parameter $\beta(\omega)$ for *Si(111):H*

Parallel to the approach followed in § 8.3.1, also in the case of *Si(111):H* it is possible to estimate the rate of energy transfer from an excited dipole to the substrate *as a function of the frequency of the emitter*. The numerical value expected in the case of the *MePTCDI* molecule deposited on *Si(111):H* is then explicitly calculated.

The molecule is assumed to lie at a distance $d_{eff} < 50$ Å from a *Si(111):H* surface, separated from it by an argon spacer. From fig. 53, it is evident that only within this distance range the general damping factor $\hat{b}$ (eq. 12) can be approximated by the near-field expression (eq. 15).

The frequency dependent proportionality constant $\beta(\omega)$ as calculated from eq. 16 is plotted in fig. 55. Once more, only the *experimental* dielectric function of *Si* [150] (§ A.1) and of argon has been used here.

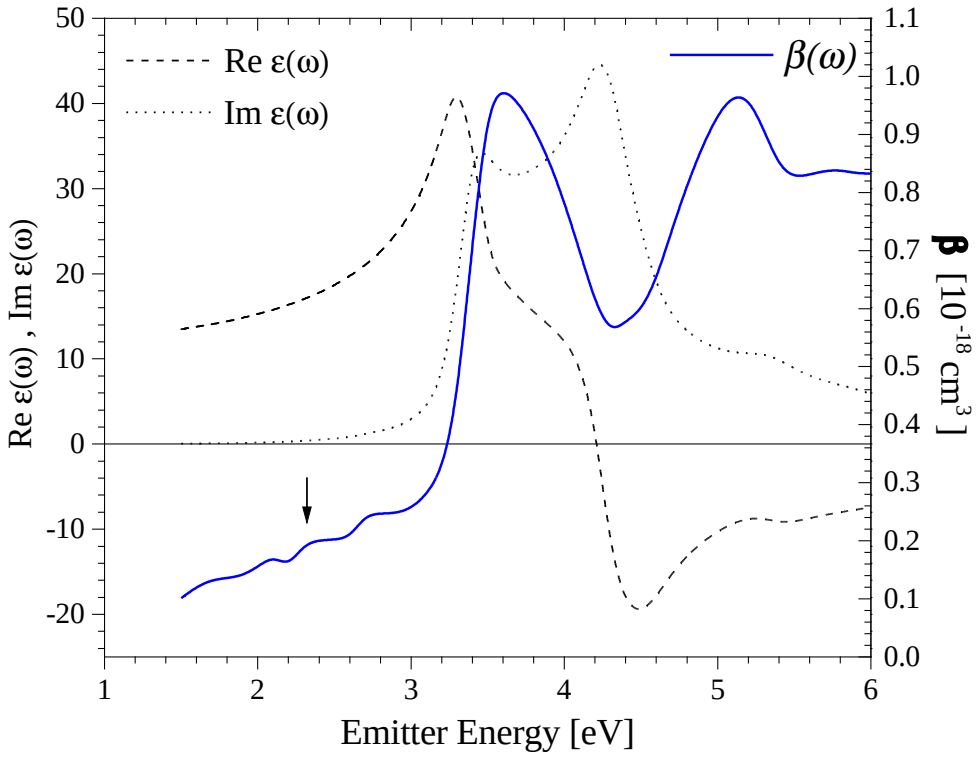

Fig. 55: Real and imaginary part of *Si(111):H* dielectric function [150] and calculated energy transfer rate parameter β as a function of emitter energy $\hbar\omega$, for a parallel emitting dipole at a distance $d_{eff} < 50$ Å from *Si(111):H* substrate. The rate is predicted to increase almost one order of magnitude above $\hbar\omega = 3.4$ eV, the onset of direct absorption across the band in silicon. The arrow indicates the emission energy of the *MePTCDI* molecule, well *below* the direct band gap.

Fig. 55 shows, together with the real and imaginary part of the *Si(111):H* dielectric function from which is derived, the energy transfer rate parameter $\beta(\omega)$ (thick line) as a function of emitter frequency for a *parallel* emitting dipole with quantum yield q=0.93. The small arrow indicates the actual emission energy of the *MePTCDI* molecule.

The strong increase predicted in $\beta(\omega)$ for energies above 3.40 eV is ascribed to the onset of the transition across the band in *Si* as evidenced by the increase in the absorption coefficient. The *MePTCDI* emission ($E_{\mathrm{mol}} = 2.32\,\mathrm{eV}$) lies therefore well below the direct energy gap.

Numerical value of β for *MePTCDI* on *Si(111):H*
In the present case, an energy transfer rate parameter $\beta_{Si} \sim 0.195 \cdot 10^{18}[\mathrm{cm}^3]$ is predicted. If $d = 10$ Å ($d = 10^{-7}$ cm, $d^{-3} = 10^{21}\,\mathrm{cm}^{-3}$), then $\hat{b}^{ET}_{Si:H} \sim 0.195 \cdot 10^{-18} \cdot 10^{21} \sim 195$; since $\tau = \tau_0/\hat{b}_{ET}$, the shortening factor is more than two orders of magnitude. This value is readily comparable with that obtained when the molecule is supposed to be deposited at the same distance ($d = 10$ Å) on the MoS_2 substrate: $\hat{b}^{ET}_{MoS_2} \sim 1700$ (§ 8.3.1); the fluorescence lifetime shortening is predicted to be on *Si(111):H* almost one order of magnitude smaller than that measured on MoS_2.

8.4.2 Calculation of the power dissipated by *MePTCDI* on *Si(111):H*

Also in the case of *MePTCDI* deposited on *Si(111):H* it is possible to calculate through what mechanisms the emitting dipole does dissipate its power when it is brought in the proximity of the semiconductor surface. Following the approach developed in § 8.3.2, the imaginary part of the integrand in eq. 12 can be plotted as a function of $u = k_x/k_1$ for various emitter-surface separations.

As discussed for *Ag* and for MoS_2 (fig. 45 and fig. 52), the value of the ratio k_x/k_1 discriminates among the possible energy transfer mechanisms: coupling to the radiation field, to resonant surface charge density oscillation modes and to electron-hole pair generation.

Fig. 56 shows the power dissipated by the emitting dipole, calculated as a function of the normalized wave vector u, for a parallel *MePTCDI* molecule placed at various distances (d_{eff}=0−600 Å, by an argon spacer) above a *Si(111):H* surface. The area under these curves is proportional to the energy transfer rate $\hat{b}$ from excited molecule to substrate, i.e. it corresponds to a point of the curve $a = \hat{b}^{-1}$ in fig. 53 at a defined distance d_{eff}.

Comments on fig. 56
By comparing fig. 52 (*MePTCDI* on MoS_2) and fig. 56, it can be observed that:

- The shape of the curves in the range $0 \leqslant u \leqslant 1$ is very similar to what already observed on MoS_2; also on *Si(111):H* there are no appreciable changes in coupling of emitter to radiation.

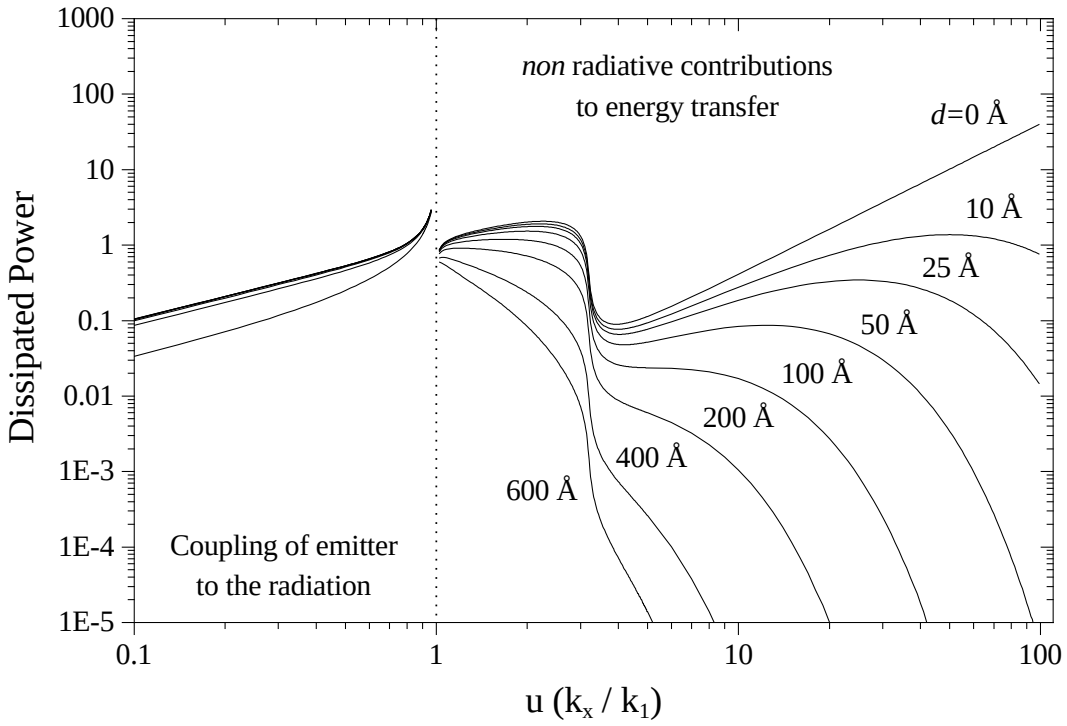

Fig. 56: Power dissipated by the emitting dipole calculated as function of the normalized wave vector $u = k_x/k_1$, for a parallel *MePTCDI* molecule located at various distances ($d_{eff} = 0-600$Å, argon spacer) above a *Si(111):H* surface. The area under these curves is proportional to the energy transfer rate from excited molecule to substrate. Log-log plot.

- No strong resonance for u slightly above 1 is predicted; the curve shows only the divergence at $u = 1$ (corresponding to l_1=0 in eq. 12) and further a strong modulation at about $u = 3.24$ (corresponding to the zero of l_2, at $u = \sqrt{\varepsilon_2/\varepsilon_1}$ with a singularity just outside the real axes). The peak associated to the resonant excitation of surface charge oscillations (SPP) *is here not present*, as on MoS_2.
- A *difference* is however observed in the region $u \gg 1$. Even in log-log scale, the plot exhibits an *evident reduction* of the contribution to dissipated power from large wave vectors. The integration in u (proportional to the energy transfer rate) turns out to be more than one order of magnitude smaller on *Si(111):H* that on MoS_2.
- As already observed on the two other substrates, the dissipated power increases progressively with the decreasing of the distance; at $d = 0$ the integral (without any applied correction, as discussed at p. 109) diverges.

The results of application of the CPS model to the study of the interaction between *MePTCDI* and *Si(111):H* are summarized in § 8.5. The nature of interaction between *MePTCDI* and *Si(111)* substrate and why the CPS model *is not able* to effectively describe the experimental data in the short distances range will be discussed in the § 8.6.

8.5 CPS model and *MePTCDI* on MoS_2 and *Si(111):H*: Summary of the results

The main results of the application of the CPS model to the quantitative description of the interaction between *MePTCDI* and MoS_2 and *Si(111):H* can be summarized as follows.

CPS and *MePTCDI* on MoS_2: summary

a.) The CPS model is successful in describing (over a wide range of distances, between 20-500 Å) the effect of non-radiative interaction between the electronically excited molecule and MoS_2. In this case the dipole energy lies *above* the direct band gap energy.

b.) From the model curves, the emitting *dipole* can be assumed mainly parallel to the substrate. From geometrical considerations, it follows that also the *MePTCDI molecule* lies mainly parallel to substrate.

c.) Eventual deviations from the model at extremely short distances ($d_{eff} < 30$ Å) are not experimentally detectable owing to the limited time resolution of the system.

d.) The energy transfer rate parameter $\beta(\omega)$ calculated at the *MePTCDI* monomer emission frequency is predicted to be stronger on MoS_2 than on *Ag*.

d.) The power of the emitting dipole is dissipated through very similar routes on MoS_2 and on *Ag*; nevertheless, on MoS_2, the contribution from SPP excitation is absent.

CPS and *MePTCDI* on *Si(111):H*: summary

a.) Differently from the case of *MePTCDI* on MoS_2, when *Si(111):H* is used as substrate the *MePTCDI* emission energy lies well *below* the direct band gap energy.

b.) Also at minimum distance ($d_{eff} = 5.7$ Å) the observed molecular fluorescence lifetime is larger than the system detection time limit.

c.) Within the considered distance range (5.7−130 Å), the CPS model does ***not*** describe adequately (particularly when $d_{eff} < 50$ Å) the effect of interaction between the electronically excited molecule and the substrate; at the lowest effective distance a discrepancy of more than one order of magnitude is observed.

d.) The energy transfer rate parameter $\beta(\omega)$ calculated at *MePTCDI* monomer emission frequency is predicted to be about 10 time weaker on *Si(111):H* than on MoS_2.

e.) The power of the emitting dipole is predicted to be dissipated through *different* routes on *Si(111):H* and on MoS_2; particularly the high wave vectors do contribute in *Si(111):H* only *poorly*; also on *Si(111):H* the contribution from SPP excitation is however absent.

8.5.1 General comments on the molecule-semiconductor interaction in the two considered cases

From the comparison of experimental data *and* calculated curves in § 8.3 and § 8.4, the most important aspects of the interaction between *MePTCDI* molecules and the chosen semiconductor substrates can be commented as follows:

- The electronically excited *MePTCDI* isolated molecule decays on *both* semiconductor surfaces orders of magnitude *faster* than the molecule in dilute solution.
- A lifetime shortening is found both on a semiconductor whose band gap is *smaller* (MoS_2) or *greater* (*Si(111):H*) than the molecular energy (E_{mol}=2.32 eV), nevertheless this effect is quantitatively different (about three and slightly more than one order of magnitude, respectively).
- The observed distance dependent lifetime is *quantitatively* described by the CPS model on the whole considered distance range *only* in the case of MoS_2 (fig. 49), a deviation of more than one order of magnitude between model predictions and experimental data is observed on *Si(111):H*.

8.6 Molecule-semiconductor interaction: the role of the band structure

The results shown in § 8.3 and § 8.4 are discussed in this section taking into account a simple band structure for MoS_2 and *Si(111):H* and making use of a further model ('SDK', *see* § 8.6.2) to complete the description of the materials given by the CPS model.

The inadequateness of a description of the solids independent from their band structure (as made in the CPS model) is at first pointed out, then the SDK model is introduced, briefly described in its main assumptions and statements and finally used to interpret the experimental results.

8.6.1 Inadequateness of the CPS model to describe semiconductors

The CPS model does not take explicitly into account the band structure of the solid: the substrate is described only by its local dielectric function only dependent on ω, but without any dependence on the k-vector.

When a semiconductor is used as substrate, its band structure is expected to have a strong influence on the fluorescence properties of an emitter placed at *short* distance from its surface, because the possibility to absorb energy is modulated by the momentum matching conditions imposed by the band structure of the solid. Deviations from the prediction of the CPS model are indeed expected.

To rationalize the subject and explain what experimentally observed, the following questions have to be answered:

- Why a strong fluorescence lifetime shortening effect is observed when the energy of the electronically excited molecule *exceeds* the semiconductor direct band gap (for example, *MePTCDI* on MoS_2).
- Why the observed distance dependent fluorescence lifetime reduction in this case seems *properly described* by the CPS model.
- Why a lifetime shortening effect is *however* observed also when the energy of the emitter *does not exceed* the semiconductor direct band gap (for example, *MePTCDI* on *Si(111):H*)
- Why the observed distance dependent lifetime reduction in the last case *is not* properly described by the CPS model.

The SDK model, introduced in the following section, permits to answer (at least qualitatively) these questions on the basis of the band structure of the considered materials.

8.6.2 The excitation of electron-hole pairs in semiconductors

In the frame of the CPS model, the solid has been described only by its dielectric function $\varepsilon(\omega)$, without any kind of microscopic treatment.

For dipole energies *above* the onset of the interband transitions within the substrate (irrespective whether metal or semiconductor), the form of $\varepsilon(\omega)$ depends almost exclusively on the specific electronic band structure of the material; as an example, the case of *Ag* has been reported in § 7.2.1.

An extended theoretical treatment that correctly takes into account, beside the frequency dependence, also the k-vector dependence of the response function of the solid is therefore expected to describe in a better way the interaction with the solid if this is a semiconductor.

As originally proposed by *Dexter* [153], the energy of a molecule optically excited within an organic film deposited on a semiconductor can be transferred to the substrate producing electron-hole pairs in the semiconductor. The energy transfer is predicted to occur via a *non-radiative* process from the excited molecule, when the excitation energy of the molecule is greater than the band gap of the semiconductor.

Successively *Stavola, Dexter and Knox* [13] proposed a semiclassical model (referred to in the present work as 'SDK model'), that describes the interaction between molecule and substrate by a dipole-dipole interaction mechanism between the excited molecular dipole and the *induced e-h dipole* in the semiconductor.

The model combines the Förster-Dexter energy transfer theory [154] [155] and a simple band model to describe the semiconductor; direct and indirect band-gap solids are treated explicitly. The model is briefly introduced in the following section.

8.6.3 The SDK model

As in the CPS model, also in the SDK one the electronically excited molecule is modelled as an emitting dipole placed at distance d from a substrate (semiconductor in this case). The volume between dipole and solid is filled with a non-absorbing medium 1 (the argon spacer in the present case), whereas the solid is described not by a macroscopic dielectric function $\varepsilon(\omega)$ as in the CPS model, but by its band structure (by $E_c(\mathbf{k}_c)$ and $E_v(\mathbf{k}_v)$, i.e. the k-vector dependent energy of conduction and valence bands, respectively).

The probability for the energy transfer from an excited molecule to the semiconductor is expressed by means of Fermi's golden rule. Within the SDK model [13], the interaction which gives rise to the transfer is the Coulomb interaction between the electrons of the excited molecule and the electrons of the semiconductor. The Coloumb interaction Hamiltonian here used contains explicitly a reference to the distribution of momentum components of the exciting field of the dipole. The emitter is assumed for simplicity to transfer all of its (sharply defined) energy.

The bands of the semiconductor are treated with a simple parabolic band approximation and the exciting energy is supposed to be $0.05-0.5\,\mathrm{eV}$ above the direct (or indirect)

band-gap energy of the semiconductor. The semiconductor is assumed to be explicitly a crystal with cubic symmetry and lattice constant a.

The expression for the damping function $\hat{b}_{\rm SDK}$ (ratio between the transfer rate from molecule to substrate and the spontaneous radiative emission rate) has the form:

$$\hat{b}_{\rm SDK} = A \int_{\rm zone} d\mathbf{k}_c \int_{\rm zone} d\mathbf{k}_v \; B(d, \mathbf{k}_c, \mathbf{k}_v) \; \delta(\underbrace{E_M - E_G}_{\Delta} - E_c(\mathbf{k}_c) - E_v(\mathbf{k}_v)) \qquad (30)$$

where A depends on the parameters of the solid, $B(d,k)$ is a function of the molecule-substrate separation and the delta function accounts for the energy conservation in the transition. Here $\Delta = E_M - E_G$ ('excess energy') is a fundamental parameter of the model and it indicates how much larger is the molecule emission energy (E_M) than the energy band gap E_G of the semiconductor; finally, $E_c(\mathbf{k}_c)$ and $E_v(\mathbf{k}_v)$ are the electronic bands of the solid, measured with respect to the lowest point of conduction and the highest point of valence band, respectively.

In eq. 30 within the integral on all the wave vectors of the zone ($\mathbf{k}_v$, in valence and $\mathbf{k}_c$, conduction band), Dirac's delta function acts to eliminate the contribution of transitions for which the energy is not conserved (if $\Delta \neq (E_c(\mathbf{k}_c) + E_v(\mathbf{k}_v))$ then $\delta = 0$).

Approximated band shape

Valence and conduction band are approximated as parabolic (with quadratic dependence in k-vector; i.e. $E_c(\mathbf{k}_c) = (\hbar^2 k_c^2)/2m_c$, $E_v(\mathbf{k}_v) = (\hbar^2 k_v^2)/2m_v$), with masses m_v and m_c; the δ function in eq. 30 is then rewritten as:

$$\delta\left(\Delta - \frac{\hbar^2 k_c^2}{2m_c} - \frac{\hbar^2 k_v^2}{2m_v}\right)$$

By introducing the variables $\mathbf{k} \equiv \Delta\mathbf{k} = \mathbf{k}_c - \mathbf{k}_v$ and $m_* = m_c m_v/(m_c + m_v)$ and solving the integral in eq. 30 with standard methods, the following expression for the energy transfer rate is obtained:

$$\hat{b}_{\rm SDK} = A\; 2\pi \left(\frac{2m_*}{\hbar^2}\right)^{3/2} \Delta^{1/2} \int d^3k \; B(d,k) \; \left(1 - \frac{\hbar^2 k^2}{2(m_c + m_v)\Delta}\right)^{1/2} \qquad (31)$$

The transfer rate is therefore a function of the integral of the product of two terms: $B(d,k)$ that takes into account the geometry of the system and the term inside the parenthesis that imposes the energy conservation.

The expression in eq. 31 is valid both for an excitation energy larger than the *direct* band gap and larger than the *indirect* band gap, changing in the two cases the form of function $B(d,k)$.

Transitions above the *direct* band gap

By analysing the functional dependence of $\hat{b}_{\mathrm{SDK}}$ on d, it is possible to evidence that when d is large, the function $B(d,k)$ is non-negligible only for *small* values of k: at distance larger than a few (5−10) lattice constants, only $B(d, k = 0)$ is in practice non zero. This observation permits to obtain a large-distance approximated solution in which the k-vector dependence is reduced to uniquely $\mathbf{k} = 0$ ('optical-limit solution'): this solution *coincides* with the d^{-3} functional dependence predicted in the CPS model.

However, when the distance d decreases ($d < 50$ Å), more and more transitions with k-vector around $\mathbf{k} = 0$ are admitted to contribute to the transfer rate by the $B(d,k)$ function.

But now the (multiplicative) energy conservation condition (represented by the δ function) tends to restrict once more the integration to the center of the zone: the requirement that energy transfer rate (eq. 31) be real, implies that the last part of the integral is real. Thus, a condition on k is obtained:

$$k^2 \leqslant \frac{2(m_c + m_v)\Delta}{\hbar^2} \tag{32}$$

The energy conservation condition *reduces* therefore the density of the allowed final states for the transition, as a function of the excess energy Δ and of the band masses: as Δ becomes smaller or the band curvature larger the condition is more restrictive. It acts to truncate the integration on k in eq. 31 and thereby to *reduce* the transfer probability with respect to the optical-limit (CPS) values: not all the k-vector components of the molecular near field can produce an electron-hole pair, but only those that satisfy the condition of eq. 32; for this reason the energy transfer rate *decreases* and this results in a deviation (less quanching) from the dependence valid at large-distance.

Fig. 57 shows the energy transfer rate predicted by the SDK model ($\hat{b}_{\mathrm{SDK}}$) as a function of the molecule-semiconductor separation d, for a direct gap material, *normalized* to the large-distance (CPS) value. $\hat{b}_{\mathrm{SDK}}/\hat{b}_{\mathrm{CPS}}$ is plotted for a number of excess energy Δ values, whereas the band masses values are kept fix. The SDK model predicts (at intermediate distances, $d = 20$−60 Å) a large deviation from the CPS expectation only for *small* Δ values ($\Delta < 0.2$ eV).

Transitions above the *indirect* band gap

Also in this case the valence and conduction bands are assumed parabolic with masses m_v and m_c, but while the valence band extremum is at zone center the conduction band extremum is assumed to be displaced from the zone center by a some wave vector $\mathbf{q}$, as sketched in fig. 58.

- Phonon-assisted transitions.

As discussed for transitions above the direct band gap of semiconductor, the contribu-

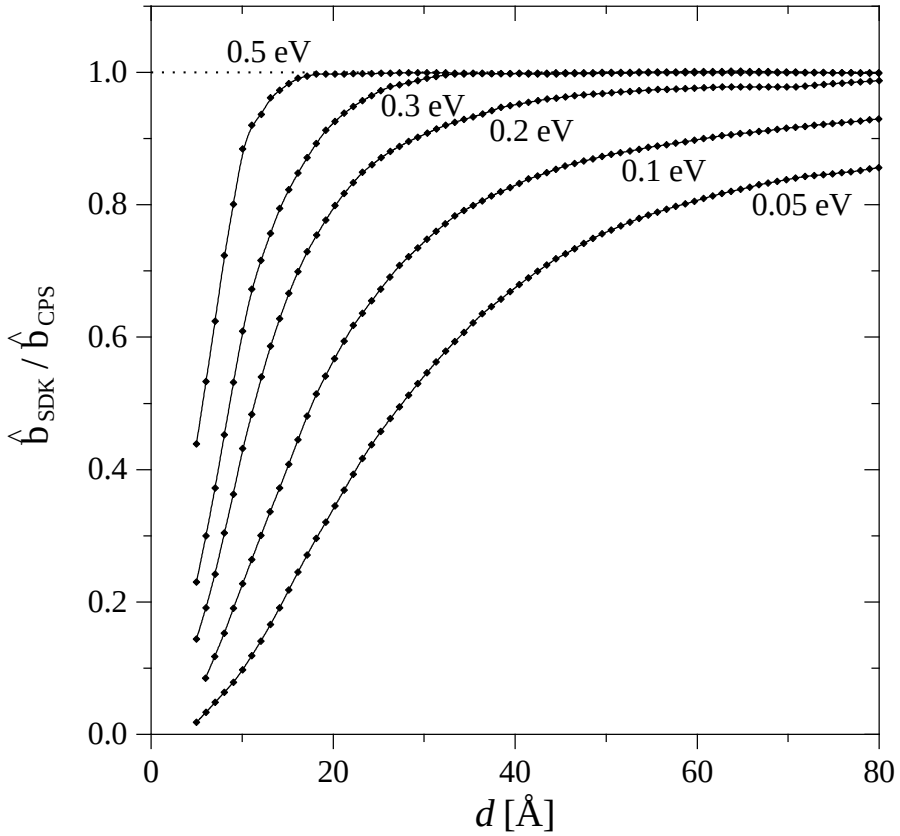

Fig. 57: SDK model predictions for the energy transfer from an electronically excited molecule to a semiconductor (via electron-hole pair generation) when the molecular energy is *larger* than the direct gap of the material, as a function of the molecule-substrate separation d. The curves, normalized to the expected CPS value (large-distance, 'optical' limit value), are calculated for various emitter excess energy Δ and constant band masses values $m_c = 0.1\, m_e$ and $m_v = 0.5\, m_e$ [13]. Energy conservation condition is predicted to limit the density of final states allowed for the transition according to eq. 32: not all the k-vector components of the molecular near field can indeed produce an electron-hole pair in the semiconductor; in this way the energy transfer deviates from CPS expectation (pointed line).

tions to the energy transfer rate integral (eq. 30) are non zero only for transitions between regions near the band extrema. In the far-field distance and for transferred energies just above the band gap (Δ very small), as the wave vector of molecular field is negligible ($\mathbf{k}_M \sim 0$), *phonon emission or absorption* (with $\mathbf{k}_{\rm ph} \sim \mathbf{q}$) is required to conserve momentum in indirect transitions across the gap in the semiconductor (fig. 58 (a)).

When the phonon-assisted band transition is the dominant mechanism to produce electron-hole pairs in the solid, the energy transfer rate $\hat{b}^{\rm phon}_{\rm SDK}$ is predicted to exhibit once

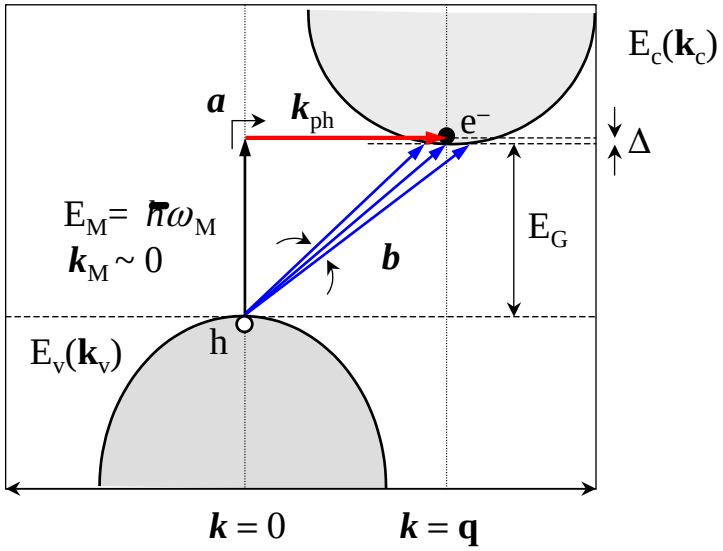

Fig. 58: Sketch of molecule-semiconductor energy transfer via electron-hole pairs generation, for molecular energy E_M just above the onset E_G of an indirect band transition. The conduction band minimum is displaced by $\mathbf{q}$ in k-space. At large emitter-substrate separation, to conserve the momentum in transition, phonon-assistance (a) is required ($\mathbf{k}_M + \mathbf{k}_{ph} = \mathbf{q}$, with $\mathbf{k}_M \sim 0$). At short emitter-substrate separation, the near-field effects become dominant: SDK model predicts that the high-wave-vector components of molecular near field can directly promote non-vertical transitions (b) without phonon-assistance. Depending on Δ's value, energy conservation (eq. 32) reduces the possible transitions only to final states around $\mathbf{k}_c \sim \mathbf{q}$. The phonon energy is neglected in figure.

more a d^{-3} dependence on the distance. Its absolute value is however expected to be smaller than that in the direct transitions: in both cases the rate is proportional to the absorption coefficient α of the solid. In case of indirect transition however α_{ind} is proportional to Δ^2, rather than $\Delta^{1/2}$ as in the direct case (α_{dir}); as a consequence, for excess energy of $\sim 0.1-0.3\,\text{eV}$, the indirect absorption is up to two orders of magnitude weaker than the direct one.

The observed energy transfer rate $\hat{b}^{\text{phon}}_{\text{SDK}}$ via phonon-assisted transition mechanism on indirect band gap materials is similarly expected to be appreciably smaller in absolute value than the rate via vertical transitions on direct gap solids.

- Non phonon-assisted transitions.
In the near-field domain the molecules transfer *non-radiatively* the excitation to the substrate. The excitation transfer is not mediated by a photon and the condition $\mathbf{k}_M \sim 0$ is no more valid. The molecular near field exhibits indeed a large distribution of k-vectors. As a consequence, the SDK model predicts that it is possible that the excited molecule does transfer energy to the semiconductor by *directly* producing electron-hole pairs via non-

vertical transitions, *without phonon assistance*, only by means of the k-vector distribution around $\mathbf{k} = \mathbf{q}$.

The production of electron-hole pairs by non-vertical transitions (fig. 58(b), slanted arrows) allows the energy transfer to take place also when the energy of the emitter is smaller than the direct band gap of the semiconductor. When caused by a mechanism involving non-vertical transitions, the model predicts that the energy transfer rate $\hat{b}$ from the molecule to the semiconductor shows a d^{-4} *dependence* on the distance.

However, at shorter distances, much as in the direct gap case, also on indirect gap semiconductors the energy conservation condition (δ function in eq. 30) truncates, as a function of Δ and of the band masses, the integration in k-space to values around $\mathbf{k}_c \sim \mathbf{q}$. This reduces the energy transfer rate and causes weaker dependence and a *deviation from the d^{-4} curve*.

Summary of the SDK model predictions

The predictions of the SDK model can be summarized as follows:

−Emitter energy larger than the *direct* band gap:

1.) For distances in the range of $d \sim 50-100$ Å, the SDK model agrees with the expectations of the CPS model and the energy transfer rate is predicted to exhibit a d^{-3} dependence.

2.) At shorter distance ($d \leqslant 50$ Å) the SDK model predicts, on the base of energy conservation reasons, *less* energy transfer than that expected by the CPS model. A *deviation* from the classical d^{-3} curve, depending on the value of excess energy Δ, is therefore expected.

−Emitter energy larger than the *indirect* band gap:

3.) The SDK model predicts two possible energy transfer mechanisms: for large molecule-substrate distances, via phonon-assisted band transitions with a d^{-3} dependence. In the range $d \sim 20-50$ Å via non phonon-assisted transitions with a d^{-4} dependence.

4.) Owing to energy conservation condition a *deviation* from the d^{-4} curve is predicted for distances $d < 20$ Å. The extent of the deviations depends on the amount of excess energy Δ and on the band structure of the semiconductor.

These aspects are evidenced in fig. 59; there, the normalized fluorescence lifetime $a = \hat{b}_{\mathrm{SDK}}^{-1}$ (according to eq. 11) is plotted versus d in case of emitter energies respectively above the direct or above the indirect band gap in a semiconductor: in the short distance range the SDK model predicts deviations from respectively the d^3 and d^4 dependence.

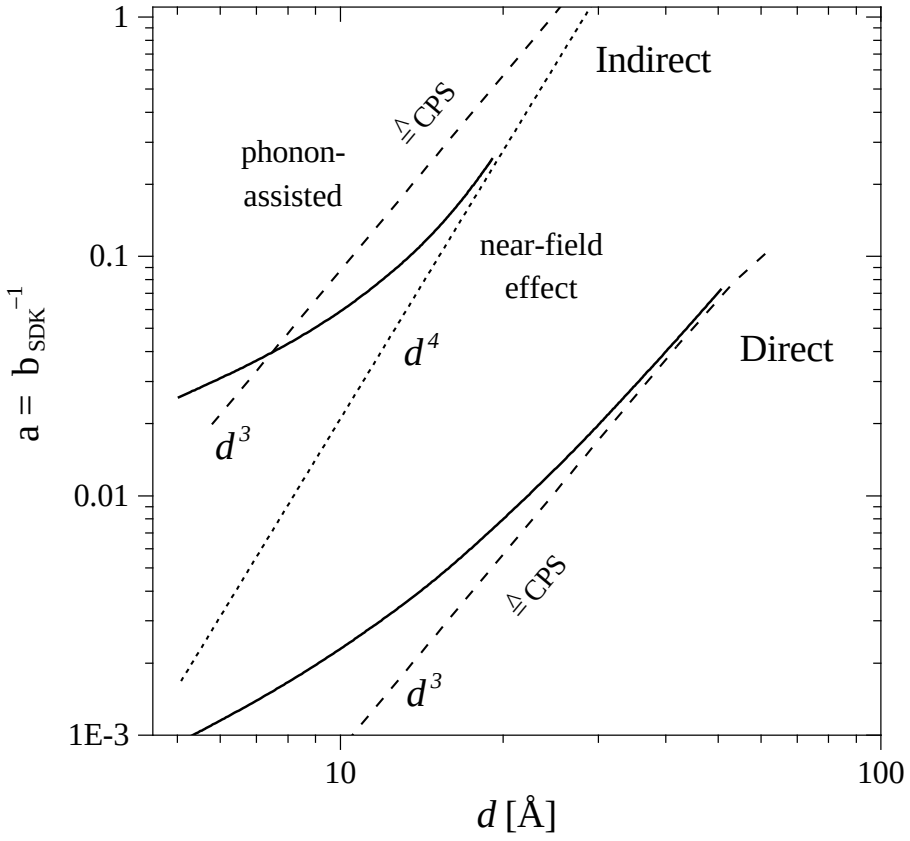

Fig. 59: SDK model predictions for excited molecules deposited on a generic direct or indirect band gap semiconductor substrate (with optical absorption of $\alpha_{\mathrm{dir}} = 50000\,\mathrm{cm}^{-1}$ and $\alpha_{\mathrm{ind}} = 500\,\mathrm{cm}^{-1}$, respectively). Distance-dependent normalized fluorescence emitter lifetime ($a = \hat{b}_{\mathrm{SDK}}^{-1}$) numerically calculated (continuous line) from eq. 31 [13] and analytically approximated in the limit of large distances (dashed and dotted lines).

Direct transitions: In the limit of large distances, the model predictions coincide with the CPS model expectations (i.e. d^3 dependence for a), whereas a deviation is expected for smaller d.

Indirect transitions: Beside phonon-assisted transitions (dashed line, with a classical d^3 dependence), non-vertical transitions from valence to conduction band are possible, because of momentum distribution in the molecular near field, without phonon-assistance ('near-field effect'): in this case a d^4 dependence is predicted at large distances (dotted line), whereas for small d a deviation is once more expected. The extent of the deviations depends on the amount of excess energy Δ and on the band structure of the semiconductor.

8.7 The SDK model applied to *MePTCDI* on MoS_2 and on *Si(111)*

In this section, the distance dependent fluorescence measurements carried out on the two semiconductors are discussed by joining the arguments of § 8.3 (for MoS_2) and of § 8.4 (for *Si(111)*) based on the quantitative calculations by the CPS model, with considerations about the specific band structure of the two semiconductors and the qualitative predictions of the SDK model, described in the last paragraph.

The fluorescence lifetime shortening is connected to the semiconductor nature of the considered solids. The distance dependence observed on *Si(111):H* (fig. 53) is interpreted by the light of the particular energy transfer mechanism predicted by the SDK model on indirect semiconductors.

8.7.1 *MePTCDI* on MoS_2: description by the SDK model

In the quantitative description of *MePTCDI* deposited on MoS_2, the introduction of the SDK model seems not necessary since the CPS model has proofed to be able to describe correctly, on a large distance range, the observed distance dependence of the fluorescence lifetime (fig. 49).

Nevertheless, the (quantitatively correct) predictions of the CPS model are exclusively founded on the use of a frequency dependent dielectric function $\varepsilon(\omega)$ (macroscopic parameter) of the material, whereas no indication is given on the *interaction mechanism*.

As shown in fig. 51, in case of MoS_2, both the dielectric function $\varepsilon(\omega)$ and the energy transfer rate parameter $\beta(\omega)$ turn out to be drastically affected by the transitions across the gap in the substrate. The fluorescence lifetime shortening effect is therefore definitely related to the *semiconductor nature* of the solid, too.

Furthermore, the calculation (within the CPS model) of the power dissipated by the *MePTCDI* molecules when deposited at various distances d from MoS_2 (fig. 52) puts in evidence that, as the separation is decreased, the largest part of the energy is transferred through *high-wave vectors components* of the molecular field.

Moreover, in the same plot, the peak related to the resonant excitation of surface plasmon polaritons (SPP) is absent. The missing of such resonance precludes the possibility to explain the observed lifetime shortening effect on MoS_2 in terms of excitations of longitudinal charge oscillations as on metallic substrates.

Finally, the *MePTCDI* energy ($E_{\mathrm{mol}} = 2.32\,\mathrm{eV}$) lies *above* the direct band gap of MoS_2 ($E^{\mathrm{gap}}_{MoS_2}$=1.95 eV) and the excess energy Δ amounts to 0.35-0.40 eV.

Taking into account all these aspects, ***the SDK model describes the energy transfer from electronically excited MePTCDI molecules to MoS_2 as the***

result of a direct electron-hole pair generation in the solid by the molecular near field.

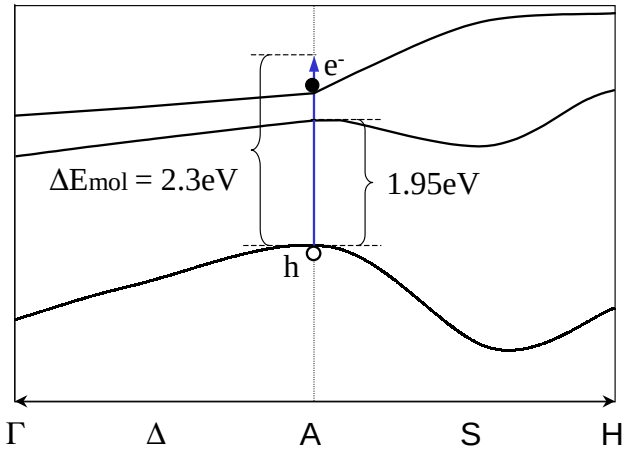

Fig. 60: Sketch of the MoS_2 band structure along the most important crystallographic axes of symmetry in the Brillouin zone (ref. [50] for details). The *MePTCDI* molecule-semiconductor energy transfer mechanism is illustrated: on MoS_2 the emitter energy ($\hbar\omega = 2.32\,\mathrm{eV}$) lies *above* the onset of the direct band transition ($\hbar\omega = 1.95\,\mathrm{eV}$) in MoS_2; the SDK model predicts that the near field of the molecule can *directly* produce e-h pairs in the solid. Consequently, a non-radiative excitation transfer from the *MePTCDI* molecule to the MoS_2 substrate takes place, resulting in a reduction (according to the distance d) of the molecular fluorescence lifetime.

Using the SDK model and the knowledge of the MoS_2 band structure it is therefore possible to *extend* the interpretation of the experimental results based only on the CPS model; in comparison with the phenomenological description by the CPS model, the application of the SDK one allows to *justify* the observed molecular lifetime shortening by introducing a mechanism for the energy transfer. This is shown in fig. 60.

Fig. 60 shows both the sketch of the band structure along the most important axes of symmetry of MoS_2 lattice (after [50]) and the SDK mechanism to explain the observed transfer. Since the *MePTCDI* energy does exceed the band gap of MoS_2, the excited molecule can promote an electron from valence to conduction band by a mechanism similar to the Förster dipole-dipole interaction [154]: in this case the 'donor' dipole is the transition dipole of the de-exciting *MePTCDI* molecule, the 'acceptor' dipole is the non-radiatively induced electron-hole pair in the solid.

It is possible to describe the case of *MePTCDI* on MoS_2 by a combination of CPS *and* SDK model:

a.) When the separation between molecule and substrate is sufficiently large ($d \sim 30$-

70 Å) *both* CPS *and* SDK model predict a d^{-3} distance dependence of the energy transfer rate: on the basis of this coincidence the quantitative description of the observed molecular lifetime shortening through the CPS model (fig. 49) turns out to be successful.

b.) When the separation d becomes shorter, the energy conservation condition (eq. 32) in the SDK model truncates in k-space the contributions to energy transfer probability, therefore *reducing* the shortening effect with respect to what is predicted by the CPS theory; as seen in the earlier paragraph and in fig. 57, the amount of the deviation from CPS model predictions depends mainly on the value of excess energy Δ.

When, as in the present case, the *MePTCDI* molecule emission lies above the band edge of the MoS_2 semiconductor by $\Delta = 0.35$–$0.40\,\text{eV}$, from fig. 57 it is possible to estimate that the distance d under which the SDK model predicts a deviation from the d^{-3} curve is $\sim 20-30\,\text{Å}$.

On MoS_2, as discussed in § 8.3 (fig. 49), a *deviation* from the d^3 curve is actually found for distances under $\sim 30\,\text{Å}$; however just under this value of d, the lifetime measurement is strongly affected by the limited time resolution of the system. It is not therefore possible to ascribe with certainty this discrepancy to the deviation of the energy transfer rate from the d^{-3} curve as predicted by the SDK model.

It is however possible to state that the mechanism responsible for the energy transfer from *MePTCDI* to the MoS_2 semiconductor is the creation of electron-hole pairs in the substrate by the near field of the electronically excited molecules.

8.7.2 *MePTCDI* on *Si(111):H*: description by the SDK model

In this paragraph the SDK model is applied to interpret the fluorescence dynamics of the *MePTCDI* molecule on *Si(111):H*. As seen in § 8.4, the CPS model fails in describing the experimental results in the range of small distances (fig. 53).

In contrast to the case of *MePTCDI* on MoS_2, when the *MePTCDI* molecule is deposited on *Si(111):H* the molecular emission energy ($E_{\text{mol}} = 2.32\,\text{eV}$) is *smaller* than the direct band gap of silicon (3.4 eV) and larger than the indirect band gap (1.16 eV).

The excitation of the silicon substrate can take place radiatively and non radiatively, depending on the actual spatial separation between molecule and substrate.

– *Excitation of the solid by the radiative field of the emitter.*
In the far-field range, the electronic transitions across the gap are induced by the *radiative* field of the molecule; they take place only with phonon assistance, since optical transitions are 'vertical'. The promotion of an electron from valence to conduction band above the indirect gap happens by emitting or by absorbing a phonon (with wave vector $\mathbf{k}_{ph}$) to conserve the momentum in the transition, as exemplified in fig. 58(a).

This mechanism is actually taken into account by the CPS model, since the phonon-assisted transitions contribute to the optical absorption of silicon, which turns out to be non-zero also below the onset of the transition across the direct band gap (in fig. A.3, tail of the dashed curve below 3.4 eV). Nevertheless, in the short distance regime, it is not possible to describe the fluorescence lifetime shortening by the CPS model (fig. 53): evidently the energy transfer mechanism is *different* from that phenomenologically taken into account by this model via the dielectric function of the material.

– *Excitation of the solid by the non-radiative field of the emitter.*
When the excitation of the solid takes place no more via the radiative field of a source placed far from the substrate, but by the non-radiative field of an electronically excited *MePTCDI* molecule deposited *very near* to silicon surface, the SDK model predicts that the high-wave vector components of the molecular near field can promote an electron from valence to conduction band of silicon via a non-vertical electronic transition across the gap, without phonon assistance (fig. 61, slanted arrow).

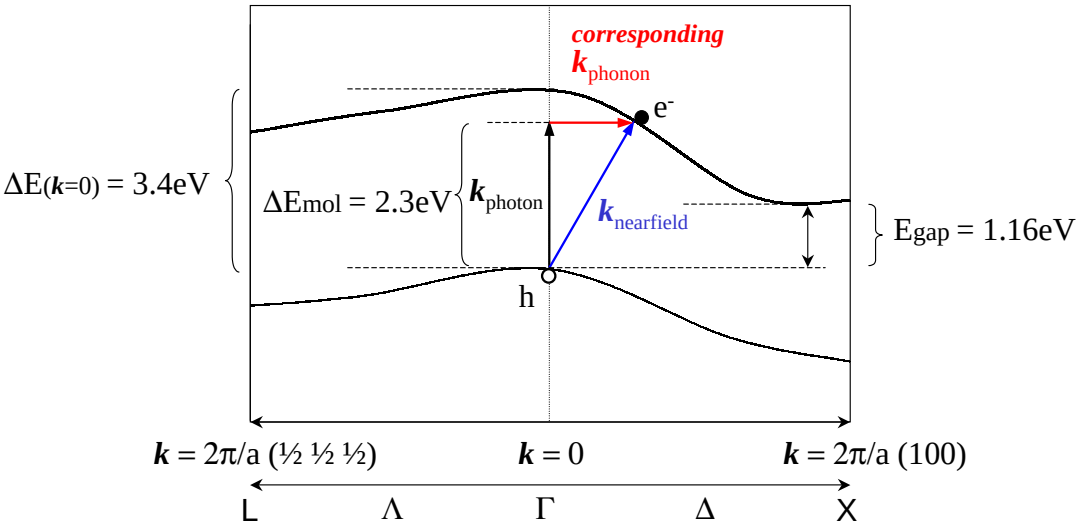

Fig. 61: Sketch of the band structure in silicon along the most important axes of symmetry in the Brillouin zone [156]. The *MePTCDI* molecule-semiconductor energy transfer mechanism is illustrated: below the onset of the direct electronic transition at 3.4 eV, the absorption of a photon usually requires simultaneous scattering of a phonon to conserve the momentum. Nevertheless, at very short separations, the SDK model predicts that the *near field* of the dipole can *directly* excite *non-vertical* electronic transitions across the gap and in this way efficiently transfer the excitation to the substrate.

Since such a process is possible only when the molecule is *physically placed in proximity* of the solid, it does not contribute to the value of the optically measured $\varepsilon(\omega)$ of

silicon [150] and consequently it is missed in the CPS model.

The molecular fluorescence lifetime shortening consequence of non phonon-assisted band transitions is expected to exhibit a *different* distance dependence than that expected by applying the CPS model.

This aspect is considered in fig. 62: the normalized *MePTCDI* fluorescence lifetime ($a = \tau_{obs}/\tau_0$) is plotted as a function of the distance from the silicon substrate (x-scale: $4-200$ Å). The CPS curve calculated using the parameters for silicon (corrected for low temperature) and the curves predicted by the SDK model for the present case are also reported.

The complete set of fluorescence lifetime data can be then interpreted as follows. At sufficiently large distances ($d > 100$ Å), the observed modulation of the molecular lifetime a has to be ascribed almost entirely to the interference effect (much as on silver, fig. 39). In this distance domain, the CPS model (thin continuous line) is found to describe adequately the experimental data.

At intermediate distances (15 Å $< d < 50$ Å), a discrepancy (estimated almost one order of magnitude at 15 Å) between the data and the CPS model expectations is observed: inside this range of distances the phenomenologic description of the CPS model starts to fail.

In the same distance range, the SDK mechanism for the fluorescence lifetime shortening is based on the molecular near field induced non-vertical electronic transitions across the gap. The thick continuous line shows the d^4 dependent curve for a; notably the vertical offsetting of the curve is a function of the band masses and of the band structure of the solid and its position is critically affected by the assumptions of the model. At shorter distances ($d < 15$ Å) a weaker dependence is expected, i.e. a deviation (up to one order of magnitude) from the d^4 curve, depending on the parameters of the system (dashed line).

In the small distance range, *both* models *overestimate* the lifetime shortening effect. At minimum distance ($d = 5.7$ Å, indicated by 'min' on the x-scale) a fluorescence lifetime value of $a = 145$ ps is observed, whereas a value of $a \sim 7$ ps is expected (at low temperature) according to CPS d^3 curve and a value of $a \sim 10 \pm 5$ ps according to the SDK model.

Whereas the phenomenological CPS model fails in the description of the lifetime shortening effect, the SDK model provides a mechanism to justify the observed dependence and permits to give a crude qualitative description of the experimental data, although still with a large discrepancy in absolute value.

However, the grade of success of these theoretical models is strictly joint to the validity of the approximations, on which the models are based. In particular, below few tens of angstroms the point-dipole approximation is no more correct and it would be necessary to account for the finite dimensions of the emitter. Furthermore, the surface of the substrate,

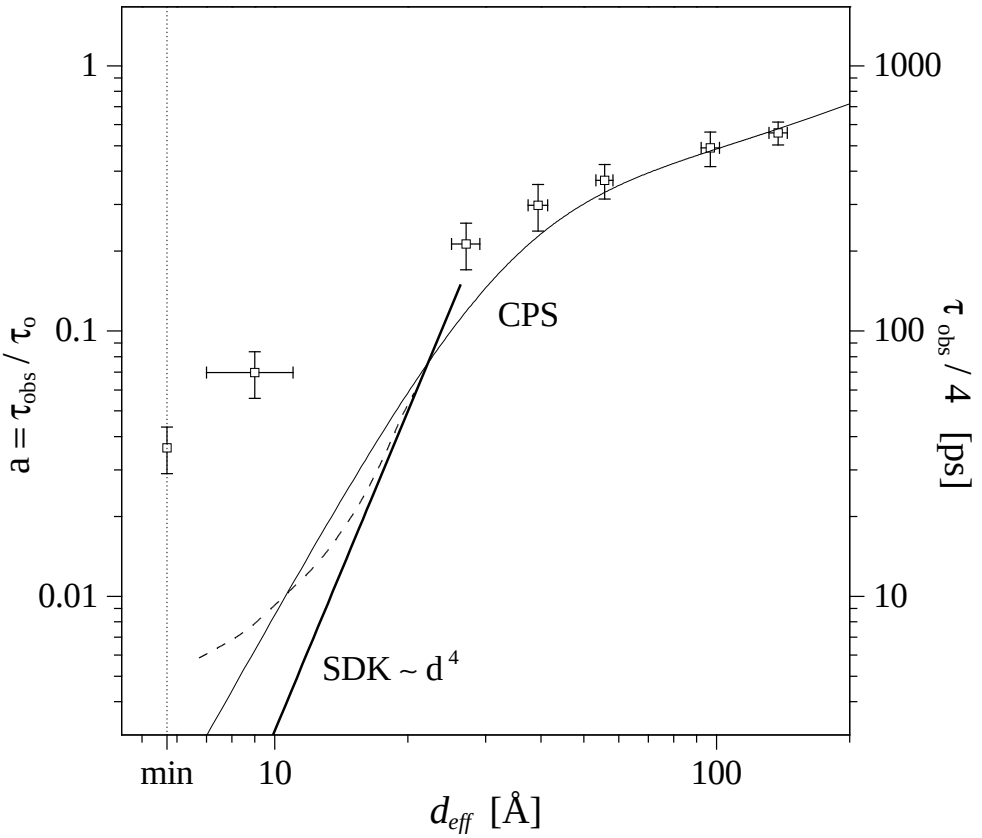

Fig. 62: *MePTCDI* on *Si(111):H*: normalized fluorescence lifetime data, CPS curve calculated for a parallel *MePTCDI* molecule (thin line) using the parameters of *Si(111):H* and curve derived by the SDK model (thick line). The CPS model calculations describe the data down to distances of ~ 50 Å. Below, the SDK predicts that molecular near field induces non-vertical band transitions in the semiconductor: the mechanism brings about a quartic distance dependence in the observed lifetime ($a \sim d^4$). At extremely small distances ($\min \leqslant d < 15$ Å), energy conservation causes a deviation from such a trend ($- - -$). With 'min' the minimum distance (5.7 Å) from *Si(111)* surface is indicated.

described as infinitely extended and flat, presents in reality finite dimensions, a grade of roughness and a certain density of defects. The substrate, considered as a continuous medium characterized only by its macroscopic dielectric function, exhibits actually a wave vector dependent response. The modellization of the boundary interface between the substrate and the surrounding media is indeed object of a series of theoretical studies finalized to overcoming the existing approximations [40]. On the other hand, the SDK model has been developed starting from rather strict initial assumptions [13], too. It is not very flexible and difficult to apply to the numerical solution of general problems, taking into account defined semiconductor band structure.

Comparison with the results of precedent researches

As briefly reported in § 1.1.4, the experimental activity concerning the study of the interaction between organic molecules and semiconductors has been up to now very limited. The experimental results of the present work carried out on silicon substrate can be compared with those of Hayashi et al. [39], Alivisatos et al. [24], Sluch et al. [42] and Gómez [43].

In the first case, the fluorescence intensity of thick films of tetracene, separated from Si by LiF spacer layers, was measured between $20\,\text{Å} < d < 400\,\text{Å}$ and analyzed by using the CPS model. A very large discrepancy was observed: the fluorescence intensity was quenched two order of magnitude *more* than expected. The presence of a strong intralayer excitation transfer component, however, did not allow to correctly estimate the molecule-substrate transfer rate.

In the second case, the fluorescence lifetime of submonolayer films of pyrene on Si(111) (Xe as spacer layer) was measured for just three distances (17, 28 and 196Å). An intralayer excitation transfer was observed in addition to the transfer to the Si substrate, making the results somewhat inconclusive; a slightly faster dependence on the distance with respect to the CPS model predictions was obtained.

Sluch et al., making use of the Langmuir-Blodgett technique to separate palmitic acid from Si, studied the distance dependence of the fluorescence intensity in a range between 25 Å and 200 Å. A deviation (weaker dependence, less quenching) was noted for separations below 50 Å in comparison with the CPS model expectations.

Gómez studied the fluorescence lifetime of *MePTCDI* films of different thickness (between 1 and 50 ML) deposited on *Si(111):H*. By a numerical integration on the film thickness, he was able to estimate the excitation transfer rate to the substrate as a function of the film thickness and to compare the value with the expectations of the CPS model. He found a good agreement for thicknesses down to ~ 6 ML (~ 30 Å) and more than one order of magnitude deviation (less quenching) for smaller thicknesses.

The present results confirm the observations of Sluch et al. and Gómez, whereas disagree with the results of the first two groups. Nevertheless, in contrast with all the precedent known researches, the isolated molecule approach followed during this work ensures that each other excitation transfer process, competing with the direct molecule-substrate interaction, is strongly reduced and at limit blocked.

The estimation of the fluorescence lifetime shortening effect turns out to be consequently more reliable than in precedent researches, as the measurement of its value is no more perturbed by the presence of any other deactivation process.

9 Conclusions

The goal of this research was the study of the *interaction mechanism* between electronically excited molecules and *semiconductor* substrates. Following the *isolated molecule approach*, ultrathin molecular films (0.01 ML) of *MePTCDI* have been deposited at helium temperature at nanometric and subnanometric distances ([0 − 500 Å]) on two prototypical semiconductors, MoS_2 and *Si(111):H*, making use of the spacer layer technique to fix the distance and of ps-time resolved single photon counting methods to measure the fluorescence signal.

By the isolated molecule approach, it is possible to stop the inter-molecular interaction (and consequently the intra-layer transport) and *measure directly* the effects induced by the presence of the substrate on the fluorescence properties of the molecule deposited on top. During this work, for the first time the fluorescence lifetime of isolated organic molecules was measured as a *function of the distance* from *semiconductor* substrates.

The treatments applied both to substrates and to argon layer and how they affect the fluorescence properties of the sample have been extensively studied and the experimental conditions accordingly optimized.

The main *experimental results* are summarized as follows.

- The electronically excited *MePTCDI* molecules deposited at a nanometric distance from the semiconductor surface exhibit (both on MoS_2 and on *Si(111):H*) *faster* fluorescence decays than the molecule in dilute solution (prototype of intrinsic molecular fluorescence lifetime).
- The distance dependence of *MePTCDI* fluorescence lifetime as measured in the range [0 − 500 Å] for MoS_2 and in [0 − 130 Å] for *Si(111):H* shows for the two semiconductors a quantitatively different lifetime shortening effect: on MoS_2 the fluorescence lifetime is observed to be shortened more then two orders of magnitude (from 3.95 ns to 25 ps), on *Si(111):H* more than one (down to 145 ps).

The theoretical model developed by Chance, Prock and Silbey (CPS) has been applied to describe *quantitatively* the observed change in fluorescence lifetime upon molecule-substrate distance variation.

Within this classical model the properties of the substrate are taken into account phenomenologically by characterizing the solid through its dielectric function $\varepsilon(\omega)$ only, without any microscopic description of the material and any indication to the interaction mechanism.

The model predicts that at short separation d, the excitation transfer rate follows a d^{-3} functional dependence, independently from the nature of the solid. It is formally correct to apply the CPS model (originally developed to describe the transfer to metals)

to the study of the interaction between excited molecule and a *semiconductor*, making use of the appropriate dielectric function.

The interaction mechanism is nevertheless physically different: in case of metals the dielectric function is mainly contributed by the free electrons and the mechanism is related to the coupling of the molecular near field to surface charge oscillations (surface plasmons); on the contrary in case of semiconductors it is related to the coupling to the bound electrons of the lattice.

On $\boldsymbol{MoS_2}$, the experimental dependence of the fluorescence lifetime is *quantitatively* described by the CPS model (i.e. by $\varepsilon(\omega)$) on the whole considered distance range.

On ***Si(111):H***, the experimental dependence can not be described by the CPS model: at minimum distance, a deviation of more than one order of magnitude in fluorescence lifetime between model predictions and experimental data is observed.

A further semi-classical model specifically developed for (direct/indirect) semiconductors by Stavola, Dexter and Knox (SDK) allows to explain the observed molecular lifetime shortening by introducing a mechanism for the energy transfer. It provides a *qualitative* description of the distance dependence of molecular fluorescence lifetime, taking into account characteristics of the semiconductor band structure.

The results have been interpreted by the SDK model as follows.
MoS_2−Prototypical case in which the molecular emission energy exceeds the semiconductor direct band gap. The near field of the molecule can non-radiatively excite an electron from the valence band to the conduction band in the semiconductor, by a dipole−(induced *e*-*h*) dipole mechanism and in this way transfer its excitation to the solid. The process is effective for distances less than 300 Å. The transfer rate is predicted to exhibit a d^{-3} dependence (like in CPS model). At short distances ($d < 50$ Å), depending on the excess molecular energy a deviation from this dependence is predicted, but not experimentally observed because of time resolution limits.

Si(111):H−Prototypical case in which the molecule emission energy does not exceed the semiconductor direct band gap. The near field of the molecule can nevertheless excite non-vertical transitions by its distribution of wave vectors, without phonon assistance and hence can be effective in creating *e*-*h* pairs. Such mechanism is predicted to exhibit a d^{-4} dependence for the transfer rate. At very short distances ($d < 25$ Å), depending on the excess molecular energy a deviation from this dependence is predicted. Applying this second model, the experimental data trend can be qualitatively mimed although with a large discrepancy in the absolute value.

A Appendix

A.1 Interband transitions and the dielectric function of *Ag*, MoS_2 and *Si*

In this section the experimental values of the dielectric function for *Ag*, MoS_2 and *Si* are reported and the influence of the interband transitions on the dielectric properties of these materials discussed.

These values have been used within the calculation of the CPS curves (fig. 39, fig. 48− 49 and fig. 53), within the calculation of the energy transfer rate parameter $\beta(\omega)$ (fig. 43, fig. 55 and fig. 51) and in that of the dissipated power of excited dipole (fig. 45, fig.52 and fig.56).

The values for *Ag* were published by *Johnson and Christy* [135], those for *Si* by *Aspnes and Studna* [150] and those for MoS_2 by *Sobolev and Sobolev* [51]. The measurements were carried out at room temperature through various techniques (*see* the respective references for details).

Dielectric function of *Ag*
Fig. A.1 shows, in the range $[2-6\,\mathrm{eV}]$, the real and the imaginary parts of the dielectric function of *Ag*: both *experimental* curve and *model* curve (calculated using the Drude's model (eq. 17) with plasmon energy $\hbar\omega_p = 9.14\,\mathrm{eV}$ and relaxation time $\tau = 1/\delta = 31 \cdot 10^{-15}\,\mathrm{s}$ [140]) are here plotted to evidence the importance of the contribution of the interband transitions to determine the form of $\varepsilon(\omega)$.

In real metals in fact, beside the contributions from free electrons (adequately described by Drude's model), the effects of interband transitions on the response of the metal have to be carefully considered. If for alkali metals, e.g. sodium and potassium, interband transitions do not affect the dielectric function in the visible range because the energy of the band gap is large, in the case of noble metals such as silver, copper and gold the influence of interband transitions from the narrow filled *d* bands well below the Fermi level into the *sp* conduction band cannot be ignored [143] [144, p.168]: in these three materials, the transitions turn out to be the $4d \to 5sp$, $3d \to 4sp$ and $5d \to 6sp$ respectively, whereas the free electrons are in the 5*s*, 4*s* and 6*s* states [140]. In the case of copper and gold the interband transitions are in the visible range (for this reason these metals are coloured), while for silver, although the absorption edge is in the ultraviolet, it affects the dielectric function in the visible range very much.

Fig. A.1 shows clearly this effect for *Ag*: the experimentally determined dielectric function is plotted as a continuous line, whereas the modelled one as a dashed line. The real and imaginary part of $\varepsilon(\omega)$ are separately reported.

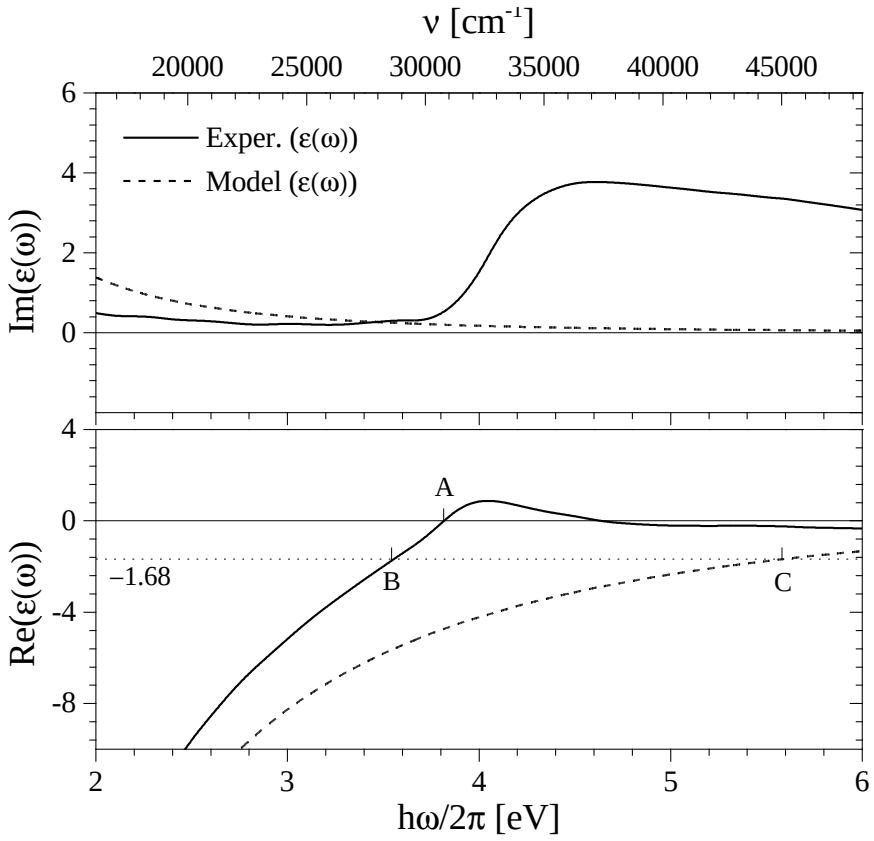

Fig. A.1: Dielectric function $\varepsilon(\omega)$ of *Ag*: real part (*below*) and imaginary part (*above*), either experimentally determined [135] (——) or theoretically calculated by the Drude's model (– – –). *See* text for details.

Imaginary part - The imaginary part of the experimental dielectric function is correctly described by a Drude's model only for energy *below* $\sim 3.8\,\mathrm{eV}$: above this threshold the description fails. At this energy the interband transition $4d \rightarrow 5sp$ takes place; since $\mathrm{Im}(\varepsilon(\omega))$ is proportional to absorption of the solid, its higher value at energies above this threshold indicates that the contribution to $\varepsilon(\omega)$ from transitions across the gap becomes dominant and the description of $\varepsilon(\omega)$ only by the free electron is inadequate. The dielectric function of a real metal is generally better approximated by the *sum* of contributions from free electrons and from interband transitions.

Real part - $\mathrm{Re}(\varepsilon(\omega))$ from Drude's model (– – –) remains negative in the whole considered range and it crosses the $\varepsilon = 0$ line at $\hbar\omega_p = 9.14\,\mathrm{eV}$ (out of the range shown in the figure); ω_p is the plasma frequency (according to eq. 19) and it depends only on the free carrier density n (in *Ag*, $n = 5.86 \cdot 10^{22}\,\mathrm{cm}^{-3}$ [147]).

The experimental curve (——) shows, differently from the model one, an appreciable modulation. Just the transitions from *d*-bands to regions of high density of states above the Fermi level are responsible for these structures. They are superimposed on a free

electron component and the resulting $\varepsilon(\omega)$ curve appears vertically offset.

For this reason, the point 'A' at which $\mathrm{Re}(\varepsilon(\omega))$ crosses zero (at energy $\hbar\omega_x$) is strongly red-shifted down to $\hbar\omega_x = 3.80\,\mathrm{eV}$. Although the condition $\varepsilon(\omega) = 0$ is satisfied, the zero-cross frequency ω_x is actually something *different* from a real 'plasma frequency' ω_p: this latter is exclusively defined by the free carrier density, independently from any band structure information, whilst the former is drawn out from a macroscopic function that takes into account contributions of various nature. The real plasma energy remains at $\hbar\omega_p = 9.14\,\mathrm{eV}$ (where the $(---)$ crosses the zero line) independently from any other contribution and the two coincide only if the interband transitions are neglected.

This aspect, although pointed out in earlier papers (*see* for example *Johnson and Christy* [135]), is usually disregarded in literature and together with a misleading on the definition of ω_p generates confusion also in well known review papers.

Energy transfer rate in presence of interband transitions

As shown in § 7.1, in the frame of the CPS theory it is possible to express the energy transfer rate between excited emitter and substrate by the parameter $\beta(\omega)$, with ω the frequency of the emitter. $\beta(\omega)$ depends (eq. 16) on the dielectric function both of the substrate and on that of the medium in which the emitter is embedded. On metals, as discussed at p. 103, a strongly enhanced energy transfer (peak of $\beta(\omega)$ in fig. 43) is predicted when the emitter frequency approaches the resonance frequency of charge density oscillation modes on the metal surface.

The frequency of these resonances is strictly dependent on the dielectric properties of the interface: the modulation induced by the interband transitions on the dielectric function of the substrate drastically affects the energy transfer rate of an excited emitter.

To make an example, the interface between an argon layer (medium 1, $\varepsilon_1 = 1.68$, near ω-independent) and a *Ag* substrate (medium 2, $\varepsilon_2(\omega)$) is explicitly considered.

The $\varepsilon_2(\omega)$ can be described either by an experimental dielectric function (that takes into account also the interband transitions) or by a simple free electron function.

In fig. 43, the predicted energy transfer rate $\beta(\omega)$ is plotted using the model function (black line) and using the experimental one (grey line). Remarkably, the curves show resonances at two *very different* energies.

According to eq. 25, the function $\beta(\omega)$ is found to show a resonance at ω_s so that the condition $\varepsilon_2(\omega_s) = -\varepsilon_1(\omega_s)$ is fulfilled. In the present case, a peak is predicted when $\varepsilon_2(\omega_s) = -1.68$.

Such a condition is fulfilled at two different energies, when the two expressions for $\varepsilon_2(\omega)$ are used: the *model* function crosses actually the line -1.68 at $\hbar\omega_{sp} = \hbar\omega_s = 5.58\,\mathrm{eV}$, whereas the function that takes into account the interband transition contributes crosses

the line at $\hbar\omega = 3.56\,\text{eV}$. In fig. A.1 these two energies are indicated by the letters B and C, for the experimental and model dielectric function, respectively. Such crossing points obviously indicate the positions of the resonances in fig. 43.

This demonstrates how the presence of interband transitions modulation in the dielectric function of the metal affects drastically the frequency dependence of the energy transfer rate.

Since the condition that determines the resonance in $\beta(\omega)$ holds for *any form* of $\varepsilon(\omega)$ (not depending this expression on an particular model of dielectric function, but just directly coming from Maxwell's equation), it continues still to have a physical meaning also when the solid is described by a *experimental* dielectric function, therefore contributed also by the interband transitions.

Dielectric function of MoS_2

Fig. A.2 shows the dielectric function of MoS_2, in the energy range from 1.0 to 4.0 eV. The onset of the transition across the gap is visible in $\text{Im}(\varepsilon(\omega))$ at $\hbar\omega \sim 1.8\,\text{eV}$.

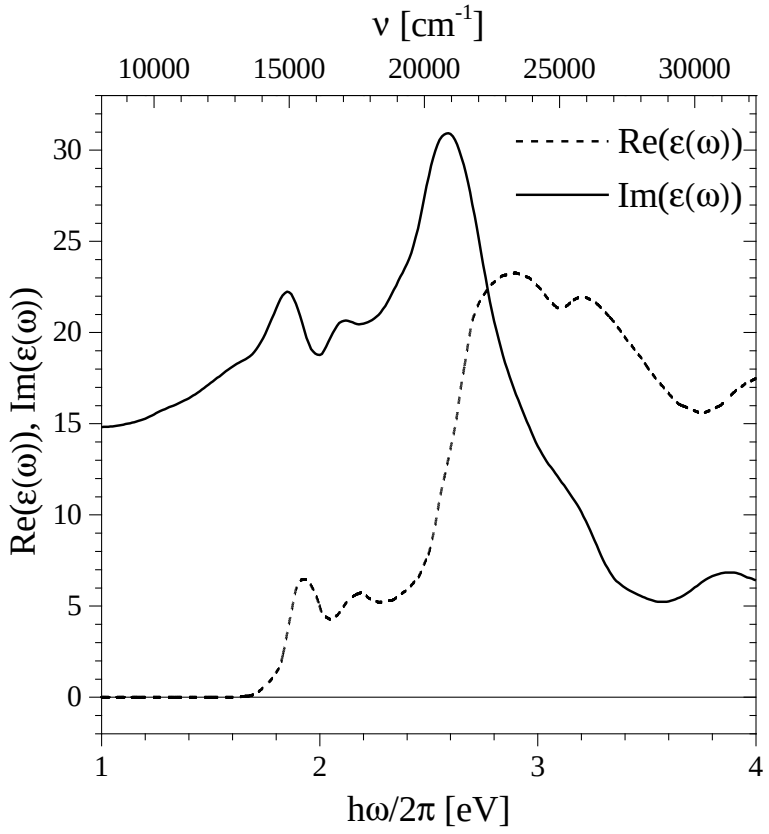

Fig. A.2: Frequency dependent real (——) and imaginary (– – –) part of dielectric function for MoS_2 (after [51]).

Dielectric function of *Si(111)*

Fig. A.3. shows the dielectric function of *Si*, in the energy range from 1.5 to 6.0 eV. The onset of the transition across the gap is visible in $\mathrm{Im}(\varepsilon(\omega))$ at $\hbar\omega \sim 3.2\,\mathrm{eV}$.

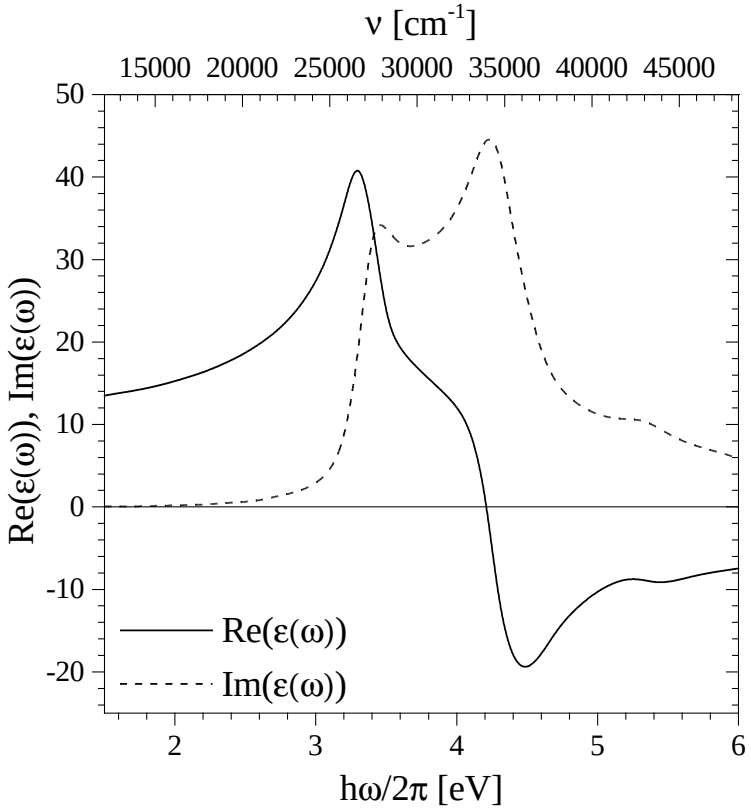

Fig. A.3: Frequency dependent real (——) and imaginary (– – –) part of dielectric function for *Si* (after [150]).

Bibliography

The order is citation order

[1] J.R. Sheats, H. Antoniadis, M. Hueschen, W. Leonard, J. Miller, R. Moon, D. Roitman und A. Stocking. *Organic electroluminescent devices.* Science, **273** (1996) 884.

[2] L.J. Rothberg und A.J. Lovinger. *Status of and prospects for organic electroluminescence.* J. Mater. Res., **11** (1996) 3174.

[3] R.H. Jordan, A. Dodabalapur, M. Strukelj und T.M. Miller. *White organic electroluminescence devices.* Appl. Phys. Lett., **68** (1996) 1192–4.

[4] S. Tasch, C. Brandstaetter, F. Meghdadi, G. Leising, G. Froyer und L. Athouel. *Red-green-blue light emission from a thin film electroluminescence device based on parahexaphenyl.* Adv. Mater., **9** (1997) 33.

[5] A.L. Burin und M.A. Ratner. *Spin effects on the luminescence yield of organic light emitting diodes.* J. Chem. Phys., **109** (1998) 6092.

[6] M.A. Baldo, S. Lamansky, P.E. Burrows, M.E. Thompson und S.R. Forrest. *Very high-efficiency green organic light-emitting devices based on electrophosphorescence.* Appl. Phys. Lett., **75** (1999) 4.

[7] M. Deussen, P.H. Bolivar, G. Wegmann, H. Kurz und H. Bässler. *Electric field-induced photoluminescence quenching in molecularly doped polymer light-emitting diodes.* Chem. Phys., **207** (1996) 147.

[8] M.C.J.M. Vissenberg und M.J.M. de Jong. *Theory of exciton migration and field-induced dissociation in conjugated polymers.* Phys. Rev. Lett., **77** (1996) 4820.

[9] A. L. Burin und M. A. Ratner. *Exciton migration and cathode quenching in organic light emitting diodes.* J. Phys. Chem. A, **104** (2000) 4704–4710.

[10] H. Kuhn. *Classical Aspects of Energy Transfer in Molecular Systems.* J. Chem. Phys., **53** (1970) 101–108.

[11] R.R. Chance, A. Prock und R. Silbey. *Molecular Fluorescence and Energy Transfer Near Interfaces.* In I. Prigogine und S.A. Rice, Editoren, *Advances in Chemical Physics*, **37**, S. 1–63. John Wiley & Sons, New York, 1978.

[12] R.R. Chance, A. Prock und R. Silbey. *Comments on the Classical Theory of Energy Transfer.* J. Chem. Phys., **62**(6) (1975) 2245–2253.

[13] M. Stavola, D.L. Dexter und R.S. Knox. *Electron-Hole Pair Excitation in Semiconductors via Energy Transfer from an External Sensitizer.* Phys. Rev. B, **31** (1985) 2277–2289.

[14] B.N.J. Persson. *Theory of the Damping of Excited Molecules Located above a Metal Surface.* J. Phys. C, **11** (1978) 4251–4269.

[15] B.N.J. Persson und N.D. Lang. *Electron-Hole-Pair Quenching of Excited States Near a Metal.* Phys. Rev. B, **26**(10) (1982) 5409–5415.

[16] G. Rempe. *Der Ein-Atom-Laser.* Phys. Bl., **51**(5) (1995) 383.

[17] K.H. Drexhage. *Monomolecular Layers and Light.* Sci. Am., **222** (1970) 108–119.

[18] K.H. Drexhage. *Influence of a Dielectric Interface on Fluorescence Decay Time.* J. Lumin., **1/2** (1970) 693–701.

[19] K.H. Drexhage. *Interaction of Light with Monomolecular Dye Layers.* In E. Wolf, Editor, *Progress in Optics*, **12**, S. 163–232. North-Holland Publishing, New York, 1974.

[20] A. Campion, A.R. Gallo, C.B. Harris, H.J. Robota und P.M. Whitmore. *Electronic Energy Transfer to Metal Surfaces: A Test of Classical Image Dipole Theory at Short Distances (Ni(111)-Ar-Pyrazine-Triplet).* Chem. Phys. Lett., **73** (1980) 447–450.

[21] P.M. Whitmore, H.J. Robota und C.B. Harris. *Electronic Energy Transfer from Pyrazine to a Silver(111) Surface between 10 and 400 Å.* J. Chem. Phys., **76** (1982) 740–741.

[22] P.M. Whitmore, H.J. Robota und C.B. Harris. *Mechanisms for Electronic Energy Transfer between Molecules and Metal Surfaces: A Comparison of Silver and Nickel.* J. Chem. Phys., **77** (1982) 1560–1568.

[23] P.M. Whitmore, A.P. Alivisatos und C.B. Harris. *Distance Dependence of Electronic Energy Transfer to Semiconductor Surfaces: $^3n\pi^*$ Pyrazine/GaAs(110).* Phys. Rev. Lett., **50** (1983) 1092–1094.

[24] A.P. Alivisatos, M.F. Arndt, S. Efrima, D.H. Waldeck und C.B. Harris. *Electronic Energy Transfer at Semiconductor Interfaces. I. Energy Transfer from Two–dimensional Molecular Films to Si(111).* J. Chem. Phys., **86**(11) (1987) 6540–6549.

[25] C. Beneking und G. Heiland. *Fluorescence of a Merocyanine Dye Adsorbed on ZnO Crystals.* J. Lumin., **43** (1989) 9–24.

[26] A. Murayama, Y. Oka und H. Fujisaki. *Picosecond Transient Spectroscopy of Fluorescence in Rhodamine 6G Adsorbed Electrochemically on Ag Surface.* Sol. State Commun., **55**(1) (1985) 91–95.

[27] A.R. Leheny, N.J. Turro und J.M. Drake. *Direct Energy Transfer from Excited Organic Adsorbates to Intrinsic Defect Sites in Silicalite.* J. Chem. Phys., **97**(5) (1992) 3736–3743.

[28] K. Kemnitz, N. Tamai, I. Yamazaki, N. Nakashima und K. Yoshihara. *Site-Dependent Fluorescence Lifetimes of Isolated Dye Molecules Adsorbed on Organic Single Crystals and Other Substrates.* J. Phys. Chem., **91** (1987) 1423–1430.

[29] K. Kemnitz, T. Murao, I. Yamazaki, N. Nakashima und K. Yoshihara. *Picosecond Fluorescence Measurement of Submono- and Mono-Layer of Adsorbed Rhodamine B on a Single Crystal of Naphthalene and on Glass.* Chem. Phys. Lett., **10**(4/5) (1983) 337–340.

[30] S. Ohshima, T. Kajiwara, M. Hiramoto, K. Hashimoto und T. Sakata. *Excited H_2TPP on a Silver Surface: Fluorescence Quenching and Interference Effects.* J. Phys. Chem., **90** (1986) 4474–4476.

[31] R.W. Kessler, S. Uhl, W. Honnen und D. Oelkrug. *Fluorescence Decay of Aromatic Hydrocarbons on γ-Aluminia Surface.* J. Lumin., **24/25** (1981) 551–554.

[32] M. Daffertshofer, H. Port und H.C. Wolf. *Fluorescence Quenching of Ultrathin Anthracene Films by Dielectric and Metallic Substrates.* Chem. Phys., **200**(1/2) (1995) 225–233.

[33] M. Daffertshofer, H. Port und H.C. Wolf. *Fluorescence Quenching of Spacer-Separated Anthracene Monolayers by Inorganic Substrates.* J. Lumin., **66/67**(1–6) (1995) 208–212.

[34] M. Daffertshofer. *Zeitaufgelöste Fluoreszenzspektroskopie ultradünner Anthracen-Schichten in Wechselwirkung mit anorganischen Substraten.* Dissertation, Universität Stuttgart, 1995.

[35] S. Suto, W. Uchida, M. Yashima und T. Goto. *Luminescence Quenching of an Ultrathin H_2TPP Film on a Conductive SnO_2 Substrate.* Phys. Rev. B, **35**(9) (1987) 4393–4397.

[36] S. Suto, M. Yashima, W. Uchida und T. Goto. *Dynamics of Optically Excited Teraphenylporphyrin Films Evaporated on a Conductive SnO_2 Substrate.* J. Lumin., **38** (1987) 308–310.

[37] S. Suto, T. Ikehara, A. Koike, W. Uchida und T. Goto. *Luminescence Decay Time of Thin Tetraphenyl-Porphyrin Films Evaporated on Au Substrate: The Role of Electronic Energy Transfer.* Sol. State Com., **73**(5) (1990) 331–334.

[38] S. Suto, M. Yashima, W. Uchida und T. Goto. *Picosecond Luminescence Approach to Charge Transfer in a Tetraphenylporphyrin/SnO_2 interface.* Surf. Sci., **205**(1/2) (1988) 230–240.

[39] T. Hayashi, T.G. Castner und R.W. Boyd. *Quenching of Molecular Fluorescence Near the Surface of a Semiconductor.* Chem. Phys. Lett., **94** (1983) 461–466.

[40] W.L. Barnes. *Fluorescence near interfaces: the role of photonic mode density.* J. Mod. Optics, **45** (1998) 661–99.

[41] M. Brandstätter, P. Fromherz und A. Offenhausser. *Fluorescent dye monolayers on oxidized silicon.* Thin Solid Films, **160** (1988) 341–346.

[42] M.I. Sluch, A.G. Vitukhnovsky und M.C. Petty. *Anomalous distance dependence of fluorescence lifetime quenched by a semiconductor.* Phys. Lett. A, **200** (1995) 61–64.

[43] U. Gómez. *Abstandsabhängiger Energietransfer ultradünner MePTCDI-Schichten zum dielektrischen Substrat.* Dissertation, Universität Stuttgart, 1997.

[44] C. Gerthsen, H.O. Kneser und H. Vogel. *Physik.* Springer, Berlin, 1989.

[45] A.B. Djurišič, T. Fritz und K. Leo. *Determination of optical constants of thin absorbing films from normal incidence reflectance and transmittance measurements.* Optics Communications, **166** (1999) 35–42.

[46] G. Klebe, F. Graser, E. Hädicke und J. Berndt. *Christallochromy as a solid-state effect: correlation of molecular conformation, crystal packing and colour in perylene-3,4:9,10-bis(dicarboximide) pigments.* Acta Cryst. B, **45**(1) (1989) 69–77.

[47] M. Runne, J. Becker, W. Laasch, D. Varding, G. Zimmerer, M. Liu und R.E. Johnson. *Exciton-Induced Desorption and Surface-Type Luminescence of Kr Atoms from Kr-Doped Solid Ar.* Nuc. Ins. & Met. in Phys. Res., **B82**(2) (1993) 301–309.

[48] E. Hädicke und F. Graser. *Structures of Eleven Perylene-3,4:9,10-bis(dicarboximide) Pigments.* Acta Cryst. C, **42**(2) (1986) 189–195.

[49] P.A. Lee. *Optical and electrical properties*, **4** der *Physics and chemistry of materials with layered structure.* D. Reidel, Dordrecht, 1976.

[50] R.V. Kasowsky. *Band structure of MoS_2 and NbS_2.* Phys. Rev. Lett., **30** (1973) 1175–78.

[51] V.V. Sobolev und V. Val Sobolev. *Optical spectra of Molybdenum Disulphide in the region between 1 and 30eV.* J. Appl. Spectr., **61** (1994) 532–5.

[52] R.C. Weast und M.J. Astle ed. *CRC Handbook of chemistry and physics.* CRC Press, Boca Raton, 1981.

[53] P.O. Hahn und M. Henzler. *Influence of Oxidation Parameters on Atomic Roughness at the Si-SiO_2 Interface.* J. Appl. Phys., **52**(6) (1981) 4122–4127.

[54] G.J. Pietsch. *Struktur und Chemie technologischer Silicium-Oberflächen*, **9/148** der *VDI Fortschritt-Berichte.* VDI Verlag, Düsseldorf, 1992.

[55] W. Kern. *Handbook of Semiconductor Wafer Cleaning Technology.* Noyes Publ., Park Ridge, NJ, 1993.

[56] W. Kern und D.A. Puotinen. *Cleaning Solutions Based on Hydrogen Peroxide for Use in Silicon Semiconductor Technology.* RCA Rev., **31** (1970) 187–206.

[57] W. Glatz. *Rastertunnelmikroskopie im Vergleich mit der Streuung hochfrequenter Phononen an freien und metallbedeckten Siliziumoberflächen.* Dissertation, Universität Stuttgart, 1992.

[58] R. Strohmaier. *STM–Bildkontrast und Monolagenkristallographie planarer Aromaten.* Dissertation, Universität Stuttgart, 1997.

[59] G.P. Lopinski, D.D.M. Wayner und R.A. Wolkow. *Self-directed growth of molecular nanostructures on silicon.* Nature, **406** (2000) 48–51.

[60] R. Lin, M. Galili, U.J. Quaade, M. Brandbyge, T. Bjornholm, A. Degli Esposti, F. Biscarini und K. Stokbro. *Spontaneous dissociation of conjugated molecule on the Si(100) surface.* J. Chem. Phys., **117** (2002) 321–30.

[61] R.J. Hamers, J.S. Hovis, Seung Lee, Hongbing Liu und Jun Shan. *Formation of ordered , anisotropic organic monolayer on the Si(001) surface.* J. Phys. Chem. B, **101** (1997) 1489–92.

[62] J.T. Jates Jr. *Surface chemistry of silicon: the behaviour of dangling bonds.* J. Phys.: Condens. Matter, **3** (1991) 143–156.

[63] J.W. Lyding, T.C. Shen, J.S. Hubacek, J.R. Tucker und G.C. Abeln. *Nanoscale patterning and oxidation of H-passivated Si(100)-2*1 surfaces with an ultrahigh vacuum scanning tunneling microscope.* Appl. Phys. Lett., **64** (1994) 2010–12.

[64] M.C. Hersam, N.P. Guisinger und J.W. Lyding. *Isolating, imaging, and electrically characterizing individual organic molecules on the Si(100) surface with the scanning tunneling microscope.* J. Vac. Sci. Technol. A, **18** (2000) 1349–53.

[65] Ph. Avouris, R.E. Walkup, A.R. Rossi, H.C. Akpati, P. Nordlander, T.-C. Shen, G.C. Abeln und J.W. Lyding. *Breaking individual chemical bonds via STM-induced excitations.* Surface Science, **363** (1996) 368–377.

[66] T.-C. Shen, C. Wang, G.C. Abeln, J.R. Tucker, J.W. Lyding, Ph. Avouris und R.E. Walkup. *Atomic-Scale desorption through electronic and vibrational excitation mechanisms.* Science, **268** (1995) 1590.

[67] G.C. Abeln, A.M.C. Hersam, D.S. Thompson, S.T. Hwang, H. Choi, J.S. Moore und J.W. Lyding. *Approaches to nanofabrication on Si(100) surfaces: Selective area chemical vapor deposition of metals and selective chemisorption of organic molecules.* J. Vac. Sci. Technol. B, **16** (1998) 3874–8.

[68] E. Umbach, M. Sokolowski und R. Fink. *Substrate-interaction , long-range order and epitaxy of large organic adsorbates.* Appl. Phys. A, **63** (1996) 565–576.

[69] U. Zimmermann, G. Schnitzler, N. Karl, E. Umbach und R. Dudde. *Epitaxial growth and characterization of organic thin films on silicon.* Thin Solid Film, **175** (1989) 85–8.

[70] J. Taborski, P. Vaterlein, H. Dietz, U. Zimmermann und E. Umbach. *NEXAFS investigations on ordered adsorbate layers of large aromatic molecules.* J. Electron Spectr., **75** (1995) 129–47.

[71] H.Lüth. *Surfaces and interfaces of solid materials.* Springer Study Edition. Springer, Heidelberg, 1995.

[72] A. Zangwill. *Physics at surfaces.* Cambridge Univ. Press, Cambridge, 1988.

[73] D.V. O'Connor und D. Phillips. *Time-Correlated Single Photon Counting.* Academic Press, London, 1984.

[74] D.F. Eaton. *Recommended Methods for Fluorescence Decay Analysis.* Pure & Appl. Chem., **62**(8) (1990) 1631–1648.

[75] U. Gómez. *Zeitaufgelöste Fluoreszenzspektroskopie an dünnen organischen Aufdampfschichten.* Diplomarbeit, Universität Stuttgart, 1994.

[76] G. Klebe, F. Graser, E. Hädicke und J. Berndt. *Christallochromy as a solid-state effect: correlation of molecular conformation, crystal packing and colour in perylene-3,4:9,10-bis(dicarboximide) pigments.* Acta Cryst. B, **45**(1) (1989) 69–77.

[77] M. Hoffmann, K. Schmidt, T. Fritz, T. Hasche, V.M. Agranovich und K. Leo. *The lowest energy Frenkel and charge-transfer excitons in quasi-one-dimensional structures: application to MePTCDI and PTCDA crystals.* Chem. Phys., **258** (2000) 73–96.

[78] K. Gustav, M. Leonhardt und H. Port. *Theoretical Investigations on Absorption and Fluorescence of Perylene and its Tetracarboxylic Derivatives.* Monatshefte für Chemie, **128** (1997) 105–112.

[79] M.H. Hennessy, Z.G. Soos, R.A. Pascal Jr. und A. Girlando. *Vibronic structure of PTCDA stacks: the exciton-phonon-charge-transfer dimer.* Chem. Phys., **245** (1999) 199–212.

[80] C.A. Parker und W.T. Rees. *Correction of Fluorescence Spectra and Measurement of Fluorescence Quantum Efficiency.* Analyst, **85** (1960) 587–600.

[81] R. Seyfang. *Selbstlokalisierte Anregungszustände in Pyrenkristallen. Dynamische und spektrale Charakterisierung durch optische Kurzzeitspektroskopie.* Dissertation, Universität Stuttgart, 1989.

[82] B. Walker. *Kurzzeitspektroskopie an Perylen-Kristallen. Untersuchungen zur Excimer-Bildungskinetik.* Dissertation, Universität Stuttgart, 1993.

[83] J. Tanaka. *The Electronic Spectra of Aromatic Molecular Crystals. II. The Crystal Structure and Spectra of Perylene.* Bull. Chem. Soc. Jpn., **36**(10) (1963) 1237–1249.

[84] H. Port, B. Walker und H.C. Wolf. *Time Resolved Excimer Dynamics in Perylene Crystals.* J. Lumin., **31/32**(2) (1984) 780–782.

[85] B. Walker, H. Port und H.C. Wolf. *The Two-Step Excimer Formation in Perylene Crystals.* Chem. Phys., **92**(2/3) (1985) 177–185.

[86] P. Fischer. *Laserspektroskopische Charakterisierung dünner organischer Aufdampfschichten.* Dissertation, Universität Stuttgart, 1991.

[87] V. Bulović, P.E. Burrows, S.R. Forrest, J.A. Cronin und M.E. Thompson. *Study of Localized and Extended Excitons in 3,4,9,10-Perylenetetracarboxylic Dianhydride (PTCDA) I. Spectroscopic Properties of Thin Films and Solutions.* Chem. Phys., **210** (1996) 1–12.

[88] K. Puech, H. Fröb, M. Hoffman und K. Leo. *Luminescence of ultrathin organic films: transition from monomer to excimer emission.* Optics Letters, **21**(19) (1996) 1606–8.

[89] U. Gómez, H. Port und H.C. Wolf. *Fluorescence Quenching of Ultrathin MePTCDI Films by Inorganic Substrates.* J. Lumin., **72–74** (1997) 496.

[90] U. Gómez, M. Leonhardt, H. Port und H.C. Wolf. *Optical Properties of Amorphous Ultrathin Films of Perylene Derivatives.* Chem. Phys. Lett., **268** (1997) 1–6.

[91] K. Puech, H. Fröb und K. Leo. *Excimer dynamics in ultrathin organic films.* J. Lumin., **72-74** (1997) 524.

[92] P.B. Bisht, K. Fukuda und S. Hiraysama. *Size-dependent fluorescence emission spectra and lifetimes of microcrystals of the dye N,N'-bis(2,5-di-tert-butylphenyl)-3,4:9,10- perylenebis(dicarboximide) (DBPI) studied by confocal fluorescence microscopy.* J. Phys. Chem. B, **101** (1997) 8054–8.

[93] K. Akers, R. Aroca, A.M. Hor und R.O. Loutfy. *Molecular organization in perylenetetracarboxylic dianhydride films.* J. Phys. Chem., **91** (1987) 2954–9.

[94] K. Akers, R. Aroca, A.M. Hor und R.O. Loutfy. *Molecular organization in perylene tetracarboxylic di-imide solid films.* Spectrochim. Acta, **44A**(11) (1988) 1129–1135.

[95] E.I Haskal, Z. Shen, P.E. Burrows und S.R. Forrest. *Excitons and exciton confinement in crystalline organic thin films grown by organic molecular-beam deposition.* Phys. Rev. B, **51** (1995) 4449–62.

[96] V. Bulović und S.R. Forrest. *Study of Localized and Extended Excitons in 3,4,9,10-Perylenetetracarboxylic Dianhydride (PTCDA) II. Photocurrent Response at Low Electric Fields.* Chem. Phys., **210** (1996) 13–25.

[97] C.I. Wu, Y. Hirose, H. Sirringhaus und A. Kahn. *Electron-hole interaction energy in the organic molecular semiconductor PTCDA.* Chem. Phys. Lett., **272** (1997) 43.

[98] M. Hoffmann. *Frenkel and Charge–Transfer Excitons in Quasi–One–Dimensional Molecular Crystals with Strong Intermolecular Orbital Overlap.* Dissertation, Technische Universität Dresden, 2000.

[99] R. Scholz, A. Yu Kobitski, I. Vragović, G. Salvan, T.U. Kampen, D.R.T. Zahn und H.P. Wagner. *Proc 26th Int. Conf. Physics Semicond.* IOP Press, (2003) in press.

[100] I. Vragović und R. Scholz. *Frenkel Exciton Model of Optical Absorption and Photoluminescence in α-PTCDA.* submitted to Phys. Rev. B, (2003).

[101] A. Yu Kobitski, R. Scholz, I. Vragović, H.P. Wagner und D.R.T. Zahn. *Low-temperature time-resolved photoluminescence characterization of 3,4,9,10-perylene tetracarboxylic dianhydride crystals.* Phys. Rev. B, **66** (2002) 153204.

[102] M. Leonhardt. *UHV-Aufdampfschichten von PTCDA: Korrelation von optischer Spektroskopie und Schichtaufbau.* Dissertation, Universität Stuttgart, 2001.

[103] M. Pope und C.E. Swenberg. *Electronic Processes in Organic Crystals*, **39** der *Monographs on the Physics and Chemistry of Materials.* Oxford University Press, New York, 1982.

[104] J.B. Birks. *Photophysics of Aromatic Molecules.* Wiley Monographs in Chemical Physics. Wiley-Interscience, London, 1970.

[105] Th. Förster und K. Kasper. *Ein Konzentrationsumschlag der Fluoreszenz.* Z. Phys. Chem., **1** (1954) 275–277.

[106] H. Port. *Zeitaufgelöste Excimer-Dynamik in Molekülkristallen, in: Photoreaktive Festkörper.* M. Wahl-Verlag, Karlsruhe, 1984.

[107] E. Glockner. *Fluoreszenzuntersuchungen am Mischkristallsystem Anthracen–Perdeuteroanthracen bei Temperaturen zwischen 1,6 K und 77 K.* Dissertation, Universität Stuttgart, 1973.

[108] D.S. McClure und O. Schnepp. *Electronic States of the Naphthalene Crystal.* J. Chem. Phys., **23**(9) (1955) 1575–1587.

[109] V.L. Broude, A.F. Prikhotko und E.I. Rashba. *Some Problems of Crystal Luminescence.* Sov. Phys. Uspekhi, **67**(2) (1959) 38–49.

[110] J. Hofmann, K.P. Seefeld, W. Hofberger und H. Bässler. *Excimers in Solid Non-Crystalline Anthracene.* Mol. Phys, **34**(3) (1979) 973–979.

[111] G. Gaisser. *Zeitaufgelöste Fluoreszenzspektroskopie an organischen Molekülschichten im Monolagebereich.* Diplomarbeit, Universität Stuttgart, 1998.

[112] C. Seidel. *Charakterisierung organischer Adsorbate auf Silbereinkristallen mit den Meßmethoden LEED und STM.* Dissertation, Universität Stuttgart, 1993.

[113] M. De Seta, D. Sanvitto und F. Evangelisti. *Direct evidence of C_{60} chemical bonding on Si(100).* Phys. Rev. B, **59** (1999) 9878–81.

[114] G.A. Reider, U. Höfer und T.F. Heinz. *Desorption kinetics of hydrogen from Si(111)7 × 7 surface.* J. Chem. Phys., **94** (1991) 4080–83.

[115] A. Otto, I. Mrozek, H. Grabhorn und W. Akemann. *Surface-enhanced Raman scattering.* J. Phys.: Condens. Matter, **4** (1992) 1143–1212.

[116] A. Dargis und J. Kundrotas. *Handbook on Physical Properties of Ge, Si, GaAs and InP.* Science and Encyclopedia Publishers, Vilnius, 1994.

[117] M.E. Levinshtein und S.L. Rumyantsev. *Handbook Series on Semiconductor Parameters*, **1**. World Scientific, London, 1996.

[118] Paul A. Temple und C.E. Hathaway. *Multiphonon Raman Spectrum of Silicon.* Phys. Rev. B, **7** (1971) 3685–97.

[119] P.J. Tarcha, J. Desaja-Gonzalez, S. Rodriguez-Llorente und R. Aroca. *Surface-enhanced fluorescence on SiO_2-coated silver island films.* Appl. Spect., **53** (1999) 43–8.

[120] R. Scholz, A.Yu. Kobitski, T.U. Kampen, M. Schreiber, D.R.T. Zahn, G. Jungnickel, M. Elstner, M. Sternberg und Th. Frauenheim. *Resonant Raman spectroscopy of 3,4,9,10-perylene-tetracarboxylic- dianhydride epitaxial films.* Phys. Rev. B, **61** (2000) 13659–69.

[121] F.S. Tautz, S. Sloboshanin, J.A. Schaefer, R. Scholz, V. Shklover, M. Sokolowski und E. Umbach. *Vibrational properties of ultrathin PTCDA films on Ag(110).* Phys. Rev. B, **61** (2000) 16933–47.

[122] R.F. Aroca und C.J.L. Constantino. *Surface-enhanced Raman scattering: imaging and mapping of Langmuir-Blodgett monolayers physically adsorbed onto silver island films.* Langmuir, **16** (5425-9) 2000.

[123] D.A. Tenne, S. Park, T.U. Kampen, A. Das, R. Scholz und D.R.T. Zahn. *Single crystals of the organic semiconductor perylene tetracarboxylic dianhydride studied by Raman spectroscopy.* Phys. Rev. B, **61** (2000) 14564–9.

[124] G. Salvan, D.A. Tenne, A. Das, T.U. Kampen und D.R.T. Zahn. *Influence of deposition temperature on the structure of 3,4,9,10- perylene tetracarboxylic dianhydride thin films on H-passivated silicon probed by Raman spectroscopy.* Organic Electronic, **1** (2000) 49–56.

[125] P. Kambhampati, C.M. Child, M.C. Foster und A. Campion. *On the chemical mechanism of surface enhanced Raman scattering: experiment and theory.* J. Chem. Phys., **108** (1998) 5013–26.

[126] T. Hasche, T.W. Canzler, R. Scholz, M. Hoffmann, K. Schmidt, Th. Frauenheim und K. Leo. *Coherent external and internal phonons in quasi-one-dimensional organic molecular crystals.* Phys. Rev. Lett., **86** (2001) 4060–4063.

[127] U. Guhathakurta-Ghosh und R. Aroca. *Surface-enhanced Raman scattering and surface-enhanced resonant Raman scattering studies of perylenetetracarboxylic derivatives on Ag-coated Sn spheres and Ag and Au island films.* J. Phys. Chem., **93** (1989) 6125–28.

[128] J. Taborski. *NEXAFS-Untersuchungen an organischen Adsorbaten auf verschiedenen (111)-Oberflächen.* Dissertation, Universität Stuttgart, 1994.

[129] C. Kittel. *Einführung in die Festkörperphysik.* R. Oldenbourg Verlag, München, 1989.

[130] R.R. Chance, A. Prock und R. Silbey. *Frequency Shifts of an Electric-Dipole Transition Near a Partially Reflecting Surface.* Phys. Rev. A, **12**(4) (1975) 1448–1452.

[131] A. Sommerfeld. *Vorlesungen über Theoretischen Physik*, **VI**. Akademische Verlagsgesellschaft, Leipzig, 1962.

[132] E. Fehlberg. *New High Order Runge-Kutta Formulas with Step Size Control for Systems of First- and Second-Order Differential Equations.* ZAMM, **44** (1964) 17–29.

[133] J. Stoer und R. Bulirsch. *Numerische Mathematik 2.* Springer Verlag, Berlin, 1990.

[134] W.H. Press, S.A. Teukolsky, W.T. Vetterling und B.P. Flannery. *Numerical Recipes in C.* Cambridge University Press, New York, 1992.

[135] P.B. Johnson und R.W. Christy. *Optical constants of the noble metals.* Phys. Rev. B, **6**(12) (1972) 4370–4379.

[136] Th. Förster. *Experimentelle und theoretische Untersuchungen des zwischenmolekularen Übergangs von Elektronenanregungsenergie.* Z. Naturforsch., **4a**(5) (1949) 321–327.

[137] H. Kuzmany. *Solid State Spectroscopy.* Springer, Heidelberg, 1998.

[138] P.Y.Yu und M.Cardona. *Fundamentals of Semiconductors.* Springer, Heidelberg, 1996.

[139] H. Raether. *Surface Plasmons.* Springer, Heidelberg, 1988.

[140] S. Kawata (Ed.). *Near-field optics and surface plasmon polariton.* Springer, Heidelberg, 2001.

[141] W.H. Weber und C.F. Eagen. *Energy transfer from an excited dye molecule to surface plasmons of an adjacent metal.* Opt. Let., **4**(8) (1979) 236.

[142] I. Pockrand, A. Brillante und D. Möbius. *Nonradiative Decay of Excited Molecules Near a Metal Surface.* Chem. Phys. Lett., **69** (1980) 499–504.

[143] H. Ehrenreich und H.R. Philipp. *Optical properties of Ag and Cu.* Phys. Rev., **128** (1962) 1622.

[144] N.F.Mott und H.Jones. *The Properties of Metals and Alloys.* Dover, New York, 1958.

[145] G.W. Ford und W.H. Weber. *Electromagnetic interactions of molecules with metal surfaces.* Phys. Rep., **113** (1984) 195–287.

[146] D.H. Waldeck, A.P. Alivisatos und C.B. Harris. *Nonradiative damping of molecular electronic excited states by metal surfaces.* Surf. Sci., **158** (1985) 103–125.

[147] N.W. Ashcroft und N.D. Mermin. *Solid State Physics.* CBS Publishing LTD, 1976.

[148] H.E. Hallam Editor. *Vibrational Spectroscopy of Trapped Species.* John Wiley & Sons, London, 1973.

[149] R.L. Amey und R.H. Cole. J. Chem. Phys., **40** (1964) 146.

[150] D.E. Aspnes und A.A. Studna. *Dielectric Functions and Optical Parameters of Si, Ge, GaP, GaAs, GaSb, InP, InAs and InSb from 1.5 to 6 eV.* Phys. Rev. B, **27**(2) (1983) 985–1009.

[151] S. M. Sze. *Physics of Semiconductor Devices.* John Wiley and Sons, New York, 1981.

[152] C.B. Roxlo, R.R. Chianelli, H.W. Deckman, A.F. Ruppert und P.P. Wong. *Bulk and surface optical absorption in molybdenum disulfide.* J. Vac. Sci. Technol. A, **5** (1987) 555–557.

[153] D.L. Dexter. *Two ideas on energy transfer phenomena: ion-pair effects involving the OH stretching mode and sensitization of photovoltaic cells.* J. Lumin., **18/19** (1979) 779–84.

[154] Th. Förster. *Zwischenmolekulare Energiewanderung und Fluoreszenz.* Ann. Phys., **6**(2) (1948) 55–75.

[155] D.L. Dexter. *A theory of sensitizes luminescence in solids.* J. Chem. Phys., **21**(5) (1953) 836–850.

[156] M. Cardona und E.H. Pollack. *Energy-band structure of Germanium and Silicon: The k·p method.* Phys. Rev., **142** (1966) 530–543.